**Universidade Federal do Rio Grande – FURG**

**Instituto de Oceanografia**

Programa de Pós-Graduação em Oceanografia

# Transporte de Sedimento na Região Central da Plataforma Interna do Atlântico Sul

**Paulo Victor de Araújo Brito Lisboa**

Tese apresentada ao Programa de Pós-Graduação em Oceanologia, como parte dos requisitos para a obtenção de grau de doutor.

Orientadora: *Prof. Dra.* Elisa Leão Fernandes

Universidade Federal do Rio Grande (FURG), Brasil

Coorientador: *Prof. Dr.* Aldo Sottolichio

Universidade de Bordeaux, França

Rio Grande, RS, Brasil

Fevereiro, 2021

# Transporte de Sedimento na Plataforma Interna do Atlântico Sul

Tese apresentada ao Programa de Pós-Graduação em Oceanologia, como parte dos requisitos para a obtenção de grau de doutor.

**Paulo Victor de Araújo Brito Lisboa**

Rio Grande, RS, Brasil

Fevereiro, 2021

LISBOA, PAULO

Transporte de Sedimento na Plataforma Interna do Atlântico Sul / Paulo Victor de Araújo Brito Lisboa. – Rio Grande: FURG, 2020.

Número de páginas 205p.

Tese (Doutorado) - Universidade Federal do Rio Grande. Doutor em Oceanologia. Área de Concentração: Física Oceânica; Geologia Marinha e Costeira;

1. Modelagem Computacional. 2. Transporte de Sedimentos. 3. Evolução do Fundo 4. Oceanografia Costeira. 5. Plataforma Interna I. Transporte de Sedimento na Plataforma Interna do Atlântico Sul.

# Agradecimentos

Como já era esperado, o doutorado foi um processo muito difícil, posso dizer um dos mais difíceis da minha vida. Mas ao mesmo tempo o doutorado me proporcionou momentos que nunca na minha vida eu imaginaria passar. Experiencias incríveis que vivi, e que acrescentou e muito na minha vivencia e no meu intelectual. Porém, nada disso seria possível sem a ajuda de pessoas que entram na minha vida para muda-la por completo e contribuíram de alguma forma para a realização dessa etapa tão importante na minha vida.

Tenho muito a agradecer primeiramente a Deus por toda a força que Ele me deu, e por não permitir que minha fé diminuísse a cada obstáculo. Quero agradecer demais a minha família por todo suporte emocional depositado em mim. Sem eles eu já teria ficado no meio do caminho, e provavelmente desistido do doutorado. Obrigado a minha mãe Lúcia, ao meu pai Paulo Accácio e a minha irmã Luana. Obrigado demais a minha namorada Kamila Mansur e toda família Mansur da Rocha, que me acolheu como um filho, em um momento muito difícil para toda a humanidade, durante a pandemia do COVID. Diante disso não tenho palavras para agradecer tudo que o Alan Carlos, Rosane Mansur e Raquel Mansur fizeram por mim.

Agradeço demais ao pessoal do LOCOSTE, em especial a minha orientadora Elisa Fernandes, que durante todos esses anos como minha orientadora, sempre cobrou o meu melhor e nunca desistiu de mim, mesmo em momentos no qual eu demonstrava desmotivação. Muito obrigado por não desistir de mim e desculpe por todas as vezes em que não me comprometi como deveria.

O doutorado me trouxe pessoas que foram vitais para essa tese, o Professor Aldo Sottolichio e meu amigo José Filho, que durante minha estadia na França foram meus grandes companheiros e sempre estavam dispostos a me ajudar.

E por fim queria agradecer a todos os meus amigos em especial ao Jean Espinoza, ao Rayton Bendô e Miguel Albuquerque. Agradeço muito por todas as horas e mais hora em frente ao computado gerando os resultados que compõem essa tese. Muito obrigado a todos.

# Índice

# Lista de Figuras

Dados prescritos como a condição de contorno no limite do oceano nos pontos L1 e L2 (elevação da superfície do mar) (A), V1 e V2 (velocidade da corrente) (B), e S1 e S2 (salinidade) (C) para o período 2005-2012.

**Figura 7:** Página 52

Séries temporais da descarga fluvial do rio Guaíba, rio Camaquã, canal São Gonçalo e Rio da Prata para o período estudado (2005-2012).

**Figura 8:** Página 53

(A) Série temporal de intensidade do vento usada como forçante superficial na simulação. (B) Rosa dos ventos para a distribuição de frequências da série temporal de intensidade e direção do vento para os anos de 2005 a 2012.

**Figura 9:** Página 57

Comparação entre as séries temporais medidas e calculadas da velocidade da corrente (A) na superfície e (B) no fundo do canal de acesso ao Porto do Rio Grande (ver Figura 2B para localização).

**Figura 10:** Página 59

Comparação entre as séries temporais medidas e calculadas da elevação do nível do mar na (A) Praia do Cassino e (B) Rio da Prata.

**Figura 11:** Página 60

Comparação entre as séries temporais de salinidade medida (linha vermelha) e calculada (linha azul) e velocidade da corrente (A) na superfície e (B) no fundo.

**Figura 12:** Página 61

Comparação entre a concentração calculada de sedimentos em suspensão (linha azul) e os dados medidos (linha vermelha) em (A) o estuário inferior, (B) médio e (C) superior do Rio da Prata, entre o dia 24 de Junho a 16 de dezembro de 2010.

**Figura 13:** Página 62

Painéis à esquerda: Concentrações de sedimentos em suspensão (SSC) na superfície obtidas com o modelo numérico (A, D) e por sensoriamento remoto (B, D) em 6 de fevereiro de 2008 (topo) e 17 de setembro, 2008 (parte inferior), respectivamente. Painéis à direita: SSC na superfície extraída dos respectivos perfis longitudinais (painéis superiores) e transversais (painéis inferiores) (C, F).

**Figura 14 - Figure 1 - Artigo 1:** Página 72

The study region defined between the latitudes of 28°S (Santa Marta Cape) and 38°S (Mar Del Plata). Blue dots represent the main effluents from the Patos Lagoon (Guaíba River, Camaquã River, and São Gonçalo Channel), green dots show important regions in the study area and black dots represent the points from where model results were extracted for the wavelet analysis (P1 and P2). T shows the transects where model results were extracted from (T1, T2, T3, T4, and T5) for empirical orthogonal function (EOF) analyses. The white lines represent the main effluents of the La Plata River (River Bermejo, River Paraná, and River Uruguay).

**Figura 15 - Figure 2 - Artigo 1:** Página 80

Computational domain and numerical mesh used for the simulations. (A) Initial and boundary conditions prescribed in the model. The points where the time series of salinity (S1 and S2), current velocity (V1 and V2), and water level (L1 and L2) prescribed as boundary conditions were extracted are also shown. (B) Zoom view of the Patos Lagoon mesh and (C) that of the La Plata River mesh.

**Figura 16 - Figure 3 - Artigo1:** Página 83

Comparison between measured and calculated time series of current velocity (A) at the surface and (B) at the bottom of the access channel to the Port of Rio Grande (see Figure 2B for location).

**Figura 17 - Figure 4 - Artigo 1:** Página 84

Comparison between the measured and calculated time series of free surface elevation at (A) Cassino Beach and (B) Rio La Plata.

**Figura 18 - Figure 5 - Artigo 1:** Página 85

Comparison between the measured (red line) and calculated (blue line) salinity and current velocity time series at (A) the surface and (B) the bottom.

**Figura 19 - Figure 6 - Artigo 1:** Página 86

Comparison between the calculated suspended sediment concentration (blue line) and the measured data (red line) in (A) the lower, (B) middle and (C) upper estuary in Rio de La Plata River, between the 24th of June to the 16th of December, 2010.

**Figura 20 - Figure 7 - Artigo 1:** Página 87

Left panels: Suspended sediment concentrations (SSC) at the surface obtained with the numerical model (A, D) and from remote sensing (B, D) on the 6th of February, 2008 (top) and the 17th of September, 2008 (bottom), respectively. Right panels: SSC at the surface extracted from the respective longitudinal (top panels) and transversal (bottom panels) profiles (C, F).

**Figura 21 - Figure 8 - Artigo 1:** Página 89

Seasonal average suspended sediment concentrations (SSC) for the study region during winter (A) and summer (C) in the neutral period (2005-2006), and during winter (B) and summer (D) in the period experienced ENSO conditions (2008-2009).

**Figura 22 - Figure 9 - Artigo 1:** Página 91

Average suspended sediment concentrations (SSC) (left column) and their averaged normal velocities (red represents outflow and blue is inflow) and the transversal velocity components (vectors; right column) along transects made across the La Plata River (T2) and the Patos Lagoon (T4), respectively, during the neutral period (2005-2006) and the period influenced by the ENSO cycle (2008-2009). The white dotted line indicates the position of the Patos Lagoon mouth. The color scale for SSC has not been standardised for easy viewing, and for the La Plata River, the red colour indicates sediment concentrations ranging between 50 and 200 mg/L.

**Figura 23 - Figure 10 - Artigo 1:** Página 92

Mass flux (red indicates export and blue import) of suspended sediment and time series of the cumulative mass flux into the cross-section in the Patos Lagoon mouth (T4) (left column) during (A) a neutral period (2005-2006) and (B) a period under the influence of the ENSO cycle (2008-2009), and in the cross-section of the La Plata River (T2) (right column) during (C) a neutral period (2005-2006) and (D) a period under the influence of the ENSO cycle (2008-2009).

**Figura 24 - Figure 11 - Artigo 1:** Página 94

The first three empirical orthogonal function (EOF) modes of suspended sediment concentration (SSC) across the domain for the neutral period (2005-2006) (left column) and for the period under the influence of an ENSO cycle (2008-2009) (right column). The red areas (positive values) represent the regions where the concentration of the suspended sediment has a high spatial pattern, in contrast, the blue areas (negative values) represent the regions where the SSC has a low spatial pattern.

**Figura 25 - Figure 12 - Artigo 1:** Página 95

The first three empirical orthogonal function (EOF) modes of suspended sediment concentration (SSC) along the longitudinal section of the La Plata River (T1) for the neutral period (2005-2006) (left column) and for the period under the influence of an ENSO cycle (2008-2009) (right column). The dotted lines represent the position of the mouth in longitudinal view. The red areas (positive values) represent the regions where the concentration of the suspended sediment has a high spatial pattern, and in contrast, the blue areas (negative values) represent the regions where the SSC has a low spatial pattern.

**Figura 26 - Figure 13 - Artigo 1:** Página 96

The first three modes of the empirical orthogonal function (EOF) analysis of suspended sediment concentrations (SSC), along the transversal profile of the La Plata River (T2) for the neutral period (2005-2006) (left column) and for the period under the influence of an ENSO cycle (2008-2009) (right column). The red areas (positive values) represent the regions where the concentration of the suspended sediment has a high spatial pattern. In contrast, the blue areas (negative values) represent the regions where the SSC has a low spatial pattern.

**Figura 27 - Figure 14 - Artigo 1:** Página 97

The first three modes of the empirical orthogonal function (EOF) analysis of suspended sediment concentrations (SSC) along the transversal profile of the Patos Lagoon mouth (T4) for the neutral period (2005-2006) (left column) and the period under the influence of an ENSO cycle (2008-2009) (right column). The dotted lines represent the position of the mouth in longitudinal view. The red areas (positive values) represent the regions where the concentration of the suspended sediment has a high spatial pattern, and in contrast, the blue areas (negative values) represent the regions where the SSC has a low spatial pattern.

**Figura 28 - Figure 15 - Artigo 1:** Página 98

The first three modes of the empirical orthogonal function (EOF) analysis of suspended sediment concentrations (SSC) on the longitudinal profile at the Patos Lagoon mouth (T5) for the neutral period (2005-2006) (left column) and for the period under the influence of an ENSO cycle (2008-2009) (right column). The dotted lines represent the position of the Patos Lagoon mouth. The red areas (positive values) represent the regions where the concentration of the suspended sediment has a high spatial pattern; in contrast, the blue areas (negative values) represent the regions where the SSC has a low spatial pattern.

**Figura 29 - Figure 16 - Artigo 1:** Página 99

(A) Time series of the La Plata River discharge (orange) and suspended sediment concentrations (SSC; blue) for the period 2005-2006 (green dot - Figure 1). (B) Cross-spectrum of local energy using Mexican hat wavelet analyses where the contour lines enclose regions with a 95% confidence interval. The dashed line indicates the region of influence where the border effects become important. (C) Average global power spectrum where the dashed line represents the 95% confidence level. (D) Time series of the La Plata River discharge (orange) and suspended sediment concentrations (blue) for the period 2008-2009 (green dot; Figure 1). (E) Cross-spectrum of local energy using the Mexican hat wavelet analysis; the contour lines involve regions with a 95% confidence interval and the dashed line indicates the region of influence where the border effects become important. (F) Average global power spectrum; the dashed line represents the 95% confidence level.

**Figura 30 - Figure 17 - Artigo 1:** Página 100

(A) Time series of fluvial discharge from the Patos Lagoon (red) and sediment concentrations (blue) for the period 2005-2006 (green dot - Figure 1). (B) Cross-spectrum of local energy using the Mexican hat wavelet analysis. The contour lines enclose regions with a 95% confidence interval and the dashed line indicates the influence with which the border effects become important. (C) Global spectrum indicating the average time of each cycle; the dashed line represents the 95% confidence level. (D) Time series of fluvial discharge from the Patos Lagoon (red) and sediment concentrations (blue) for the period 2008-2009 (green dot - Figure 1). (E) Cross-spectrum of local energy using the Mexican hat wavelet analysis; the contour lines involve regions with a 95% confidence interval and the dashed line indicates the influence with which the border effects become important. (F) Global spectrum indicating the average time each cycle takes place over. The dashed line represents the 95% confidence level.

**Figura 31 - Figure 18 - Artigo 1:** Página 101

(A) Time series of wind intensity (orange) and suspended sediment concentrations (SSC) in the La Plata River (blue) for the period 2005-2006 (green dot - Figure 1). (B) Cross-spectrum of local energy between the time series using Morlet wavelet analysis. The contour lines enclose regions with a 95% confidence interval. The dashed line indicates the region of influence where the border effects become important. (C) Average global power spectrum where the dashed line represents the 95% confidence level. (D) Time series of wind intensity (orange) and SSC of the La Plata River (blue) for the period 2008-2009 (green dot - Figure 1). (E) Cross-spectrum of local energy between the time series using Morlet wavelet; the contour lines involve regions with a 95% confidence interval and the dashed line indicates the region of influence where the border effects become important. (F) Average global power spectrum, where the dashed line represents the 95% confidence level.

**Figura 32 - Figure 19 - Artigo 1:** Página 102

(A) Time series of wind intensity (orange) and suspended sediment concentrations (SSC) in the Patos Lagoon (blue) for the period 2005-2006 (green dot - Figure 1). (B) Cross-spectrum of local energy between the series using Morlet wavelet; the contour lines enclose regions with a 95% confidence interval and the dashed line indicates the region of influence where the border effects become important. (C) Average global power spectrum; the dashed line represents the 95% confidence level. (D) Time series of wind intensity (red) and SSC in the Patos Lagoon (blue) for the period 2008-2009 (green dot - Figure 1). (E) Cross-spectrum of local energy between series using Morlet wavelet analysis; the contour lines involve regions with a 95% confidence interval and the dashed line indicates the influence with which the border effects become important. (F) Average global power spectrum; the dashed line represents the 95% confidence level.

**Figura 33 - Figure 20 - Artigo 1:** Página 103

(A) Time series of discharge from the La Plata River for the period influenced by the ENSO cycle. (B) Hovmöller diagram elaborated with the time series of suspended sediment concentrations (SSC) extracted along transect T6. SW is the limit of the closest transect to the La Plata River and NE the closest limit to the Patos Lagoon. (C) Time series of discharge in the north of the Patos Lagoon for the neutral period.

**Figura 34 - Figure 21 - Artigo 1:** Página 104

(A) Time series of discharge from the La Plata River for the period influenced by the ENSO cycle. (B) Hovmöller diagram elaborated with the time series of suspended sediment concentrations (SSC) extracted along transect T6. SW is the limit of the closest transect to the La Plata River and NE the closest limit to

the Patos Lagoon. (C) Time series of discharge in the north of the Patos Lagoon for the period influenced by the ENSO cycle.

**Figura 35 - Figure 22 - Artigo 1:** Página 105

The first three empirical orthogonal function (EOF) modes of suspended sediment concentrations (SSC) along the T6 transect on the internal platform for the neutral period (2005-2006) (left column) and for the period under the influence of an ENSO cycle (2008-2009) (column right). The red areas (positive values) represent the regions where the concentration of the suspended sediment has a high spatial pattern and in contrast, the blue areas (negative values) represent the regions where the concentration of the suspended sediment has a low spatial pattern.

**Figura 36 - Figure A1 - Artigo 1:** Página 129

Summary of the methodological steps used in this work.

**Figura 37 - Figure B1 - Artigo 1:** Página 130

Salinity fields used as an initial condition in the surface layer of the model in January 2005 (A) and January 2008 (B).

**Figura 38 - Figure B2 - Artigo 1:** Página 130

Data prescribed as the boundary condition at the ocean boundary at points L1 and L2 (sea surface elevation) (A), V1 and V2 (current velocity) (B), and S1 and S2 (salinity) (C) for the period 2005-2006. The boundary conditions for 2008-2009 are not presented.

**Figura 39 - Figure B3 - Artigo 1:** Página 131

Time series of the freshwater discharge from the Guaíba River, Camaquã River, São Gonçalo Channel and the La Plata River for both studied periods (2005-2006 and 2008-2009).

**Figura 40 - Figure B4 - Artigo 1:** Página 132

Wind Rose for the frequency distribution of the time series of wind intensity and direction, for the years 2005-2006 (A) and 2008-2009 (B).

**Figura 41 - Figure B5 - Artigo 1:** Página 132

Time series of intensity used as a superficial forcing in the simulation.

**Figura 42 - Figure E1 - Artigo 1:** Página 139

Seasonal behavior of sea level for the study region, in the summer 2005-2006 (A), summer 2008-2009 (B), winter 2005-2006 (C) and winter 2008-2009 (D).

**Figura 43 - Figure E2 - Artigo 1:** Página 141

Seasonal behavior of the salinity field for the study region, in the summer 2005-2006 (A), summer 2008-2009 (B), winter 2005-2006 (C) and winter 2008-2009 (D).

**Figura 44 - Figure E3 - Artigo 1:** Página 142

Seasonal behavior of the speed field for the study region, in the summer 2005-2006 (A), summer 2008-2009 (B), winter 2005-2006 (C) and winter 2008-2009 (D).

**Figura 45 - Figure 1 - Artigo 2:** Página 146

The study region defined between the latitudes of 28°S (Santa Marta Cape) and 38°S (Mar Del Plata). Blue dots represent the main effluents from Patos Lagoon (Guaíba River, Camaquã River, and São Gonçalo Channel), green dots are important geomorphological regions in the study area and black dots represent points from where model results where extracted for the Wavelet analysis, the deposition flux and the bed evolution (P1 and P2).

**Figure 46 - Figure 2 - Artigo 2:** Página 152

Computational domain and numerical mesh used for the simulations. (A) Initial and boundary conditions prescribed in the model. (B), detail of La Plata River mouth (C), and Patos Lagoon (C).

**Figura 47 - Figure 3 - Artigo 2:** Página 154

Time series of fluvial discharge from the Guaíba River, Camaquã River, São Gonçalo Channel and La Plata River for the period studied (2005-2012) (A) Time series of intensity used as surface forcing in the simulation. (B) The wind rose for the frequency distribution of the time series of wind intensity and direction, for the

years 2005 to 2012 (C) Times series of salinity from the ocean boundary (D). Times series of tidal from the ocean boundary.

**Figura 48 - Figure 4 - Artigo 2:** Página 157

Comparison between the measured (red line) and calculated (black line) salinity time series at (A) the surface and (B) the bottom, current velocity time series at (C) the surface and (D) the bottom, and free surface time series (E).

**Figura 49 - Figure 5 - Artigo 2:** Página 158

Comparison between the calculated suspended sediment concentration (black line) and the measured data (red line) in (A) the lower, (B) middle and (C) upper estuary in Rio de La Plata River, between the 24th of June to the 16th of December, 2010.

**Figura 50 - Figure 6 - Artigo 2:** Página 159

Mean-field of concentration of bottom sediment (A), Mean-field of erosion flow (B) and deposition flow (C) for the study region, during the period from 2005 to 2012.

**Figura 51 - Figure 7 - Artigo 2:** Página 160

Seven years (2005–2012) calculated Deposition Flux, Erosion Flux, and SSC means for the austral seasons: a) Summer (Dec – Jan – Feb), b) Winter (Mar – Apr – May), c) Fall (Jun – Jul – Aug), and d) Spring (Sep – Out – Nov).

**Figure 52 - Figure 8 - Artigo 2:** Página 161

The first three EOF modes of the bottom sediment concentration for the entire domain in the simulated years (2005 - 2012).

**Figura 53 - Figure 9 - Artigo 2:** Página 163

(A) Time series of deposition flow at the La Plata mouth (blue) and fluvial discharge for the cross-analysis (orange) (black dot - P1, Figure 1). (B) Cross spectra of local energy between the series using Mexican Hat wavelets. The level curves involve regions with a 95% confidence interval. The dashed line indicates the region of influence where the effects of borders become important. (C) Mean global power spectrum. The dashed line represents the 95% confidence level.

(D) Time series of deposition flow at the La Plata mouth (blue) and the intensity of the wind for the cross-analysis (orange). (E) Cross spectra of local energy between the series using Morlet wavelets. The level curves involve regions with a 95% confidence interval. The dashed line indicates the region of influence where the effects of borders become important. (F) Mean global power spectrum. The dashed line represents the 95% confidence level.

**Figura 54 - Figure 10 - Artigo 2:** Página 164

(A) Time series of deposition flow at the Patos Lagoon mouth (blue) and fluvial discharge for cross-analysis (orange) (black dot - P1, Figure 1). (B) Cross spectra of local energy between the series using Mexican Hat wavelets. The level curves involve regions with a 95% confidence interval. The dashed line indicates the region of influence where the effects of borders become important. (C) Mean global power spectrum. The dashed line represents the 95% confidence level. (D) Time series of deposition flow at the Patos Lagoon mouth (blue) and wind intensity for the cross-analysis (orange). (E) Cross spectra of local energy between the series using Morlet wavelets. The level curves involve regions with a 95% confidence interval. The dashed line indicates the region of influence where the effects of borders become important. (F) Mean global power spectrum. The dashed line represents the 95% confidence level.

**Figure 55 - Figure 10 - Artigo 2:** Página 165

(A) Bed Evolution rate for the entire domain after 2920 simulated days, (B) Mean friction velocity field.

**Figura 56 - Figure 12 - Artigo 2:** Página 166

(A) The South Oscillation Index (SOI) for the analysis period (2005 - 2012), (B) deposition flux and bed evolution for the mouth of the La Plata River (P1), (C) and deposition flux and bed evolution for the mouth of the Patos Lagoon (P2).

# Lista de Tabelas

Rating scale for the relative mean absolute error (RMAE) (Sutherland et al., 2004 and Walstra et al., 2001).

**Tabela 8 - Table D1 - Artigoo 1:** Página 136

Parameters used in the calibration of the model, with the respective RMAE results for each of the tests (Patos Lagoon and La Plata River level). The results of the RMAE for the test with the best approximation in relation to the measured values are marked in bold.

**Tabela 9 - Table 1 - Artigo 2:** Página 155

Rating scale for the relative mean absolute error (RMAE) (Sutherland et al., 2004 and Walstra et al., 2001)

**Tabela 10 - Table 2 - Artigo 2:** Página 156

Better parameterization of the model found by the calibration exercises.

# Resumo

A Plataforma Continental do Atlântico Sudoeste é uma das maiores plataformas continentais do Hemisfério Sul e uma das mais importantes na produção biológica, devido à grande contribuição continental exercida tanto pelo Rio da Prata quanto pela Lagoa dos Patos. Estudos na região mostram que esses rios são significativamente afetados pelo efeito do El Niño – Oscilação Sul (ENOS), que pode interferir expressivamente na disponibilidade de material em suspensão inserido na região costeira. Apesar do grande esforço de diversos autores para compreender esses processos, algumas questões permanecem sem resposta. Assim, este trabalho visa preencher essa lacuna, respondendo a questões relacionadas à contribuição do sedimento de origem continental e seu comportamento na Plataforma Interna do Atlântico Sudoeste. O comportamento do sedimento em suspensão foi investigado com o auxílio do modelo hidromorfodinâmico TELEMAC-3D, através de 3 simulações devidamente calibrada e validada: uma representando anos normais, ou seja, sem o efeito do ENSO (2005-2006), outro experimentando o efeito do ENSO (2008-2009) e uma terceira simulação de longo prazo (2005-2012) para analisar os processos de deposição e evolução do fundo. Os resultados foram baseados em análises estatísticas, como Ondaletas e Análise Empírica da Função Ortogonal (EOF), além de séries temporais. Os resultados mostram que a Plataforma Interna do Atlântico Sudoeste é influenciada principalmente pela descarga fluvial do Rio da Prata e da Lagoa dos Patos, e pelo vento local. Além disso, a análise dos resultados da taxa exportação de sedimento para a plataforma interna mostra que o Rio da Prata é o maior exportador de sedimentos em suspensão da região, com uma taxa aproximada de $1,2x10^8$ ton/ano em anos neutros (normais) e $3,0x10^8$ ton/ano em anos sob influência do ENOS (fase quente e fria). Já a Lagoa dos Patos exporta aproximadamente $1,25x10^7$ ton/ano no período sem o efeito ENOS e $1,35x10^7$ ton/ano no período influenciado pelo ENOS. Os resultados também mostram que a descarga fluvial e o vento interagem com o sedimento em escalas sazonais a interanuais e sinóticas, respectivamente. Sobre a evolução de fundo, os resultados mostram que a Plataforma Interna do Atlântico Sudoeste tem um comportamento deposicional, apesar da presença de alguma área erosivas. Além disso, ficou evidente a influência do ENSO no fluxo de

deposição na plataforma, refletindo na taxa de sedimentação, que variou desde 50mm/ano até 120mm/ano.

Palavras-Chave: Concentração de Sedimento; Deposição; Erosão, Evolução de Fundo Plataforma Interna do Atlântico Sudoeste; Modelagem Numérica, Rio da Prata; Lagoa dos Patos; ENSO.

# Abstract

The Southwest Atlantic Inner Shelf is the largest continental shelf in the Southern Hemisphere and one of the most important in biological production, due to the great continental contribution exerted by both the La Plata River and the Patos Lagoon. Studies in the region show that these rivers are significantly affected by the effect of El Niño - South Oscillation (ENSO), which can significantly interfere with the availability of suspended material inserted in the coastal region. Despite the great effort of several authors to understand these processes, some questions remain unanswered. Thus, this work aims to fill this gap, answering questions related to the contribution of sediment of continental origin and its behavior on the Southwest Atlantic Inner Shelf. The behavior of the suspended sediment was investigated with the help of the hydromorphodynamic model TELEMAC-3D, through 3 simulations properly calibrated and validated: one representing normal years, that is, without the effect of ENSO (2005-2006), another experiencing the effect ENSO (2008-2009) and a third long-term simulation (2005-2012) to analyze the deposition and the bed evolution. The results were based on statistical analysis, such as Wavelets and Empirical Orthogonal Function Analysis (EOF), in addition to time series. The results show that the Southwest Atlantic Inner Shelf is influenced mainly by the fluvial discharge of the La Plata River and Patos Lagoon, and by the local wind. The La Plata River is the largest exporter of suspended sediments in the region, with an approximate rate of $1.2x10^8$ ton/year in neutral (normal) years and $3.0x10^8$ ton/year in years under the influence of ENSO. The Patos Lagoon exports approximately $1.25x10^7$ ton/year in the period without the ENSO effect and $1.35x10^7$ ton/year in the period influenced by ENSO. The results also show that fluvial discharge and wind interact with the sediment on seasonal to interannual and synoptic scales, respectively. Regarding the bed evoluiton, the results show that the Southwest Atlantic Inner Shelf has a depositional behavior, despite the presence of some erosive area. In addition, the influence of ENSO on the deposition flow on the platform was evident, reflecting on the sedimentation rate, which ranged from 50mm/year to 120mm/year.

Keywords: Sediment Concentration; Deposition; Erosion; Bed Evolution; Southwest Atlantic Inner Shelf; Numerical Modelling; La Plata River; Patos Lagoon; ENSO.

# Lista de Acrônimos e Abreviações

## A

ADPC – Acoustic Doppler Current Profiler;

ALM – Agência da Lagoa Mirim;

ANA – Agência Nacional de Águas;

## C

CAPES – Coordenação de Aprimoramento de Pessoal de Nível Superior;

CTD – Condutividade Temperatura Profundidade;

## D

DHN – Diretoria de Hidrografia e Navegação;

## E

ECMWF – Centro Europeu de Previsões Meteorológicas de Médio Prazo;

EDF – Companhia de Eletricidade da França;

ENSO – El Niño-Oscilação do Sul;

EOF – Análise Empírica de Funções Ortogonais;

## L

LEPLAC – Projeto de Levantamento da Plataforma Continental Brasileira;

## N

NASA – Agência Espacial Norte Americana;

## P

PCAS – Plataforma Interna do Atlântico Sudoeste;

## R

RMAE – Erro Absoluto Médio;

RMSE – Erro Quadrático Médio;

## S

SAIS – Plataforma Interna do Atlântico Sudoeste;

SAS – Plataforma Continental do Atlântico Sudoeste;

SHN - Serviço de Hidrografia Naval da Argentina;

SPM – Material particulado em suspensão;

SSC – Concentração de sedimentos em suspensão.

# **Capítulo I:** Introdução

# 1. Introdução

## Porque estudar as regiões estuarinas e costeiras?

Os estuários são comumente definidos como corpos de água costeiros semiconfinados, com ligação livre para a região costeira, que se estende ao longo de um rio até o limite de influência da maré, onde interior a água do mar é mensuravelmente diluída pela água doce oriunda da drenagem continental (Dyer, 1997). Esses ambientes apresentam a dinâmica altamente complexa e muito importante sobre o ponto de vista ambiental e econômico. Ao mesmo tempo que agem como fontes de compostos químicos (Santoro, 2017), os estuários e a região costeiras são reservatórios de sedimentos finos derivados das bacias continentais (Silva et al., 2014). Nesse contexto, a dinâmica desse sedimento fino em ambientes costeiros e estuarinos é pertinente devido seu impacto na produção primária, no transporte de compostos químicos e poluentes, e na evolução do fundo em virtude dos processos erosivos e deposicionais da região costeira.

Compreender a dinâmica dos sedimentos ajuda na previsão da contínua mudança nas zonas estuarinas e costeiras globais, gerado em parte por conta de forçantes físicas resultantes de diversos processos oceanográficos que frequentemente ocorrem nessas regiões, como por exemplo a descarga fluvial, os regimes de maré e de vento, as correntes costeiras e a ação das ondas (Rosa et al., 2013). Diversos autores focam seus estudos no intuito de conhecer de forma aprofundada as origens e consequências dessas alterações na região e na dinâmica costeira. E como resultado desses estudos, muito autores fomentam a importância do transporte de sedimento nos processos costeiros (Mahiques, 1995; Rodrigues et al., 2006; Marques et al., 2009; Rosa et al., 2013).

Além do contexto ecológico, as regiões costeiras são reconhecidas por sua significativa importância socioeconômica, sendo de fundamental relevância a compreensão dos aspectos ambientais que interferem na sua dinâmica (Dean, 1973). Por isso, a percepção do processo relativo a contribuição continental para a plataforma interna é de suma importância, pois estes afetam diretamente as condições oceanográficas que regem o ecossistema costeiro, dentre eles se destacam o padrão da circulação costeira (Gavine, 1974), a produção biológica (Mann e Lazier, 1996), a configuração da geomorfologia marinha (Muehe, 2018), além de outros fatores.

O transporte das águas oriundas de rios e estuários para o oceano é um elemento importante da dinâmica em muitas plataformas continentais, pois são responsáveis por

descarregar grande quantidade de água doce, sedimentos, material orgânico e substâncias dissolvidas na região costeira. De forma geral, a introdução dessa água doce nos ecossistemas costeiros produz um impacto significativo nas propriedades físicas, químicas e biológicas do oceano (Piola et. al., 2008), resultando na intensificação dos efeitos baroclínicos, no enriquecimento de nutrientes das águas costeiras, e consequentemente no aumento da produtividade primária (Garvine, 1974). Além disso, as condições dinâmicas, somadas aos padrões de dispersão e de assentamento destes sedimentos, criam características morfológicas ao longo das zonas costeiras, que podem ser modificadas em um amplo espectro de variabilidade espacial e temporal.

## Qual a importância do sedimento fino na região costeira?

O sedimento encontrado nas regiões costeiras e estuarinas podem ser classificados de acordo com o seu tamanho médio de grão ($D_{50}$). Metha (2014) propõe diferentes critérios para essa classificação, variando desde sedimentos grossos (incluindo areia, cascalho e seixo), a sedimentos finos (como argila e silte), podendo estes representar até 90% do total de carga sólida transportada em suspensão por rios para a região costeira. (Ward & Trimble, 1995).

Diante de um cenário de intensa mudança da região costeira global, entender o comportamento e a dinâmica do sedimento fino representa compreender o desenvolvimento da evolução costeira (Frenchetal, 2008). Sendo assim, mesmo com a grande quantidade de pesquisa relacionada ao assunto, a dinâmica de sedimento nas regiões costeiras ainda apresenta diversas questões que continuam sem respostas.

Visto que até 90% dos sedimentos de origem terrígena são eventualmente depositados nas margens oceânica (McCave, 2002), os estuários desempenham papel importante nos processos de distribuição do sedimento desde sua fonte terrígena até os sumidouros marinhos, sendo esse um dos processos mais importantes no qual moldam a morfologia do assoalho marinho. Sendo assim, o entendimento do comportamento dos sedimentos finos, quando em suspensão e quando depositados, é essencial para os estudos da dinâmica de sedimentos na região costeira (Milligan & Loring, 1997).

## Qual a importância das plumas estuarinas na dinâmica costeira?

As vazões continentais desempenham papel fundamental na distribuição do sedimento fino na região costeira, e tendem a serem menos densa e, portanto, mais leves do que a água da plataforma costeira, a contribuição dos estuários chega na região costeira através de feições conhecidas como plumas (salina ou sedimentar) (Garvine et. al., 2002; Marques et. al., 2010). As plumas normalmente se formam quando a água flutuante, auxiliada pelas correntes costeiras, se espalha para longe da boca do estuário, se desenvolvendo a jusante (Garvine et. al., 2002). Além disso, outra característica das plumas costeiras é a sua capacidade de transportar para a plataforma interna elevadas concentrações de sedimento em suspensão (Marques *et al.,* 2010), visto que, muitos estuários e rios tem aporte fluvial suficientemente grande para perpetuar uma pluma sedimentar por longas distâncias pela região costeira adjacente. Uma vez na costa, esta contribuição é capaz de influenciar a sedimentação da plataforma interna devido a sua interação com a dinâmica costeira (Mestres *et. al.* 2007). Nesse contexto, a estrutura dinâmica formada pelo processo de descarga de água de origem costeira, chamada pluma costeira, assume um papel de destaque em relação as trocas entre o continente e a plataforma continental (Wright, 1995), e no transporte e redistribuição de sedimentos. Isso torna os ecossistemas fluviais e estuarinos protagonistas devido à sua importância no enriquecimento das águas costeiras, e consequente aumento da produtividade (Geyer et al.,2004).

Diversos autores consideram as plumas como feições altamente complexas devido os inúmeros tipos de fontes fluviais, e a existência de diversos rios e estuários de variados tamanhos e localizações, espalhados em inúmeras plataformas continentais ao redor do planeta, sendo os responsáveis pela dinâmica costeira atual de maneira bastante específica (Marques et. al., 2010). Associado a isso, a dinâmica das plumas e o transporte de sedimento estão relacionados a diversos processos lineares e não-lineares, tais como o efeito da densidade em processos como erosão e deposição, mistura turbulenta, fricção, entre outros. Sendo assim, quanto maior a densidade da pluma costeira, maior a complexidade das interações da pluma com as águas da plataforma interna (Gelfenbaum e Stumpf, 1993), dando origem a significativos gradientes horizontais de densidade ao longo da profundidade e a frentes costeiras (Lentz, 1992). Logo, o papel das plumas costeiras na dinâmica sedimentar de regiões de plataforma interna é preponderante.

A densidade é uma propriedade tão importante no desenvolvimento das plumas, que Bates (1953) classificou as plumas de origem fluvial de acordo com o contraste da densidade com as águas oceânicas em três categorias: plumas hipopicnais, homopicnais e hiperpicnais. As plumas hipopicnais tem como característica uma flutuabilidade positiva causada pelo fato de a água fluvial ser menos densa que a água oceânica, causando assim um espalhamento horizontal da pluma. Nas plumas homopicnais não existe diferença entre as densidades, gerando massas de água altamente misturadas e com flutuabilidade nula. Já nas hiperpicnais, as águas de origem continentais são mais densas que as águas oceânicas, causando uma flutuabilidade negativa, o que gera um espalhamento horizontal junto as camadas de fundo.

Souza e Robinson (2004), afirmaram que a interação entre as correntes costeiras, o regime de vento, o efeito da maré, e as plumas de rios pode acarretar diversos efeitos sobre a dinâmica costeira. Visto que, as correntes costeiras ao mesmo tempo que podem atuar como uma barreira dinâmica a propagação de águas continental, inibindo a advecção de propriedades sobre a plataforma continental (Blanton, 1981), a presença de uma corrente costeira na mesma direção de propagação da pluma pode ajudar o transporte dessa pluma ao longo da plataforma continental (Soares et. al. 2007b), estando dependente apenas da direção de propagação da pluma (Pimenta et. al., 2002). De acordo com Wright e Nittrouer (1995) o destino dos sedimentos que chegam à zona costeira adjacente passa por pelo menos 5 estágios: suprimento através das plumas, deposição inicial, ressuspensão, transporte por processos marinhos, e por fim acumulação em larga escala de tempo.

Vários autores (Chao, 1988b, Kourafalou et. al. 1996a, Xia et. al., 2007, Marques et. al., 2009, por exemplo) analisaram o efeito do vento sobre plumas costeiras no mundo. Os autores afirmaram que as plumas são altamente sensíveis as perturbações causadas pela mudança na direção preferencial do vento (Kourafalou et. al. 1996b; Ghisolfi e Mckee, 2003; Soares et. al., 2007a; 2007b). Já as marés tem efeito modulador sobre as plumas costeiras, reduzindo o efeito de estratificação do vento, e aumentando o processo de mistura (Chao, 1990; Garvine, 1999; Pritchard, 2000; Guo & Valle- Levinson, 2007; Marques et. al., 2010b). Os processos de mistura ocorrem tanto durante enchente quanto durante a vazante, visto que, a pluma se forma durante a fase vazante, e durante a enchente a pluma se separa da costa em forma de pulsos de água doce (Hickey, 2000). As marés

ainda tem um papel importante no espalhamento da pluma em direção ao oceano (Chao, 1990).

## Avanços nos estudos das plumas estuarinas

A análise das plumas estuarinas vem sendo realizadas ao longo do tempo utilizando principalmente três principais metodologias: obtenção e análise de medidas diretas (dados *in situ*), rastreamento superficiais e subsuperficiais de imagens orbitais, e o aprimoramento de modelos numéricos e analíticos. Em virtude da evolução computacional nas ultimas décadas, da complexidade dos processos relacionados na análise das plumas estuarinas, além do alto custo na aquisição direta dos dados, a ferramenta da modelagem numérica se tornou, nos últimos anos, a forma mais produtiva para analisar tais processos e feições. A utilização de modelos numéricos não-lineares para o estudo da dinâmica costeira se tornou uma importante ferramenta para o estudo da formação, manutenção e desenvolvimento de plumas. Essa metodologia vem sendo bastante utilizada por diversos autores (Royer & Emery, 1985; Chao e Boicourt, 1986; Chao, 1988; Garvine, 1999; Xia *et al.*, 2007; Soares *et al.*, 2007; Marques *et al.*, 2009; 2010).

O pioneirismo no uso de modelos numéricos na análise de plumas estuarinas foi de Garvine e Monk (1974), ao observarem uma pluma de pequena escala na década de 70. Esse trabalho revolucionou os modelos numéricos, e incentivou o desenvolvimento de modelos que representassem de forma satisfatória os processos físicos que regem a formação e desenvolvimento das plumas costeiras. Com o avanço da utilização da modelagem numérica, modelos 3D foram desenvolvidos com o intuito de analisar como as plumas afetam os processos físicos e as características da coluna d'agua. Dentre os autores que fizeram uso dessa ferramenta, Chao (1988a), Kourafalou et. al. (1996a) e Garvine (1999) verificaram com o uso de modelos tridimensionais a interferência a declividade do fundo no desenvolvimento, manutenção e dissipação das plumas. Os resultados desses trabalhos mostram que a inclinação do assoalho estuarino amplifica a circulação vertical, intensificando a mistura no estuário.

O sensoriamento remoto foi introduzido nos estudos das plumas costeiras e nos processos de transporte de sedimento pelo final da década de 70. Para verificar a o comportamento de frentes estuarinas formadas pela inserção de plumas na costa inglesa,

Simpson e Bowers (1979), fizeram uso imagens orbitais. Com essa metodologia foi possível verificar que o processo de mistura tem uma escala temporal semanal devido a atuação das marés da região. Atualmente, técnicas de sensoriamento remoto são amplamente utilizadas para o estudo das plumas costeiras (Munday e Fedosh, 1981; Dinnel *et al.* 1990; Stumpf, 1991), possibilitando a estimativa da morfologia das plumas e da concentração de material em suspensão que é transportado para o ambiente costeiro (Piola e Romero, 2004), assim como a validação de modelos numéricos que calculam o transporte do sedimento em suspensão (Marques et al., 2010).

Com o desenvolvimento de diversas metodologias no estudo dos processos oceanográficos que controlam a formação e desenvolvimentos das plumas costeiras, vários autores estudaram o processo de interação entre plumas e suas plataformas continentais adjacentes por todo o mundo. Para a região da Ásia, Milliman et. al. (1984) estudaram contribuição de material em suspensão do estuário de Changjiang para a Plataforma Continental Chinesa e a interação desse sedimento com a Corrente de Taiwan e a Corrente Costeira de Jiangsu. O resultado do trabalho mostra uma grande relação entre o transporte de sedimento e o regime de maré local, sendo responsável por levar 60% do sedimento para a região costeira adjacente, enquanto o restante se deposita no interior do estuário. Ainda na Ásia, na região do Ganges-Brahmaputra, Haque et. al. (2016) verificaram o comportamento do sedimento em relação ao fluxo volumétrico estuarino. A análise dos autores mostrou que o fluxo de vazante na região é muito maior que o fluxo de enchente, resultando num padrão de circulação estuarina no sentido horário, causando o retorno do sedimento do mar para o estuário, levando assim a uma sedimentação local.

Na Europa, a modelagem numérica foi utilizada por Diaz et. al. (2020) no Golfo Biscaia. Os autores avaliaram a influência da parametrização empírica do modelo MARS3D nos fluxos residuais de sedimentos, além de estimar as incertezas no processo de transferência de lama e areia na foz do estuário de Gironde através de uma análise sensitiva do modelo. Os resultados mostraram que o transporte de sedimento na região é altamente sensitivo à parametrização do modelo, principalmente aos parâmetros de sedimentação e erosão, ao período de spin-up do modelo e ao processo de deslizamento do sedimento. O modelo tridimensional ainda mostrou que tanto a circulação estuarina quanto a oscilação da maré induzem a exportação do sedimento durante a maré alta. O sedimento fino é exportando por uma pluma costeira no período de alta vazão, mesmo

com o transporte líquido de lama tendendo a crescer nas regiões interiores do estuário, devido o aumento da circulação baroclínica em regimes de baixa vazão.

Na costa brasileira, Kineke e Sternberg (1995) usaram dados coletados em campo para estudarem os sedimentos em suspensão do Rio Amazonas, e sua colaboração para a Plataforma Amazônica para entender a ligação entre os parâmetros físicos e a contribuição continental em diferentes escalas de tempo. Os autores mostraram que a estrutura vertical da lama na região tem um comportamento espaço-temporal variável, com variabilidade quinzenal na região próxima da foz do rio. Os autores ainda constataram que o volume do estoque total do sedimento em suspensão na plataforma continental nos períodos de alta vazão é próximo ao valor da descarga anual de sedimento em suspensão no rio ($1{,}2x10^9$ ton/ano), sendo mais de 90% desse estoque composto por lama fluida. Gabiox et. al. (2005), utilizando um modelo 2D, estudaram o efeito do sedimento em suspensão na Plataforma Amazônica. Os autores constataram que o sedimento em suspensão presente próximo ao fundo representa um importante elemento na dinâmica da Plataforma Amazônica, visto que esse sedimento reduz a tensão de cisalhamento do fundo ao ponto de dissipar a energia, afetando assim a amplitude da maré na região.

## O que sabemos sobre a pluma estuarina na Plataforma Interna de Atlântico Sudoeste?

No caso da Plataforma Interna de Atlântico Sudoeste (PIAS), que é a região de interesse desse estudo, trabalhos vêm sendo desenvolvidos por diversos autores (Soares e Möller, 2001; Costa e Möller, 2011), por esta ser uma região estratégica devido à sua relevância econômica e multidisciplinar. A contribuição continental para a Plataforma Interna do Atlântico Sudoeste é exercida principalmente pelo Rio da Prata e pela Lagoa dos Patos (Soares et al. 2007). À esta contribuição continental se somam os efeitos das correntes, o efeito da maré, e o efeito dos ventos (Souza e Robinson, 2004). A combinação destes fatores gera um complexo cenário (Palma et al, 2008).

A influência das águas das águas do Rio da Prata é reconhecida desde os primeiros estudos oceanográficos na região (Emilson, 1961; Guerreiro et. al., 1997; Depetris e Pasquini, 2007b). Möller et. al. (2008) demostraram que a intrusão das águas do Rio da

Prata na plataforma continental resulta na formação de uma pluma salina que se expande por 1300 km da faixa costeira (Piola et. al., 2005). Uma vez na região costeira, essa pluma interfere na circulação, na estratificação e na distribuição dos nutrientes e espécies biológicas. Ao avançar na zona costeira, a água de doce de origem continental forma um grande gradiente salino na plataforma, gradiente este, modulado pela ação sinótica do vento local (Pereira, 1989; Zavialov et. al., 1998; Pimenta et. al., 2005).

Quanto ao efeito do vento, Piola et.al. (2005) fizeram o uso da modelagem numérica ao parametrizarem o modelo com dados hidrográficos e series históricas de vento da PIAS para determinar a variabilidade sazonal da dinâmica do Rio da Prata, sua relação com a magnitude da vazão do rio e a intensidade do vento. Os resultados mostraram que o regime vento ao longo da costa foi o responsável pela variabilidade sazonal da dinâmica do Rio da Prata. A modelagem numérica também foi utilizada por Soares et. al. (2007b) para analisar a importância da mistura turbulenta no desenvolvimento da pluma do Rio da Prata e o comportamento da Pluma ao se espalhar na plataforma adjacente. Os resultados do modelo 3D mostraram que durante o outono a pluma do Rio da Prata se espalha preferencialmente pela margem norte da plataforma interna, devido a ação do vento local. Já durante a primavera, a pluma tende a ficar aprisionada na foz do rio pela atuação da maré, visto que o vento nesse período perde intensidade na região. Pimenta et. at. (2001) utilizando o modelo POM mostraram que o desenvolvimento da pluma do Rio da Prata sobre a plataforma depende principalmente do alto volume da descarga fluvial, associado a ação contínua do vento de Sudeste. Atualmente Santoro et. al., 2017 implementou o modelo TELEMAC e o capacitou para simular a dinâmica de sedimentos do Rio da Prata, em especial a região da Baía de Montevideo. Como resultados dos testes de sensibilidade dos parâmetros do modelo, os autores afirmaram que o TELEMAC representou se forma satisfatória a dinâmica dos sedimentos da região de estudo.

Outro importante corpo d'água que tem papel preponderante na região de interesse é a Lagoa dos Patos. A influência da Lagoa dos Patos vem sendo amplamente abordada por diversos autores com o passar dos anos (Marques et al.,2009; Monteiro et. al. 2011). As forças físicas que controlam a dinâmica da pluma da Lagoa dos Patos foram estudadas por Marques et. al. (2009). Nesse trabalho os autores concluíram que a pluma costeira tem um comportamento característico de uma pluma de pequena escala, como modo de variabilidade relacionado ao transporte de sul, sendo controlado pela convergência da

variabilidade sazonal e do regime de vento nordeste da região. Monteiro et. al. (2011) analisou o quanto a rotação da Terra, a vazão do rio, a maré e o regime de ventos podem influenciar na dinâmica da pluma. Os autores afirmaram em seu trabalho que a rotação do planeta é responsável pela assimetria do fluxo da pluma, já as marés controlam o processo de mistura, enfraquecendo a penetração da pluma na plataforma interna adjacente. Além disso os autores concluíram que existe um equilíbrio entre a descarga fluvial e o vento, tornando-os responsáveis pela mobilidade interna e externa da pluma.

## Efeito ENSO sobre a dinâmica das plumas estuarinas no sul do Brasil

A região sul do Brasil é reconhecida em diversos trabalhos por ser altamente influenciada pelo efeito ENSO, sendo com uma maior magnitude na região norte da plataforma (litoral brasileiro) se comparado a região sul (litoral uruguaio e argentino). Segundo Grimm et. al. (1998), na América do Sul, os ciclos ENSO são um padrão climático periódico caracterizado por dois modos: a fase quente, conhecida como El Niño e a fase fria, conhecida como La Niña, com ciclos recorrentes a cada dois a sete anos. Em especial na região sul do Brasil, anomalias fortes e consistentes na precipitação podem estar relacionadas com esses eventos (Grimm et. al., 1998; Grimm et. al., 2000). Porém, ainda são escassos os estudos relacionados ao impacto dos ciclos do ENSO na Plataforma Interna do Atlântico Sudoeste. Ciotti et. al. (1995) ao analisarem as atividades biológicas na região, afirmaram que a quantidade de clorofila na região costeira está vinculada aos nutrientes oriundos da descarga fluvial dos principais efluentes da região. Sendo assim, os autores sugerem que as anômalias pluviométricas promovidas pelo efeito ENSO, tem forte impacto na variabilidade da produção de fitoplâncton, que por sua vez, interfere diretamente nos ciclos biogeoquímicos da Plataforma Interna do Atlântico Sudoeste. Enquanto isso, Berbery e Barros (2002) ao estudarem a ciclo hidrográfico do Rio da Prata, descobriram que os máximos históricos da vazão do rio acontecem em anos de El Niño, podendo alcançar o triplo da média típica local. No entanto, Piola et. al. (2005) afirmaram que os efeitos de anomalias de vento e precipitação tendem a compensar o aumento do fluxo, evitando extensões anômalas de plumas de nordeste associadas a grandes eventos de fluxo. Sendo assim, a descarga do Rio da Prata se espalha para o mar.

Mais recentemente, García-Rodríguez et. al. (2014) investigaram variações geoquímicas na seção intermediária do estuário do Rio da Prata durante o evento ENSO

2009-2010. Os autores perceberam que durante a fase quente do ENSO, a vazão do rio chegou a valores 5 vezes maiores do que os níveis históricos médios. Ainda sobre o efeito do ENSO na vazão do Rio da Prata, Dogliotti et. al. (2016) analisaram a variabilidade espaço-temporal da turbidez na região baseados em uma série temporal 15 anos de dados orbitais MODIS. Os autores encontraram uma forte variabilidade sazonal nos estuários superior e médio, com alto fluxo ocorrendo de março a maio, e baixa turbidez de junho a janeiro. A influência do ENSO ocorre em escalas de tempo interanuais, mostrando um aumento da turbidez quando ocorrem anomalias de descarga fluvial negativa, mas isso nem sempre está relacionado a eventos de La Niña, uma vez que esses eventos não são os únicos responsáveis pelo período de seca na região.

Távora et. al. (2020) utilizaram uma avaliação de 17 anos de dados orbitais de sedimentos em suspensão do sensor MODIS-Áqua na Lagoa dos Patos, e observaram forte variabilidade interanual de material particulado em suspensão (SPM) correlacionada com eventos ENSO. E por fim, a partir de simulações de modelos TELEMAC-3D ao longo de cinco anos, Bitencourt et. al. (2020) também observaram a influência do ENSO em valores de alta concentração de sedimentos em suspensão (SSC) ao longo da Lagoa dos Patos em uma escala de variabilidade interanual.

Apesar do grande número de estudos sobre a dinâmica costeira na Plataforma Interna do Atlântico Sudoeste, focando principalmente nos processos relacionados ao transporte de sedimento, em destaque as plumas costeiras, pouco se sabe sobre o comportamento da concentração de sedimento, seja em suspensão ou de fundo nesta região. Isto é, as consequências que o sedimento em suspensão e o sedimento de fundo causam na dinâmica e na morfologia da plataforma interna. Assim, este trabalho visa preencher essa lacuna, respondendo as seguintes questões cientificas: Qual o tamanho da contribuição dos efluentes no processo de sedimentação da plataforma continental? Como se comporta espacialmente e temporalmente esse sedimento ao atingir a plataforma interna? Como os processos de erosão e deposição contribuem para a morfologia da região? E como o efeito ENSO afeta nos processos relacionados ao transporte de sedimento para a plataforma?

# **Capítulo II:** Hipótese

## 2. Hipótese

A descarga fluvial do Rio da Prata e da Lagoa dos Patos apresentam uma significativa variabilidade interanual, o que é determinante para os padrões de transporte de sedimento em suspensão e de fundo na Plataforma Interna Atlântico Sudoeste.

# **Capítulo III:** Objetivos

# 3. Objetivos

## 3.1. Geral

Avaliar as contribuições continentais do Rio da Prata e da Lagoa dos Patos para a dinâmica do sedimento em suspensão e de fundo da Plataforma Interna do Atlântico Sudoeste (PIAS).

## 3.2. Específico

- Caracterizar o comportamento médio e sazonal da concentração do sedimento em suspensão e de fundo;
- Avaliar o processo de exportação de sedimento em suspensão para a plataforma interna através das plumas costeiras da Lagoa dos Patos e do Rio da Prata;
- Analisar a variabilidade temporal e espacial da distribuição do sedimento superficial e de fundo na região de estudo;
- Avaliar como os ciclos interanuais afetam os aportes de sedimento do Rio da Prata e da Lagoa dos Patos.

# **Capítulo IV:** Área de Estudo

# 4. Área de Estudo

A região de estudo está limitada entre a latitude 28°S (Cabo de Santa Marta) e 38°S (Mar Del Plata), correspondendo à região central da Plataforma Continental do Atlântico Sudoeste (Figura 1), que se estende desde a Terra do Fogo ( 55 ° S), para Cabo Frio (22 ° S) (Palma et. Al., 2008). É uma plataforma continental de contorno oeste no Oceano Atlântico Sul, formada por uma suave linha de costa, com longas praias arenosas e lagoas costeiras (Figueredo, 1980).

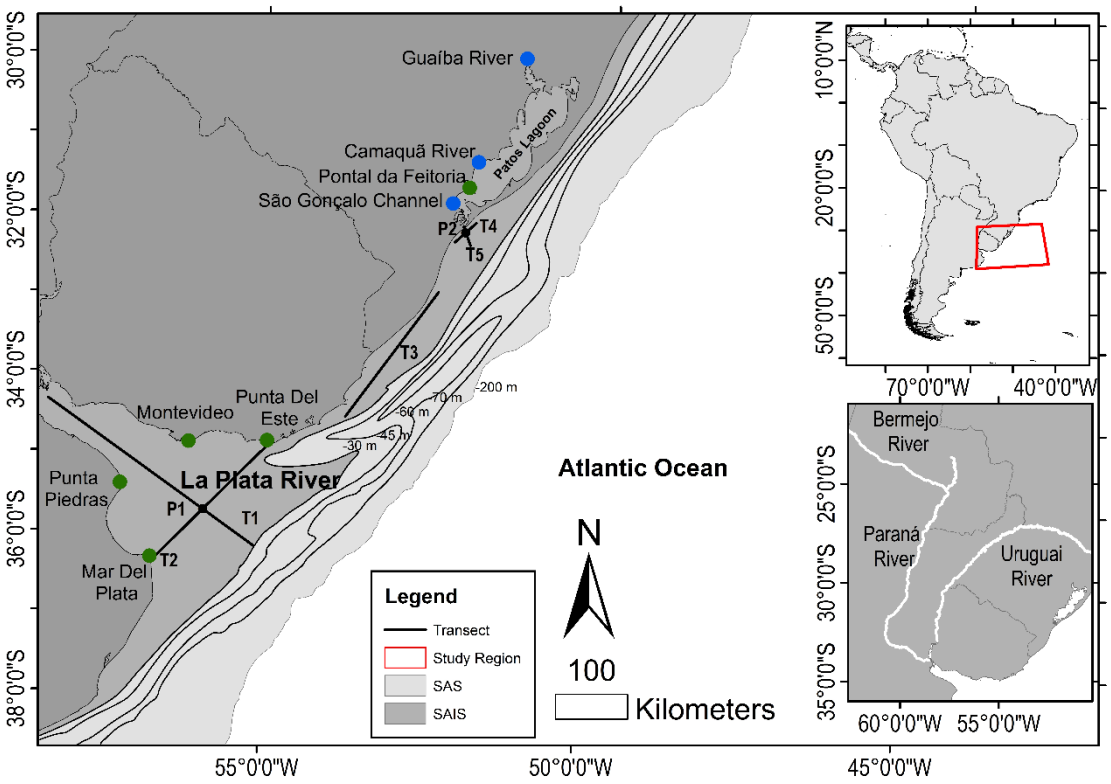


Figura 1 - Região de estudo definida entre as latitudes 28 ° S (Cabo Santa Marta) e 38 ° S (Mar Del Plata). Os pontos azuis representam os principais efluentes da Lagoa dos Patos (Rio Guaíba, Rio Camaquã e Canal de São Gonçalo), os pontos verdes mostram regiões importantes na área de estudo e os pontos pretos representam os pontos de onde os resultados do modelo foram extraídos para a análise das ondaletas, do fluxo de deposição e da evolução do fundo (P1 e P2). T mostra os transectos de onde os resultados do modelo foram extraídos (T1, T2, T3, T4 e T5) para análises de função ortogonal empírica (EOF). As linhas brancas representam os principais efluentes do rio La Plata (rio Bermejo, rio Paraná e rio Uruguai)

## Plataforma Continental do Atlântico Sudoeste

Sobre a Plataforma Continental do Atlântico Sudoeste, é possível observar duas principais feições hidrodinâmicas principais, a Corrente do Brasil e a Corrente das Malvinas, como Correntes de Contorno Oeste (Figura 2) (Matano et al., 2010). A Corrente do Brasil é definida por muitos autores como sendo um fluxo associado ao movimento da Água Tropical, da Água Subtropical e da Água Central do Atlântico Sul (Cirano et al., 200). É uma corrente baroclínica e tem origem vinculada a 10°S, transportando águas quentes da região tropical para a região subtropical até alcançar a região da Confluência Brasil-Malvinas (38°S – 42°S), onde suas águas quentes interagem com as águas frias da Corrente das Malvinas (Olson et al., 1988; Gordon, 1989; Legeckis & Gordon, 1982). Já a Corrente das Malvinas é um ramo estreito da Corrente Circumpolar Antártica, que flui rapidamente e de forma barotrópica para o norte, ao longo do talude continental, até alcançar a Confluência Brasil-Malvinas próximo a desembocadura do Rio da Prata, gerando uma região com alta variabilidade em mesoescala (Matano et al., 2010).

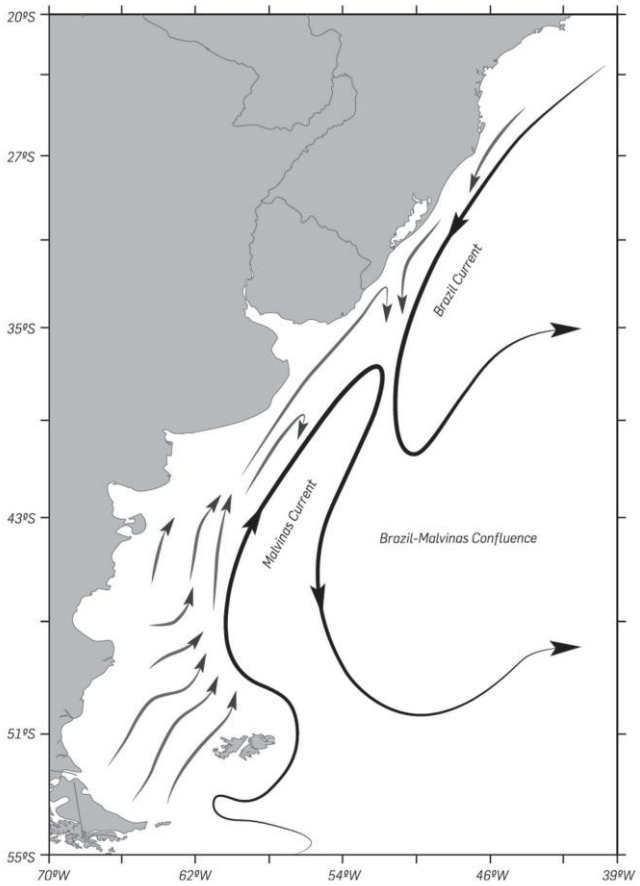


Figura 2 - Representação esquemática das correntes de superfície na região da Corrente das Malvinas e da Corrente do Brasil (Morel et al., 2014)

Sobre as feições sedimentares, em conformidade com os estudos realizados por Martins et al. (2003), o piso sedimentar da Plataforma Continental do Atlântico Sul é caracterizado pela presença dominante de sedimento arenoso. Uma grande concentração de areia pode ser encontrada numa faixa mais litorânea no trecho entre o Rio Grande e Chuí, e outra, mais extensa, numa região externa, entre Punta Del Este e Mar Del Plata (Figura 1 e 3). Em contra partida, nas regiões como a desembocadura da Lagoa do Patos, e na altura de região de Maldonado, justificada pela alta taxa de deposição de lama ocasionada pelas vazões lagunares, são áreas de baixa concentração de areia.

Quanto a concentração de lama, Martins et al. (2003) indicaram a presença de três grandes corpos com uma maior concentração de lama, distribuídos pela região (Figura 3). Na área do Cone de Rio Grande existe um aumento gradativo da percentagem de lama, culminando com uma concentração 100% da mesma. Um outro corpo lamoso está localizado na desembocadura da Lagoa dos Patos. Já o terceiro corpo com uma alta concentração de lama encontra-se na desembocadura do Rio da Prata.

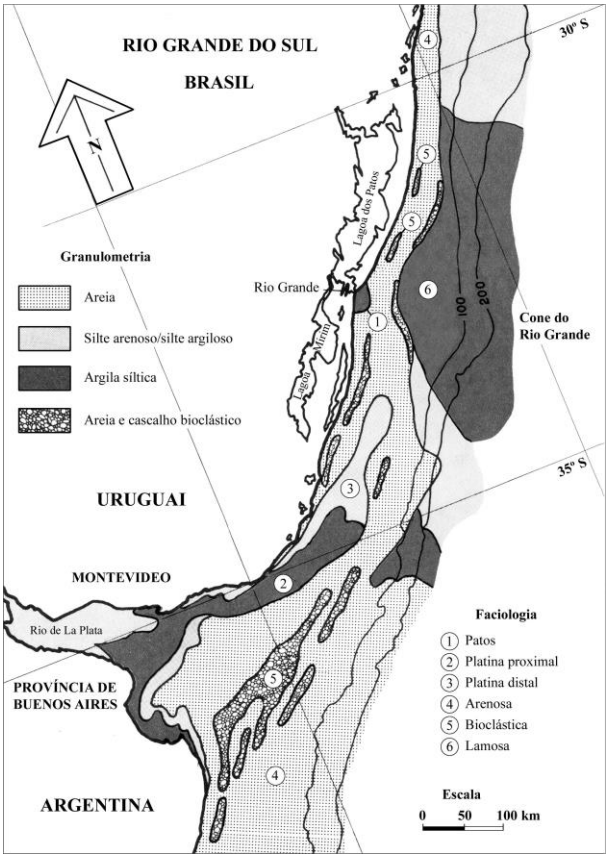


Figura 3 - Morfologia e Sedimentos da Plataforma continental do Rio Grande – Argentina (Martins et al., 2003)

## Plataforma Interna do Atlântico Sudoeste

Já a Plataforma Interna do Atlântico Sudoeste está localizada dentro da Plataforma Continental do Atlântico Sudoeste. Tem seu limite meridional, das plataformas interna e média, relacionado a presença do Canal do Albardão (ou "poço de lama") (Capítoli & Bemvenuti, 2006; Attisano, 2007), e é reconhecida como a área de pesca mais importante da costa brasileira (Haimovici et. al., 1989; Castello et. al., 1990). A região recebe mais de 95% de sua descarga dos Rios Paraná e Uruguai através do Rio da Prata (Depetris e Paolini, 1991), e outros afluentes que atingem o litoral sul do Brasil, como o Sistema Patos-Mirim, o complexo estuarino de Laguna, além do Rio Itajaí-Açu.

Soares e Möller (2001) demonstraram que as águas de baixa salinidade originárias das vazões do Rio da Prata e da Lagoa dos Patos são de suma importância na plataforma interna, participando na distribuição e na formação de massas de água, enquanto que as aguas transportadas pela Corrente do Brasil e pela Correntes das Malvinas são as principais águas na plataforma externa e talude.

O Rio da Prata é a segunda maior bacia hidrográfica da América do Sul (3,170,000 $km^2$) A descarga fluvial do Rio da Prata tem uma média anual de 22.000 $m^3/s$, com picos de descarga podendo variar de 90.000 $m^3/s$ a 8.000 $m^3/s$ durante condições extremas relacionadas aos ciclos ENSO (Berbery e Barros, 2002) . Tem um formato afunilado de aproximadamente 300 km de extensão no sentido de noroeste para sudeste, que se estreita de 220 km em sua foz para 40 km na extremidade superior (Moreira et al., 2016), resultando em uma área estuarina de 35.000 $km^2$.

## Rio da Prata

A região estuarina do Rio da Prata apresenta uma geometria e batimetria altamente varável, configurando uma dinâmica rio-estuário-oceano de alta complexidade. Sendo assim, alguns autores preferem dividir a região estuarina em duas partes, seguindo suas características geomorfológicas: região interna-intermediária e região externa (Framiñan et. al., 1996). Essas partes são separadas por uma feição topográfica conhecida como Barra del Indio (Fossati et. al., 2014), sendo esta, uma área rasa que cruza o estuário entre Punta Piedras e a região de Montevidéu, sendo responsável por marcar o limite marítimo onde a frente de salinidade está localizada (Sepúlveda et. al., 2004). Esta região é

caracterizada por um regime fluvial com influência das marés e sem estratificação. Já a região externa é formada por águas salobras de salinidade variável, influenciadas pelas marés, ventos e a contribuição da água doce da bacia hidrográfica (Santoro et. al., 2016). A densidade no estuário externo é controlada pela salinidade, visto que, a temperatura exibe um pequeno gradiente horizontal, mesmo que a variabilidade interanual possa ser alta na região (Guerrero et. al., 1997; Simionato et. al., 2010). Em contrapartida, a estratificação da água é controlada pela confluência das descargas continentais com alta flutuabilidade, que avançam para o mar, se colocando acima da água mais densa da plataforma que penetra no estuário como uma cunha salina controlada pela topografia. Esta cunha de sal tem normalmente entre 100 e 250 km de comprimento e define uma frente de salinidade de fundo sobre o baixio da Barra del Indio acompanhando aproximadamente a isóbata de 10 m (Guerreiro et. al., 1997). Devido a ação do regime de vento predominante (Simionato et. al., 2001), tanto a frente salina superficial quanto a de fundo apresentam um ciclo sazonal que altera amplamente a cunha salina desde a primavera-verão até o outono-inverno (Guerreiro et. al., 1997). O vento da região é caracterizado pela alta variabilidade (Simionato et. al., 2005), que por sua vez, implica uma variabilidade significativa em escalas de tempo sinópticas para as outras variáveis estuarinas (Meccia et. al., 2009).

Sobre a maré, podemos afirmar que se trata de uma região sobre influência do regime de micromaré, com a componente principal da maré astronômica sendo a M2. Contudo, a componente O1, assim como as componentes semidiurnas S2 e N2 também são relevantes na região (Fossati et. al., 2014; Santoro et. al., 2016). A amplitude de maré é maior na costa argentina, (na ordem de 1 metro), se comparado à costa uruguaia (cerce de 0.4 metros). As marés meteorológicas são geradas principalmente na plataforma argentina e se propagam para o norte como ondas costeiras até atingir o estuário (Santoro et. al., 2013). As marés ainda são responsáveis pela presença de correntes dentro do estuário, que podem atingir valores maiores que 0.3 m/s no fundo e maiores que 0.5m/s na superfície (Fossati e Piedra-Cueva, 2013).

O Rio da Prata chega a despejar no Oceano Atlântico Sul 160 milhões de toneladas de sedimento em suspensão por ano (Menéndez e Sarubbi, 2007). O alto estuário e a plataforma continental adjacente são cobertos principalmente por areia, enquanto que no baixo e médio estuário ocorre uma predominância de sedimento fino (Moreira et. al., 2016). A pluma do Rio da Prata pode alcançar longas distâncias a norte pela plataforma

interna, afetando as regiões costeiras uruguaia e brasileira (Piola et. al., 2000; Piola et. al., 2005).

## Lagoa dos Patos

Outro grande importante afluente presente na região de interesse, é a Lagoa dos Patos. A Lagoa dos Patos está localizada no extremo sul do Brasil (entre 30°S e 32°S), sendo considerada a maior lagoa costeira do tipo estrangulado do mundo (Kjerfve, 1986), com 250 km de comprimento e 40 km de largura, totalizando uma área de aproximadamente 10.360 $km^2$ (Delaney, 1965). A região lagunar é considerada um corpo d'água raso, com profundidade média de 5 m, com as maiores profundidades atingindo 16 m na região do canal navegação, sendo esse canal localizado na foz do estuário o responsável pela conexão da lagoa com o Oceano Atlântico Sul.

A Lagoa dos Patos possui uma extensa bacia de drenagem com aproximadamente 201.626 $Km^2$, composta pelos rios Guaíba, Camaquã e Canal São Gonçalo como os principais afluentes da parte norte, central e sul da lagoa, respectivamente. Os rios apresentam um comportamento característico de zonas subtropicais, isto é, com alta vazão no final do inverno e início da primavera, seguida de uma vazão baixa a moderada no verão e no outono (Möller et. al., 2001). A média anual de descarga do rio Guaíba é de aproximadamente 2.000$m^3$/s, porém variações relacionadas com a sazonalidade foram observadas no local, podendo ocorrer vazões de 700 $m^3$/s durante o verão austral (fim de dezembro até março) e de 3000$m^3$/s durante a primavera austral (setembro até fim de dezembro) (Marques e Möller, 2009). Os maiores picos de vazão na região foram relatados por Möller et. al. (1996), alcançando valores próximos a 25.000 $m^3$/s sob efeito do ENSO. Já a vazão do Canal São Gonçalo tem a presença de uma eclusa para controlar o nível do canal, que por sua vez é fechada quando o nível do canal alcança valores superiores a 1 metro. Com isso, a descarga fluvial na porção inferior da lagoa varia entre 700 e 3000 $m^3$/s, sendo mais intensa no período de inverno/primavera (Hartmann et. al., 1990).

A circulação na Lagoa dos Patos é controlada por diversos mecanismos, dependendo da área considerada: a ação do vento sobre a porção lagunar (vento local), a ação do vento sobre a porção estuarina e costeira (vento remoto), e a descarga fluvial da porção lagunar. (Fernandes et. al., 2002; 2005; Moller et. al., 1996). Em cenários de vazão

baixa ou moderada do rio, o vento se torna o principal mecanismo que rege a circulação na Lagoa dos Patos (Möller e Castaing, 1999). Segundo Möller et. al. (2001), o vento nordeste gera um gradiente de pressão barotrópica em direção ao oceano devido a atuação do transporte de Ekman, que age a 90º na direção do vento, resultando num cenário de vazante para o estuário. Em contra partida, quando se trata do vento sudoeste, o resultado é um aumento do nível das águas na região costeira, promovendo um gradiente de pressão barotrópica em direção ao continente e inibindo a descarga fluvial, gerando um cenário de enchente para a Lagoa dos Patos. Esse padrão não ocorre durante períodos de alta vazão (>2.000 m3/s), visto que o efeito do vento sudoeste é superado pela vazão do rio (Möller e Castaing, 1999; Castelão e Möller, 2003).

Sobre a maré local, a região é caracterizada por ser mista com predominância diurna, tendo amplitude média de 0,23 m (Möller et. al., 2001) e caracterizando um sistema de micromaré. O efeito das marés é de importância secundária para a dinâmica do sistema, ficando restrito à região costeira e à porção estuarina da Lagoa dos Patos. Fernandes et. al. (2004) demonstraram que o canal de acesso atual como um filtro amortecedor do efeito da maré conforme ela entra no estuário.

Sobre as características morfológicas da Lagoa dos Patos, existe uma predominância de sedimentos grosseiros nas áreas rasas e de sedimentos finos nas regiões mais profundas, especialmente na zona estuarina. O contorno oeste da lagoa é coberto predominantemente por areia média e grossa (Martins et. al.,1987; Toldo et. al., 1991), trazida principalmente pelo rio Camaquã. Já nas margens leste e norte, o sedimento é composto por areia fina do sistema litoral-marinho (Toldo et. al., 1991). Sobre a concentração do sedimento em suspensão (SSC), Hartmann et. al. (1986) indicaram que a concentração média variava em torno de 43 a 196 mg/L baseado em três anos de amostragem ao longo do eixo principal da lagoa e na foz dos principais afluentes. Os mesmos autores numa análise qualitativa do sedimento em suspensão, relataram que a região tem grande predominância de silte (>80%), seguido de argila e areia fina, evidenciando que a lagoa é uma fonte de silte e argila para a região litorânea.

# **Capítulo V**: Material e Métodos

# 5. Material e Métodos

Para realizar a análise e investigação do comportamento e a variabilidade do sedimento em suspensão e de fundo na Plataforma Interna do Atlântico Sudoeste foi utilizada a modelagem numérica, onde foram realizadas três simulações hidro e morfodinâmicas (Tabela 1). Para os estudos do sedimento em suspensão, foram realizadas duas simulações com duração de 730 dias, sendo uma delas realizada para os anos de 2005-2006 enquanto a outra foi para os anos de 2008-2009. A escolha dos períodos analisados está relacionada com a ação do efeito ENSO na região, onde 2005-2006 é considerado um período neutro (sem efeito significativo do ENSO) e 2008-2009 é um período afetado tanto pela La Niña (início de 2008) quanto pelo El Niño (final de 2009). Já para os estudos do sedimento de fundo, foi realizada uma simulação com duração de 2920 dias entre os anos de 2005 e 2012. A escolha desse período, assim como nos anteriores, tem relação direta com a ação do efeito ENSO na região. A diferença fica na duração da simulação, isso é justificável pelo fato de os processos relacionados aos sedimentos de fundo demandarem uma escala de tempo maior para se tornar perceptível a alteração do fundo devido os processos de erosão e deposição.

**Tabela 1 - Parametrização das simulações**

| Simulação | Descrição | Descarga do La Plata | Descarga da Lagoa dos Patos | 2005-2006 | 2008-2009 | 2005-2012 |
|---|---|---|---|---|---|---|
| **SUP 1** | **Modelo com todas as forçantes físicas para o período de 2005 a 2006;** | **X** | **X** | **X** | | |
| **SUP 2** | **Modelo com todas as forçantes físicas para o período de 2008 a 2009;** | **X** | **X** | | **X** | |
| **FUN** | **Modelo com todas as forçantes físicas para o período de 2005 a 2012;** | **X** | **X** | | | **X** |

## 5.1. Modelo Hidrodinâmico

As simulações hidrodinâmicas foram realizadas utilizando o modelo TELEMAC-3D (www.opentelemac.org). O sistema TELEMAC possui módulos para o estudo de aspectos relacionados à hidrodinâmica, transporte de sedimento, ondas, qualidade de água de regiões costeiras e oceânica, entre outros. O modelo resolve as equações de Navier-Stokes considerando as variações locais na superfície livre do fluido, desconsiderando as variações de densidade na equação de conservação de massa, e considerando as aproximações de Boussinesq e hidrostática para resolver as equações de momentum (Hervouet, 2007). Santoro et. al., (2017) e Orseau et. al. (2019) utilizaram o modelo TELEMAC para analisar a dinâmica de sedimentos do Rio da Prata e do Estuário de Gironde, descrevendo com bastante detalhes todo o equacionamento do modelo.

## 5.2. Modelo de Transporte de Sedimento em Suspensão

O transporte de sedimentos em suspensão do sistema TELEMAC 3D, é simulado utilizando o módulo SED-3D (V7P0), onde as equações são resolvidas aplicando a técnica dos elementos finitos, sendo a decomposição fracionária realizada em etapas (Janin e Marcos, 1997). O sedimento em suspensão é considerado pelo modelo como um traçador livre e ativo, que junto com a salinidade e a temperatura, formam os traçadores do modelo que podem promover flutuações no campo da densidade. A fim de representar os efeitos coesivos no transporte de sedimentos em suspensão, a influência do processo de floculação na velocidade de sedimentação é calculada pelo modelo em função da concentração do sedimento, da temperatura, da salinidade e do gradiente de velocidade de sedimentação (constante) de acordo com a parametrização da fórmula de Van Leussen (Van Leussen, 1994), que foi aplicado a esta região por Marques et. al. (2010a, 2010b) e Bitencourt et. al. (2020).

O transporte do sedimento coesivo em suspensão ocorre através da combinação dos processos de difusão e advecção. No modelo SED-3D, a equação 3D da difusão e da advecção é resolvida levando em consideração que as partículas de sedimento coesivo se movimentam na mesma velocidade do fluxo:

$$\frac{\partial C}{\partial t} + U_j \frac{\partial C}{\partial x_j} = \frac{\partial}{\partial x_j}\left(\frac{v_t}{\sigma_t}\frac{\partial C}{\partial x_j} + w_s C \delta_{ij}\right) \qquad (1)$$

Na equação 1, $U$ é a velocidade média do fluxo (m/s), $t$ é o tempo (s), $x_j$ representa os componentes do vetor coordenado (m), $\upsilon_t$ é a viscosidade turbulenta ($m^2/s$), $\sigma_t$ é o Número de Prandtl-Schmidt turbulento (ou seja, a razão de $\upsilon_t$ para a difusividade turbulenta das partículas de sedimento), $C$ é a concentração de sedimento ($g.l^{-1}$) ou ($kg.m^{-3}$), $w_s$ é a velocidade de sedimentação média (m / s ) e $\delta_{ij}$ é o delta de Kronecker.

Na interface entre a coluna de água e a camada de fundo, ocorrem processos de erosão devido à tensão de cisalhamento do fundo induzida pelo fluxo. O fluxo de erosão é calculado pela fórmula de Partheniades (Partheniades, 1965), Equação 2. O fluxo de erosão, assim como a tensão de cisalhamento, depende da composição do material do fundo, bem como do estado de consolidação do material. Como este último processo não é considerado, ambos os parâmetros tem que ser definidos pelo usuário em cada classe de grão (considerada silte fino no presente trabalho).

$$E = \begin{cases} M\left(\frac{\tau_b}{\tau_{ce}} - 1\right) & if\ \tau_b > \tau_{ce} \\ 0 & otherwise \end{cases} \qquad (2)$$

Na equação 2, $M$ é a constante de erosão de Krone-Partheniades ($kg.m^{-2}.s^{-1}$), $\tau_b$ é a tensão de cisalhamento do fundo e $\tau_{ce}$ a tensão de cisalhamento crítica do fundo para a erosão. Portanto, a erosão só ocorre quando a tensão de cisalhamento do leito é maior do que a tensão de cisalhamento crítica para a erosão definida pelo usuário. A constante de erosão $M$ determina a intensidade do fluxo de erosão. Um valor maior significará mais erosão, se ocorrer erosão.

A tensão de cisalhamento do fundo é dada por:

$$\tau_b = \rho_w u_* |u_*| \qquad (3)$$

Onde $\rho_w$ é a densidade da água e $u_*$ é a velocidade de atrito. No SEDI-3D, a lei quadrática do atrito é usada com um coeficiente de arrasto $C_D$ para calcular $\tau_b$ em um

regime rugoso. Quando a fórmula de Nikuradse é usada, a equação assume a seguinte forma:

$$\tau_b = \frac{1}{2}\rho_w C_D \overline{U}|\overline{U}| \quad (4)$$

onde:

$$C_D = 7.831 ln\left(12\frac{h}{k_s}\right) \quad (5)$$

$\overline{U}$ é a velocidade média de fundo (que também é calculada pelo SEDI-3D), $k_s$ é o grau de rugosidade e $h$ é a profundidade da coluna d'água. Depois de determinar a tensão de cisalhamento, a velocidade de cisalhamento é calculada e então imposta na parte inferior como uma condição de contorno para resolver as equações de conservação de momentum dos fluxos. A lei deposicional empírica de Krone é implementada no SEDI-3D para estimar o fluxo de deposição dos sedimentos. Aqui, o fluxo de deposição é aproximado pelo produto da concentração local de sedimentos com a velocidade de sedimentação, multiplicado por uma probabilidade de deposição:

$$D = \begin{cases} w_s C\left(1 - \frac{\tau_b}{\tau_{cd}}\right) & if\ \tau_b > \tau_{cd} \\ 0 & otherwise \end{cases} \quad (6)$$

Onde, $\tau_{cd}$ é a tensão de cisalhamento crítica para a deposição, $w_s$ é a velocidade de sedimentação (m/s) e C é concentração de sedimento em suspensão ($g.l^{-1}$) ou ($kg.m^{-3}$). Se a tensão de cisalhamento de fundo for menor do que o cisalhamento de fundo crítico para deposição, o sedimento se depositará.

Nesta versão do SEDI-3D, apenas uma fração de sedimento coeso pode ser modelada. Com base no principal tamanho de grão do sedimento suspenso observado por Toldo et. al. (2006), Fossati e Cuevas (2013) e Moreira e Simionato (2019) para a região de estudo, foi escolhido o silte como o tamanho de partícula, característico de 50 μm. O gradiente de velocidade de sedimentação foi considerado constante em toda a simulação,

e o valor escolhido foi de 0,5 mm/s, de acordo com o tamanho do grão e com base em Van Leussen et. al. (1994), Winterwerp et. al. (2002) e Lee et. al. (2011). A densidade do sedimento foi fixada em 2650 kg/m$^3$. O processo de floculação foi desconsiderado no estudo. A tensão de cisalhamento crítica para erosão foi fixada em 0,15 Pa, a tensão de cisalhamento crítica para deposição foi de 0,05 Pa e o coeficiente de Partheniades foi de 2,0E$^{-6}$ kg.m$^{-2}$.s$^{-1}$ (Marques et. al., 2010a). Esses três parâmetros são parâmetros de calibração relativos ao transporte de sedimentos em suspensão.

## 5.3. Modelo de transporte de Sedimento e Evolução do fundo: SISYPHE

O transporte de sedimento de fundo e a evolução do fundo foi simulado no modelo SISYPHE (Tassi & Villaret, 2014). O SISYPHE trabalha tanto com sedimento não coesivo quanto com sedimento coesivo. Aqui o foco dos processos relacionados será na modelagem do sedimento fino.

O Transporte do sedimento de fundo é calculado segundo a equação de advecção-difusão:

$$\frac{\partial C}{\partial t} + U\frac{\partial C}{\partial x} + V\frac{\partial C}{\partial y} = \left[\frac{\partial}{\partial x}\left(\epsilon_s \frac{\partial C}{\partial x}\right) + \frac{\partial}{\partial y}\left(\epsilon_s \frac{\partial C}{\partial y}\right)\right] + \frac{(E-D)_{z=a}}{h} \qquad (7)$$

Na equação 7, $C$ é a profundidade média da concentração de sedimento, $\epsilon_s$ é o coeficiente difusivo turbulento do sedimento, $U$ e $V$ são as componentes da velocidade da profundidade médias nas direções $x$ e $y$, respectivamente, $h$ é a profundidade, e $E$ e $D$ são respectivamente o fluxo de erosão e o fluxo de deposição.

O SISYPHE utiliza a equação de Exner (Exner, 1920 e Exner, 1925) para calcular a evolução do fundo em todos os passos de tempo da simulação. O cálculo da evolução do fundo leva em consideração o fluxo de sedimento no fundo e o balanço entre a deposição e a erosão.

$$(1-n)\frac{\partial Z_f}{\partial t} + \nabla . Q_b + (E-D)_{z=a} = 0 \qquad (8)$$

Na equação 8, $n$ é o valor da porosidade do sedimento de fundo, $Z_f$ é a evolução do fundo, $Q_b$ é o fluxo de sedimento no fundo, e $E$ e $D$ são as taca de erosão e deposição na elevação $z = a$, profundidade correspondente entre a interface água-sedimento. Duas camadas de espessura do fundo, inicialmente vazias foram escolhidas. Se silte foi depositada nessas camadas, a densidade da camada de silte foi definida para 1500 kg/m$^3$.

## 5.4. Domínio e Malha Numérica

O domínio definido para este trabalho (Figura 4) se estende desde as latitudes 28°S (Cabo de Santa Marta - SC) a 38°S (Mar del Plata) e longitudes de 49°W a 52°W, atingindo profundidades de aproximadamente 300 m. Dados de diferentes fontes foram combinados para obter a melhor representação das características batimétricas do Rio da Prata, da Lagoa dos Patos, do seu estuário e da região costeira adjacente.

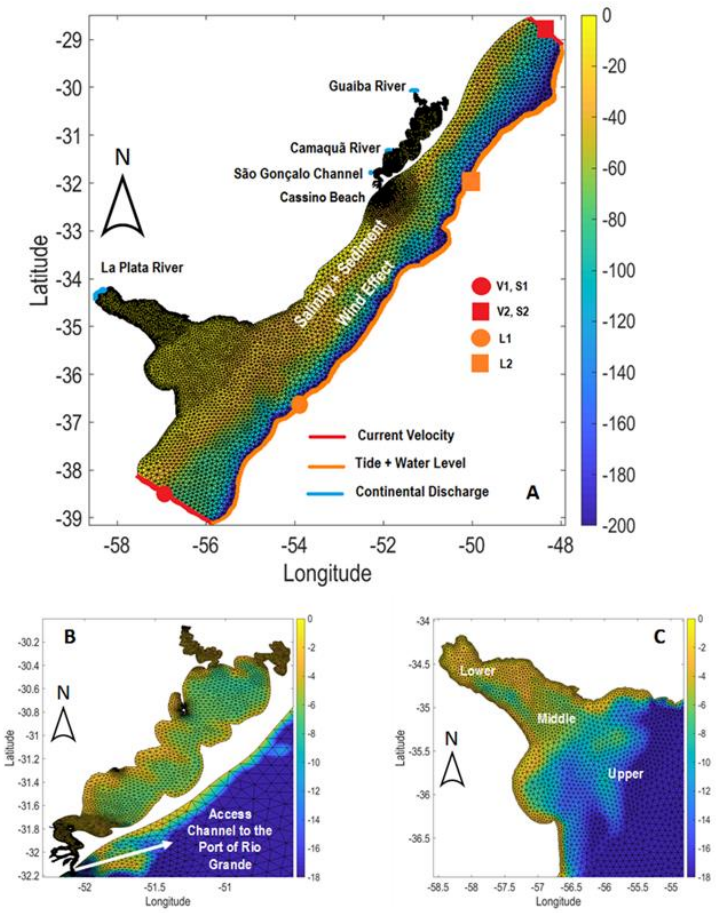


Figura 4 - Domínio computacional e malha numérica utilizada para as simulações. (A) Condições iniciais e de contorno prescritas no modelo. Os pontos onde as séries temporais de salinidade (S1 e S2), velocidade da corrente (V1 e V2) e nível do

mar (L1 e L2) prescritos como condições de contorno foram extraídas também são mostrados. (B) Vista ampliada da malha da Lagoa dos Patos e (C) da malha do Rio da Prata.

Para a região da Lagoa dos Patos, dados batimétricos foram extraídos das cartas náuticas da Diretoria de Hidrografia e Navegação (DHN) da Marinha do Brasil. Buscando melhorar a qualidade da informação batimétrica no principal canal de acesso ao Porto do Rio Grande, foram utilizados dados de levantamentos realizados entre 2006 e 2010 pela autoridade portuária e dados complementares de levantamento batimétrico realizado pela Marinha do Brasil no âmbito do Projeto de Levantamento da Plataforma Continental Brasileira (LEPLAC). Já para a batimetria do Rio da Prata e de sua região costeira adjacente, dados da Marinha argentina foram interpolados e complementados com os dados de Smith e Sandwell (1997) para profundidades superiores a 200 m (Palmas et. al., 2008).

O domínio numérico foi inicialmente discretizado com elementos triângulares com 10 km de aresta no contorno oceânico, 6 km na Plataforma Interna, 3 km na região costeira e 1,5 km na foz do Rio da Prata; e próximo à foz da Lagoa dos Patos as arestas dos elementos triangulares variaram entre 130 m a 20 m. A malha não estruturada 2D resultante (Figura 2) tem 18275 nós e 33296 elementos triangulares, discretizados verticalmente em 11 níveis sigmas, para os quais as equações do modelo foram resolvidas.

## 5.5. Condição Inicial e de Contorno

A determinação das condições iniciais e de contorno (figura 5 e 4A) é etapa crucial para que o modelo represente de forma satisfatória a dinâmica da região. Para isso, a malha numérica conta com 7 fronteiras abertas: as fronteiras continentais do Rio da Prata e da Lagoa dos Patos, a fronteira oceânica, as fronteiras norte e sul, e a fronteira superficial.

As condições iniciais de salinidade são apresentadas na Figura 3, o valor do nível do mar foi constante e igual e 0,4m e a velocidade inicial de corrente igual a 0,5 m/s foram incialmente prescritos no contorno oceânico da malha conforme a figura 2A.

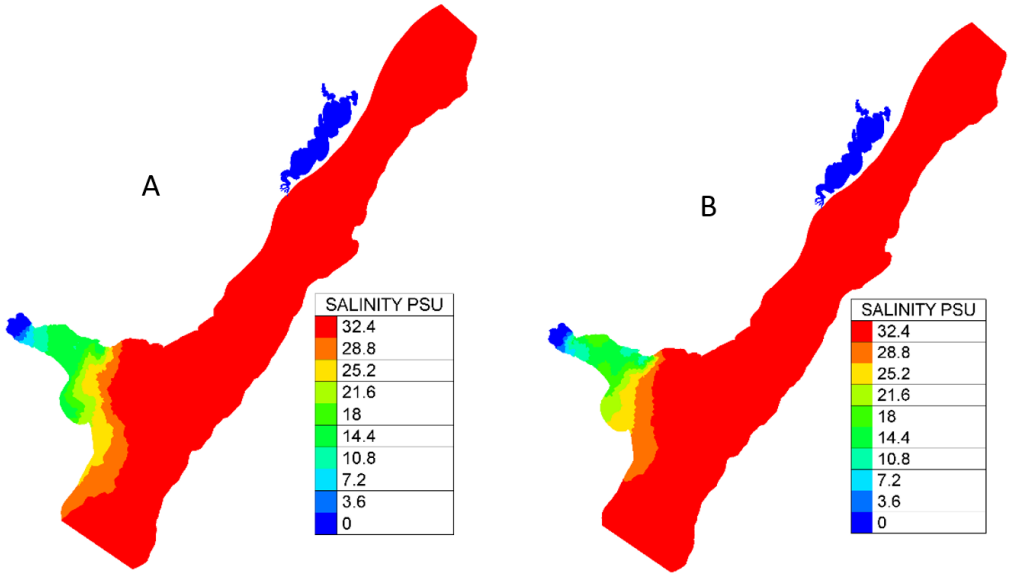


Figura 5 - Campos de salinidade usados como condição inicial na camada superficial do modelo em janeiro de 2005 (A) e janeiro de 2008 (B).

Na fronteira oceânica (figura 4), foram prescritos dados de maré astronômica e nível médio do mar (0.4m) (fronteira oceânica) (figura 6A), velocidade da corrente (fronteiras norte e sul) (figura 6B) e salinidade (figura 4C). A maré foi calculada pela solução inversa das equações de Laplace (Edgbert et. Al., 1994), e 33 componentes harmônicos da maré foram usados para gerar uma estimativa confiável do comportamento do nível do mar. A velocidade da corrente, por sua vez, foi estimada usando campos regionais de velocidade da corrente de maré, obtidos com o OSU Tidal Inversion Software-OTIS (Edgbert e Erofeeva, 2002), acoplado internamente ao TELEMAC. Já os campos de salinidade foram obtidos do modelo global HYCOM + NCODA Global (Hybrid Coordinate Ocean Model, https://hycom.org), com resoluções temporais e espaciais de 3 horas e 0,08 °, respectivamente.

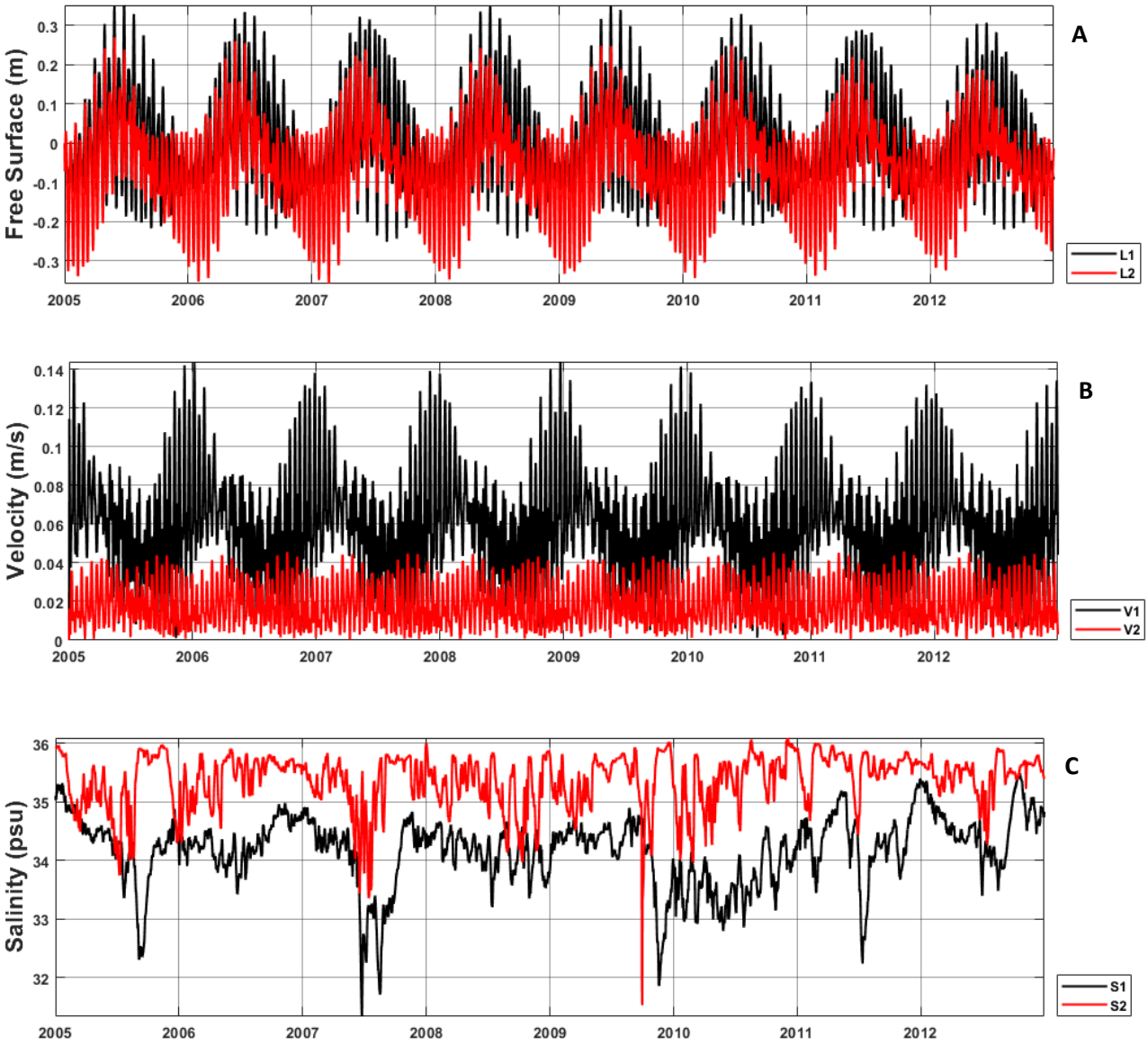


Figura 6 - Dados prescritos como a condição de contorno no limite do oceano nos pontos L1 e L2 (elevação da superfície do mar) (A), V1 e V2 (velocidade da corrente) (B), e S1 e S2 (salinidade) (C) para o período 2005-2012.

As condições de contorno continental (figura 4) para a Lagoa dos Patos correspondem aos dados de vazão diária dos Rios Guaíba e Camaquã (figura 7), fornecidos pela Agência Nacional de Águas (ANA - www.hidroweb.ana.gov.br). Para o terceiro afluente (Canal São Gonçalo), não há série temporal de descargas sistemáticas e os dados de nível da água obtidos através da Agência da Lagoa Mirim (ALM, https://wp.ufpel.edu.br/alm) foram convertidos em dados de descarga fluvial diários por Oliveira et. al. (2015) usando um método de curva de chave. Para a região do Rio da

Prata, os dados diários de vazão foram fornecidos pelo Serviço de Hidrografia Naval da Argentina (SHN, https://argentina.gob.ar/armada).

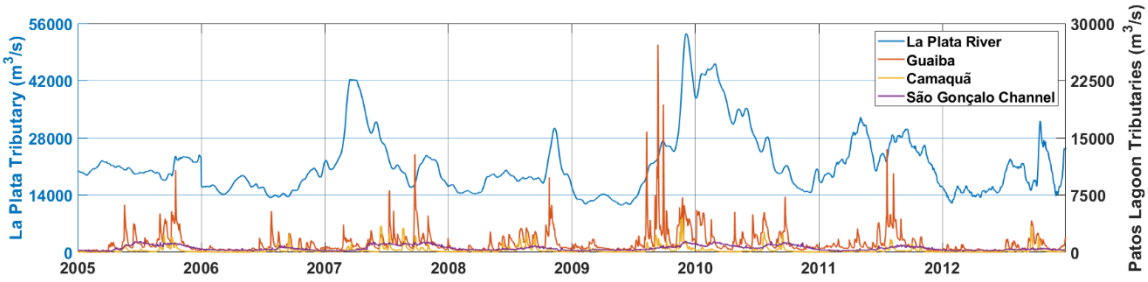


Figura 7 - Séries temporais da descarga fluvial do rio Guaíba, rio Camaquã, canal São Gonçalo e Rio da Prata para o período estudado (2005-2012)

Para os fluxos de sedimentos em suspensão dos rios, não há medições disponíveis para construir séries temporais suficientemente realistas para serem utilizadas como condição de contorno do modelo. Diante disso, as concentrações de sedimento em suspensão dos rios foram consideradas constantes no modelo, de modo que os fluxos de sedimentos são dependentes apenas do fluxo do rio. Os valores atribuídos para as concentrações de sedimento em suspensão foram 200 $mg.l^{-1}$, 100 $mg.l^{-1}$, 150 $mg.l^{-1}$ para o Rio Guaíba, Rio Camaquã e Canal São Gonçalo, respectivamente (Marques et. al., 2010), e 230 $mg.l^{-1}$ para o Rio da Prata (Moreira e Simionato, 2019). A classe de sedimentos em suspensão usada neste estudo foi silte fino (Marques et. al., 2010b; Fossati et. al., 2013).

Os dados de vento do *European Centre for Medium-Range Weather Forecasts (*ECMWF*), ERA Interim* (http://www.ecmwf.int) foram prescritos na fronteira superficial (oceano-atmosfera) (figura 6), com uma escala temporal de 6 h e resolução espacial de 0,75 °, interpolados no tempo e no espaço para cada nó da malha numérica.

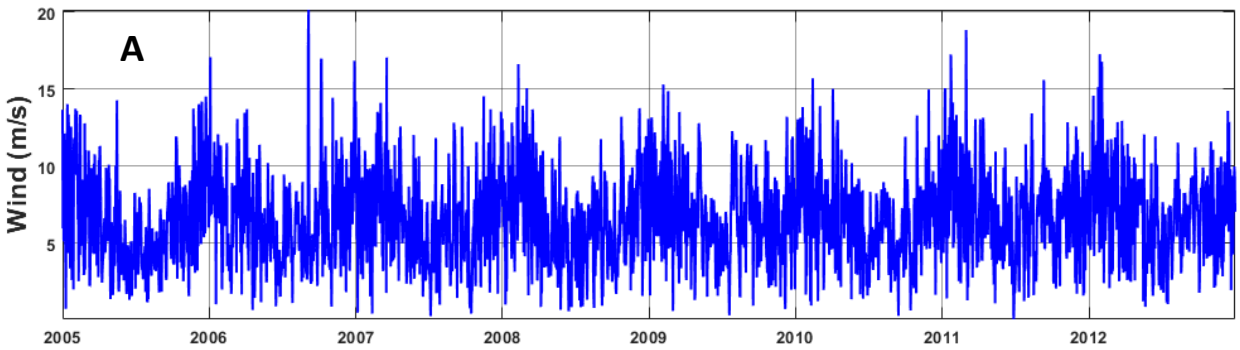

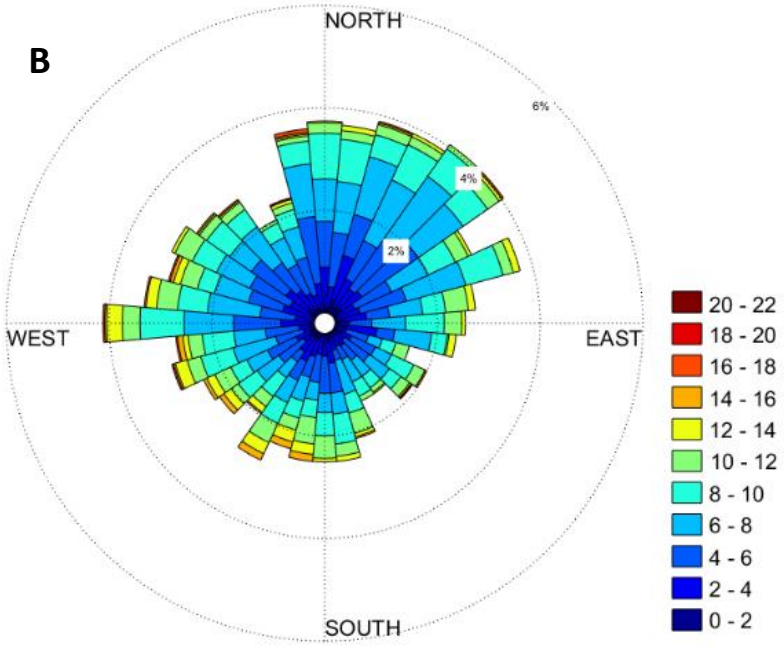


Figura 8 - (A) Série temporal de intensidade do vento usada como forçante superficial na simulação. (B) Rosa dos ventos para a distribuição de frequências da série temporal de intensidade e direção do vento para os anos de 2005 a 2012.

**Tabela 2 - Resumo das fontes dos dados prescritos como condições iniciais e de contorno.**

| Forçante | Fonte do Dado |
|---|---|
| **Descarga Continental** | Guaíba e Camaquã – ANA;<br>São Gonçalo – Método da Curva Chave (Oliveira *et al.*, 2015);<br>Rio da Prata – SHN |
| **Vento** | ECMWF – ERA Interim |
| **Maré** | TPXO |
| **Velocidade** | TPXO |
| **Nível** | TPXO |
| **Salinidade** | HYCOM + NCODA 1/12º |
| **Sedimento em Suspensão** | Silte Fino |
| **Sedimento de Fundo** | Silte Fino |
| **Concentração do Sedimento em Suspensão** | Lagoa dos Patos - Marques et al., 2010<br>Rio da Prata - Moreira and Simionato, 2019 |

## 5.6. Limitações do estudo

A utilização de modelos numéricos possibilita a análise de processos em uma ampla escala temporal e espacial e detalhista o quanto necessária. Porém, existem algumas limitações intrínsecas associadas à aplicação da ferramenta da modelagem numérica:

- ✓ O desconhecimento dos mecanismos físicos de todos os processos relacionados aos fenômenos estudados, devido a representação idealizada dos processos analisados pela modelagem, como a utilização de coeficientes para representar a influência do vento, mecanismo de arrasto de fundo e nas bordas laterais, as trocas no interface oceano-atmosfera, além dos processos de pequena escala relacionado aos fluxos turbulentos.
- ✓ A não incorporação de processos importantes como a maré meteorológica, o regime de onda local, a floculação dos sedimentos, a consolidação do fundo oceânico pode alterar de forma significativa os mecanismos relacionados ao transporte de sedimento. Com isso o resultado dessa modelagem pode ter certa diferença se comparados a outros trabalhos que consideram tais processos.
- ✓ A imperícia de se inserir todos os processos relativos a hidrodinâmica a ao transporte de sedimento, como por exemplo as aproximações e as simplificações necessárias na equação de Navier-Stokes em seu aspecto hidrostático e para os fluidos incompressíveis. O modelo funciona de forma adequada, porém negligenciando algumas implicações que nem sempre deveriam ser desprezadas.
- ✓ Um problema enfrentado nesse trabalho está associado as escalas espaciais e temporais dos distintos corpos d'água analisados. Na modelagem numérica é comum a escolha de parâmetros que se adequam a representar determinados processos, mas que não são adequados para distintas escalas. Por exemplo, a parametrização das influencia do vento para uma região, pode não ser satisfatória para a outra região, devido à grande escala espacial da região de estudo, que abrange diferentes sistemas aquáticos.
- ✓ Os erros relacionados aos dados de entrada podem resultar numa diferença nos resultados finais. Por exemplo, na falta de uma serie temporal longa o suficiente para abranger todo o período analisado, foi adotado um valor

médio para tal parâmetro, podendo gerar uma diferença nos resultados obtidos.

## 5.7. Calibração e Validação do Modelo

O modelo TELEMAC-3D foi extensivamente calibrado e validado para a região da Lagoa dos Patos (Fernandes et. al., 2001; 2002; 2005; 2007; Marques et. al., 2009; 2010a; 2010b; Lisboa et. al., 2015; Silva et. al., 2015, Oliveira et. al., 2019; Bitencourt et. al., 2020). Neste estudo, o domínio do modelo foi ampliado (Figura 4) e foram realizados exercícios complementares de calibração e validação.

A calibração e validação do modelo consistem em comparações entre os resultados do modelo e os dados in situ para o mesmo período e local. A capacidade do modelo de reproduzir os dados medidos é quantificada com base em análises estatísticas como o Erro Quadrático Médio (RMSE) e o Erro Absoluto Médio (MAE) (Janssen et al., 1997; Lalbeharry, 2001; Lalbeharry et al., 2001; Wastra et al., 2001; 2004; Bidlot et al., 2002; Sutherland et al., 2004). Neste estudo, esta capacidade foi avaliada com base nos mesmos parâmetros estatísticos apresentados por Fernandes et. al. (2001), Marques et. al., (2009) e Lisboa et. al., (2015), conforme abaixo.

O Erro Quadrático Médio (RMSE) determina a magnitude do módulo do erro quadrático médio (ou seja, sem considerar se o número é negativo ou positivo) entre as observações e os valores calculados pelo modelo, de acordo com a seguinte expressão matemática:

$$RMSE = \sqrt{\frac{\sum_{i=1}^{n}(m_i - o_i)^2}{n}} \qquad (9)$$

Onde, $m$ é o resultado do modelo, $o$ é o ponto de dados medidos ou observados e $n$ é o número de pontos.

O RMAE indica o Erro Absoluto Médio entre os dados medidos e os resultados obtidos pelo modelo, o qual foi utilizado para quantificar a qualidade dos resultados encontrados no melhor experimento de calibração e nos testes de validação do modelo TELEMAC (Wastra et al., 2001). O valor absoluto médio dos valores observados e os valores modelados é dado por:

$$\langle|X|\rangle = \frac{1}{n}\sum_{i=1}^{n}|X_n| \quad (10)$$

$$\langle|Y|\rangle = \frac{1}{n}\sum_{i=1}^{n}|Y_n| \quad (11)$$

Onde $X$ são valores observados e $Y$ são valores modelados, com cada um dos valores na mesma posição espacial e temporal. Esses valores podem ser escalares (altura da onda ou nível da água) ou vetores (correntes). O parêntese angular expressa a média e, respectivamente, os módulos $X$ e $Y$. Da mesma forma, o erro absoluto médio (MAE) é dado por:

$$MAE = \langle|Y - X|\rangle \quad (12)$$

A qualidade da modelagem pode ser avaliada pelo valor RMAE, da seguinte forma:

$$RMAE = \frac{\langle|Y-X|\rangle}{\langle|X|\rangle} = \frac{MAE}{\langle|X|\rangle} \quad (13)$$

Walstra et. al. (2001) e Sutherland et. al. (2004) utilizaram uma escala de coeficientes que indicam a qualidade dos resultados do modelo de acordo com o método de RMAE.

**Tabela 3 - Escala de classificação para o Erro Absoluto Médio (RMAE) (Sutherland et al., 2004 e Walstra et al., 2001)**

| D | Excelente | Boa | Razoável | Pobre | Ruim |
|---|---|---|---|---|---|
| **RMAE** | ≤0.2 | 0.2 – 0.4 | 0.4 – 0.7 | 0.7 – 1.0 | > 1.0 |

Nos exercícios de calibração hidrodinâmica, os dados de velocidade de corrente e salinidade, de 22 de outubro a 30 de novembro de 2006 e de 15 de outubro a 19 de novembro de 2011 foram coletados na costa usando um ADPC (*Acoustic Doppler Current Profiler*) modelo Sontek Argonalta 1000 kHz e um CTD (Condutividade Temperatura Profundidade) instalado no canal de acesso do Porto do Rio Grande,

respectivamente. Também foram utilizados dados de elevação da superfície livre do mar de 16 de maio a 24 de outubro de 2005 e de 19 de março a 31 de agosto de 2010 obtidos no canal de navegação do Rio da Prata no âmbito do projeto FREPLATA-IFREMER.

Na primeira etapa dos exercícios de calibração, diferentes valores de parâmetros físicos selecionados foram testados. Como a dinâmica da região é fortemente afetada pelo vento, o primeiro parâmetro investigado foi o Coeficiente de Influência do Vento, com valores variando de $10^{-4}$ a $10^{-6}$ (quanto maior o Coeficiente de Influência do Vento, maior a influência do vento). Outros parâmetros físicos importantes aplicados nos exercícios de calibração foram: o passo de tempo de 60 s, o coeficiente de Coriolis igual a -7,70735 x $10^{-5}$ $Nm^{-1}.s^{-1}$, Smagorinsky como modelo de turbulência horizontal (30 para salinidade e $1E10^{-4}$ para sedimento), Comprimento de Mistura (Prandlt) como modelo de turbulência vertical ($1.E10^{-6}$) e Manning como a lei do atrito de fundo (0,02 $s/m^{1/3}$). Os melhores resultados do modelo em comparação com dados de campo foram obtidos com o Coeficiente de Influência do Vento igual a $3x10^{-6}$ ao comparar a velocidade da corrente medida e calculada na superfície (Figura 9A) e no fundo (Figura 9B) no canal de acesso ao Porto do Rio Grande. Neste exercício de calibração, os valores encontrados foram considerados bons (RMAE = 0,24 e 0,20) de acordo com a classificação estatística de Waltra et. al. (2001) e Sutherland et. al. (2004a; 2004b).

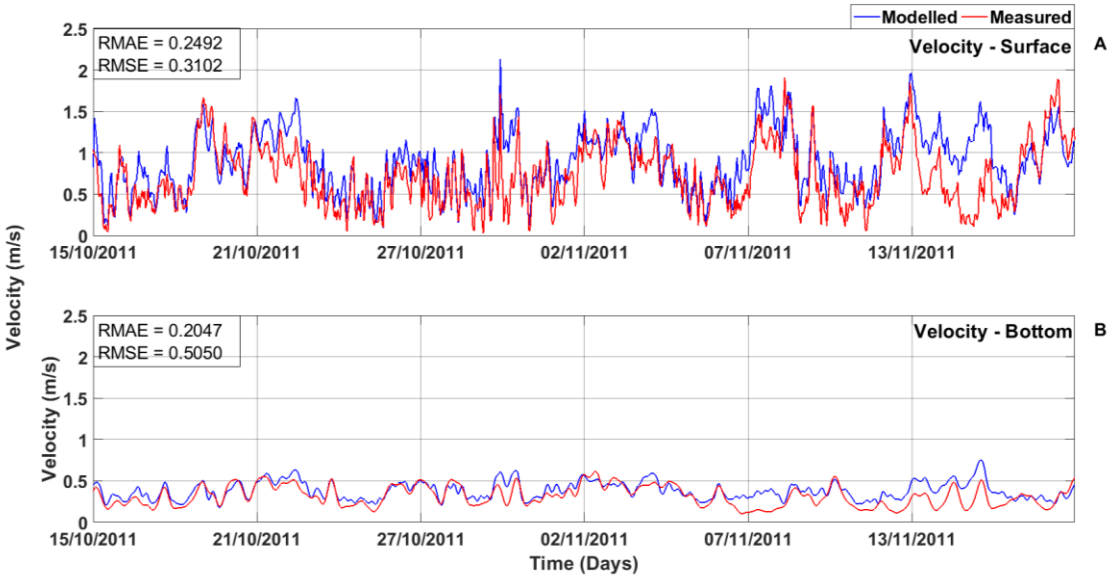


Figura 9 - Comparação entre as séries temporais medidas e calculadas da velocidade da corrente (A) na superfície e (B) no fundo do canal de acesso ao Porto do Rio Grande (ver Figura 2B para localização).

Após definir o Coeficiente de Influência do Vento ($3x10^{-6}$) adequado para a região, novas calibrações foram realizadas variando os modelos de turbulência horizontal (Smagorinsky, K-Epsilon) e vertical (Tsanis, Prandlt e K-Epsilon), bem como leis de atrito com o fundo (Manning e Nikuradse), conforme mostrado nos exercícios de calibração para a elevação do nível do mar na Praia do Cassino e Rio da Prata, na Tabela 4.

**Tabela 4 - Parâmetros utilizados na calibração do modelo, com os respectivos resultados do RMSE para teste (Lagoa dos Patos e nível do Rio da Prata). Os resultados do RMSE para o teste com a melhor aproximação em relação aos valores medidos estão marcados em negrito.**

| Teste | Coeficiente de Influência do Vento | Modelo de Turbulência Vertical | Modelo de Turbulência Horizontal | Lei de Fricção de Fundo | Coeficiente de Fricção | RMAE Praia do Cassino | RMAE Rio da Prata |
|---|---|---|---|---|---|---|---|
| 01 | $3x10^{-6}$ | K-ε | Smagorinsky | Manning | 0.01 | 0.1452 | 0.2993 |
| 02 | $3x10^{-6}$ | K-ε | Smagorinsky | Manning | 0.02 | 0.3573 | 0.2478 |
| 03 | $3x10^{-6}$ | K-ε | Smagorinsky | Manning | 0.03 | 0.3919 | 0.2612 |
| 04 | $3x10^{-6}$ | K-ε | Smagorinsky | Manning | 0.04 | 0.2547 | 0.3641 |
| 05 | $3x10^{-6}$ | K-ε | K-ε | Manning | 0.01 | 0.1987 | 0.2998 |
| 06 | $3x10^{-6}$ | K-ε | K-ε | Manning | 0.02 | 0.1825 | 0.2664 |
| 07 | $3x10^{-6}$ | K-ε | K-ε | Manning | 0.03 | 0.2564 | 0.2334 |
| 08 | $3x10^{-6}$ | K-ε | K-ε | Manning | 0.04 | 0.2417 | 0.1785 |
| 09 | $3x10^{-6}$ | Prandlt | Smagorinsky | Manning | 0.01 | 0.3214 | 0.4568 |
| **10** | **$3x10^{-6}$** | **Prandlt** | **Smagorinsky** | **Manning** | **0.02** | **0.1521** | **0.1801** |
| 11 | $3x10^{-6}$ | Prandlt | Smagorinsky | Manning | 0.03 | 0.1625 | 0.3698 |
| 12 | $3x10^{-6}$ | Prandlt | Smagorinsky | Manning | 0.04 | 0.1847 | 0.3667 |
| 13 | $3x10^{-6}$ | Prandlt | K-ε | Manning | 0.01 | 0.1965 | 0.3412 |
| 14 | $3x10^{-6}$ | Prandlt | K-ε | Manning | 0.02 | 0.1752 | 0.1987 |
| 15 | $3x10^{-6}$ | Prandlt | K-ε | Manning | 0.03 | 0.3412 | 0.3438 |
| 16 | $3x10^{-6}$ | Prandlt | K-ε | Manning | 0.04 | 0.2987 | 0.3360 |
| 17 | $3x10^{-6}$ | Tsanis | Smagorinsky | Manning | 0.01 | 0.3024 | 0.3978 |
| 18 | $3x10^{-6}$ | Tsanis | Smagorinsky | Manning | 0.02 | 0.4125 | 0.3682 |
| 19 | $3x10^{-6}$ | Tsanis | Smagorinsky | Manning | 0.03 | 0.4187 | 0.3769 |
| 20 | $3x10^{-6}$ | Tsanis | Smagorinsky | Manning | 0.04 | 0.3657 | 0.3572 |
| 21 | $3x10^{-6}$ | Tsanis | K-ε | Nikuradse | $1x10^{-5}$ | 0.4126 | 0.4409 |
| 22 | $3x10^{-6}$ | Tsanis | K-ε | Nikuradse | $2x10^{-5}$ | 0.3952 | 0.4215 |
| 24 | $3x10^{-6}$ | Tsanis | K-ε | Nikuradse | $3x10^{-5}$ | 0.3458 | 0.4712 |
| 25 | $3x10^{-6}$ | Tsanis | K-ε | Nikuradse | $4x10^{-5}$ | 0.2147 | 0.4412 |
| 26 | $3x10^{-6}$ | K-ε | Smagorinsky | Nikuradse | $1x10^{-5}$ | 0.1452 | 0.4181 |
| 27 | $3x10^{-6}$ | K-ε | Smagorinsky | Nikuradse | $2x10^{-5}$ | 0.3878 | 0.4571 |
| 28 | $3x10^{-6}$ | K-ε | Smagorinsky | Nikuradse | $3x10^{-5}$ | 0.2478 | 0.2347 |
| 29 | $3x10^{-6}$ | K-ε | Smagorinsky | Nikuradse | $4x10^{-5}$ | 0.1698 | 0.4516 |
| 30 | $3x10^{-6}$ | K-ε | K-ε | Nikuradse | $1x10^{-5}$ | 0.4215 | 0.3219 |
| 31 | $3x10^{-6}$ | K-ε | K-ε | Nikuradse | $2x10^{-5}$ | 0.4987 | 0.3315 |
| 32 | $3x10^{-6}$ | K-ε | K-ε | Nikuradse | $3x10^{-5}$ | 0.3651 | 0.2669 |

| | | | | | | | |
|---|---|---|---|---|---|---|---|
| 33 | $3x10^{-6}$ | K-ε | K-ε | Nikuradse | $4x10^{-5}$ | 0.3412 | 0.2033 |
| 34 | $3x10^{-6}$ | Prandlt | Smagorinsky | Nikuradse | $1x10^{-5}$ | 0.2981 | 0.2155 |
| 35 | $3x10^{-6}$ | Prandlt | Smagorinsky | Nikuradse | $2x10^{-5}$ | 0.2786 | 0.2029 |
| 36 | $3x10^{-6}$ | Prandlt | Smagorinsky | Nikuradse | $3x10^{-5}$ | 0.4127 | 0.9785 |
| 37 | $3x10^{-6}$ | Prandlt | Smagorinsky | Nikuradse | $4x10^{-5}$ | 0.4579 | 0.2049 |
| 38 | $3x10^{-6}$ | Prandlt | K-ε | Nikuradse | $1x10^{-5}$ | 0.3217 | 0.3284 |
| 39 | $3x10^{-6}$ | Prandlt | K-ε | Nikuradse | $2x10^{-5}$ | 0.3258 | 0.4569 |
| 40 | $3x10^{-6}$ | Prandlt | K-ε | Nikuradse | $3x10^{-5}$ | 0.2569 | 0.5214 |
| 41 | $3x10^{-6}$ | Prandlt | K-ε | Nikuradse | $4x10^{-5}$ | 0.1987 | 0.4396 |
| 42 | $3x10^{-6}$ | Tsanis | Smagorinsky | Nikuradse | $1x10^{-5}$ | 0.2356 | 0.4789 |
| 43 | $3x10^{-6}$ | Tsanis | Smagorinsky | Nikuradse | $2x10^{-5}$ | 0.2147 | 0.2369 |
| 44 | $3x10^{-6}$ | Tsanis | Smagorinsky | Nikuradse | $3x10^{-5}$ | 0.2987 | 0.4213 |
| 45 | $3x10^{-6}$ | Tsanis | Smagorinsky | Nikuradse | $4x10^{-5}$ | 0.4126 | 0.4978 |
| 46 | $3x10^{-6}$ | Tsanis | K-ε | Nikuradse | $1x10^{-5}$ | 0.2713 | 0.2336 |
| 47 | $3x10^{-6}$ | Tsanis | K-ε | Nikuradse | $2x10^{-5}$ | 0.2678 | 0.2245 |
| 48 | $3x10^{-6}$ | Tsanis | K-ε | Nikuradse | $3x10^{-5}$ | 0.2956 | 0.2668 |
| 49 | $3x10^{-6}$ | Tsanis | K-ε | Nikuradse | $4x10^{-5}$ | 0.2456 | 0.2987 |

Os melhores resultados foram obtidos para o Teste 10, com RMSE de 0,15 e 0,18 para a Praia do Cassino (Figura 10A) e Rio da Prata (Figura 10B), respectivamente; esses valores são classificados como excelentes de acordo com Walstra et. al. (2001). Assim, o melhor conjunto de parâmetros físicos foi definido como uma combinação da lei de Manning do atrito do fundo (coeficiente de atrito = 0,02 $s/m^{1/3}$), o modelo de turbulência horizontal de Smagorinsky (30 para salinidade e $1.E10^{-4}$ para sedimentos) e o modelo de turbulência vertical do comprimento da mistura (Prandlt) ($1.E10^{-6}$).

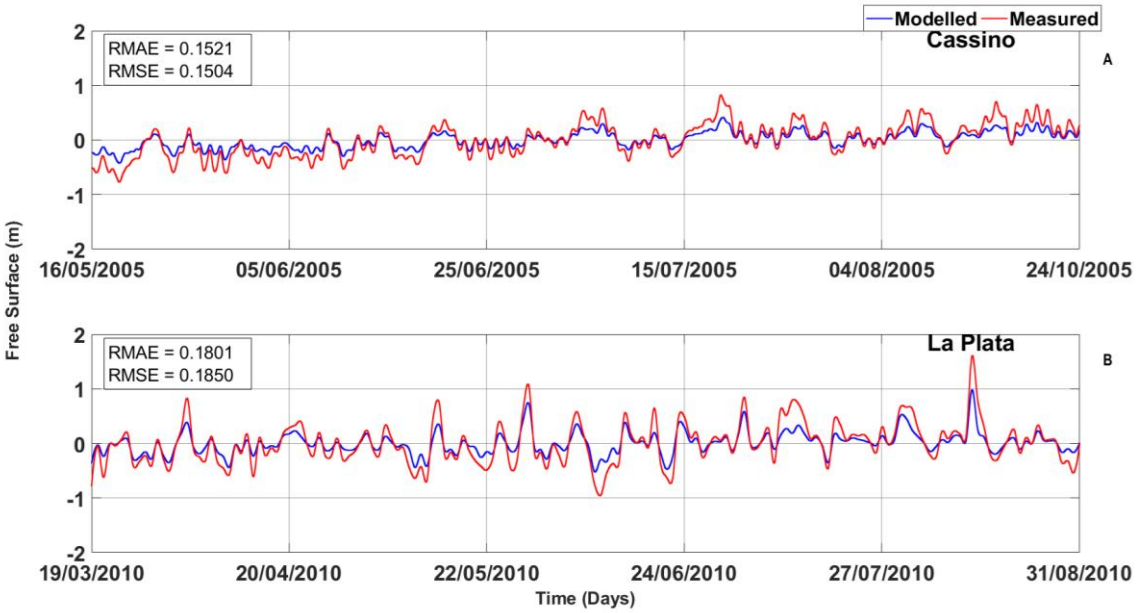


Figura 10 - Comparação entre as séries temporais medidas e calculadas da elevação do nível do mar na (A) Praia do Cassino e (B) Rio da Prata.

Após definir o melhor conjunto de parâmetros físicos para o modelo hidrodinâmico, exercícios de validação adicionais foram realizados para o período entre 22 de outubro a 30 de novembro de 2006, e o desempenho do modelo para reprodução de salinidade e velocidade de corrente foi avaliado (Figuras 11A e 11B). O desempenho do modelo para simular a salinidade na superfície e próximo ao fundo do estuário da Lagoa dos Patos foi classificado como excelente de acordo com Walstra et. al. (2001), com RMAE de 0,17 e 0,19, respectivamente. Os valores RMSE variaram de 5,68 a 9,06 psu. Considerando a série temporal da velocidade da corrente medida e calculada, a capacidade do modelo também foi classificada como excelente de acordo com Walstra et. al. (2001), com RMAE de 0,17 e 0,18 na superfície (Figura 11A) e no fundo (Figura 11B), respectivamente. Os valores de RMSE variaram de 0,17 a 0,39 m/s. Uma análise geral dos exercícios de calibração e validação indica que o Modelo TELEMAC é uma ferramenta adequada para simular a hidrodinâmica do domínio.

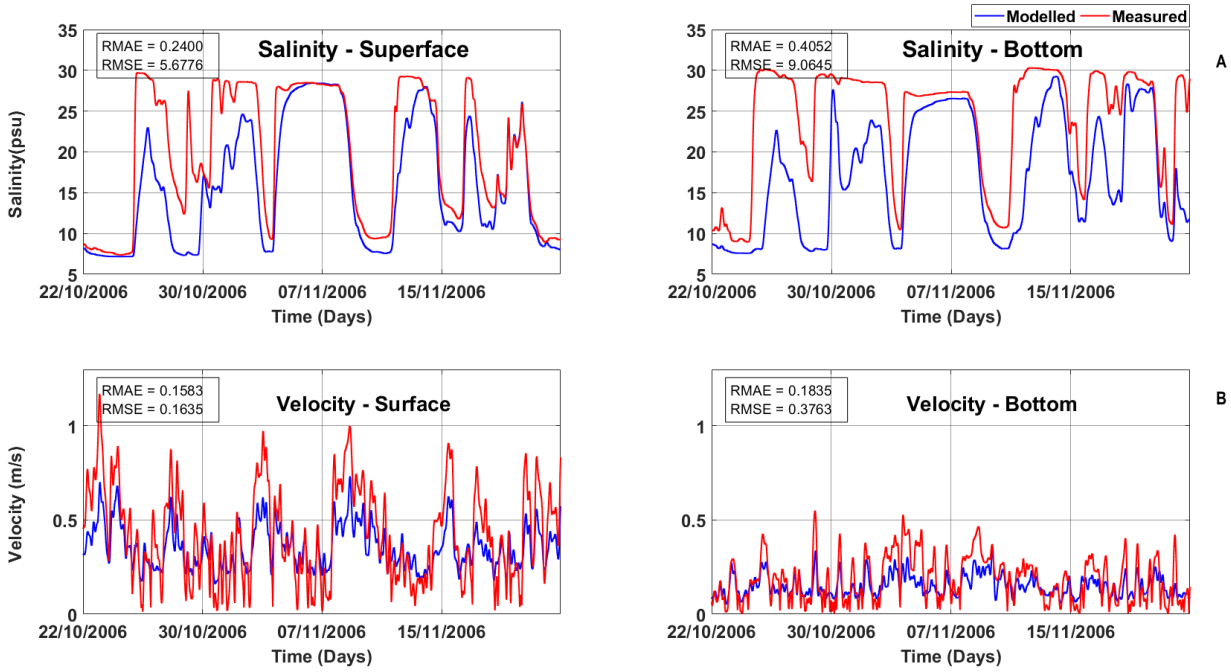


Figura 11 - Comparação entre as séries temporais de salinidade medida (linha vermelha) e calculada (linha azul) e velocidade da corrente (A) na superfície e (B) no fundo.

Para a validação da concentração de sedimento em suspensão calculada pelo modelo, foram utilizados dados de Rio da Prata entre os dias 26 de novembro de 2009 e 16 de dezembro de 2010 (FREPLATA-IFREMER Projeto). Detalhes sobre os

procedimentos de aquisição de dados foram descritos por Fossati et. al. (2014). A Figura 12 mostra a evolução temporal da concentração de sedimento em suspensão calculada e medida no estuário inferior, médio e alto do Rio da Prata, resultando em valores RMSE variando de 14,05 a 15,53 mg.l$^{-1}$ e um RMAE = 0,21, no limite entre a classificação de uma reprodução excelente e boa (Walstra et. al., 2001).

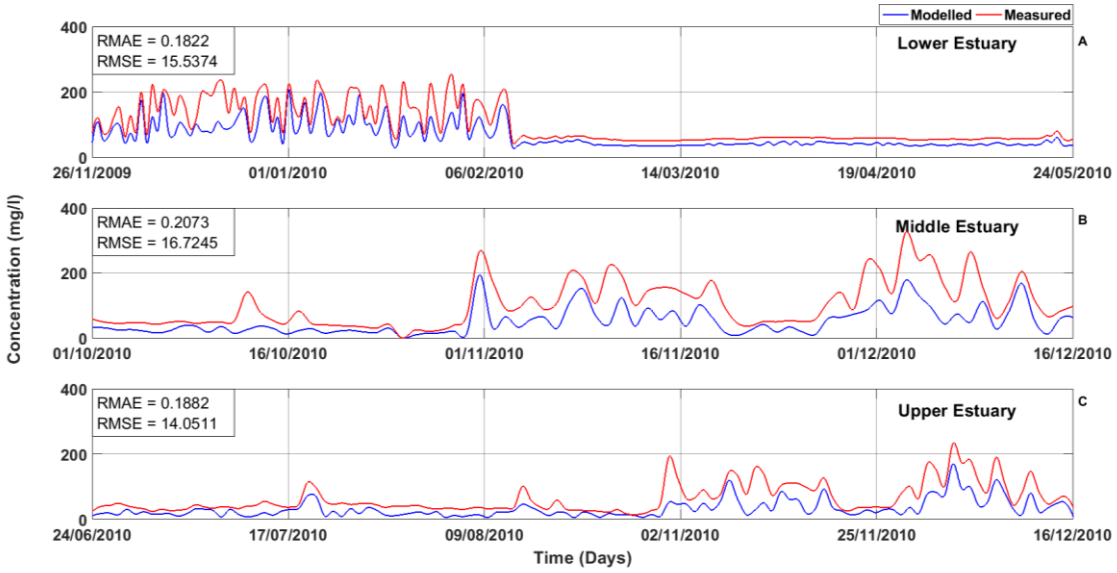


Figura 12 - Comparação entre a concentração calculada de sedimentos em suspensão (linha azul) e os dados medidos (linha vermelha) em (A) o estuário inferior, (B) médio e (C) superior do Rio da Prata, entre o dia 24 de Junho a 16 de dezembro de 2010.

Devido à falta de dados da concentração de sedimento em suspensão observada para calibração do modelo numérico no sul do Brasil, foi utilizada uma metodologia alternativa baseada em produtos de sensoriamento remoto para a região. Três imagens LandSat 5 da American Space Agency (NASA) (https://earthexplorer.usgs.gov/) foram utilizadas (6 de fevereiro de 2008; 3 de outubro de 2008; 17 de setembro de 2008), e processadas de acordo com Peixoto et. al. (2018) para obter produtos com resolução espacial de 30 m para posterior comparação com mapas calculados da concentração de sedimento em suspensão de superfície em dois perfis (Figura 11).

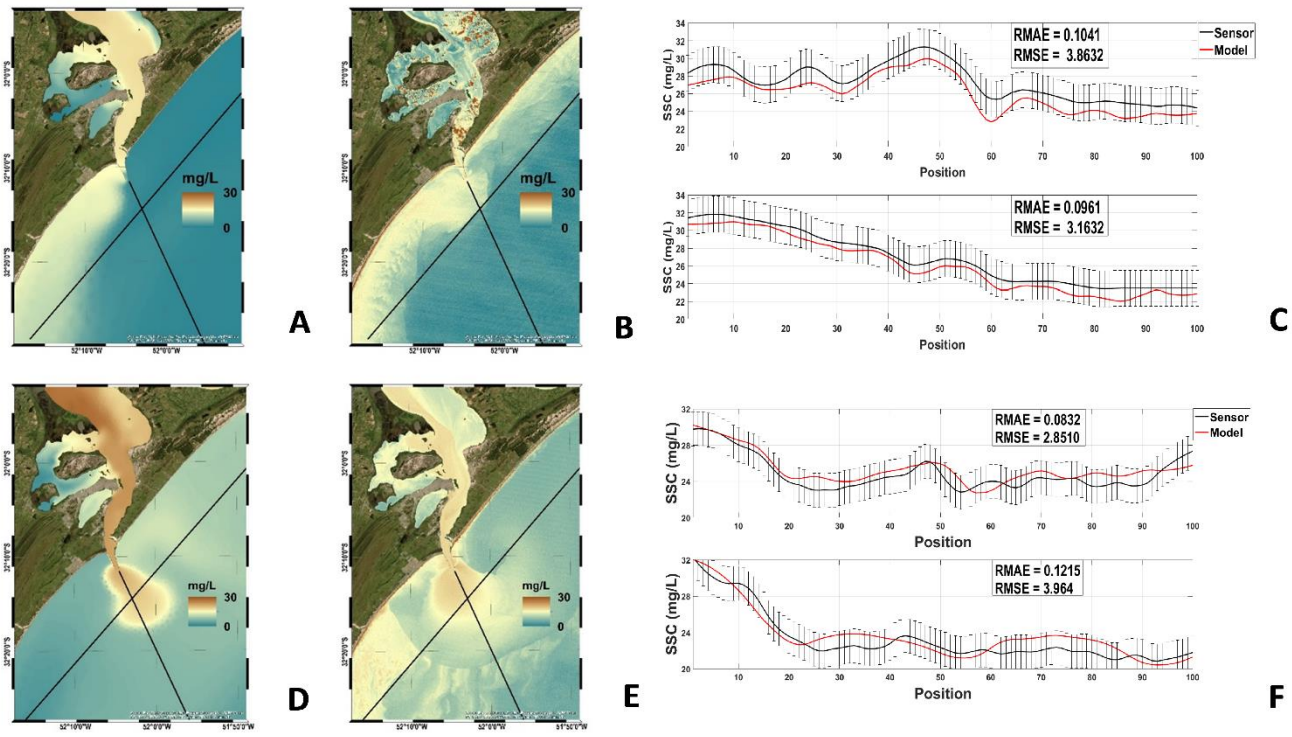


Figura 13 - Painéis à esquerda: Concentrações de sedimentos em suspensão (SSC) na superfície obtidas com o modelo numérico (A, D) e por sensoriamento remoto (B, D) em 6 de fevereiro de 2008 (topo) e 17 de setembro, 2008 (parte inferior), respectivamente. Painéis à direita: SSC na superfície extraída dos respectivos perfis longitudinais (painéis superiores) e transversais (painéis inferiores) (C, F).

Uma comparação entre a concentração de sedimento em suspensão calculada pelo modelo numérico e as informações do sensoriamento remoto indica que o modelo pode reproduzir algumas características da pluma costeira da Lagoa dos Patos, como sua orientação e espalhamento. Além disso, os perfis selecionados para comparação (Figuras 13C e 13F) indicam que os resultados do modelo e as informações de sensoriamento remoto são semelhantes, com valores RMSE de 4,0 e 2,9 $mg.l^{-1}$ para o litoral (painéis superiores) e 3,2 e 3,9 $mg.l^{-1}$ para perfis transversais (painéis inferiores).

# **Capítulo VI**: Resultados

# 6. Resultados

Para se obter o título de Doutorado pelo Programa de Pós-Graduação em Oceanografia da FURG (PPGO – FURG), é requerido que o doutorando submeta pelo menos dois artigos científicos como primeiro autor em periódico com Qualis A1 ou A2 (Qualis CAPES), e este artigo esteja em revisão para que a defesa da tese possa ser agendada.

Dessa forma, os resultados da pesquisa desenvolvida durante o período de doutorado, assim como a discussão e conclusão dos mesmos resultados serão apresentados em forma de dois artigos científicos neste Capítulo.

Os dois manuscritos, tiveram autoria e a participação de Paulo Victor de Araújo Brito Lisboa, Elisa Helena Fernandes, Aldo Sottolichi, Nicolas Huybrecht e Antônio Raylton Bendô, sendo o primeiro intitulado "Coastal Plumes Contribution to the Suspended Sediment Transport in the Southwest Atlantic Inner Continental Shelf", e submetido para publicação no periódico "*Journal of Marine Systems*". Já o segundo tem como título "Bottom Evolution Patterns in the Southwest Atlantic Inner Continental Shelf", foi submetido para a publicação no periódico "*Environmental Modelling & Software*".

## 6.1. Article 1

# Coastal Plumes Contribution to the Suspended Sediment Transport in the Southwest Atlantic Inner Continental Shelf

Paulo Victor Lisboa a,b,*, Elisa H. Fernandes a, Aldo Sottolichio b, Nicolas Huybrecht c, Raylton Bendô d.

[a]*Laboratótio de Oceanografia Costeira e Estuarina - LOCOSTE, Instituto de Oceanografia - PPGO, Universidade Federal do Rio Grande, Rio Grande, RS, 96203-900, Brazil*

[b]*Environnements et Paléo-Environnements Océaniques et Continentaux – EPOC Laboratory, University of Bordeaux, 33615 Pessac, France.*

[c] *Cerema, Direction Technique Eau, Mer et Fleuves, 134 rue de Beauvais – CS 60039-60280 Margny-lès-Compiègne – France.*

[d]*Escola de Engenharia – PPGE, Universidade Federal do Rio Grande, Rio Grande, RS, 96203-900, Brazil.*

* Corresponding author

E-mail address: paulovictor_fjv@hotmail.com

**Abstract**

Global coastal zones are constantly changing due to the actions of various physical forces. Recent studies show that the supply of suspended sediment of continental origin plays an important role in these changes. Once in the coastal region, this sediment significantly influences the sedimentation process on the internal platform. Knowing this, understanding the transport and destination of these sediments is crucial to interpreting the morphodynamic evolution of the seabed and biogeochemical processes in the ocean. The Southwest Atlantic Shelf is the largest continental shelf in the Southern Hemisphere and one of the most important in biological production, because of the great continental contribution exercised by both the La Plata River and the Patos Lagoon. Studies in the region show that these effluents are significantly affected by the El Niño–Southern Oscillation (ENSO) effect, which can significantly interfere with the availability of suspended material inserted into the coastal region. Despite the great efforts of several authors to understand

these changes and their interactions with the environment, some questions remain unanswered. Thus, this work aims to fill this gap by answering questions related to the contribution of sediment of continental origin and its behavior on the Southwest Atlantic Inner Shelf. The behavior of suspended sediment was investigated in two distinct periods using the hydromorphodynamic model TELEMAC-3D: one representing normal years, that is, without the effect of ENSO (2005-2006) and the other experiencing the effect of ENSO (2008-2009).The model was calibrated and validated using field data for both studied periods and for other periods. The results were based on statistical analyses, such as wavelet and empirical orthogonal function (EOF) analyses, in addition to time series. The results show that the Southwest Atlantic Inner Shelf is mainly influenced by the fluvial discharge of the La Plata River and the Patos Lagoon, and by the local wind. The La Plata River being the largest exporter of suspended sediment in the region, with an approximate rate of $1.2x10^8$ tons/year in neutral (normal) years and $3.0x10^8$ tons/year in years under the influence of ENSO. The Patos Lagoon, on the other hand, exports approximately $1.25x10^7$ tons/year in the period without the ENSO effect and $1.35x10^7$ tons/year in the period influenced by ENSO. The results also show that the fluvial discharge interacts with the suspended sediment in seasonal to interannual scales, while the wind contributes to the concentration of suspended sediment on synoptic scales. Still on the local wind regime, the results show that the local wind regime gains importance particularly when the suspended sediment reaches the coastal region.

*Keywords: Suspended Sediment Concentration; Southwest Atlantic Inner Continental Shelf; Numerical Modelling; La Plata River; Patos Lagoon; ENSO.*

## Introduction

Coastal zones are constantly changing due to the continuous action of winds, waves, currents, tides, and river discharges (Wright and Friedrichs, 2006; Rosa et. al., 2013). Although their study started decades ago (Helder and Ruardij, 1982; Blanton, 1988; Zavialov et. al., 1998), current studies still aim to understand these changes and interactions between different coastal environments, with different physical forcings, particularly in relation to the importance of suspended sediment transport in the sediment supply and the dispersion processes on the adjacent costal shelf (Rodrigues et. al., 2006; Rosa et. al., 2013; He et. al., 2018).

The global sedimentary budget of the world's rivers indicates that approximately 15-20 billion tons of suspended sediment are annually transported towards the ocean (Milliman and Syvitski, 1992). This riverine suspended sediment is transported seawards mainly by coastal plumes (Wright and Nittrouer, 1995). Among various estuaries and rivers, some have a fluvial

contribution sufficiently large to perpetuate a coastal plume during significant periods (on a weekly scale) and over large distances in the continental shelf (Menandro et. al., 2015). According to Simpson and Sharples (2012), the influence of freshwater on the continental shelf depends on several widely complex physical processes, inducing significant buoyancy in the coastal region. Horizontal density gradients tend to generate a circulation in the coastal region analogous to an estuarine setting, with the difference being that this flow can be modified by the action of the Coriolis effect when generating currents parallel to the coastline. According to the authors, the combined action of the tide with the wind is also responsible for the vertical stratification and the displacement of the plume across the coastal region.

Once in the coastal seas, this fluvial contribution can influence sedimentation in the inner shelf due its interaction with coastland shelf dynamics (Mestres et. al., 2007), and can be trapped in deltas, deposited on the adjacent nearshores, distributed in the continental shelf, or delivered to the deep sea over the shelf break or via submarine canyons (Meade, 1996). Only the four world's largest rivers in terms of suspended sediment load (Amazon, Ganges-Brahmaputra, Yangtze and Yellow before damming) contribute together about 4 billion tons of suspended sediment into the oceans, accounting for 20% of the total global discharge (Milliman and Syvitski, 1992). These rivers are extensively studied in terms of river processes, sediment characteristics, river plume dynamics, sedimentary properties, and shelf sediment transport (Montanher et. al., 2018; Haque et. al., 2016; He et. al., 2018; Ye et. al., 2019).

Understanding the transport and fate of riverine suspended sediment is crucial for interpreting seabed morphodynamic evolution and biogeochemical processes in the ocean. This is because continental waters carry high amounts of organic matter and nutrients, which help in the intensification of biogeochemical processes and support coastal primary productivity and fishing stocks. They can also promote hypoxia in the inner continental shelf due to their proximity to coastal processes such as an intensification of biological activities (Mann and Lazier, 1991; Geyer et. al., 2004). In general, the intrusion of these continental waters into the coastal region significantly interferes with the chemical, physical and biological properties of the ocean (Piola et. Al., 2008), since continental waters tend to be less saline compared to ocean waters, forming features known as feathers (Garvine et. al., 2002; Marques et. al., 2010). Several authors (Lentz, 1992; Gelfenbaum e Stumpf, 1993) consider the plumes as features of great complexity, mainly due to the variety of rivers and estuaries capable of generating this feature, and the amount of non-inertial processes, such as density, correlated with sediment transport.

Density is such an important property in the development of plumes that Bates (1953) classified plumes of fluvial origin according to the contrast of density with ocean waters in three categories: hypopicnal, homopycnal and hyperpycnal plumes. Hypopicnal plumes are characterized by positive buoyancy caused by the fact that river water is less dense than ocean water, thus causing a horizontal spread of the plume. In homopycnal plumes there is no difference between densities, generating highly mixed water masses with zero buoyancy. In the hyperpycnais, the continental waters are denser than the ocean waters, causing negative buoyancy, which generates a horizontal spread along the bottom layers.

Several authors have investigated the interaction between continental suspended sediment contributions and their adjacent coastal regions throughout the world. The fate and behavior of suspended sediments in the continental shelf are controlled by linear and non-linear processes that can be studied through field data analyses, remote sensing, and analytical and numerical models (e.g., Milliman et. al., 1985, Kourafalou et. al., 1996; Foster and Carter, 1997; Rodrigues et. al., 2006; Warrick et. al., 2013; Brodie et. al., 2010). In Asia, Milliman et. al. (1985) studied the contribution of suspended material from the Chengjiang estuary to the Chinese Continental Shelf and its interaction with the Taiwan Current and the Jiangsu Current in the Yellow Sea. The authors showed that sediment transport is directly related to the riverine ebb and flood regime, but the tidal phase (spring or neap) also plays an important role; it was estimated that 40% of the riverine suspended sediment load is deposited inside the estuary. The remaining suspended sediment is deposited directly in the adjacent continental shelf during flood seasons, being resuspended and carried southwards by the coastal current. Still in Asia, Haque et. al. (2016) studied the mechanism of sediment transport in the Ganges - Brahmaputra Delta region using 1D and 2D dynamic models (HEC RAS and Delft 3D) to analyze the volumetric flow distribution in estuarine systems. Their results show that the distribution patterns of the freshwater inlet and water storage are much higher than those of the saltwater inlet and storage flow. This results in a clockwise estuarine residual circulation pattern causing the sediments to return from the sea to the central estuarine system and leading to significant local sedimentation. In the North Atlantic Bay of Biscay, Diaz et. al. (2020) used the realistic 3D hydrodynamic and sediment transport model MARS3D to evaluate the influence of the model's empirical parameterizations on residual sediment fluxes and to estimate the uncertainties in the transfer of mud and sand at the macrotidal Gironde estuary mouth. The results revealed that simulated residual fluxes are not only sensitive to sedimentation and erosion parameters, but also to the spin-up period and the sliding process of sediments. The model also highlighted the strong seasonal variability in sediment fluxes, importing suspended sediment during high river flow and slowly exporting it during a low river flow.

Kineke and Stemberg (1995) studied the Amazon River suspended-sediment exportation and its contribution to the Amazon Shelf to understand the link between physical processes and the fate of Amazon River suspended sediment at different time scales. Results based on field data showed that the vertical structure of benthic fluid mud varies through space and time, with fortnightly variability close to the river mouth. The authors also concluded that the total suspended sediment inventory on the shelf during the high discharge season is approximately equal to the annual suspended sediment discharge from the river ($1.2x10^9$ tons/year) and more than 90% of that inventory is fluid mud. Gabioux et. al. (2005) presented a study with a 2D numerical model of the effects of suspended sediments on the Amazon shelf. The results showed that the presence of suspended sediment close to the bottom of the shelf represents an important factor in the dynamics of the continental shelf in the Amazon, reducing the bottom shear stress to the point of generating energy dissipation, which in turn affects the amplitude of the wave tide on the spot.

The Southwest Atlantic Shelf (SAS) is the largest continental shelf in the Southern Hemisphere and one of the most biologically productive areas in the oceans globally, (Castello and Möller, 1977; Bisbal, 1995; Acha et. al., 2004) because of the high phytoplankton biomass sustained by the Patos Lagoon and the La Plata River runoffs and shelf-break upwelling (Ciotti et. al., 1995; Bauer et. al., 2017). Particularly in the brazilian part of SAS, the impact of the La Plata's waters on the shelf has been recognized since the first oceanographic studies in the region (Emilson, 1961; Guerrero et. al., 1997; Depetris and Pasquini, 2007b). Möller et. al. (2008) showed that the intrusion of La Plata water into the continental shelf forms a saline plume, that extends along a coastal strip of 1300 km (Piola et. al., 2005). This plume affects the circulation, stratification, and the distributions of nutrients and biological species over a broad extension of the adjacent continental shelf. The presence of this large amount of freshwater in the coastal zone generates a salinity gradient in the region, strongly modulated by the synoptic action of the wind (Pereira, 1989; Zavialov et. al., 1998; Pimenta et. al., 2005). Piola et. al. (2005), combined hydrographic and wind historical data with numerical simulations to determine the seasonal and interannual variability of the La Plata River dynamics, in addition to its relationship with the magnitude of the river discharge and the intensity and direction of the wind. Their results indicated that the seasonal variability of the river plume is controlled by the alongshore component of the wind. Soares et. al. (2007b) then analyzed the importance of turbulent mixing for the evolution of the La Plata plume and its spreading on the platform towards the Patos Lagoon using 3D numerical modelling results. It was shown that the La Plata plume tends to expand along the northern margin in the presence of local

winds during autumn and is more restricted to the mouth of the river during spring, when winds are weaker and the tidal regime prevails in the region.

The influence of the Patos Lagoon waters in the continental shelf has also been widely studied (Marques et. al., 2009; 2010a; Monteiro et. al., 2011). Marques et. al. (2009) studied the physical forcings controlling the dynamics of the Patos Lagoon coastal plume. They concluded that the coastal plume behaves as a small spatial scale plume, and the dominant mode of variability is associated with a transport towards the south, controlled by the combination of dominant north quadrant winds and the seasonal variability of river discharge in the region. Marques et. al. (2010a) investigated the importance of straining and advection processes of the water column along the region that is influenced by the Patos Lagoon, in the Southern Brazilian inner shelf. The study was carried out through 3D numerical modelling experiments. Results showed that the freshwater discharge intensity controls the straining and advection, which in turn were the most important mechanisms for the bed evolution in the adjacent coastal region. The different forcings that control the dynamics of the plume of the Patos Lagoon were studied by Monteiro et. al. (2011). The authors analyzed the influence of the Earth's rotation, the flow of the river, the tide, and the winds in the dynamics of the plume. The results showed that the Earth's rotation plays an important role in the asymmetry of the plume flow; the tides control the mixing process, reducing the penetration of the plume on the inner shelf. The results also showed that the balance between fluvial discharge and the wind is responsible for the internal and external displacement of the plume in the Patos Lagoon estuary.

The effects of three distinct west contour currents can be added to these continental contributions in the South Atlantic Inner Shelf (SAIS): the Malvinas Current, the Brazilian Current and the Coastal Currents, as well as the effects of tides and winds (Souza and Robinson, 2004). The interaction between the Coastal Currents and the coastal plumes can have several effects on the coastal dynamics (Soares et. al., 2007a). The Coastal Current is a dynamic help in plume transport along the continental shelf, depending only on the wind patterns that control the direction of plume propagation (Soares et. al., 2007b).

The region is also subject to ENSO cycles, although their magnitude is greater in the north of SAIS in comparison with the southern part. In South America, ENSO cycles are a periodic climate pattern characterized by two modes: warm (El Niño) and cool (La Niña) phases, with recurring cycles taking place between every two to seven years (Grimm et. al., 1998). Particularly in the southern region of Brazil, strong and consistent anomalies in precipitation can be associated with these events (Grimm et. al., 1998; 2000). Little is known, however, about how ENSO cycles affect

the Southwest Atlantic Shelf. García-Rodríguez et. al. (2014) analyzed changes in geochemical variables in the middle section of the La Plata River estuary during the 2009-2010 ENSO event. The authors realized that during the warm phase of the ENSO event, the flow of the river was 5 times greater than the average historical levels. Meanwhile, Berbery and Barros (2002) found that the historical maxima of the river flow during the year following the start of El Niño can triple the typical average flow of the river. However, according to Piola et. al. (2005), the effects of wind and precipitation anomalies tend to compensate for the increased flow, preventing anomalous extensions of northeast plumes associated with large flow events. Therefore, the discharge from the La Plata River spreads into the sea. Still on the effect of ENSO on the flow of the La Plata River, Dogliotti et. al. (2016) analyzed the spatio-temporal variability of turbidity in the region from 15 years of MODIS satellite data. The authors found a strong seasonal variability in the upper and middle estuaries, with high flow occurring from March to May and low turbidity from June to January. The influence of ENSO occurs at interannual time scales, showing an increase in turbidity when negative fluvial discharge anomalies occur, but this is not always related to La Niña events since these events are not the only drought predictions in the region. Ciotti et. al. (1995) stated that the amount of chlorophyll in the coastal region is directly related to the nutrients provided by the fluvial discharge. Therefore, extreme precipitation rates and different wind patterns suggest that ENSO events have an important impact on the variability of phytoplankton production, thus affecting biogeochemical cycles in the region of the SAIS.

Távora et. al. (2020) used a 17-year assessment of MODIS-aqua surface suspended sediments in the Patos Lagoon, in southern Brazil, and observed strong suspended particulate matter (SPM) interannual variability correlated with ENSO events. From TELEMAC-3D model simulations over five years, Bitencourt et. al. (2020) also observed the ENSO influence on high suspended sediment concentration (SSC) values throughout the Patos Lagoon on an interannual variability scale.

Although many studies have been conducted on the coastal plumes of the La Plata River and the Patos Lagoon, little is known about how these continental contributions actually affect the sediment dynamics and morphological features on the SAIS. Thus, this paper aims to fulfill this gap by answering two scientific questions: how big is the contribution of continental suspended sediment to the SAIS? And how does this suspended sediment behave when it reaches the inner shelf?

## Study Region

The study region is comprised between the latitude of 28° S (Santa Marta Cape) and 38°S (Mar Del Plata), corresponding to the central region of the SAS (Figure 1), which extends from Tierra del Fuego (55°S), to Cabo Frio (22°S) (Palma et. al., 2008).

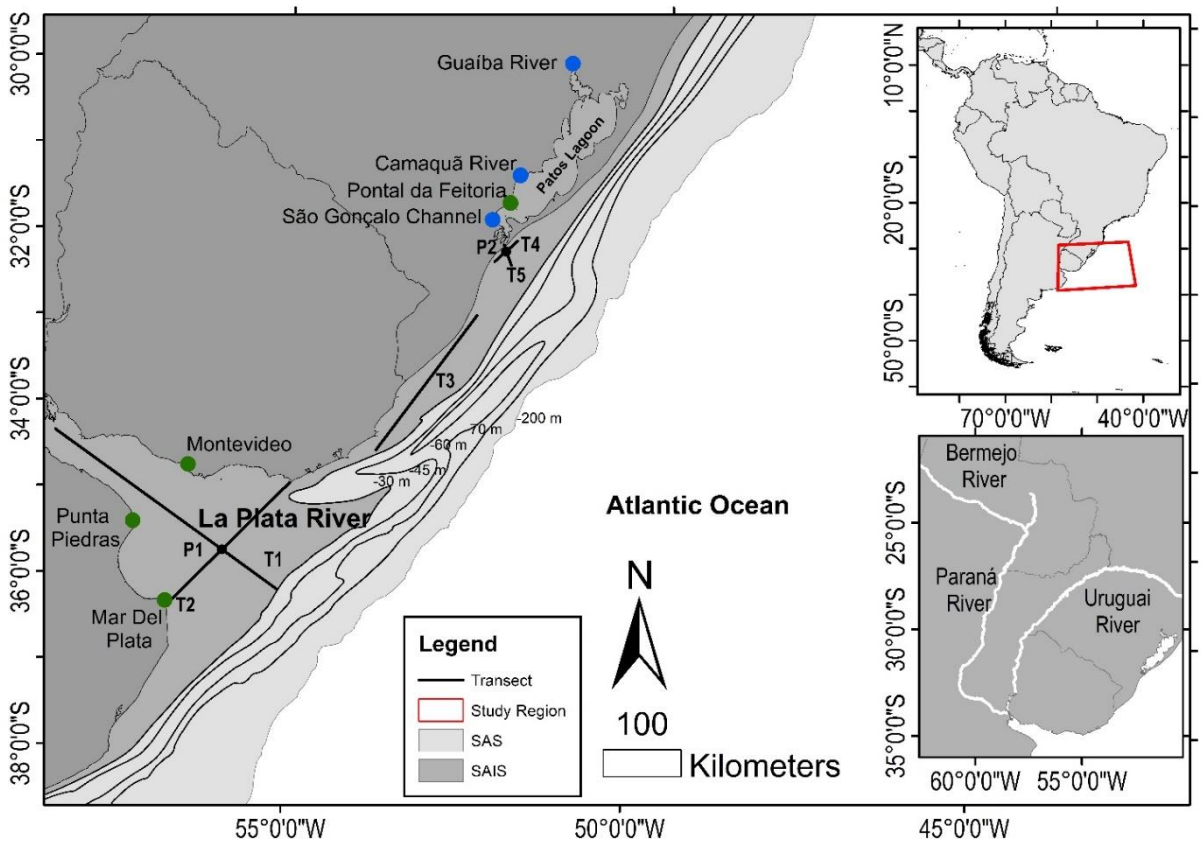


Figura 14 - Figure 1 - Artigo 1 -The study region defined between the latitudes of 28°S (Santa Marta Cape) and 38°S (Mar Del Plata). Blue dots represent the main effluents from the Patos Lagoon (Guaíba River, Camaquã River, and São Gonçalo Channel), green dots show important regions in the study area and black dots represent the points from where model results were extracted for the wavelet analysis (P1 and P2). T shows the transects where model results were extracted from (T1, T2, T3, T4, and T5) for empirical orthogonal function (EOF) analyses. The white lines represent the main effluents of the La Plata River (River Bermejo, River Paraná, and River Uruguay)

The Southwest Atlantic Inner Shelf (SAIS) is located inside the Southwest Atlantic Shelf (SAS) and it is the most important fishing area of the Brazilian coast (Haimovici et. al., 1989; Castello et. al., 1990). The region receives more than 95% of its discharge from the Paraná and Uruguay Rivers (Depetris and Paolini, 1991), and other tributaries reaching the southern coast of Brazil, such as the Patos-Mirim System, the estuarine complex of Laguna, and the Itajaí-Açu River.

The La Plata River is the second largest watershed in South America (3,170,000 $km^2$), extending from the subequatorial zone through to the tropics. The La Plata freshwater discharge is around 22,000 $m^3/s$ on annual average and peaks of discharge as high as 90,000 $m^3/s$ and as low as 8,000 $m^3/s$ can be observed during extreme conditions related to ENSO cycles (Berbery and Barros, 2002). It has an approximately 300 km long northwest to southeast-oriented funnel shape that narrows from 220 km at its mouth to 40 km at the upper end (Moreira et al., 2016), resulting in an estuarine area of 35,000 $km^2$.

The La Plata River estuary displays a variable geometry and bathymetry, resulting in highly complex river-estuary-ocean dynamics. Therefore, the estuarine region is classically divided into two parts, according to its geomorphology: inner-intermediate and outer regions (Framiñan et. al., 1996). These parts are separated by a topographical feature known as the Barra del Indio shoal (Fossati et. al., 2014), a shallow area that crosses the estuary between Punta Piedras and Montevideo, marking the seaward limit of which both the river cross-sectional area and depth increase and where the salinity front is located (Sepúlveda et. al., 2004). The region is characterized by a fluvial regime with tidal influence and no stratification. The outer region is formed by brackish waters of variable salinity influenced by tides, winds, and the contribution of freshwater from the river basin (Santoro et. al., 2016). Density in the outer estuary is controlled by salinity, whereas temperature exhibits a small horizontal gradient, even though interannual variability may be high (Guerrero et. al., 1997; Simionato et. al., 2010). Water stratification is controlled by the confluence of highly buoyant continental discharge advecting offshore, lying on denser shelf water that intrudes into the estuary as a topographically controlled salt wedge. This salt wedge is typically between 100 and 250 km long and defines a bottom salinity front over the Barra del Indio shoal following approximately the 10 m isobath (Guerreiro et. al., 1997). Forced by the prevailing winds (Simionato et. al., 2001) both surface and bottom salinity fronts show a seasonal cycle that largely modifies the salt wedge structure from spring-summer to autumn-winter (Guerreiro et. al., 1997). The high wind variability that characterizes the region (Simionato et. al., 2005) also forces significant variability on synoptic time scales in the estuarine variables (Meccia et. al., 2009).

The tidal regime is microtidal and dominated by the M2 component, followed by O1 component which is responsible for diurnal inequality (Fossati et. al., 2014; Santoro et. al., 2016). The tidal amplitude is greater along the Argentinean coast (order of 1 m), while is about 0.4 m along the Uruguayan coast. The meteorological tides are mainly generated in the Argentinean continental shelf and then propagate northward as trapped coastal waves until they reach the estuary (Santoro et. al., 2013). Currents at the estuary are controlled by the oceanic tide, reaching values close to

0.3 m/s at the bottom and 0.5 m/s at the surface, near Montevideo city (Fossati and Piedra-Cueva, 2013).

La Plata River discharges more than 160 million tons/year of suspended sediment into the South Atlantic Ocean, mainly carried by the Paraná River. The outer estuary and the adjacent continental shelf are covered with sand, while silty clays, clayey silts, and silts, are confined to the upper and middle portions of the estuary. The La Plata plume is advected alongshore towards the north, covering long distances and spreading along the coasts of Argentina, Uruguay and Brazil (Piola et. al., 2000; 2005).

The Patos Lagoon, located on the southernmost part of Brazil (between 30°S and 32°S), is the largest choked coastal lagoon in the world (Kjerfve, 1986), being 250 km long and 40 km wide and covering an area of 10.360 $km^2$. The lagoon is considered as a shallow system with a mean depth of 5 m and higher depths occurring in the estuarine channel. The latter is narrow (less than 1 km wide at the mouth) and deep (about 16 m) and connects the lagoon to the South Atlantic Ocean.

The Lagoon drains a drainage basin of approximately 201,626 $km^2$, consisting of the Guaíba, Camaquã Rivers and the São Gonçalo Channel as the main tributaries in the north, central and south part of the lagoon, respectively. The rivers have a midlatitude pattern with high discharge in late winter and early spring followed by low to moderate discharge through summer and autumn (Möller et. al., 2001). The mean annual freshwater contribution in the north of the Patos Lagoon is 2,000 $m^3/s$; seasonal variations are observed from 700 $m^3/s$ during summer (late December–March) up to 3,000 $m^3/s$ during spring (September–early December). Moller et. al. (1996) reported river discharge peaks of 12,000 and 25,000 $m^3/s$ during El Niño years and which impact the lagoon residence time (Fernandes et al., 2002). Meanwhile, the flow of the São Gonçalo Channel is controlled by gates that are only closed when the levels are above 1 m. Consequently, the discharge of freshwater from the upper part of the lagoon to the estuary is variable (700 to 3000 $m^3/s$), generally being more intense during winter and spring (Hartmann et. al., 1990).

Circulation in the Patos Lagoon is controlled by various mechanisms depending on the considered area: a combination of a local wind-driven set-up and set-down mechanism in the main lagoon, the non-local wind action in the estuarine and coastal regions and the river discharge in the north of the lagoon (Fernandes et. al., 2002; 2005; Moller et. al., 1996). The wind action dominates during periods of low to moderate river discharge (< 2,000 $m^3/s$) (Möller and Castaing, 1999). Möller et. al. (2001) demonstrated that the northeast wind causes a barotropic pressure

gradient towards the ocean because of the Ekman Transport acting at 90° to the wind direction, resulting in freshwater discharge into the continental shelf. In contrast, the southwest wind causes an increase in the water level at the coast, promoting a barotropic pressure gradient towards the continent and inhibiting the fluvial discharge from the Patos Lagoon estuary. This pattern does not occur during high river discharge periods (> 2,000 $m^3/s$) because the southwest wind effect is overcome by the river discharge. In this situation, the estuarine zone occurs in the adjacent coastal region (Möller & Castaing, 1999).

The tidal signal in the region is mixed (mainly diurnal), having a mean amplitude of 0.23 m (Moller et. al., 2001) and characterizing a microtidal system. The tidal effect is of secondary importance for the dynamics of the system, being restricted to the coastal region and to the estuarine portion of the Patos Lagoon. Fernandes et. al. (2004) demonstrated that the Patos Lagoon access channel acts like a filter damping the tidal signal as it moves up the estuary.

The morphological characteristics of the Patos Lagoon show a dominance of coarse sediment in the shallow areas and fine grains in the deeper ones, especially in the estuarine zone. The west margin of the Patos Lagoon is covered by medium to coarse sand (Martins et. al., 1987; Toldo, 1991), carried out mainly by the Camaquã River. At the east and north margins, sediment is composed of fine sand from the coastal-marine depositional system. Hartmann et. al. (1986) indicated that the average suspended sediment concentration (SSC) varies from 43 to 196 mg/L based on three years of sampling along the lagoon's main axis and at the mouth of the main tributaries. In a qualitative analysis of the suspended sediment, Hartmann et. al. (1986), reported that the region has a predominance of silt (>80%), followed by clay, and little sand (5%), indicating that the lagoon is a source of silt and clay for the adjacent coastal region. Calliari and Fachin (1993) mapped silty clay and clayey silt in the southern region of the Patos Lagoon mouth, between 15 and 17 m isobaths, but fine sediments can be found at up to 22 m depths. Calliari et. al. (2009) found a sediment accumulation rate of around 25 mm/year based on the 210Pb dating method.

Toldo et. al. (2006) estimated the short-term sedimentation rate for the Patos Lagoon based on data of 210Pb of surface deposits, defining the sedimentation rate as ranging from 3.5 to 8.3 mm/year. These values corroborate those presented by Ivanoff et. al. (2020) in the same study region. The authors estimated a sedimentation rate ranging from 7 mm/year, in the northern region of the lagoon, passing values around 4.4 to 5.5 mm/year in the central portion, up to values close to 4.8 mm/year in the southern region of the lagoon. As for the impact of ENSO cycles on the region, Ivanoff et. al. (2020) estimated that the sedimentation rate in the north cell of the Patos

Lagoon increases by 135% during El Niño years, while in the central and south regions it increases by 164% and 170%, respectively. In the estuarine region, this increase is around 262%.

The estuarine region occupies about 10% of the Patos Lagoon area and is characterized by an increase in cross section with distance from the mouth (Möller et. al., 2001). The lagoon and the estuary are separated by a morphological step formed by sandbanks situated around the region called Ponta da Feitoria (Figure 1). In addition to the contribution from the main lagoon, the São Gonçalo Channel is an important source of sediment to the Patos Lagoon estuary (Hartmann et. al., 1990; Oliveira et. al., 2015; 2019). The sedimentology of the estuarine area is more diverse than in the lagoon, presenting sand in the shallow banks and a combination of silt and clay in the deeper areas (Calliari et. al., 2009).

## Materials and methods

The behavior and variability of the suspended sediment in the SAIS was investigated using numerical simulations. Two hydrodynamic simulations with a duration of 730 days were carried out, with one simulation performed for the years 2005-2006, and another for 2008-2009 (Appendix A, Table A1). The choice of the analyzed periods is related to the ENSO influence over the region, where 2005-2006 is a neutral period (without the ENSO effect) and 2008-2009 is a period affected by La Niña (2008) and El Niño (2009). Details about the model set-up and the methodological steps developed in this work are presented in Appendix A.

## The Numerical Models

Hydrodynamic simulations were performed using the 3D model TELEMAC-3D, (www.opentelemac.org), developed by the "Laboratoire National d´Hydraulique et Environnement of the Electricité de France Company (EDF)". The model solves the Navier-Stokes equations considering the local variations in the free surface of the fluid, disregarding density variations in the mass conservation equation, and considering the Boussinesq and hydrostatic approximations for solving momentum equations (Hervouet, 2007).

The transport of suspended sediments is calculated with the TELEMAC-3D system using the SED-3D (V7P0) module, where equations are solved based on the finite element method, with fractional decomposition being performed in steps (Janin and Marcos, 1997). The suspended sediment is treated as an active tracer, but together with salinity and temperature, it can promote

fluctuations in the density field. To represent the cohesive effects on suspended sediment transportation, the settling velocity was calculated as a function of the sediment concentration, temperature, salinity and velocity gradient according to the Van Leussen formulation (Van Leussen, 1994), which was applied to this region by Marques et. al. (2010a; 2010b).

Cohesive suspended sediment transport occurs through the combination of advection and diffusion. In SEDI-3D, a 3D advection-diffusion equation is solved by considering the cohesive sediment particles moving at the same velocity as the fluid:

$$\frac{\partial C}{\partial t} + U_j \frac{\partial C}{\partial x_j} = \frac{\partial}{\partial x_j}\left(\frac{\upsilon_t}{\sigma_t}\frac{\partial C}{\partial x_j} + w_s C \delta_{ij}\right) \quad (1)$$

In this equation $U$ is the mean flow velocity (m/s), $t$ is the time (s), $x_j$ represents the components of the coordinate vector (m), $\upsilon_t$ is the eddy viscosity (m$^2$/s), $\sigma_t$ is the turbulent Prandtl-Schmidt number (i.e. the radio of $\upsilon_t$ to the eddy diffusivity of the sediment particles), $C$ is the sediment concentration (g/L) or (kg/m$^3$), $w_s$ is the representative mean settling velocity (m/s) and $\delta_{ij}$ is the Kronecker delta.

At the interface between the water column and the bed layer, erosion processes take place because of the bottom shear stress induced by the flow. The erosion flux is computed with the Partheniades formula – Equation 2 – (Partheniades, 1965). The erosion flux is the product of an erosion rate multiplied with a probability factor as a function of the shear stress in excess of a critical erosion shear stress.

$$E = \begin{cases} M\left(\frac{\tau_b}{\tau_{ce}} - 1\right) & if\ \tau_b > \tau_{ce} \\ 0 & otherwise \end{cases} \quad (2)$$

Here, $M$ is the Krone-Partheniades erosion constant (kg.m$^{-2}$.s$^{-1}$), $\tau_b$ is the bed shear stress and $\tau_{ce}$ the critical bed shear stress for erosion. So, erosion only occurs when the bed shear stress is higher than the critical bed shear stress for erosion set by the user. The erosion constant $M$ determines the intensity of the erosion. A larger value will mean more erosion, if erosion occurs. The bed shear stress is given by:

$$\tau_b = \rho_w u_* |u_*| \quad (3)$$

Where, $\rho_w$ is the density of the water and $u_*$ is the friction velocity. In SEDI-3D, a quadratic friction law is used with a drag coefficient $C_D$ to computed $\tau_b$ in a rough regime. When a Nikuradse formula is used, the equation looks as follows:

$$\tau_b = \frac{1}{2}\rho_w C_D \overline{U}|\overline{U}| \quad (4)$$

With:

$$C_D = 7.831 ln\left(12\frac{h}{k_s}\right) \quad (5)$$

Here, $\overline{U}$ is the depth-averaged velocity (which also calculated is SEDI-3D), $k_s$ is the roughness size and $h$ is the water depth. After determining the shear stress, the shear velocity is calculated and is then imposed at the bottom as a boundary condition for solving the momentum conservation equations of the flows. The empirical depositional law from Krone is implemented in SEDI-3D to estimate sediment deposition. Here the deposition flux is approximated by the product of local sediment concentration with the settling velocity, multiplied with a deposition probability:

$$D = \begin{cases} w_s C\left(1 - \frac{\tau_b}{\tau_{cd}}\right) & if\ \tau_b > \tau_{cd} \\ 0 & otherwise \end{cases} \quad (6)$$

Where, $\tau_{cd}$ is the critical shear stress for mud deposition, $w_s$ is the settling velocity (m/s), and $C$ is SSC (g/L) or (kg/m$^3$). If the bottom shear stress is smaller than the critical bottom shear for deposition, the sediment is settling.

The bed evolution in SEDI-3D is calculated with the Exner equation (Exner, 1925):

$$(1-\lambda)\frac{\partial_{z_b}}{\partial t} + (E - D) = 0 \quad (7)$$

Where, $\lambda$ is the bed porosity and $z_b$ is the bed level.

In this version of SEDI-3D only one fraction of cohesive sediment can be modelled. Based on the main suspended sediment grain size observed by Toldo et. al. (2006), Fossati and Cuevas (2013), and Moreira and Simionato (2019) for the study region, a characteristic silt particle diameter

of 50 µm was chosen. The constant settling velocity of 0.5 mm/s was chosen according to the grain size and based on Van Leussen et. al. (1994), Winterwerp et. al. (2002) and Lee et. al. (2011). The sediment density was set to 2650 kg/m$^3$. Flocculation and hindered settling were not considered. Two initially empty bed layers were chosen. If mud was deposited in these layers, the mud layer density was set to 1500 kg/m$^3$. The critical shear stress for erosion was set to 0.15 Pa, the critical shear stress for deposition was 0.05 Pa, and the Partheniades coefficient was 2.0e$^{-6}$ kg.m$^{-2}$.s$^{-1}$. These three parameters are calibration parameters regarding suspended sediment transport.

**Domain and Numerical Mesh**

The domain defined for this work (Figure 2) extends from latitudes 28°S (Cabo de Santa Marta - SC) to 38° S (Mar del Plata) and longitudes of 49°W to 52°W, reaching depths of approximately 300 m, it data from different sources was combined to acquire for the best representation of the bathymetric characteristics of the La Plata River, the Patos Lagoon and its estuary and the adjacent coastal region.

For the estuarine region, the lagoon and the northern coast, bathymetric data extracted from the nautical charts of the Diretoria de Hidrografia e Navegação (DHN) of the Brazilian Navy. In order to improve the quality of bathymetric information in the main access channel to the Port of Rio Grande, data from a survey carried out in 2006 and 2010 by the port authorities and complementary data from a bathymetric survey carried out by the Brazilian Navy as part of the Brazilian Continental Shelf Survey Project (LEPLAC) were used. The bathymetry of the La Plata River and its adjacent coastal region was interpolated with data from the Argentinean Navy, and complemented with data from Smith and Sandwell (1997) for depths greater than 200 m (Palmas et. al., 2008).

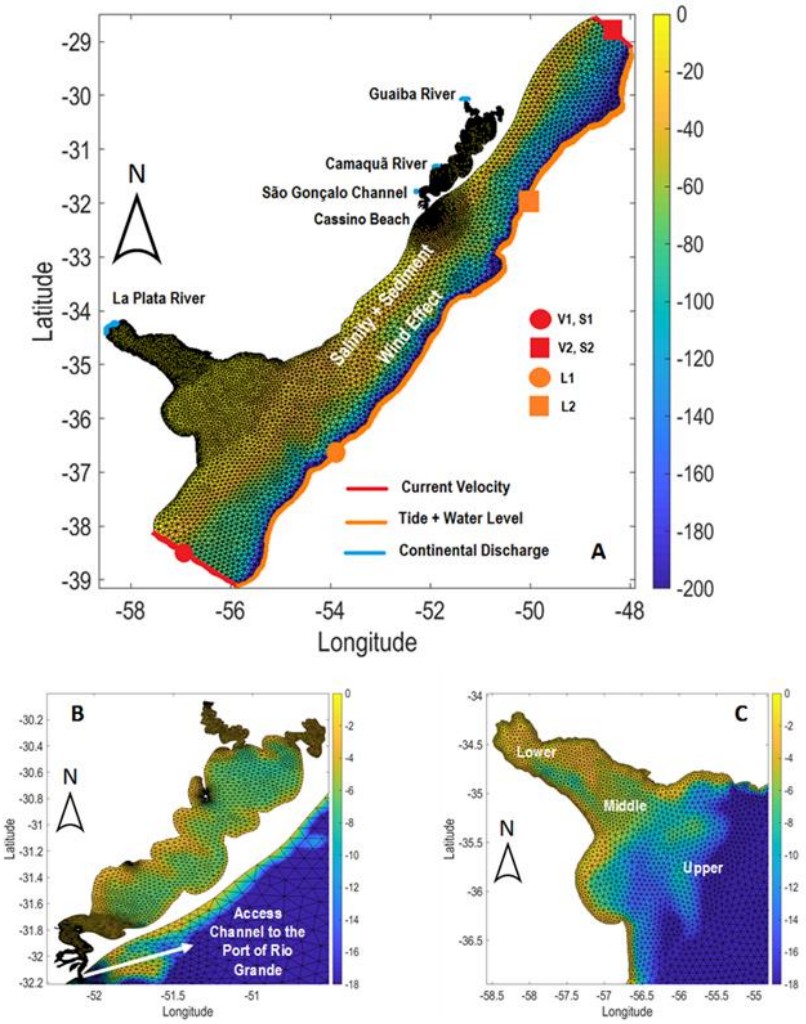


Figura 15 - Figure 2 - Artigo 1 - Computational domain and numerical mesh used for the simulations. (A) Initial and boundary conditions prescribed in the model. The points where the time series of salinity (S1 and S2), current velocity (V1 and V2), and water level (L1 and L2) prescribed as boundary conditions were extracted are also shown. (B) Zoom view of the Patos Lagoon mesh and (C) that of the La Plata River mesh.

The numerical domain was initially discretized with triangles measuring 10 km at the oceanic edge, 6 km in the Inner Platform, 3 km in the coastal region and 1.5 km at the mouth of the La Plata River; near the mouth of the Patos Lagoon the triangle edges varied between 130 m to 20 m. The resulting 2D unstructured mesh (Figure 2) has 18275 nodes and 33296 triangular elements, discretized vertically with 11 sigma levels, for which the equations were solved.

**Initial and Boundary Conditions**

Together with initial conditions, the model needs boundary conditions to better represent the dynamics of the region. The numerical mesh (Figure 2A) has 7 open boundaries: the continental boundaries in the north of the Rio de La Plata and the Patos Lagoon, the oceanic boundary, the coastal north and south boundaries, and the surface boundary. Details about the data used as initial and boundary conditions are presented in Appendix B.

Initial salinity conditions (Appendix B, Figure B1), a constant water level of 0.4 m and an initial current velocity of 0.5 m/s were initially prescribed throughout the domain in the hydrodynamic module (TELEMAC3D).

In the oceanic boundary, tide and constant mean water level (eastern boundary), current velocity (north and south boundaries) and salinity data were prescribed (Figure 2A and Appendix B, Figure B1). The tide was calculated by the inverse solution of Laplace's equations (Edgbert et. al., 1994), and 33 harmonic components of the tide were used to generate a reliable estimate of the sea level behaviour (Appendix B, Figure B1). Current velocity was estimated using regional tidal current velocity fields, obtained with the OSU Tidal Inversion Software-OTIS (Edgbert and Erofeeva, 2002), internally coupled in TELEMAC. Salinity fields were obtained from HYCOM + NCODA Global (Hybrid Coordinate Ocean Model, https://hycom.org/), with temporal and spatial resolutions of 3 h and 0.08°, respectively.

The continental boundary conditions for the Patos Lagoon correspond to daily river discharge data (Appendix B, Figure B3) from the Guaíba and Camaquã Rivers, provided by the Brazilian National Water Agency (ANA – www.hidroweb.ana.gov.br). For the third tributary (Canal São Gonçalo), there is no systematic discharge time series and the water level data obtained from the Mirim Lagoon Agency (ALM, https://wp.ufpel.edu.br/alm/) was converted into daily freshwater discharges by Oliveira et. al. (2015) using a rating curve method. For the La Plata River, daily river discharge data were provided by the Argentine Naval Hydrography Service (https://argentina.gob.ar/armada). For the suspended sediment fluxes from the rivers, there are no available measurements to build realistic time series. Riverine SSC was therefore considered constant in the model, so sediment fluxes are only dependent on the river flow. Values assigned for SSC were 200 mg/L, 100 mg/L, 150 mg/L for the Guaíba River, Camaquã River and São Gonçalo Channel, respectively (Marques et. al., 2010), and 230 mg/L for the La Plata River (Moreira and Simionato, 2019). The suspended sediment class used in this study was fine silt (Marques et. al., 2010b).

Wind data from the European Centre for Medium-Range Weather Forecasts (ECMWF), ERA Interim (http://www.ecmwf.int) was prescribed at the surface boundary, with a 6 h temporal scale and 0.75° spatial resolution, interpolated in time and space for every point of the numerical mesh (Appendix B, Figures B4 and B5).

**Model Calibration and Validation**

The TELEMAC-3D model has been extensively calibrated and validated for the Patos Lagoon (Fernandes et. al., 2001; 2002; 2005; 2007; Marques et. al., 2009; 2010a; 2010b; Silva et. al., 2015, Oliveira et. al., 2019). In this study, the model domain has been significantly extended (Figures 1 and 2) and complementary calibration and validation exercises were carried out. The model's ability to reproduce measured data was evaluated based on statistical parameters such as those presented by Fernandes et. al.(2001), Marques et. al., (2009) and Lisboa and Fernandes, (2015) (Appendix C).

In the hydrodynamic calibration exercises, current velocity, direction and salinity data, from the 22nd of October to the 30th of November of 2006 and from the 15th of October to the 19th of November of 2011 were collected at the coast using an ADPC (Acoustic Doppler Current Profiler) model Sontek Argonalta 1000 kHz and a CTD (Conductivity Temperature Depth) installed in the access channel of the Port of Rio Grande, respectively. Free surface elevation data from the 16th of May to the 24th of October of 2005, and from the 19th of March to the 31st of August of 2010 obtained in the Rio de La Plata navigation channel as part of the FREPLATA-IFREMER project were also used.

In the first stage of the calibration exercises, different values of specific physical parameters were tested. Because the dynamics of the region are strongly affected by the wind, the first parameter investigated was the Wind Influence Coefficient, with values varying from $10^{-4}$ to $10^{-6}$ (the higher the Wind Influence Coefficient, the strongest the wind influence). Other important physical parameters applied in the calibration exercises were a time step of 60 s, a Coriolis coefficient of -7.70735 x $10^{-5}$ N.m-1.s-1, a Smagorinsky in the horizontal turbulence model (30 for salinity and 1.e10-4 for sediment), a mixing length (Prandlt) in the vertical turbulence model (1.E$10^{-6}$) and Manning as the law of bottom friction (0.02 s/$m^{1/3}$). The best model results were obtained with the Wind Influence Coefficient equal to 3x$10^{-6}$ when comparing measured and calculated current velocity at the surface (Figure 3A) and at the bottom (Figure 3B) in the access channel to the Port of Rio Grande. In this calibration exercise, the values found were considered excellent

(RMAE = 0.16 and 0.18) according to the statistical classification Waltra et. al. (2001) and Sutherland et. al. (2004a; 2004b).

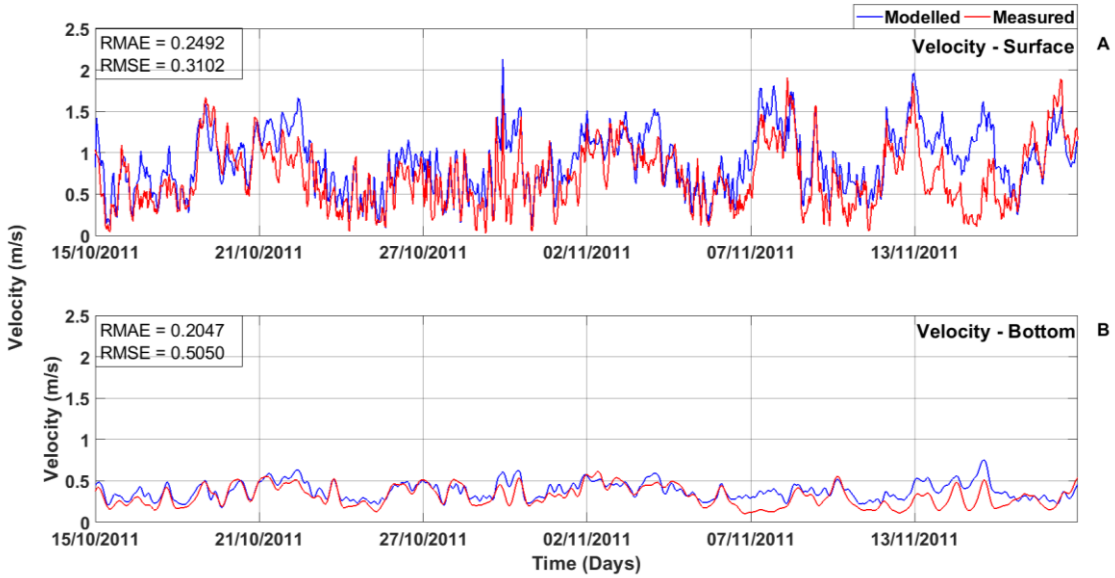


Figura 16 - Figure 3 - Artigo1- Comparison between measured and calculated time series of current velocity (A) at the surface and (B) at the bottom of the access channel to the Port of Rio Grande (see Figure 2B for location).

After defining the adequate Wind Influence Coefficient ($3x10^{-6}$) for the region, further calibrations were carried out varying the horizontal (Smagorinsky, K-Epsilon) and vertical (Tsanis, Prandlt and K-Epsilon) turbulence models, as well as the bottom friction laws (Manning and Nikuradse), as shown in the calibration exercises for the free surface elevation at Cassino Beach and Rio La Plata, in Appendix D. The best results were achieved for Test 10, with RMAE of 0.15 and 0.18 for Cassino Beach (Figure 4A) and Rio de La Plata (Figure 4B), respectively; these values are classified as excellent according to Walstra et. al. (2001). Thus, the best set of physical parameters was defined as a combination of the Manning law of bottom friction (friction coefficient= 0.02 s/m1/3), the Smagorinsky horizontal turbulence model (30 for salinity and $1.E10^{-4}$ for Sediment) and the mixture length (Prandlt) vertical turbulence model ($1.E10^{-6}$).

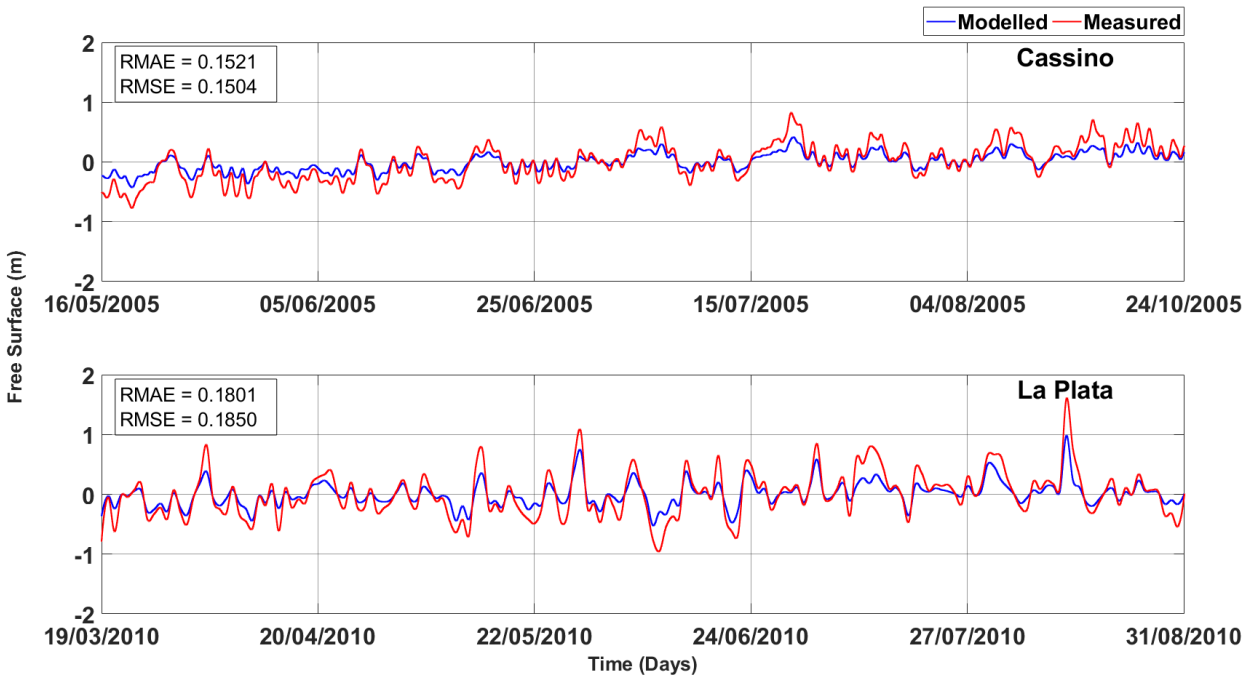


Figura 17 - Figure 4 - Artigo 1 - Comparison between the measured and calculated time series of free surface elevation at (A) Cassino Beach and (B) Rio La Plata.

After defining the best set of physical parameters for the hydrodynamic model, further validation exercises were carried out for the period between the 22nd of October to the 30th of November of 2006, and the model's performance for reproducing salinity and current velocity was evaluated (Figures 5A and 5B). The model's performance for simulating salinity at the surface and near the bottom of the Patos Lagoon estuary was classified as good according to Walstra et. al. (2001), with RMAE of 0.24 and 0.40, respectively. The RMSE values ranged from 5.68 to 9.06 psu. Considering the measured and calculated current velocity time series, the model's capacity was also classified as excellent according to Walstra et. al. (2001), with RMAE of 0.16 and 0.18 at the surface (Figure 5A) and bottom (Figure 5B), respectively. RMSE values ranged from 0.16 to 0.37 m/s. An overall analysis of the calibration and validation exercises indicates that the TELEMAC Model is an adequate tool for simulating the hydrodynamics of the domain.

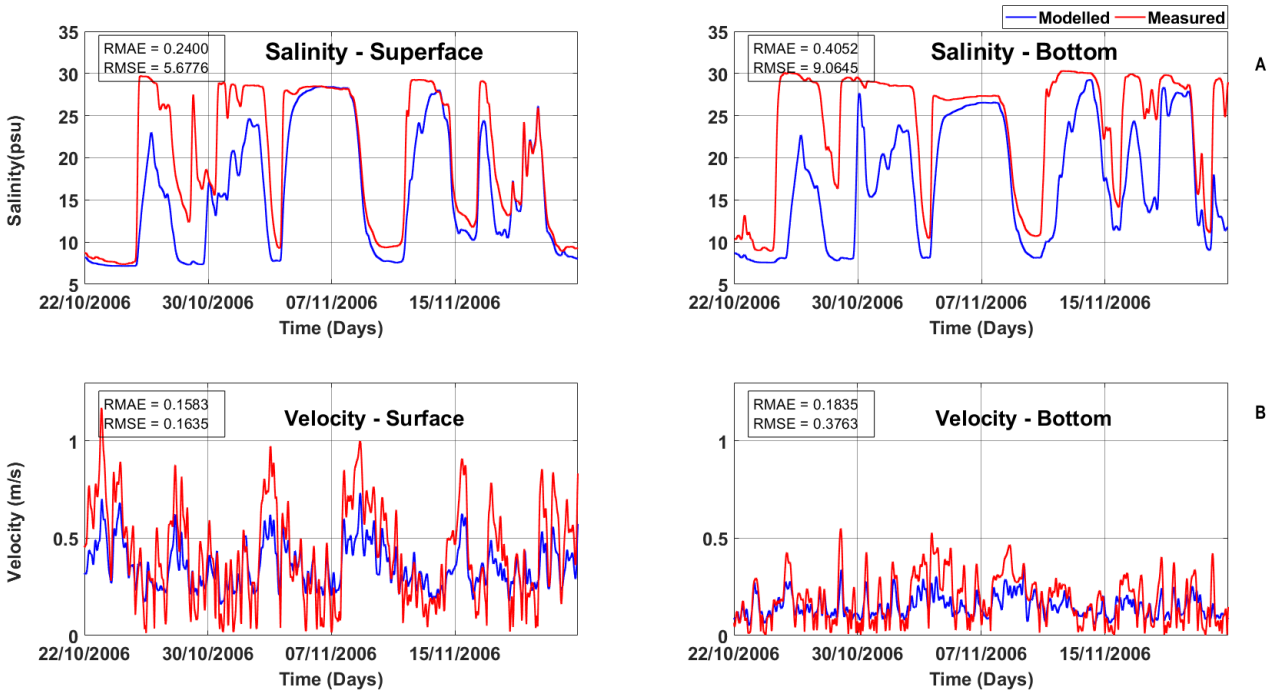


Figura 18 - Figure 5 - Artigo 1 - Comparison between the measured (red line) and calculated (blue line) salinity and current velocity time series at (A) the surface and (B) the bottom.

For the validation of calculated SSC, data from Rio de La Plata between the 26th of November of 2009 and the 16th of December of 2010 (FREPLATA-IFREMER Project) were used. Details about data acquisition procedures were described by Fossati et. al. (2014). Figure 6 shows the temporal evolution of the calculated and measured SSC in the lower, middle and upper Rio de La Plata estuary, resulting in RMSE values ranging from 14.05 to 15.53 mg/L and a RMAE = 0.21, at the limit between the classification of an excellent and a good reproduction (Walstra et. al., 2001).

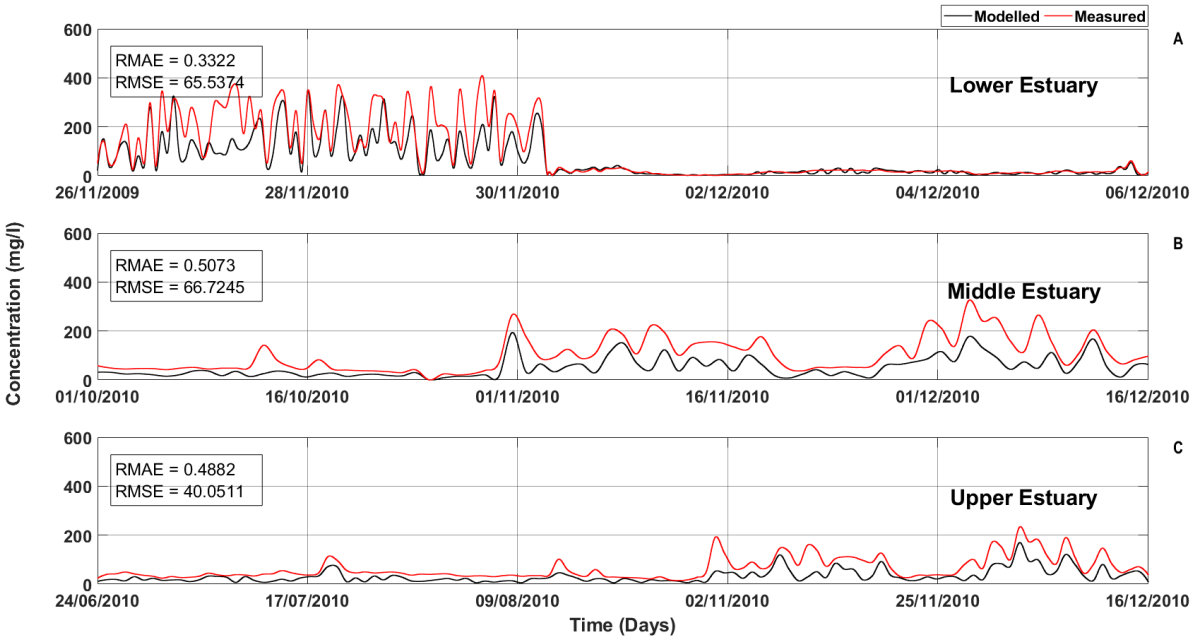


Figura 19 - Figure 6 - Artigo 1 - Comparison between the calculated suspended sediment concentration (blue line) and the measured data (red line) in (A) the lower, (B) middle and (C) upper estuary in Rio de La Plata River, between the 24th of June to the 16th of December, 2010.

Due to the lack of observational SSC data for the calibration of the numerical model in southern Brazil, an alternative methodology based on remote sensing products for the region were used. Three LandSat 5 images from the American Space Agency (NASA) (https://earthexplorer.usgs.gov/) were used (6th of February, 2008; 3rd of October, 2008; 17th of September, 2008), and processed according to Peixoto et. al. (2018) to obtain products with a 30 m spatial resolution for further comparison with calculated maps of surface SSC in two profiles (Figure 7).

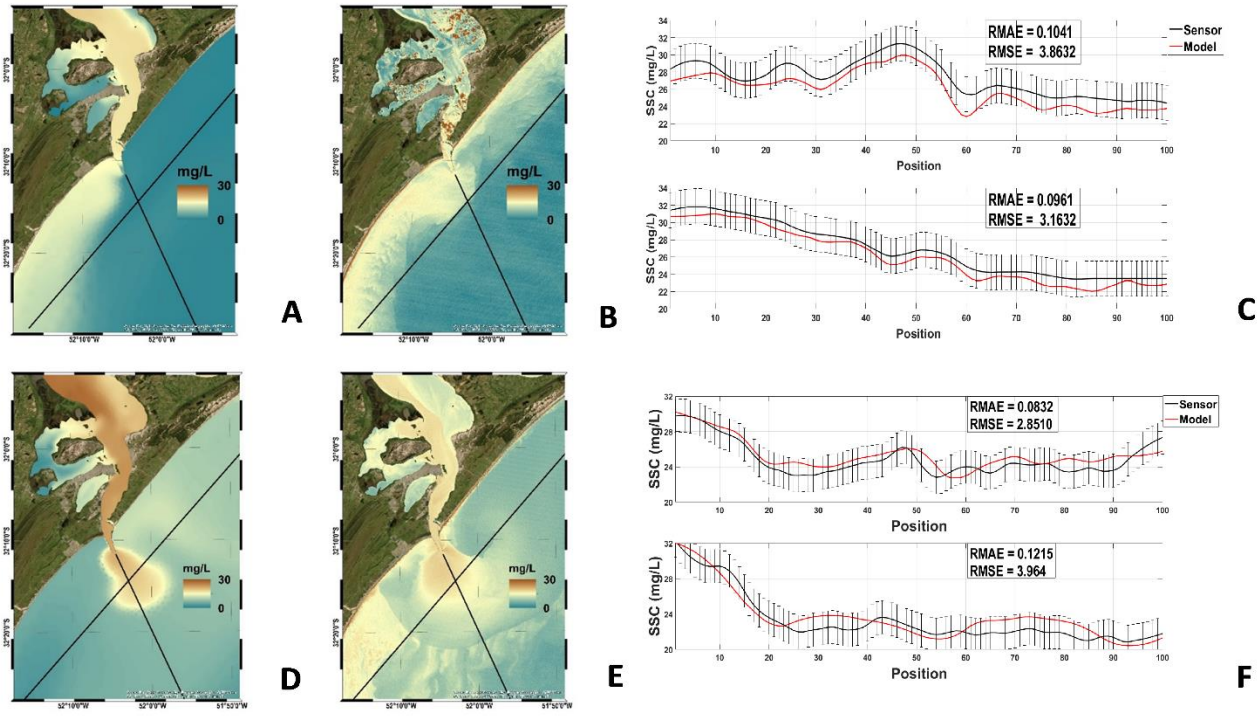


Figura 20 - Figure 7 - Artigo 1 - Left panels: Suspended sediment concentrations (SSC) at the surface obtained with the numerical model (A, D) and from remote sensing (B, D) on the 6th of February, 2008 (top) and the 17th of September, 2008 (bottom), respectively. Right panels: SSC at the surface extracted from the respective longitudinal (top panels) and transversal (bottom panels) profiles (C, F).

A comparison between the SSC calculated by the numerical model and information from remote sensing indicates that the model can reproduce some features of the Patos Lagoon coastal plume such as its orientation and spreading. Furthermore, the profiles selected for comparison (Figures 7C and 7F) indicate that numerical and remote sensing information is as similar, with RMSE values of 3.96 and 2.85 mg/L for the alongshore, and 3.16 and 3.86 mg/L for cross shore profiles (Figure 7C and 7F).

**Time series analysis**

Results from the numerical experiments indicate the contribution of the Patos Lagoon and Rio de Plata coastal plumes to the South Atlantic Inner Shelf. The analysis of their spatial and temporal variability in distinct regions of the domain, however, is not straightforward and depends on the scale of the SSC. This regional variability can be accessed using the empirical orthogonal function (EOF) analysis, which provides a compact description of the spatial and temporal variability of simulated data series in terms of statistic modes, where most of the variance of the spatially

distributed series can be observed in the first few orthogonal functions (Emery and Thomson, 1998). Knowing the regions that the coastal plumes are located in during the majority of the time is essential for identifying potential regions where the fine sediments transported via river discharge could be initially deposited after reaching the coastal region.

The spatial and temporal variability of SSC calculated for the domain with the numerical model was analyzed based on the first three EOF analyses for the neutral period (2005-2006) and for the period affected by an ENSO cycle (2008-2009). Three spatial representations were considered: 1) a horizontal plan; 2) longitudinal and transversal vertical transects at the mouth of the Rio de La Plata; and 3) longitudinal and transversal vertical transects at the mouth of the Patos Lagoon.

A wavelet analysis (continuous wavelet transform), regarded as a better option for dynamic analysis (Farge, 1992), was applied to this study to evaluate the spatial and temporal variability of SSC. This wavelet spectrum (or local energy cross-spectrum) provides energy variations along a frequency-time axis, which enables the determination of the dominant modes of variability and how those modes vary in time (Torrence & Compo, 1998). The contour line (dashed lines) enclosing regions is indicated to a 95% confidence level to the correlation between the time series varying in both space and time. For the global spectrum, the influence of the analyzed variable is only representative if power values are greater than the 95% confidence level (dashed line). The choice of mother-wavelets (or wavelets function) is essential for adequate results (Jalón-Rojas et. al., 2016). Thus, for the present study the Mexican hat (for higher frequencies – seasonal, annual, and interannual time scales) mother-wavelets were selected to analyses river discharge relations with SSC, while the Morlet wavelet was applied to analyses wind relations with SSC, as mentioned by Marques et. al. (2014), Oliveira et. al. (2015) and Costi et. al. (2018).

## Results

### Distribution of the Patos Lagoon and La Plata River Plumes in the South Atlantic Inner Shelf

The results of SIM1 (Appendix A – Table A1) show the simultaneous behavior of the Patos Lagoon and La Plata River plumes in winter and summer (Figure 8). During the winter of the neutral period (Figure 8A), both plumes are spread on the inner shelf, with the plume of the Patos Lagoon moving south and that of the La Plata River to the north, reaching a latitude of 30ºS. In this case, SSC values are continuously high (> 10 mg/L) along the coast between the two outlets. Due to the

large difference in fluvial discharge values between the two estuaries, it was noted that the plume of the La Plata River penetrates the Patos Lagoon estuary, near the entrance. The results still show that the La Plata plume is dense enough to merge with or even dominate over the Patos Lagoon plume during the southern winter. In summer (Figure 8C), the predominance of northeast winds and the lower continental discharge associated with the drier season produce less spreading of the two plumes on the inner shelf, and their meeting does not seem to happen, since a SSC minimum (1 mg/L) is observed close to the coast, between two more concentrated areas close to the two outlets. During the period of influence of the ENSO cycle (Figures 8B and 8D), the SSC values did not change much. The differences were more due to the displacement of the plume, which reached shorter distances, both along the coast and along the ocean, characterizing a more coastal plume when compared to the previous (neutral) period.

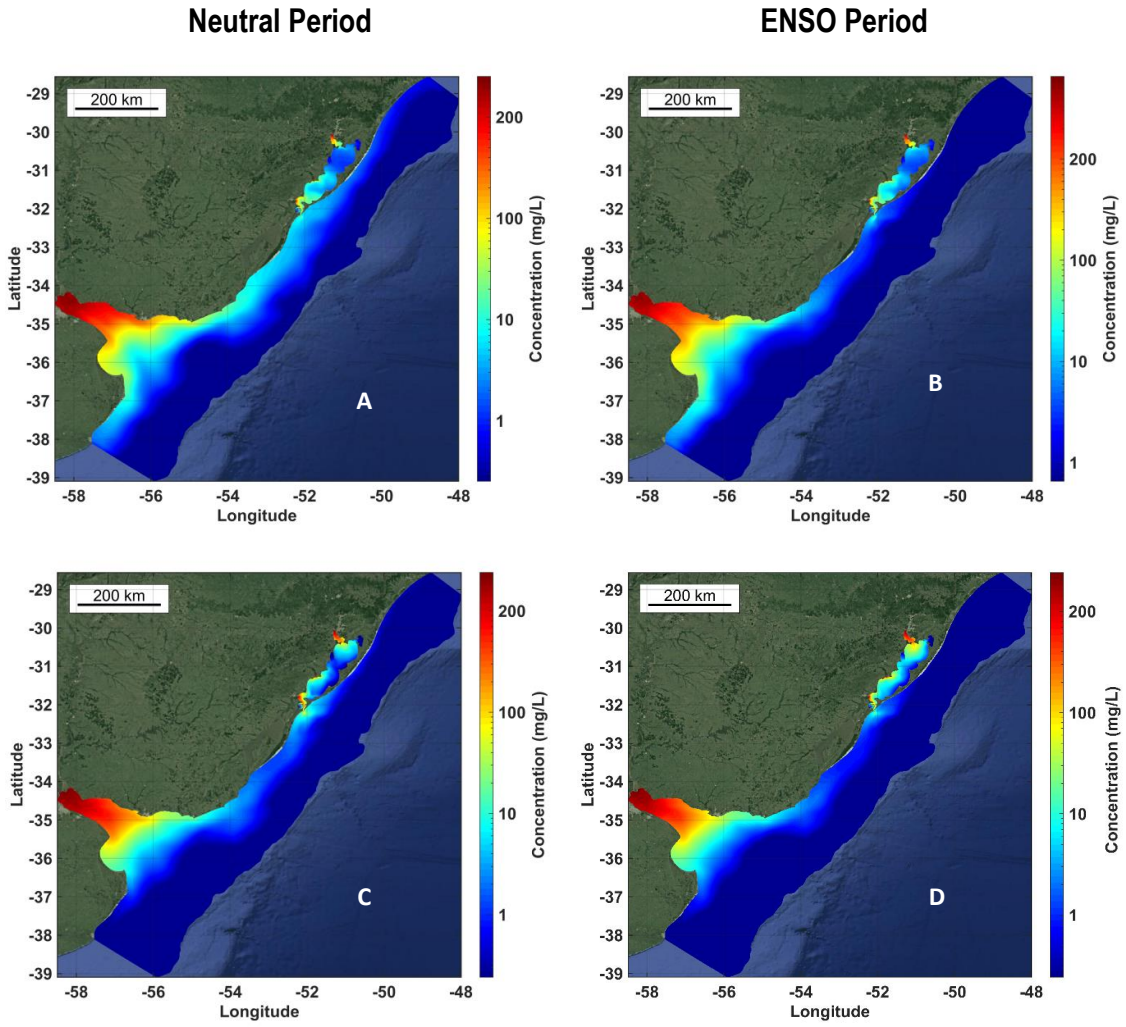


Figura 21 - Figure 8 - Artigo 1 - Seasonal average suspended sediment concentrations (SSC) for the study region during winter (A) and summer (C) in the neutral period (2005-2006), and during winter (B) and summer (D) in the period experienced ENSO conditions (2008-2009).

Figure 9 shows the average SSC and the normal and transverse velocities calculated by the model along the water column for transverse transects across the La Plata River (T2) and the Patos Lagoon (T4) mouths during the simulated periods (SIM1 and SIM2). The results indicate that the coastal plumes of the La Plata River and the Patos Lagoon exhibit different behaviors. Under neutral conditions, the La Plata River (Figures 9A and 9B) assumes a homopycnal flow pattern, with uniform SSC over the entire water column, longitudinal velocities indicating residual outflow (red tones) and higher SSC close to the margins towards the coastal region (reaching up to 200 mg/L).The Patos Lagoon (Figures 9C and 9D) shows a larger SSC vertical gradient, where the highest values are concentrated in the center of the transect and near the surface, assuming a characteristic of hypopycnal plume with positive buoyancy (Figure 9C). The residual flow chart (Figure 9D) shows residual outflow over the water column in the central part of the transect, in line with the lagoon outlet, while inflow is observed at the north and the south of the transect, with higher valuer in the south. During the period affected by the ENSO cycle, these patterns are maintained in both transects (Figures 9E to 9H), with small differences with the neutral period. In the region of La Plata, an increase in the suspended sediment concentration and a weakening of the continental discharge are observed. On the other hand, in Patos Lagoon, there is a noticeable decrease in suspended sediment concentration and, as La Plata, a weakening in the residual flow are observed due to the weaker continental contributions resulting from the predominant La Niña event.

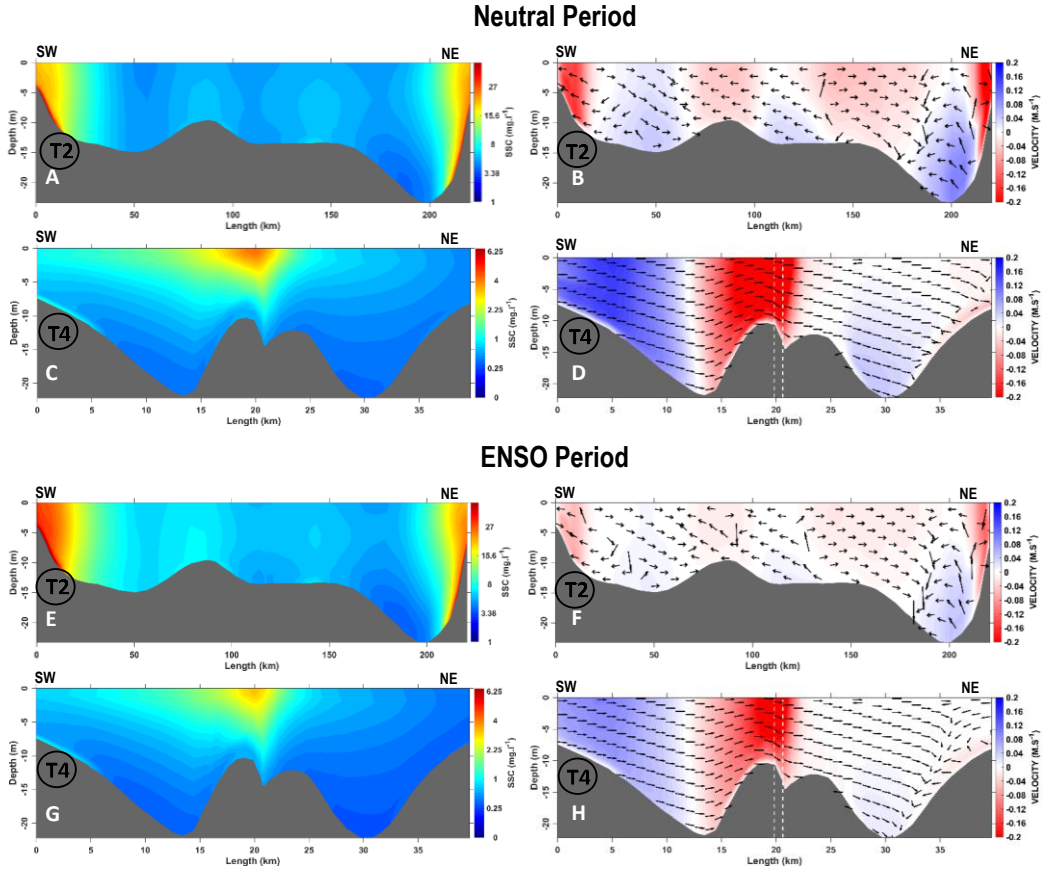


Figura 22 - Figure 9 - Artigo 1 - Average suspended sediment concentrations (SSC) (left column) and their averaged normal velocities (red represents outflow and blue is inflow) and the transversal velocity components (vectors; right column) along transects made across the La Plata River (T2) and the Patos Lagoon (T4), respectively, during the neutral period (2005-2006) and the period influenced by the ENSO cycle (2008-2009). The white dotted line indicates the position of the Patos Lagoon mouth. The color scale for SSC has not been standardised for easy viewing, and for the La Plata River, the red colour indicates sediment concentrations ranging between 50 and 200 mg/L.

As a way of quantifying how much suspended sediment the La Plata River and the Patos Lagoon export to the adjacent inner shelf, the section-averaged suspended matter flux was calculated along the transects T2 and T4 (Figure 10), based on the average SSC and the normal velocity component in the cross-section (Figure 9).

The results of Figure 10C indicate the predominance of a negative mass flux in the Patos Lagoon during the neutral period, showing that the region exports suspended sediment to the coastal region during most of the analyzed period. The highest peaks are observed between July and December of 2005 when the Patos Lagoon exports $3.0 \times 10^4$ tons/day of suspended sediment to the inner shelf. The time series of the cumulative mass flux of suspended sediment in the cross-section indicates that the Patos Lagoon exported $2.5 \times 10^7$ tons of suspended sediment during the

years 2005-2006 and presented an average annual flow of 1.25x10$^7$ tons/year. In the period under the influence of the ENSO cycle (Figure 10D), predominantly La Niña, the export pattern of suspended sediment from the Patos Lagoon remained the same, but with less accumulative mass flux during the period (1.0x10$^7$ tons/year) and, consequently, less annual flow (2.2x10$^4$ tons/day). However, a strong ebbing event at the end of 2009 due to an El Niño event raised the suspended sediment flux into the platform to 4.5x10$^4$ tons/day, generating an accumulative mass flux of 2.7 x10$^7$ tons of suspended sediment exported in that period, which results in an annual rate of 1.35 x10$^7$ tons/year.

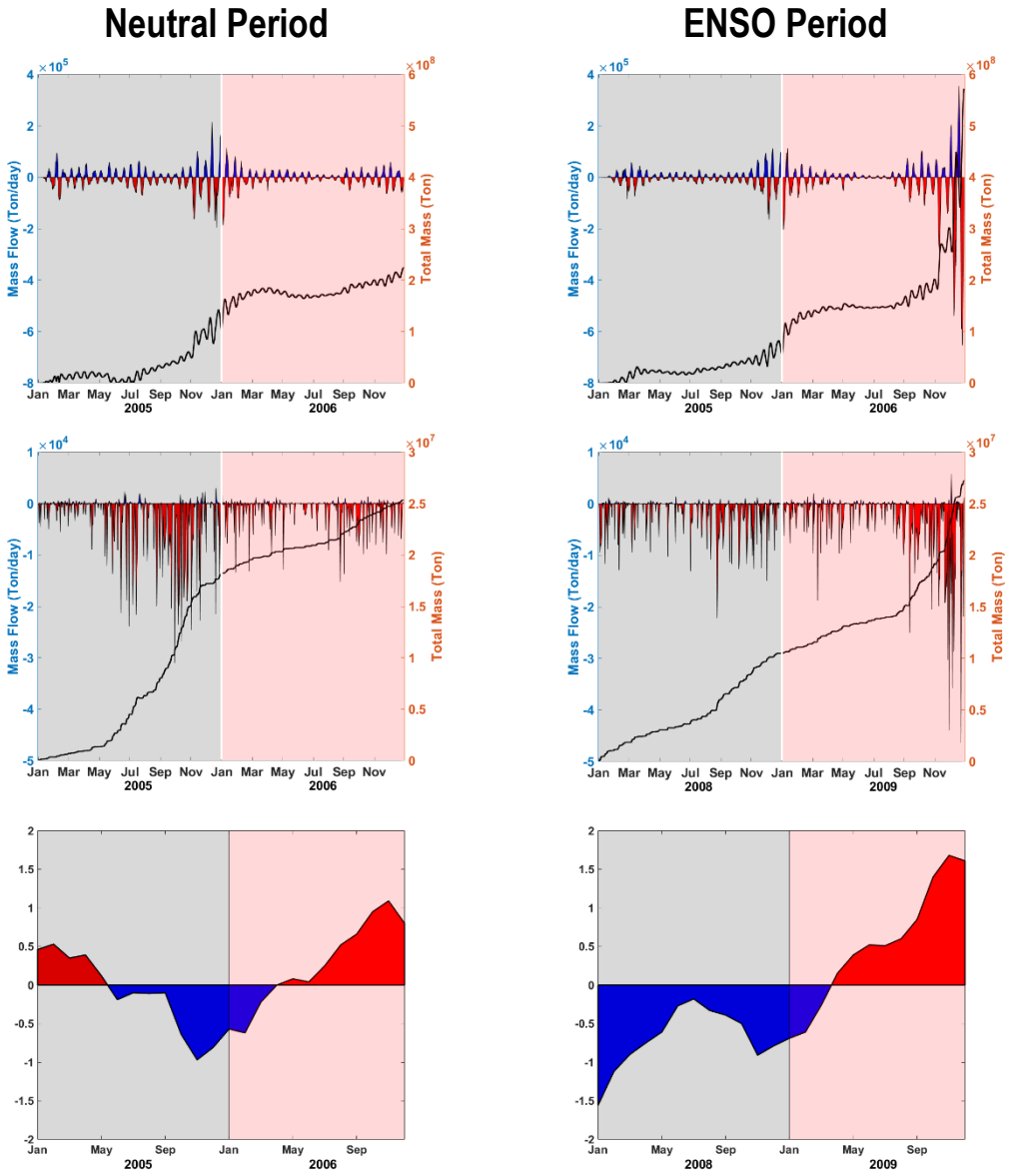


Figura 23 - Figure 10 - Artigo 1 - Mass flux (red indicates export and blue import) of suspended sediment and time series of the cumulative mass flux into the cross-section in the La Plata River

mouth (T4) (left column) during (A) a neutral period (2005-2006) and (B) a period under the influence of the ENSO cycle (2008-2009), and in the cross-section of the Patos Lagoon (T2) (right column) during (C) a neutral period (2005-2006) and (D) a period under the influence of the ENSO cycle (2008-2009).

Figures 10A and 10B present the same analysis for the cross-section at the La Plata River mouth (Figure 1), where a synoptic-scale modulation can be observed promoting the alternation between suspended sediment export and import. The largest exports of suspended sediment occurred at the end of 2005 and the beginning of 2006 (summer in the Southern Hemisphere). During this period, the La Plata River exported a maximum flux of $2x10^5$ tons/day of suspended sediment to the inner shelf. In contrast to what happened in the Patos Lagoon, in the La Plata River, periods of positive mass flux are significant for the region, with a suspended sediment import flux of $2.5x10^5$ tons/day at the end of 2005 and early 2006 (summer in the Southern Hemisphere), approximately ten times greater than the flux found for the Patos Lagoon. The accumulative mass flux of suspended sediment suggests that the La Plata River exported $2.3x10^8$ tons of suspended sediment during the years 2005-2006, with an annual average flux of $1.2x10^8$ tons/year. The results for the period subjected to the ENSO cycle (Figure 10B) show that similarly to the Patos Lagoon, the La Plata River maintained the pattern of mass flux behavior during this period and maintained lower concentrations of suspended sediment until the moment that the El Niño event began (October 2009). As of this moment, the mass flux underwent a significant increase reaching $5.8x10^8$ tons/day at the end of 2009. As a result, the accumulative mass flux reached $6.0x10^5$ tons/day, and the annual integrated mass flux was $3.0x10^8$ tons/year.

**Spatial Variability of Coastal Plumes**

The EOF analyses of the entire studied domain presented in this article resulted in a map depicting the spatial variability of the coastal plumes of the La Plata River and the Patos Lagoon on the South Atlantic Inner Shelf (Figure 11). Under neutral conditions, the first EOF represents 61% of the variance (Figure 11A) and indicates a high SSC amplitude in the north of the Patos Lagoon and on the south coast of the La Plata River, mainly in the regions near Punta Piedras, where tributaries contribute the highest SSC. The second EOF represents 22% of the variance and is located near Montevideo (Figure 11C), while the third EOF represents only 8% of the variance (Figure 11E). During the period influenced by the ENSO cycle, the first EOF mode represents 51% of the variance, while the third EOF mode remained unchanged (Figures 11B and 11F). However,

due to the lower discharge values observed, the modes of variability underwent changes in the second EOF, which explain 14% of the observed variability (Figure 11D).

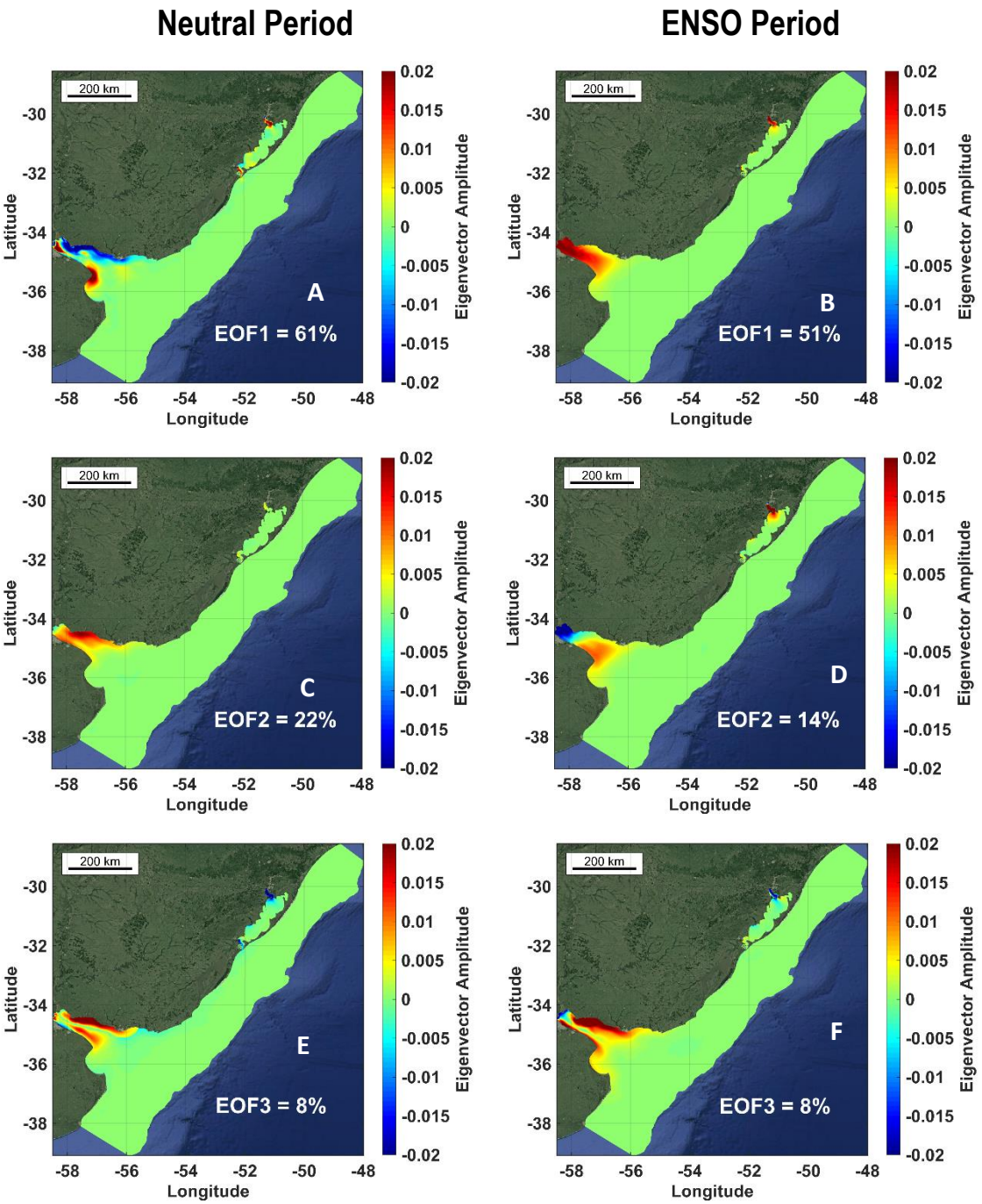


Figura 24 - Figure 11 - Artigo 1 - The first three empirical orthogonal function (EOF) modes of suspended sediment concentration (SSC) across the domain for the neutral period (2005-2006) (left column) and for the period under the influence of an ENSO cycle (2008-2009) (right column). The red areas (positive values) represent the regions where the concentration of the suspended sediment has a high spatial pattern, in contrast, the blue areas (negative values) represent the regions where the SSC has a low spatial pattern.

Similar EOF analyses are presented for SSC along the longitudinal transect of the La Plata River (T1, Figure 12). During the neutral period, the first EOF represents 49% of the variance and higher SSC close to the continental inflow, mainly at the estuary bottom (Figure 12A). The second EOF represents 28% of the variance (Figure 12C) and the third 4% (Figure 13E) indicating the presence of high SSC moving towards the inner shelf. During the period under the influence of the ENSO cycle, the first EOF represented 67% (Figure 12B), the second 22% (Figure 12D) and the third 4% (Figure 12F) of the variance, presenting lower SSC that spread more across the adjacent coastal region. The occurrence of higher SSC near the bottom is evident in the three modes of variability of the EOF.

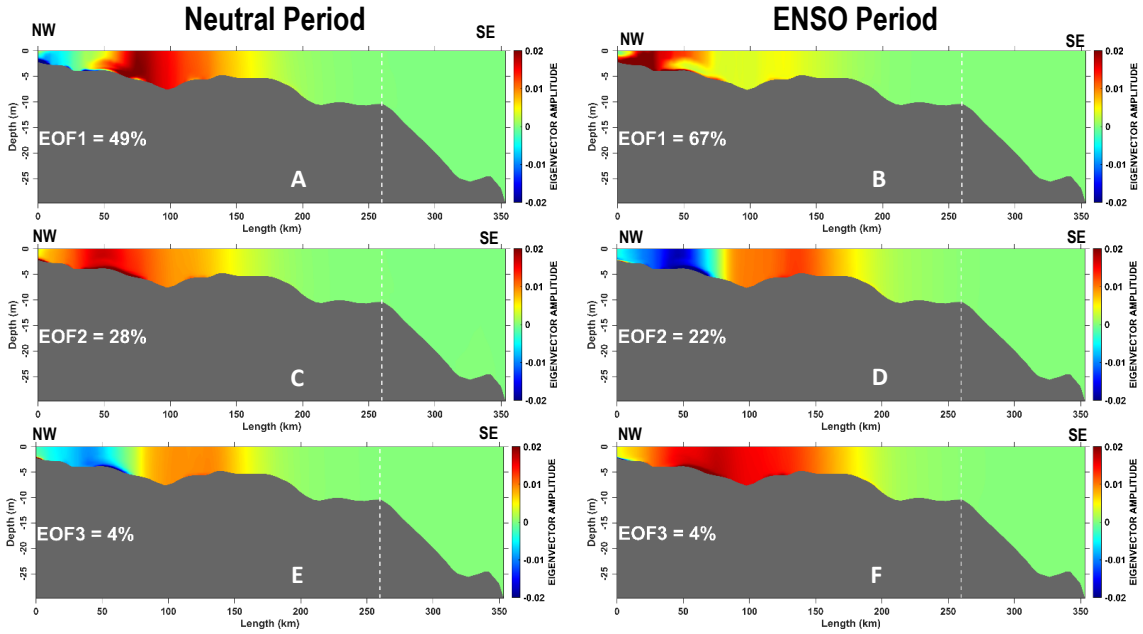


Figura 25 - Figure 12 - Artigo 1 - The first three empirical orthogonal function (EOF) modes of suspended sediment concentration (SSC) along the longitudinal section of the La Plata River (T1) for the neutral period (2005-2006) (left column) and for the period under the influence of an ENSO cycle (2008-2009) (right column). The dotted lines represent the position of the mouth in longitudinal view. The red areas (positive values) represent the regions where the concentration of the suspended sediment has a high spatial pattern, and in contrast, the blue areas (negative values) represent the regions where the SSC has a low spatial pattern.

In the transversal profile of the La Plata River mouth (T2, Figure 1) during the neutral period (Figures 13A, 13C, 13E), the first EOF represents 48% of the variability of SSC located near the south margin of the river mouth. The second mode (32%) corroborates that the highest SSC occurs

in the north margin of the river mouth, as can also be seen in the normal velocity component of the cross-section of the mouth (Figures 9B and 9F); the third mode (9%) indicates the occurrence of high SSC in both margins and low SSC in the central part of the profile. Again, the occurrence of the highest SSC near the bottom is evident.

When we consider the period under the influence of the ENSO cycle (Figures 13B, 13D, and 13F), the first EOF presents 77% of the variability very close to the south margin of the La Plata River mouth (Figure 13B), and this pattern spreads slightly to the north margin of the mouth in the second EOF (12%; Figure 13D). The first two EOF analyses corroborate the intensification of ebb currents observed in this region in Figure 9F. The third EOF (9%, Figure 13F) behaves similarly to the previous period, indicating the occurrence of high SSC in both margins of the estuary and low SSC in the central part of the profile.

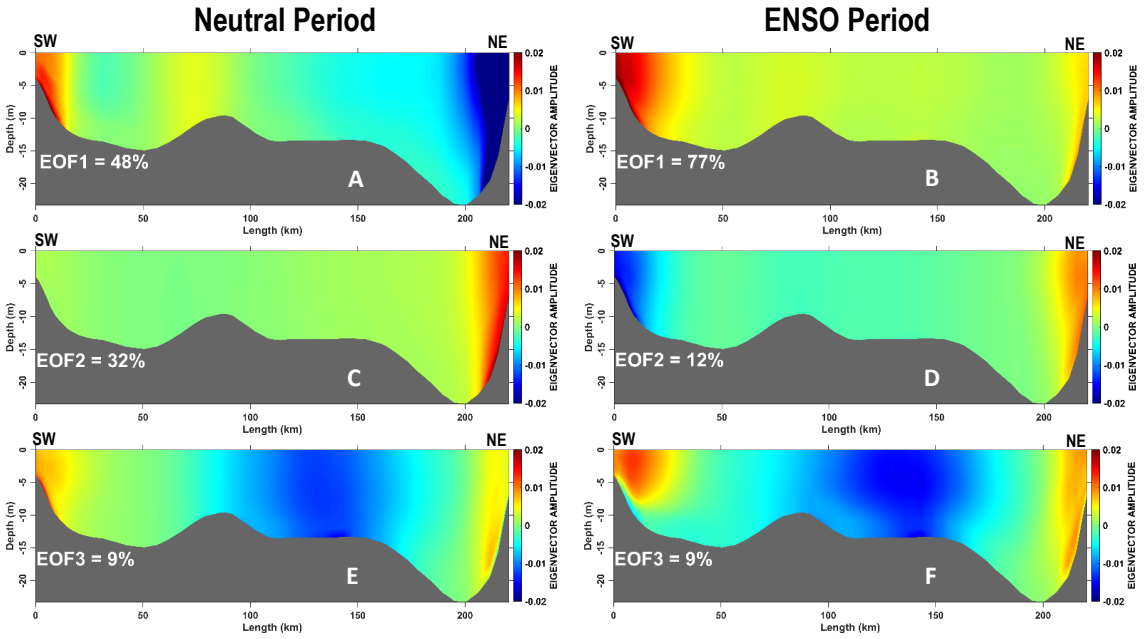


Figura 26 - Figure 13 - Artigo 1 - The first three modes of the empirical orthogonal function (EOF) analysis of suspended sediment concentrations (SSC), along the transversal profile of the La Plata River (T2) for the neutral period (2005-2006) (left column) and for the period under the influence of an ENSO cycle (2008-2009) (right column). The red areas (positive values) represent the regions where the concentration of the suspended sediment has a high spatial pattern. In contrast, the blue areas (negative values) represent the regions where the SSC has a low spatial pattern.

Along the longitudinal transect of the Patos Lagoon mouth (T4, Figure 1), the first EOF represents 93% of the variance and higher SSC towards the south of the Rio Grande jetties bar (dotted line, Figure 14A). The second EOF represents only 3% of the variance (Figure 14C) and

the third 2% (Figure 14E), always remaining concentrated south of the bar jetties. The EOF represents the residual outflow of the suspended sediment shown in Figures 8A and 8C, showing the hypopycnal flow characteristics of the plume when leaving the Patos Lagoon estuary (Figures 9C and 9G), through the bar jetties. During the period under the influence of the ENSO cycle, the same pattern was observed, with the first EOF representing 92% of the variance (Figure 14B), the second 4% (Figure 14D) and the third 2% (Figure 14F), indicating that the hypopycnal flow characteristics of the plume persist in extreme events.

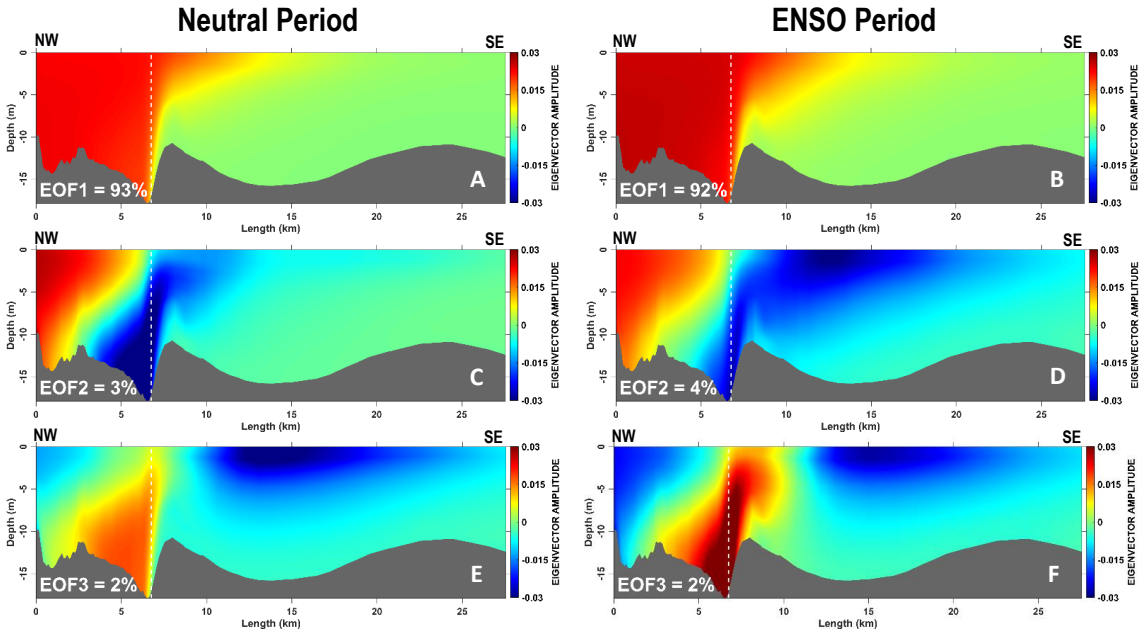


Figura 27 - Figure 14 - Artigo 1 - The first three modes of the empirical orthogonal function (EOF) analysis of suspended sediment concentrations (SSC) along the longitudinal profile of the Patos Lagoon mouth (T4) for the neutral period (2005-2006) (left column) and the period under the influence of an ENSO cycle (2008-2009) (right column). The dotted lines represent the position of the mouth in longitudinal view. The red areas (positive values) represent the regions where the concentration of the suspended sediment has a high spatial pattern, and in contrast, the blue areas (negative values) represent the regions where the SSC has a low spatial pattern.

In the transversal profile to the Patos Lagoon mouth during the neutral period (figure 15A, 15C, 15E), in the first EOF, which represents 73% of the SSC variability, a core of maximum pattern towards the ocean can be identified, corroborating the results presented in figures 9C and 9G which show the superficial position of the sediment plume at the mouth. The second EOF (12%) shows a well-marked pattern in the behavior of the plume with a preference in transgressing towards the south of the mouth, while the third EOF (6%) shows the slightly tendency of the plume to migrate to the north of the mouth.

When we consider the period under the influence of the ENSO cycle (Figure 15B, 15D and 15F), the first EOF shows 70% of the variability maintaining the pattern (spatial distribution) found in neutral years, but more intensified. This behavior is repeated both for the second EOF (11%) and for the third (6%), showing a pattern in the displacement of the plume to the south and to the north of the Patos Lagoon mouth, respectively.

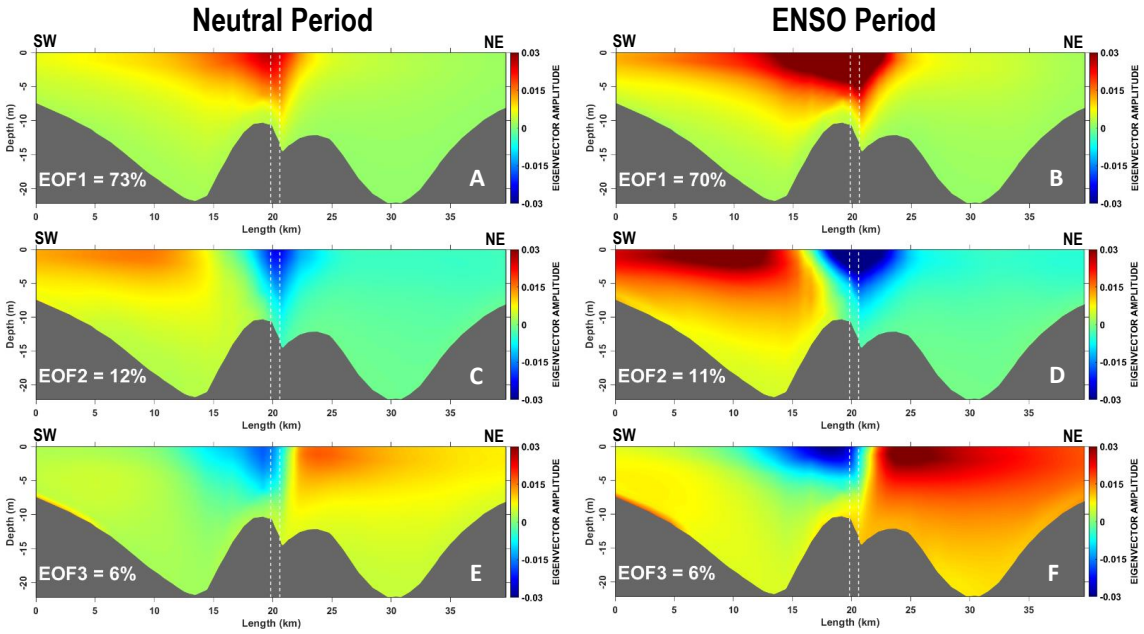


Figura 28 - Figure 15 - Artigo 1 - The first three modes of the empirical orthogonal function (EOF) analysis of suspended sediment concentrations (SSC) on the transversal profile at the Patos Lagoon mouth (T5) for the neutral period (2005-2006) (left column) and for the period under the influence of an ENSO cycle (2008-2009) (right column). The dotted lines represent the position of the Patos Lagoon mouth. The red areas (positive values) represent the regions where the concentration of the suspended sediment has a high spatial pattern; in contrast, the blue areas (negative values) represent the regions where the SSC has a low spatial pattern.

**Temporal Variability of Coastal Plumes**

In order to better evaluate the temporal variability of SSC in the La Plata River and Patos Lagoon estuaries, a cross-wave analysis was performed on the calculated time series of SSC, correlating its behavior with fluvial discharge from the river (Figures 16 and 17). The relationship of SSC with the wind was also assessed (Figures 18 and 19)

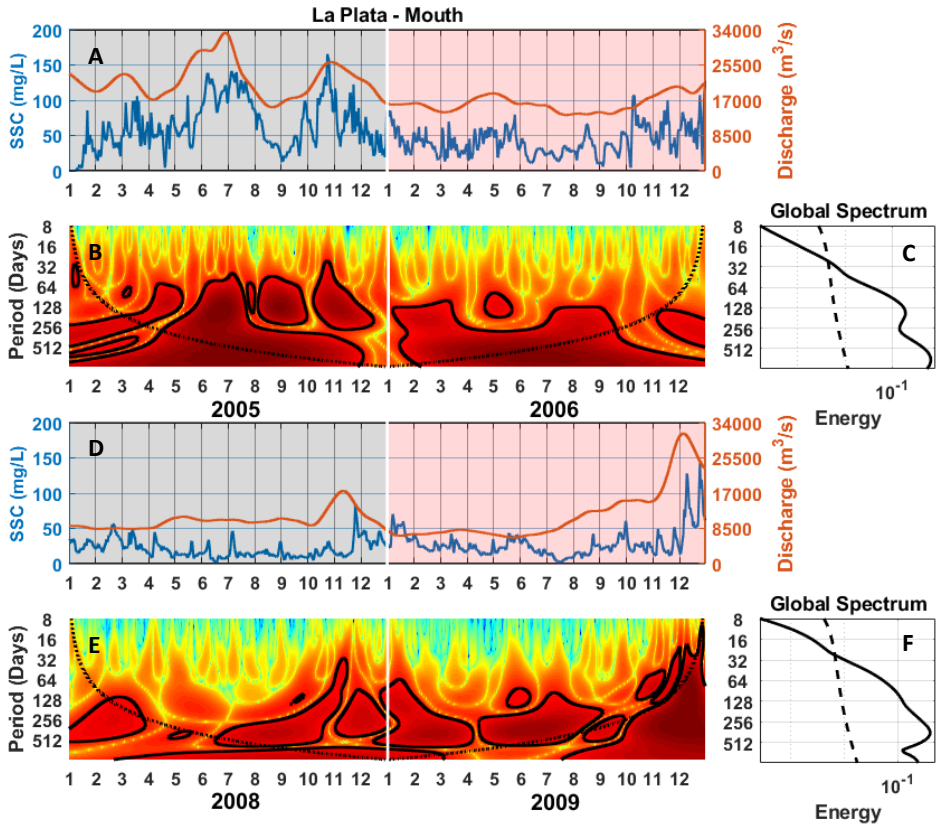


Figura 29 - Figure 16 - Artigo 1 - (A) Time series of the La Plata River discharge (orange) and suspended sediment concentrations (SSC; blue) for the period 2005-2006 (green dot - Figure 1). (B) Cross-spectrum of local energy using Mexican hat wavelet analyses where the contour lines enclose regions with a 95% confidence interval. The dashed line indicates the region of influence where the border effects become important. (C) Average global power spectrum where the dashed line represents the 95% confidence level. (D) Time series of the La Plata River discharge (orange) and suspended sediment concentrations (blue) for the period 2008-2009 (green dot; Figure 1). (E) Cross-spectrum of local energy using the Mexican hat wavelet analysis; the contour lines involve regions with a 95% confidence interval and the dashed line indicates the region of influence where the border effects become important. (F) Average global power spectrum; the dashed line represents the 95% confidence level.

The results show that during the neutral period (Figure 16A) the relationship between SSC and fluvial discharge from the La Plata River occurs in time intervals between 32 and 256 days during 2005, and part of 2006, as can be observed by the occurrence of regions delimited by black contour lines that occur within the area of significance (dashed line) of Figure 16B. This result is in line with the global power spectrum (Figure 16C), which indicates that the power (solid line) is greater than the 95% confidence interval (dotted line), for periods longer than 32 days.

When analyzing the results during the period under the influence of the ENSO cycle (Figure 16D), the cross-analysis between the SSC and the river discharge in the La Plata River region extends the interval to between 32 and 512 days, during the two years, as delimited by the black

line in the figure, within the significance range (dashed line) of Figure 16E. The global power spectrum (Figure 16F) corroborates this result, indicating that the power (solid line) is greater than the 95% confidence interval (dotted line) for periods longer than 32 days.

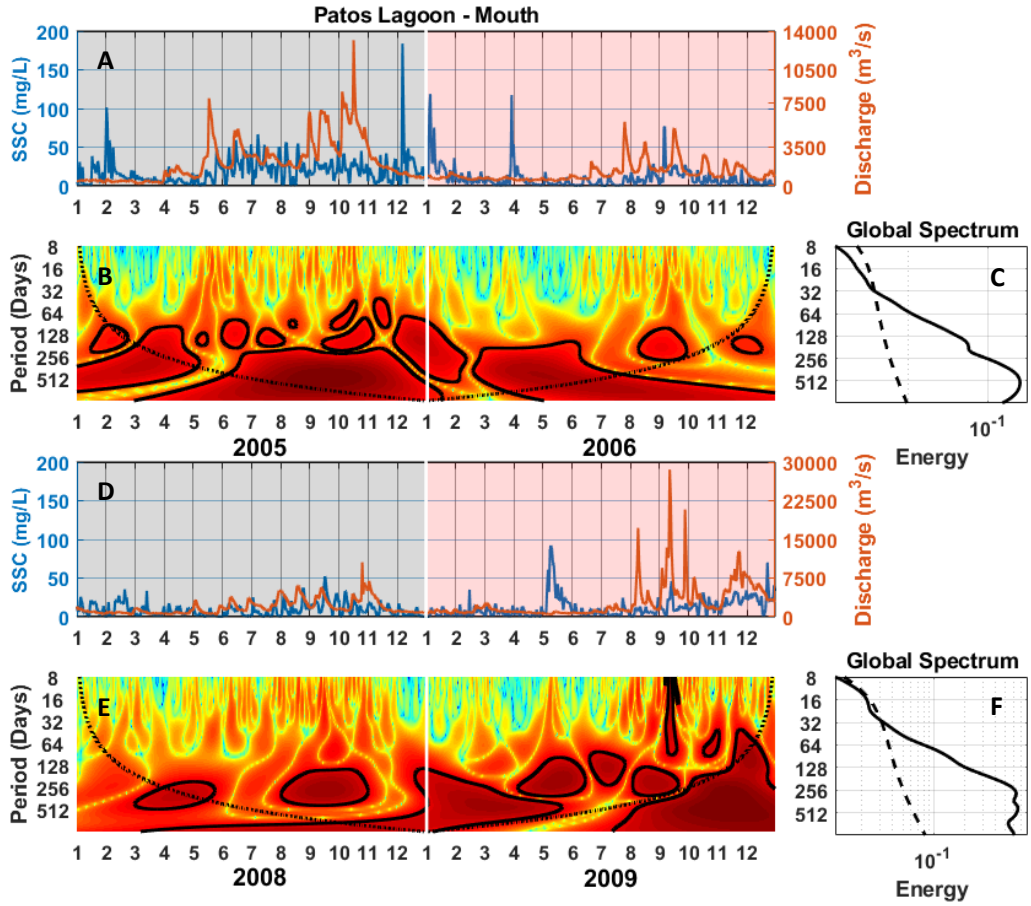


Figura 30 - Figure 17 - Artigo 1 - (A) Time series of fluvial discharge from the Patos Lagoon (red) and sediment concentrations (blue) for the period 2005-2006 (green dot - Figure 1). (B) Cross-spectrum of local energy using the Mexican hat wavelet analysis. The contour lines enclose regions with a 95% confidence interval and the dashed line indicates the influence with which the border effects become important. (C) Global spectrum indicating the average time of each cycle; the dashed line represents the 95% confidence level. (D) Time series of fluvial discharge from the Patos Lagoon (red) and sediment concentrations (blue) for the period 2008-2009 (green dot - Figure 1). (E) Cross-spectrum of local energy using the Mexican hat wavelet analysis; the contour lines involve regions with a 95% confidence interval and the dashed line indicates the influence with which the border effects become important. (F) Global spectrum indicating the average time each cycle takes place over. The dashed line represents the 95% confidence level.

For the Patos Lagoon region, the results show that during the neutral period (Figure 17A) the cross-analysis between the SSC and the fluvial discharge occurs in time intervals between 32 and 512 days during 2005 and 2006, as can be observed by the occurrence of regions bounded by black contour lines that occur within the area of significance (dashed line) of Figure 17B. This

result is in line with the global power spectrum (Figure 17C), which indicates that the power (solid line) is greater than the 95% confidence interval (dotted line), for periods longer than 32 days.

When analyzing the results during the period under the influence of the ENSO cycle (Figure 17D), the cross-analysis between the SSC and the Patos Lagoon fluvial discharge reduces the interval to between 32 and 256 days, during the two years, as delimited by the black line in the figure, within the significance range (dashed line) of Figure 17E. The global power spectrum (Figure 17F) corroborates this result, indicating that the power (solid line) is greater than the 95% confidence interval (dotted line) for periods longer than 32 days.

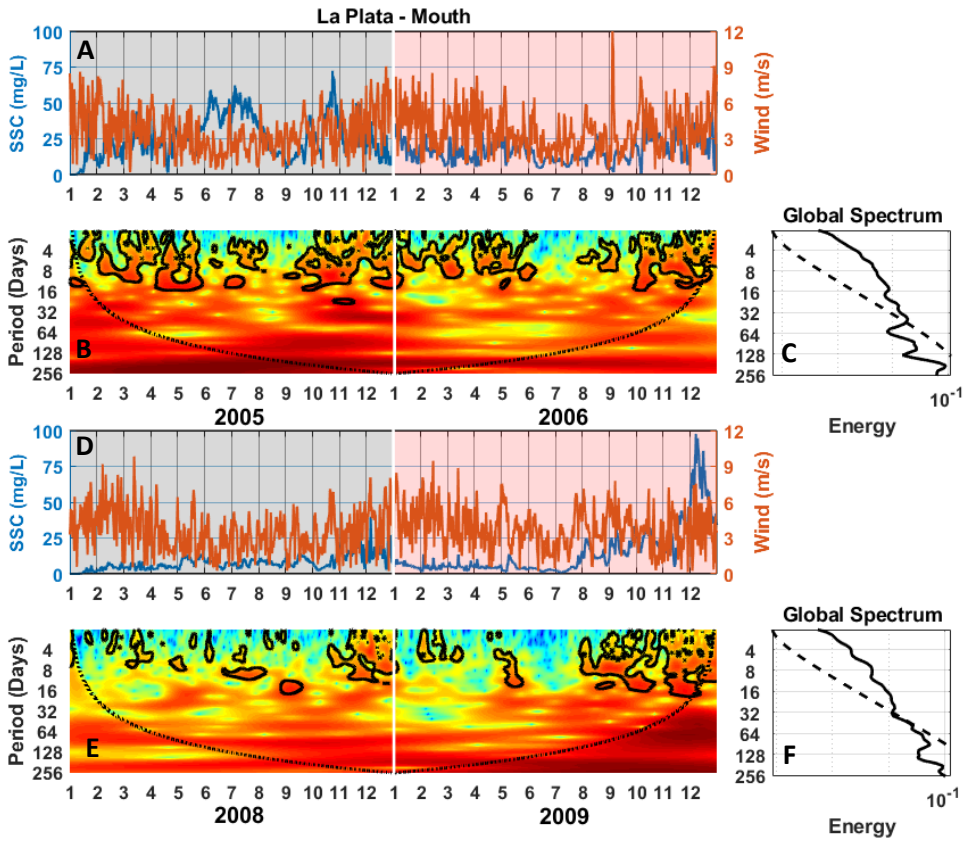


Figura 31 - Figure 18 - Artigo 1 - (A) Time series of wind intensity (orange) and suspended sediment concentrations (SSC) in the La Plata River (blue) for the period 2005-2006 (green dot - Figure 1). (B) Cross-spectrum of local energy between the time series using Morlet wavelet analysis. The contour lines enclose regions with a 95% confidence interval. The dashed line indicates the region of influence where the border effects become important. (C) Average global power spectrum where the dashed line represents the 95% confidence level. (D) Time series of wind intensity (orange) and SSC of the La Plata River (blue) for the period 2008-2009 (green dot - Figure 1). (E) Cross-spectrum of local energy between the time series using Morlet wavelet; the contour lines involve regions with a 95% confidence interval and the dashed line indicates the region of influence where the border effects become important. (F) Average global power spectrum, where the dashed line represents the 95% confidence level.

The relationship between the wind and the SSC of the La Plata River for the simulated periods is shown in Figure 18. During the neutral period (Figure 18A and 18B), the relationship of the wind with the suspended sediment occurs on a synoptic time scale between 2 and 16 days, as can be seen by the occurrence of regions bounded by black contour lines that occur within the area of significance (dashed line) of Figure 18B. This result is in accordance with the global power spectrum (Figure 18C), which indicates that the power (solid line) is greater than the 95% confidence interval (dotted line), for periods shorter than 16 days. The same behaviour was observed for the period under the influence of an ENSO cycle (Figures 18D-18F), but only in the summer of 2008 and spring and summer of 2009 (Southern Hemisphere).

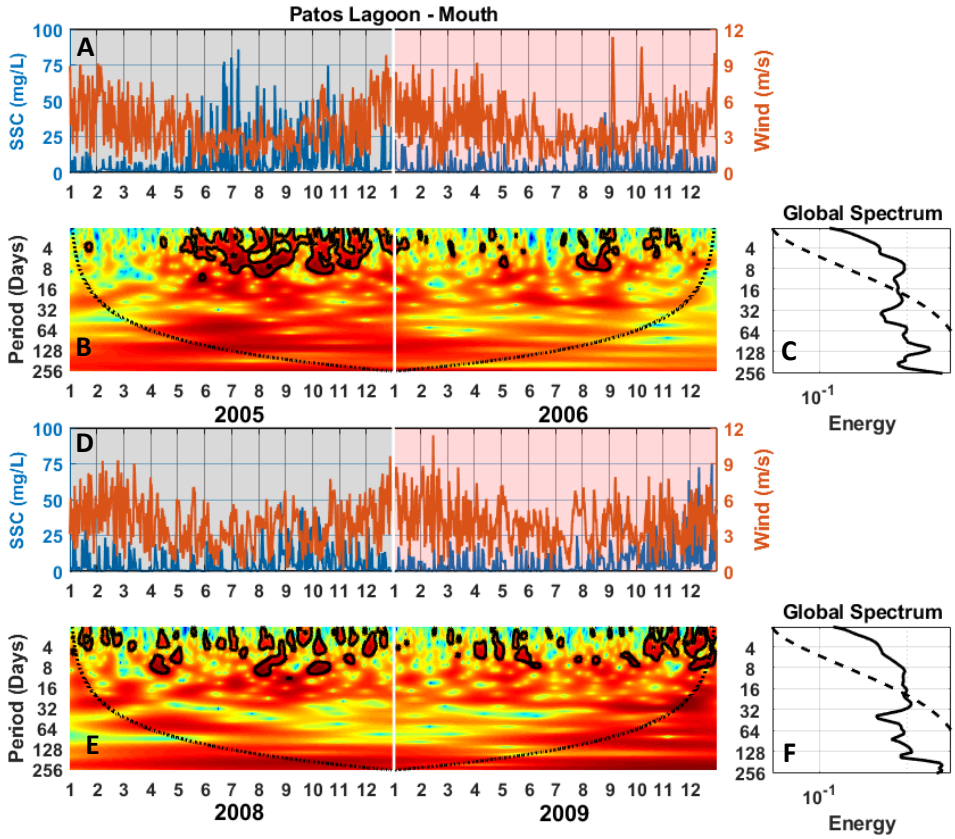


Figura 32 - Figure 19 - Artigo 1 - (A) Time series of wind intensity (orange) and suspended sediment concentrations (SSC) in the Patos Lagoon (blue) for the period 2005-2006 (green dot - Figure 1). (B) Cross-spectrum of local energy between the series using Morlet wavelet; the contour lines enclose regions with a 95% confidence interval and the dashed line indicates the region of influence where the border effects become important. (C) Average global power spectrum; the dashed line represents the 95% confidence level. (D) Time series of wind intensity (red) and SSC in the Patos Lagoon (blue) for the period 2008-2009 (green dot - Figure 1). (E) Cross-spectrum of local energy between series using Morlet wavelet analysis; the contour lines involve regions with a 95% confidence interval and the dashed line indicates the influence with

which the border effects become important. (F) Average global power spectrum; the dashed line represents the 95% confidence level.

A similar analysis made for the Patos Lagoon shows that SSC (Figure 19) is also correlated with the wind on a synoptic time scale between 2 and 16 days both in the neutral period (Figures 19B and 19C) and in the period under the influence of the ENSO cycle (Figures 19E and 19F).

**Behavior of Sediment in Suspension on the Inner Shelf**

In order to understand the behavior of suspended sediment on the South Atlantic Inner Shelf, daily time series of SSC were extracted from a cross-section established along the inner shelf (T6, Figure 1) for the simulated periods, and its spatial and temporal distribution were analyzed in the Hovmöller diagram (Figures 20 and 21). This diagram shows the time on the ordinate axis and the geographic coordinate on the abscissa axis, with the southwest being the limit of the closest transect to the La Plata River and the northeast the closest limit to the Patos Lagoon.

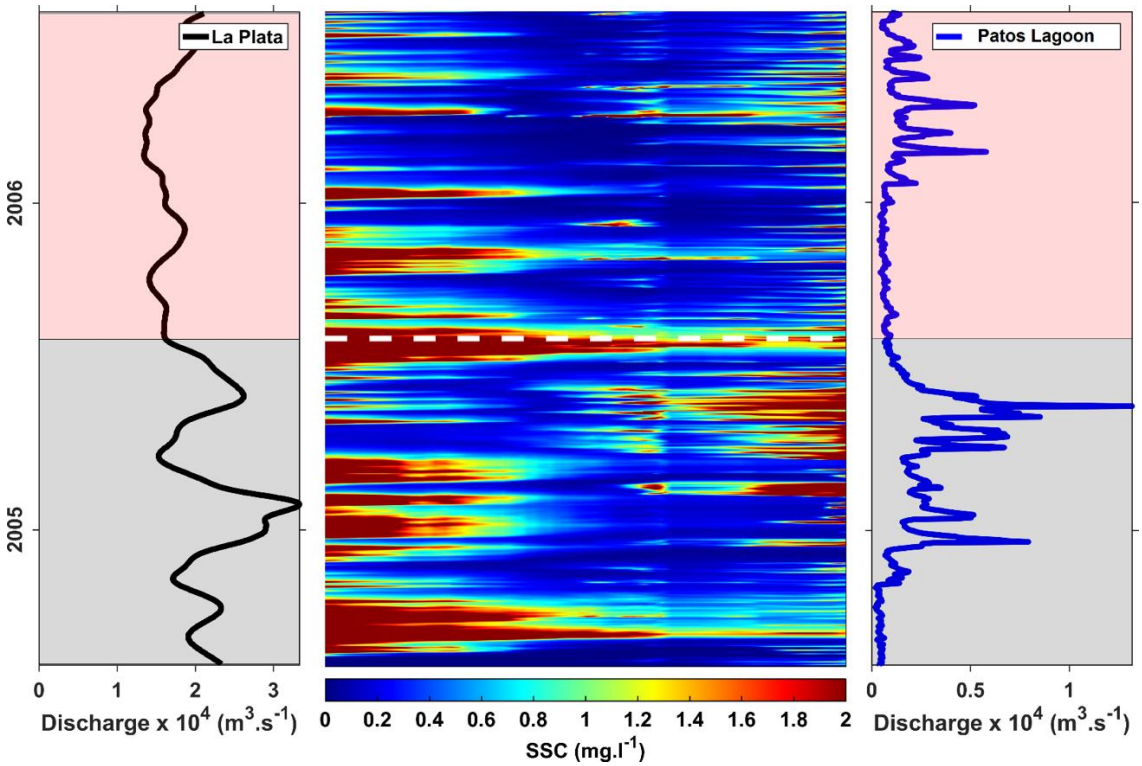


Figura 33 - Figure 20 - Artigo 1 - (A) Time series of discharge from the La Plata River for the period influenced by the ENSO cycle. (B) Hovmöller diagram elaborated with the time series of suspended sediment concentrations (SSC) extracted along transect T6. SW is the limit of the closest transect to the La Plata River and NE the closest limit to the Patos Lagoon. (C) Time series of discharge in the north of the Patos Lagoon for the neutral period.

The spatial and temporal distribution of the SSC along T6 (Figure 1) on the inner shelf appears to have a direct relationship with the SSC from the continental discharge of the La Plata River and the Patos Lagoon (Figures 20A and 20C) most of the time during the neutral period, because following the continental discharge peaks of these contributors, high SSC are observed distributed along the adjacent coast. This behavior is especially evident for the Patos Lagoon during the winter and spring of 2005 (Southern Hemisphere) (Figure 20C), although it does not always apply to the La Plata River, as seen in the summer of 2005-2006 (Southern Hemisphere), when high SSC are observed on the inner shelf (Figure 20B), but discharge peaks in the La Plata River are not evident (Figure 20A).

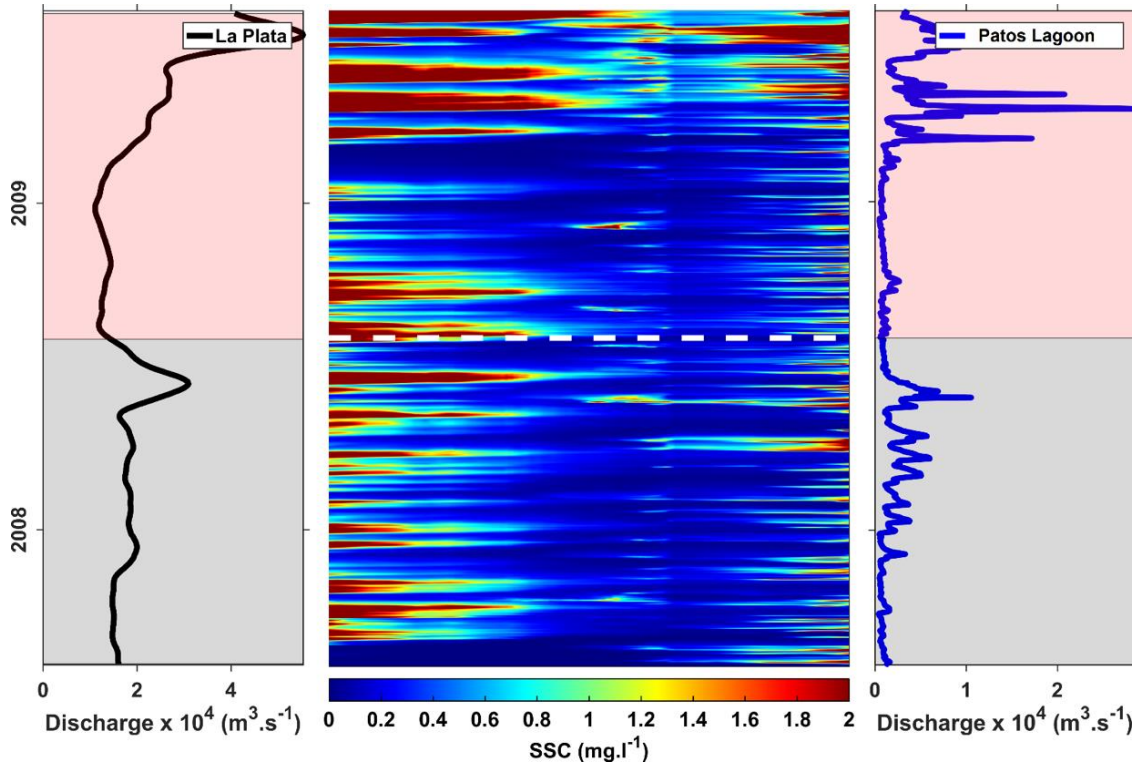


Figura 34 - Figure 21 - Artigo 1 - (A) Time series of discharge from the La Plata River for the period influenced by the ENSO cycle. (B) Hovmöller diagram elaborated with the time series of suspended sediment concentrations (SSC) extracted along transect T6. SW is the limit of the closest transect to the La Plata River and NE the closest limit to the Patos Lagoon. (C) Time series of discharge in the north of the Patos Lagoon for the period influenced by the ENSO cycle.

In Figure 21, a similar analysis is made for the period affected by the ENSO cycle. The results indicate that the direct relationship between continental discharge and SSC is maintained in the Patos Lagoon (Figure 21C) both during the La Niña period (2008 and the 1st semester of 2009) and during the El Niño period (the 2nd semester of 2009 for the La Plata River; Figure 21A);

the continental discharge peaks observed at the end of 2008 (La Niña) and at the end of 2009 (El Niño) were reflected in peaks of SSC in the inner shelf.

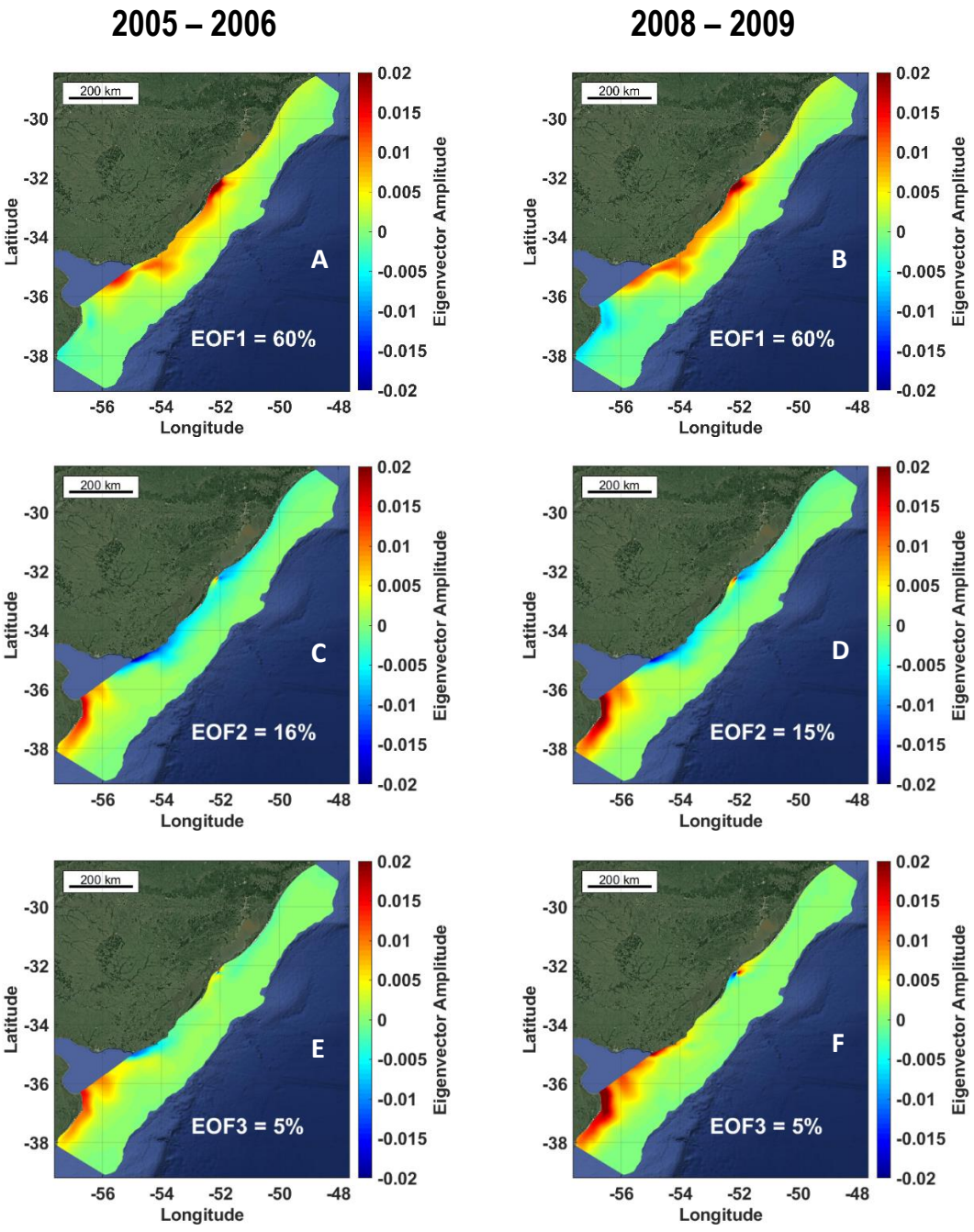


Figura 35 - Figure 22 - Artigo 1 - The first three empirical orthogonal function (EOF) modes of suspended sediment concentrations (SSC) along the T6 transect on the internal platform for the neutral period (2005-2006) (left column) and for the period under the influence of an ENSO cycle (2008-2009) (column right). The red areas (positive values) represent the regions where the concentration of the suspended sediment has a high spatial pattern and in contrast, the blue areas (negative values) represent the regions where the concentration of the suspended sediment has a low spatial pattern.

The preferred regions of occurrence of the highest SSC in the inner shelf were determined through an EOF analysis of the region during the two simulated periods (Figure 22). Both during the neutral period and during the period influenced by the ENSO cycle, the first EOF represented 60% (Figures 22A and 22D) and the second EOF 15% (Figures 22B and 22E) of the variance, indicating higher SSC in the region of inner shelf between the mouths of the La Plata River and the Patos Lagoon; this suggests an interaction between the contributions from the two environments. The third EOF (5% variance, Figures 22C and 22F) is related to the high SSC exactly in front of the mouth of the tributaries.

**Discussion**

Since the calibration and validation exercises resulted in statistic parameters considered adequate, the model's ability to reproduce the realistic behavior of the system was considered effective (Appendix E). Thus, our results show that the model reproduced the variability of the SSC over a neutral period (2005-2006) and over a period under the effect of ENSO, predominantly La Niña (2008–September of 2009), with the appearance of an El Niño event from October of 2009 for the SAIS.

**Distribution of Patos Lagoon and La Plata River Plumes in the South Atlantic Inner Shelf**

The SSC distributions in the Southwest Atlantic Inner Shelf (Figure 8) show a relationship with the seasonality of the Patos Lagoon and the La Plata River plumes for both periods analyzed. The southern winter (Figures 8A and 8B), is when the higher SSC values associated with the regions being most influenced by the La Plata River occurred, and when the seasonal cycle had a robust signal, as also observed by Guerrero et. al. (1997). As analyzed by Campos et. al., 1999, Piola et. al. (2004), Pimenta et. al. (2005), Soares et. al. (2007a) and Simionato and Moreira (2018), among others, during the southern winter the La Plata River estuarine plume expands widely as a coastal strip in a northeast direction along the coast of Uruguay and southern Brazil (Moreira et. al., 2013), reaching latitudes close to 26ºS; this shows the plume can reach more than 1,000 km of distance from the mouth of the La Plata River. During the southern summer (figures 8C and 8D) the influence of SSC on the inner platform occurs through a relatively thin coastal strip that migrates to the north, reaching latitudes close to 30ºS and through another portion that is concentrated in the region of the mouth of the La Plata River (Piola et. al., 2004).

Like for the La Plata River, the Patos Lagoon SSC contribution to the adjacent coastal region is influenced by the seasonal character of the suspended sediment coastal plume (Marques et. al., 2010a; 2010b). Higher SSC values occur during the southern winter (Figures 8A and 8B) when the river discharge is stronger in the region. Additionally, during the southern summer (Figures 8C and 8D) the region has lower SCC values, when the observed values of fluvial discharge are below average (Marques et. al., 2009). Still on the importance of fluvial discharge, Burrage et. al. (2008) stated that due to the contrast between fluvial discharge regimes from the two estuaries (22,000 m3/s for the La Plata River compared to 2,000 m3/s for the Patos Lagoon), the La Plata River plume normally penetrates beyond the entrance to the Patos Lagoon Estuary, fully incorporating it by merging or even dominating the plume of the Patos Lagoon, corroborating the results in this work.

It is worth noting that the region studied during the years influenced by the ENSO phenomenon may present precipitation anomalies (Grimm et. al., 1998; Grimm et. al., 2000). Thus, the years under the influence of El Niño tend to be more humid with a high rate of precipitation, and the opposite is observed in La Niña years, when a drought period is expected.

During the period influenced by the ENSO phenomena – predominantly La Niña – (Figures 8B and 8D) the SSC patterns showed high interannual variability. According to Dogliotti et. al. (2016), low turbidity values were observed during El Niño years and high turbidity values during some La Niña years. However, the La Niña (El Niño) effect is not always the only dry (flood) forecast in the region. This is due to the fact that the main contributor of suspended sediment to the La Plata River and the Bermejo River (approximately 70% of the total sediment), is not greatly affected by ENSO phenomena (Pasquini and Depedris, 2007; Dogliotti et. al., 2016). However, the main effluents that supply more than 97% of the La Plata's freshwater are highly influenced by the rainfall anomaly caused by the ENSO effect (Dogliotti et. al., 2016), which may increase the average of river discharge by 3-5 times (Berbery and Barros, 2002; García-Rodríguez et. al., 2014). Therefore, the influence of the ENSO phenomena on SSC acts essentially by diluting the concentration of the sediment due to the increased flow of the main effluents.

For the Patos Lagoon, the interannual variability and its contribution to local dynamics has been investigated by several authors (Möller et. al., 2001; Fernandes et. al., 2002; Vaz et. al., 2006; Marques et. al., 2010a; 2010b, Távola et. al., 2020; Bitencourt et. al., 2020). It has been shown that there is an anomalous pattern in fluvial discharge, with values that exceed the average during the El Niño years and values that vary from the average to below average during La Niña years, significantly changing the SSC, as shown in figures 8B and 8D. Marques et. al. (2010b) reported a

direct relationship between the fluvial discharge and the SSC, which intensifies towards the Atlantic Ocean during strong El Niño events.

Regarding the influence of wind in the region, Piola et. al. (2004) and Moreira et. al. (2013) confirmed that there is strong seasonal variability in wind stress along the coast. During the summer (Figures 8C and 8D), winds of moderate speed from the north and northeast directions dominate, being responsible for the minimum displacement of the coastal plume (Piola et. al., 2004; Soares et. al., 2007a). During the winter (Figures 8A and 8B), the wind exhibits the opposite behavior: strong southwest winds become frequent and important in the maximum insertions of coastal plumes to the north during the austral winter (Piola et. al., 2004; Soares et. al., 2007a).

Regarding the hydrodynamics of the La Plata River estuary, Fossati and Cuevas (2013) qualified the wind action, together with the river discharge and meteorological tide, as the main forces of local estuarine circulation, in addition to the strong participation of the local bathymetry in local hydrodynamics. Figure 9B and 9F show that flood and ebb flows are highly influenced by local bathymetry, as confirmed by Fossati and Cuevas (2013). This is because in the high estuary, near the river mouth, ebb flows are commonly observed in shallow areas, such as coastal or shoal zones (Figures 9B and 9F). On the other hand, flood flows are found in the deeper areas, mainly in those closest to the Uruguayan coast (Figures 9B and 9F). These results corroborate those found by Fossati and Cuevas (2013) when observing an inflow of salt water through the deepest regions near the northern coast of the estuary. The ENSO effect in the region (Figure 9F) was noticeable in the results when de-intensifying the flood and ebb currents, as was observed by Guerrero et. al. (1997) in the La Plata River estuary. When analyzing the hydrodynamics of the Patos Lagoon through the cross section (Figures 9D and 9H), a unidirectional circulation pattern is observed in the channel region, with the results indicating a dominance (mean) of the ebb flow. During the La Niña years studied, the Patos Lagoon, like the La Plata River, suffered a slight weakening of the current speed (Figure 9H), as a result of the predicted drought period (Grimm et. al., 2000).

Local hydrodynamics control the distribution of suspended sediment across the La Plata River estuary (Moreira et. al., 2019). Results in figures 9A and 9E show a homopycnal profile in the plume of the La Plata River (occupying the entire water column), with a preference for high SSC, in the upper estuary, along the northern coast (Uruguay) and the southern coast (Argentina). According to Monteiro et. al. (2013), the relatively higher SSC observed along the southern coast of the upper estuary (Figures 9A and 9E) may be linked, at least in part, to the higher suspended solid flow of the Paraná River compared to the Uruguay River (two of the main effluents in the La Plata River). As a result, waters from the Paraná River tend to occupy the southern coast in the

upper portion of the estuary, whereas waters from the Uruguay River are limited to the northern coast. The influence of the ENSO phenomenon (Figure 9E) becomes explicit by increasing the value of SSC both on the south coast and on the north coast, as has also been observed by Dogliotti et. al., (2016) when analyzing SSC during La Niña years. For the Patos Lagoon the local hydrodynamics suggest the formation of a hypopycnal plume (positive buoyancy), with a high SSC at its core (Figure 9C), where the maximum occur associated with the maximum discharge events, which most of the time migrate southwards in the coastal region (as a result of northeast winds); during the occurrence of winds from the south quadrant, previously exported materials can be reinserted into the estuarine region, as observed by Marques et. al. (2010b). When considering the years controlled by the ENSO effect (Figure 9G), we find a more weakly concentrated plume compared to normal years. This result found in the present article for the La Niña event, corroborating the results presented by Marques et. al. (2010b), in which the authors show that the freshwater discharge from the Patos Lagoon has a high interannual variability and directly influences the export of suspended material to the adjacent coastal zone. According to the authors, the events El Niño and La Niña can also intensify and considerably reduce the normal seasonal flow pattern, respectively.

Regarding the average behaviors of the suspended sediment and the current at the mouth of the La Plata River and the Patos Lagoon, we observed that both systems export waters and suspended sediments of continental origin to the Southwest Atlantic Inner Shelf. The total mass flux estimated through its integration along the cross section at the mouth of the La Plata River (Figures 10A and 10B) resulted in time series with very similar inflow and outflow patterns and intensities, where the maxima occur associated with the maximum events of fluvial discharge (Figure B3 - Appendix B), with a delay of approximately one month between the maximum flow and the peak of suspended sediment, was as has also observed by Simionato et. al. (2009), Moreira et. al. (2013) and Dogliotti et. al. (2016). These authors state that this time lag may be the result of the travel time of the sediment from downstream to the mouth. Marques et. al. (2010a) made a similar analysis for the Patos Lagoon in the years 1998-1999. As in the present work, the authors integrated the mass flow (Figures 10A and 10B) along a cross section of the access channel resulting in a time series with a profile similar to that of the river discharge (Figure B3 - Appendix B), where the maximum peaks show some correlation with the maximum flow. The ebb and flow periods are directly related to the north/northeast and south quadrant winds, respectively.

Weather conditions can influence the behavior of suspended sediment in some coastal regions, as seen by Marques et. al. (2010a) for the south of Brazil and Talke and Stacey (2008) for

the San Francisco bay. Thus, when analyzing the years under the influence of ENSO, it is clear that when the ENSO index is above 1 (Figures 10E and 10F), there is an evident response in river discharge, significantly influencing the mass flux. It can be seen that at the beginning of 2008 the region is under the effect of a moderate La Niña event which is already sufficient to alter the values of the mass flux both in the La Plata River and in the Patos Lagoon. At the end of 2009 however, an El Niño with an index above 1.5 was enough to increase the amount of suspended sediment exported by the La Plata River and the Patos Lagoon.

As for the cumulative value of the transported mass, Menéndez and Sarubbi (2007) stated that the La Plata River exports $1.6x10^8$ tons/year of sediment. In the current work, cumulative mass transport for the neutral years (2005–2006) reached an export rate around $1.2x10^8$ tons/year (in the same order of magnitude as the values cited by Menéndez and Sarubbi, 2007), while for the years affected by the ENSO phenomenon, the rates were around $3.0x10^8$ tons/year. For the Patos Lagoon, Marques et. al. (2010b) found a suspended sediment export rate equal to $1.4x10^7$ tons/year, whereas in the present work this rate was slightly lower, hovering around $1.3x10^7$ tons/year. For the years affected by ENSO, this value increased to 1.35x107 tons/year, which is closer to the rate reported by Marques et. al. (2010b).

**Spatial Variability of Coastal Plumes**

EOF analyses are widely used for oceanographic parameters such as salinity, temperature and chlorophyll, among others, to detect the influence of environmental and oceanographic processes on the spatial variability of the analyzed parameters. In the present work, this analysis was used on the SSC exported by the La Plata River and the Patos Lagoon to the Southwest Atlantic Inner Shelf, in order to understand how the suspended sediment is distributed in suspension in the studied region.

Our results point to the dominance of two main modes controlling the spatial variability of the SSC in the La Plata River and the Patos Lagoon. The first horizontal mode (Figure 11A) explains the spatial distribution of the plumes in 61% of the simulated period, with persistent features in the north of the Patos Lagoon and east and west coasts of the La Plata River. These dominant patterns result from the combination of available waters of continental origin towards the coastal zone due to the formation of coastal plumes, with the action of the wind from the north quadrant in both systems (Möller et. al., 2001; Fernandes et. al., 2002; Marques et. al., 2010a) aligned with the Coriolis effect and the tide acting in the La Plata River (Moreira et. al., 2013;

Simionato and Moreira, 2018). When studying the period influenced by ENSO (Figure 11B), the first horizontal mode explains the suspended sediment variability 51% of the time. This may be a result of the influence that ENSO has on the river discharge of the Paraná and Uruguay Rivers, as stated by Moreira et. al. (2013) and Dogliotti et. at. (2016).

For the Patos Lagoon, Toldo et. al. (2006) stated that there is a high correlation between the SSC and the fluvial discharge from the Guaíba River. The pattern defined by the first EOF mode (Figures 11A and 11B) for the Patos Lagoon shows this correlation not only for the Guaíba River but also for the other two main effluents in the lagoon, the Camaquã River and the São Gonçalo Channel, as has also been mentioned by Hartmann et. al. (1991) and Oliveira et. al. (2015). The Patos Lagoon access channel also plays a role in the trapping of suspended sediment (Figure 11A). Marques et. al. (2010a) analyzed the plume formation in the Patos Lagoon and showed the importance of the navigation channel in this process, since the presence of this channel intensifies the vertical circulation, favoring the formation of the coastal plume. For the La Plata River, the water supply of the Paraná River takes place mainly along the south coast of the La Plata River estuary, showing its importance on local sedimentary dynamics (in red - Figure 11A). On the north coast, where the Uruguay River is mainly responsible for the river contribution, the suspended sediment variability has a negative character (blue - Figure 11A), showing the high variability of this effluent on the dynamics of the estuary. These results agree with those of Guerrero at al. (1997), Moreira et. al. (2013) and Moreira et. al. (2019).

The second mode of variability (Figures 11C and 11D) represents about 22% of the behavior of SSC for the period considered neutral period (Figure 11C) and 14% for the period under the ENSO influence (Figure 11D), with an evident attenuation of the Guaíba River plume during the neutral period (Figure 11C) and its intensification during the ENSO period (Figure 11D). For the La Plata River this second mode of variability in SSC for the neutral period suggests a preference of the coastal plume in concentrating on the northern coast of the La Plata estuary. In the ENSO period (Figure 11D), however, the opposite happens (the plume is closer to the southern coast) and there is a negative pattern in the region of the low estuary of the La Plata River (blue region), showing the high variability of sediment concentration in the region. When analyzing the seasonal and interannual behavior of the suspended material, Dogliotti et. al. (2016) also showed a high temporal variability in the lower La Plata River estuary.

For the third mode (Figures 11E and 11F), the SSC in the neutral period and the period under the ENSO effect represent only 8% of the variability. A well-defined pattern in practically the entire south and north coast of the La Plata River can be identified for the two analyzed periods

(Figures 11E and 11F). For the Patos Lagoon this third mode shows a negative pattern (great variability) for the main effluents, both in the neutral period and in the period under the ENSO effect; this is a sporadic event for the region, since the region is characterized by the exportation of suspended sediment to the inner Patos Lagoon (Toldo et. al., 2006).

To investigate the behavior of the suspended sediment in the water column, similar EOF analyses were carried out for longitudinal and transversal sections at the mouth of both systems (Figures 12, 13, 14, and 15). For the longitudinal section of the La Plata River (Figure 12), the first three EFOs (49%, 28%, and 4%) account for 87% of the variability of the SSC during the neutral period (Figures 12A, 12C, and 12E), while during the ENSO period the first three modes account for approximately 93% of the variability (Figures 12B, 12D, and 12F). Results indicate the presence of suspended sediments throughout the intermediate region (mainly near Punta Piedras; Figure 1), and this was already stated by Moreira et. al. (2013) and Dogliotti et. al. (2016), who related this spatial distribution pattern to the fluvial discharge of the main tributaries of the La Plata River and the resuspension of sediment caused by the tides. On the other hand, in the region of the low estuary, it is possible to perceive a high variability in the SSC (blue region), due to the influence of the main effluents of the La Plata River (the Paraná River and Uruguay River) (Guerreiro et. al., 1997; Moreira et. al., 2103; Dogliotti et. al., 2016)

At the mouth of the La Plata River (Figure 13), the first EOF analysis along the transversal profile during the neutral period suggests that the suspended sediment is exported to the coastal zone through to the southern side of the estuary 48% of the time coming from the Paraná River (Figure 13A), and through the northern margin 32% of the time coming from the Uruguay River (Figure 13C). During the ENSO period the contribution from the Paraná River represents the suspended sediment variability 77% of the time, while the Uruguay River accounts for only for 12% of the variability, evidencing the influence of ENSO in the two main effluents of the La Plata River, as stated by Berbery and Barros (2002), García-Rodríguez et. al. (2014), and Dogliotti et. al. (2016).

Although the Uruguay and Paraguay rivers contribute approximately 97% of the continental discharge reaching the La Plata River and are subjected to ENSO effects, it is worth mentioning that the Bermejo River is responsible for 70% of the suspended sediment exported to the La Plata River estuary, and it is not significantly affected by ENSO cycles. Thus, considering that the amount of suspended sediment arriving in the La Plata River estuary does not change significantly due to the La Niña effect present during the 2008-2009 ENSO period, the main factor responsible for the calculated concentration of suspended sediment is the availability of continental water. As a result,

the large amount of suspended sediment exported to the adjacent coastal region is the result of low continental discharge during this period.

When analyzing the longitudinal profiles at the mouth of the Patos Lagoon (Figure 14), a floating plume which turns to the SE end of the profile (leaving the estuary) can be observed. This dominant pattern, represented by the first EOF mode (Figures 14A, 14B) during the neutral and ENSO periods (representing 93 and 92% of the suspended sediment variability, respectively), can be generated by the combination of fluvial discharges and the action of the north quadrant wind during most of the simulated period, and was also observed by Marques et. al. (2009; 2010b). The second and the third EOF modes (Figures 14C, 14D, 14E, and 14F) presented small variability for both periods.

The transversal profiles at the mouth of the Patos Lagoon (Figure 15), on the other hand, indicate a feature similar to a floating plume (hypopycnal) as a result of the bathymetry constraining the low-density waters closer to the surface. This dominant pattern is represented by the first EOF mode (Figures 15A and 15B) during the neutral and ENSO periods (representing 73 and 70% of the suspended sediment variability, respectively).The second EOF mode highlights the presence of higher SSC in the main channel (southwest limit of the profile), representing 12 and 13% of the variability during the neutral (Figure 15C) and the ENSO periods (Figure 15D), respectively. The third EOF mode represents only 6% of the variability observed in the simulated period (Figures 15E and 15F), where negative values (blue areas) indicate low SSC inside the Patos Lagoon access channel as a result of south quadrant winds (Möller et. al., 2001; Castelão and Möller, 2006; Marques et. al., 2009; 2010a).

**Temporal Variability of Coastal Plumes**

The temporal variability of the suspended sediment coastal plumes during both studied periods (Figures 16-19) showed temporal scales from days to years for both the La Plata River mouth and the Patos Lagoon mouth when related to wind and freshwater discharge. The action of the wind is observed in cycles shorter than 15 days, which is related to the passage of weather fronts over the areas and is in accordance with the synoptic time scales observed by Möller et. al. (1996; 2001), Guerrero et. al. (1997), Simionato et. al. (2005) and Simionato et. al. (2007). The discharge however is related to the SSC on time scales from one month to one year covering intraseasonal, seasonal and interannual cycles associated with the precipitation patterns over the regions, which is in agreement with Acha et. al. (2008) and Marques et. al. (2010a).

**Behavior of suspended sediment on the Inner Shelf**

The SSC throughout the inner shelf (Figures 20 and 21) show a well-defined pattern between fluvial discharge and SSC in the Patos Lagoon, with the higher SSC occurring during the winter, when the discharge is higher (Marques et. al., 2009). In the La Plata River this relation presents a time-lag between the flow and SSC (Möller et. al., 1998; Marques et. al., 2010; Dogliotti et. al., 2016). As mentioned earlier, this delay is related to the distance between the effluents of the La Plata River and the location chosen to generate the diagram (transect T6 - Figure 1), as observed by Guerrero et. al. (1997) and Dogliotti et. al. (2016).

As for the interannual variations, there is a difference between the neutral years and the years affected by the ENSO phenomena. The effects on the suspended sediment distribution on the inner shelf of La Niña during 2008 and those of El Niño occurring at the end of 2009 were evident (Figure 21), but not sufficient to affect the SSC observed on the inner shelf during the neutral period (Figure 20). These results contradict the findings made by Dogliotti et. al. (2016), where the authors observed that during the La Niña years there was an increase in the concentration of suspended material compared to the El Niño years. This difference may be due to the location of the T6 profile (Figure 1).

When looking at the variability associated with the SSC on the inner shelf, the first two modes of the EOF analyses (Figure 22) represent approximately 75-76% of the sediment distribution observed during the simulated periods, respectively. The first EOF modes (Figures 22A and 22B), indicate a very similar distribution of suspended sediment on the inner shelf, with a well-defined pattern located in a small coastal strip, responding to the seasonal variation of SSC in the region (Figure 8). For the second EOF mode the suspended sediment variability indicates the influence of the north quadrant winds in the dynamics of the Patos Lagoon and the La Plata River plumes towards the south, as was also observed by Marques et. al. (2010b) and Simionato et. al. (2005). Thus, the wind becomes an important force on the internal platform, since the sediment moves away from the dynamic influence of the flow, both from the La Plata River and from the Patos Lagoon (Soares et. al., 2007a).

**Conclusion**

The Southwest Atlantic Inner Shelf is a region influenced by continental discharge and local wind. This influence is dominant in the suspended sediment transport process of the region, which is affected significantly from seasonal and interannual variations promoted by the ENSO cycles,

mainly in its fluvial discharge regime. The La Plata River is the major exporter of suspended sediment in the region, with an approximate rate of $1.2x10^8$ tons/year in a neutral period. For years under the ENSO influence, this rate rises to $3.0x10^8$ tons/year. The Patos Lagoon also contributes to the increase in SSC in the coastal region ($1.25x10^7$ tons/years without ENSO effect and 1.35 x $10^7$ tons/years with ENSO), but on a smaller scale compared to the La Plata River.

Regarding spatial variability in neutral years, there is a strongly defined SSC pattern in the Punta Piedras region, as well as on the south coast of the La Plata estuary, while on the north coast the sediment behavior presents greater variability due to the influence of the Uruguay River on the Uruguayan coast. In the periods affected by ENSO, the SSC shows low variability in practically all sectors of the estuary, evidencing the strong impact of the flow of the river on the distribution of sediments in the estuary. For the Patos Lagoon, there was no great difference in the spatial variability of sediments in the region. A well-defined pattern is observed in the region influenced by the Guaíba River, one of the principal suppliers of sediment to the Patos Lagoon.

Regarding spatial variability, results at the mouth of the rivers confirmed that in the La Plata River the plume behaves with homopycnal characteristics (affecting the whole water column), and the sediment is preferentially distributed toward the southern coast of the estuary, as a result of the Paraná River contribution. In the Patos Lagoon, the plume is classified as hypopycnal and tends to migrate southwards mainly due to the action of the predominant northeast wind.

As for temporal variability, the fluvial discharge interacts with the SSC on a seasonal up to an interannual scale, while the wind contributes to the SSC's variability on a synoptic time scale. Upon arriving at the inner shelf, the suspended sediment preferentially occupies a narrow coastal strip close to the shore. The wind, in turn, gains importance on the platform, as the sediment moves away from the influence of the flow, both from the La Plata River and the Patos Lagoon.

**Work limitations and future projection**

Because the present study does not consider the effect of waves in the region, it would be very relevant to use a wave model to analyze their contribution to this process. According to the literature (Santoro et. al., 2015), the waves are responsible for the remobilization of the bottom sediments back toward the water column, thus being important for the SSC distribution and behavior on the internal platform.

Another point to be highlighted is the period we chose to analyze the ENSO effects. During 2008 and 2009, the influence of La Niña was noticed most of the time, and El Niño only toward the

end of the period. However, the presence of the two distinct effects within a short period of time made the analysis of the results very difficult. The most appropriate thing would be to analyze a period completely influenced by only one of the effects, either El Niño or La Niña.

Finally, due to the lack of a long SSC time series in the analyzed periods, the values used as SSC in the effluents were annual averages used by other authors who had previously studied the same region. Despite the calibration exercises, which presents statistically satisfactorily results, the estimated values may be slightly different from true values.

**Funding:** This research was partially funded by the SUNSET project from CAPES nº 88881.192857/2018-01, edict COFECUB 382/2019.

**Acknowledgments:** The authors would like to thank CAPES (Coordination for Personal Improvement of Personnel) for sponsoring the doctoral scholarship of the first author (P.V.L.) through the Graduate Program in Oceanography (PPGO). We are also grateful to Team LOCOSTE (Laboratory of Coastal and Estuarine Oceanography) and team METHIS (Modélisation Expérimentale et Télédétection en Hydrodynamique Sédimentaire) for their support during this research, to Osmar Möller and to the FREPLATA project for providing the in-situ data used for calibration and validation of the TELEMAC-3D model.

**Conflicts of interest:** The authors declare that there are no conflicts of interest.

## References

Acha, E.M., Mianzan, H., Guerrero, R., Carreto, J., Giberto, D., Montoya, N., Carignan, M., 2008. An overview of physical and ecological processes in the Rio de la Plata Estuary. Continental Shelf Research, Vol 28 (13),1579-1588.

Acha, E.M., Mianzan, H.W., Guerrero, R., Favero, M., Bava, J., 2004. Marine fronts at the continental shelves of austral South America, Physical and ecological processes, J. Mar. Syst., 44, 83-105.

Bauer, W., Abreu, P.C., Poersch, L.H., 2017. Plankton and water quality variability in an estuary before and after the shrimp farming effluents: possible impacts and regeneration, Brazilian Journal of Oceanography, 65(3):495-508.

Berbery, E.H., Barros, V.R., 2002. The hydrologic cycle of the La Plata basin in South America. Journal of Hydrometeorology, 3, pp. 630-645.

Bisbal, G.A., 1995. The southeast South American shelf large marine ecosystem: Evolution and components, Mar. Policy, 19, 21-38.

Bitencourt, L.P., Fernandes, E.H., Möller, O., Ross, L., 2020.The contribution of ENSO cycles to the salinity spatio-temporal variability in a bar-built microtidal estuary, Regional Studies in Marine Science, Vol 40,101496.

Blanton, J., Oey, L-Y., Amft, J., Lee, T. N., 1989. Advection of momentum and buoyancy in a coastal frontal zone. Journal of Physical Oceanography 19, 98-15.

Brodie, J., Schroeder, T., Rohde, K., Faithful, J., Masters, B., Dekker, A., Brando, V., Maughan, M., 2010. Dispersal of suspended sediments and nutrients in the Great Barrier Reef lagoon during river-discharge event: conclusions from satellite remote sensing and concurrent flood-plume sampling. Marine and Freshwater Research, 61, 651-664.

Burrage, D., Wesson, J., Martinez, C., Pérez, T., Möller Jr, O., Piola, A., 2008. Patos Lagoon outflow within the Río de la Plata plume using an airborne salinity mapper: Observing an embedded plume. Continental Shelf Research. 28, 1625-1638.

Calliari, D., Brugnoli, E., Ferrari, G., Vizziano, D., 2009. Phytoplankton distribution and production along a wide environmental gradient in the South-West Atlantic off Uruguay. Hydrobiology 620, 47-61.

Calliari, L.J., Fachin, S., 1993. Laguna dos Patos. Influência nos Depósitos Lamíticos Costeiros. Pesquisas. 20(1), 57-69.

Campos, J.D., Lentini, C.A., Miller, J.L., Piola, R.A., 1999. Inter-annual variability of the sea surface temperature in the South Brazilian Bight. Geophysical Research Letters, 26(14), 2061-2064.

Castelão, R.M., Möller, O.O., 2006. A modeling study of Patos Lagoon (Brazil) flow response to idealized Wind and river discharge: Dynamical analysis. Brazilian Journal of Oceanography. 54(1), 1-17.

Castello, J., Duarte, A., Möller, O.O., Niencheski, F., Odebredcht, C., Weiss, G., Habiaga, R., Bellotto, V., Kitzmann, D., Souto, C., Souza, R., Ciotti, A., Fillmann, G., Schwingell, P., Bersano, J., Cirano, M., Freire, K., Lima, I., Mello, R., Monteiro, A., Resgalla, C., Soares, I., Suzuki, M., 1990.

On the importance of coastal and subantartic waters for the shelf ecosystem off Rio Grande do Sul. Anais do II Simpósio de Estrutura, Função e Manejo de Ecossistemas da Costa Sul e Sudeste, São Paulo – Brazil, I: 112-129.

Castello, J.P., Möller Jr., O.O., 1977. Sobre as condições oceanográficas no Rio Grande do Sul, Brasil. Atlântica 2, 25-110.

Ciotti, A.M., Odebrecht, C., Fillmann, G., Möller, O.O., 1995. Freshwater outflow and subtropical convergence influence on phytoplankton biomass on the southern Brazilian continental shelf. Continental Shelf Research. 15(14), 1737-1756.

Costi, J., Marques, W.C., Kirinus, E.P., Duarte, R.F., Arigony-Neto, J., 2018. Water level variability of the Mirim-São Gonçalo System, a large, subtropical, semi-enclosed coastal complex. Adv. Water Resour, 117, 75-86.

Depetris, P.J., Pasquini, A.I., 2007b. Discharge trends and flow dynamics of southern southamerican rivers draining the southern Atlantic seabord: an overview. Journal of hydrology 333:385-399.

Depetris, P.J., Paolini, J.E., 1991. Biogeochemical aspects of South American rivers: the Paraná and the Prinoco. In: Degens, E.T., Demp, S.J.E. Richey (Eds.), En: Biogeochemistry of Major World Rivers, Scope 42. John Wiley & Sons, New York, pp. 165–194.

Diaz, M., Grasso, F., Le Hir, P., Sottolichio, A., Caillaud, M., Thouvenin, B., 2020. Modeling mud and sand transfers between a macrotidal estuary and the continental shelf: Influence of the sediment transport parameterization. Journal of Geophysical Research: Oceans, 125.

Dogliotti, A.I., Ruddick, K., Guerrero, R., 2016. Seasonal and inter-annual turbidity variability in the Río de la Plata from 15 years of MODIS: El Niño dilution effect. Estuar. Coast. Shelf Sci. 182, 27-39.

Edgbert, G.D., Erofeeva, S.Y., 2002. Efficient Inverse Modeling of Barotropic Ocean Tides. Journal of Atmospheric and Oceanic Technology,19:183-204.

Emilson, I., 1961. The Shelf and coastal waters off southern Brazil. Boletim do Instituto Oceanográfico da Universidade de São Paulo 11 (2), 101-112.

Exner F.M., 1925. über die wechselwirkung zwischen wasser und geschiebe in flüssen, Akad. Wiss. Wien Math. Naturwiss. Klasse, 134,165-204.

Farge, M., 1992. Wavelet transforms and their applications to turbulence. Annu. Rev. Fluid Mech. 24, 395-457.

Fernandes, E.H.L., Dyer, K.R., Möller, O.O., 2005. Spatial gradients in the flow of the southern Patos Lagoon. Journal of Coastal Research, v. 21, n. 4, p. 759-769.

Fernandes, E.H.L., Dyer, K.R., Möller, O.O., Niencheski, L.F.H., 2002. The Patos Lagoon Hydrodynamics during an El Nino event (1998). Continental Shelf Research, England, v. 22, n. 11-13, p. 1699-1713.

Fernandes, E.H.L., Dyer, K.R., Niencheski, L.F.H., 2001. Calibration and validation of the TELEMAC-2D model to the Patos Lagoon, Brazil. Journal of Coastal Research, USA, v. 34, p. 470-488.

Fernandes, E.H.L., Mariño-Tapia, I., Dyer, K.R., Möller, O.O., 2004. The attenuation of tidal and subtidal oscillations in the Patos Lagoon estuary. Ocean Dynamics, Alemanha, v. 54, n. 4, p. 348-359.

Fernandes, E.H.L., Monteiro, I., Möller, O.O., 2007. On the dynamics of Mangueira Bay - Patos Lagoon (Brazil). Journal of Coastal Research, v. 47, p. 97-107.

Fossati M, Piedra-Cueva I., 2013. A 3D hydrodynamic numerical model of the Río de la Plata and Montevideo's coastal zone. Appl Math Modell. 37: 1310-32

Fossati, M., Cayocca, F., Piedra-Cueva, I., 2014. Fine sediment dynamics in the Río de la Plata. Advanced Geosciences, 39,75-80.

Foster, G., Carter, L., 1997. Mud sedimentation on the continental shelf at an accretionary margin - Poverty Bay, New Zealand, New Zealand Journal of Geology and Geophysics, 40:2, 157-173.

Framiñan, M.B., Brown, O.B., 1996. Study of the Río de la Plata turbidity front: I. Spatial and temporal distribution. Continental Shelf Research, 16, 1259-1282.

Gabioux, M. Vinzon, S.B. and Paiva, A. M., 2005. Tidal propagation over fluid mud layers on the Amazon shelf. Continental Shelf Research 25, 113-125.

García-Rodríguez, F., Brugnoli, E., Muniz, P., Venturini, N., Burone, L., Hutton, M., Rodríguez, Pita, A., Kandratavicius, N., Perez, L., Vercai, J., 2014. Warm-phase ENSO events

modulate the continental freshwater input and the trophic state of sediments in a large South American estuary. Marine Freshwater research 65:1-11.

Geyer, W.R., Hill, P.S., Kineke, G.C., 2004. The transport, transformation and dispersal of sediment by buoyant coastal flows. Continental Shelf Research, v.24, p.927-949.

Grimm, A.M., Barros, V.R., Doyle, M.E., 2000. Climate variability in southern south America associated with El Niño and La Niña events. American Meteorological Society 2000:35-57.

Grimm, A.M., Ferraz, S.E.T., Julio, G., 1998. Precipitation anomalies in southern Brazil associated with El Niño and La Niña events. American Meteorological Society 1998:2863-2879.

Guerrero, R.A., Acha, E.M., Framiñan, M.B., Lasta, C.A., 1997. Physical oceanography of the Río de la Plata estuary Argentina. Continental Shelf Research 17 (7), 727-742.

Haimovici, M., Pereira, S.D., Vieira, P.C., 1989. La pesca demersal en el sur de Brasil en el periodo 1975-1985. Frente maritmo, S(A), 151-163.

Haque, A., Rahman, M., 2016. Flow distribution and sediment transport mechanism in the estuary systems of Ganges-Brahmaputra-Meghna Delta. International Journal of Environmental Science and Development, Vol. 7, No. 1.

Hartmann, C. Sano, E.E., Paz, R. S., Möller, O.O., 1986. Avaliação de um período de cheia (junho de 1984) na região sul da Laguna dos Patos, através de dados de sensoriamento remoto, meteorológicos e oceanográficos. 4o Simpósio Brasileiro de Sensoriamento Remoto. Gramado, RS. 685-693.

Hartmann, C., Calliari, L.J., Möller, O.O., 1990. Material Em Suspensão No Estuário da Laguna dos Patos, Rs, Fase I. Obs. Preliminares, Abril 79 A Dez. 80. Sociedade & Natureza.

Hartmann, C., Schettini, C.A.F., 1991. Aspectos hidrológicos na desembocadura da Laguna dos Patos, RS. Revista Brasileira de Geociências, 21(4): 371-377.

He, L., Chen, D., Zhang, S., Liu, M., Duan, G., 2018. Evaluating Regime Change of Sediment Transport in the Jingjiang River Reach, Yangtze River, China. Water, 10, 329.

Helder, W. and Ruardij, P., 1982. A one-dimensional mixing and flushing model of the Ems-Dollard Estuary. Neth. J. Sea Res., 15: 293-312.

Hervouet, J-M., 2007. Free surface flows: Modelling with the finite element methods. John Wiley & Sons Ltd, Copyright © 2007, England.

Ivanoff, M.D., Toldo, E.E., Figueira, R.C.L., Ferreira, P.A.L., 2020. Use of 210Pb and 137Cs in the assessment of recent sedimentation in Patos Lagoon, southern Brazil. Geo-Mar Lett.

Jalon-Rojas, I., Schmidt, S., Sottolichio, A., 2016. Evaluation of spectral methods for high-frequency multiannual time series in coastal transitional waters: advantages of combined analyses. Limnol. Oceanogr.: Methods 14, 381-396.

Janin, J.M., Marcos, F., 1997. Code TELEMAC-3D – Version 2.2: Note Théorique, Report HE-42/97/049/B, Electricité de France/LNHE, Paris.

Kineke, G.C., Sternberg, R.W., 1995. Distribution of fluids muds on the Amazon continental shelf. Marine Geology, 125, 193-233.

Kjerfve, B., 1986. Comparative oceanography of coastal lagoons, p. 63-81. In D. A. Wolfe (ed.), Estuarine Variability. Academic Press, New York.

Kourafalou, V.H., Oey, L-Y., Wang, J.D., Lee, T.N., 1996a. The fate of river discharge on the continental shelf. 1. Modeling the river plume and the inner shelf coastal current. J. Geophys. Res. 101, 3415-3434.

Lee, B.J., Toorman, E., Molz, F.J., Wang, J., 2011. A two-class population balance equation yielding bimodal flocculation of marine or estuarine sediments. Water Research 45(5):2131-2145.

Lisboa, P.V., Fernandes, E.H., 2015. Anthropogenic influence on the sedimentary dynamics of a sand spit bar, Patos Lagoon Estuary, RS, Brazil. Journal of Integrated coastal Zone Manegement. 15 (1), 35-46.

Mann, K.H., Lazier, J.R.N., 1991. Dynamics of Marine Ecosystems: Biological–Physical Interactions in the Oceans. Blackwell Scientific Publications, Oxford 466pp.

Marques, W.C., Möller, O.O., 2009. Variabilidade temporal em longo período da descarga fluvial e níveis de água da Lagoa dos Patos, Rio Grande do Sul, Brasil. Revista Brasileira de Recursos Hídricos 13, 155-163.

Marques, W.C., Fernandes, E.H.L., Moraes, B.C., Möller, O.O., Malcherek, A., 2010b. Dynamics of the Patos Lagoon coastal plume and its contribution to the deposition pattern of the Southern Brazilian inner shelf. Journal of Geophysical Research, 115(C10):1-22.

Marques, W.C., Fernandes, Möller, O.O., 2010a. Straining and advection contributions to the mixing process of the Patos Lagoon coastal plume, Brazil. Continental Shelf Research. v. 116, n. C3, p. C03016.

Martins, L.R., Villwock, J.A., 1987. Eastern South America quaternary coastal and marine geology. Reports in Marine Sciences, UNESCO 43, 28-86.

Meade, R.H., 1996. River-sediment inputs to major deltas. In Sea-level Rise and Coastal Subsidence (Milliman, S.D. & Haq, B.U., eds). Kluwer Academic Press, Boston, pp. 63-85.

Meccia, V.L., Simionato, C.G., Fiore, M.M.E., D'Onofrio, E., Dragani, W.C., 2009. Sea surface height variability in the R´ıo de la Plata estuary from synoptic to inter-annual scales: Results of numerical simulations. Estuarine, Coastal and Shelf Science, 85(2), 327-343

Menandro, P.S., Bastos, A.C., Quaresma, V.S., Vinzón; S.B., 2015. Acoustic response of Amazon Shelf muddy sediments. Revista Brasileira de Geofísica 33(4): 625-636.

Menéndez, A.N., Sarubbi, A., 2007. A Model to Predict the Paraná Delta Front Advancement. Workshop on Morphodynamic Processes in Large Lowland Rivers, (Santa Fe, Argentina), pp. 25.

Milliman, J. D.; Shen, H.; Yang, Z.; Meade, R.H., 1985. Transport and deposition of river sediment in the Changjiang estuary and adjacent continental shelf. Continental Shelf Research, Vol.4, pp. 37-45.

Milliman, J.D., Syvitski, J.P.M., 1992. Geomorphic/tectonic control of sediment discharge to the ocean: the importance of small mountainous rivers. Journal of Geology 100, 525-544.

Möller, O.O., Castaing, P., 1999. Hydrographical characteristics of the estuarine area of Patos Lagoon (30° S, Brazil), p. 83-100. In G. M. Perillo, M.C. Piccolo, M. Pino (eds.), Estuaries of South America: Their Geomorphology and Dynamics. Springer Verlag, Berlin.

Möller, O.O., Castaing, P., Salomon, J.C., Lazure, P., 2001. The influence of local and non-local forcing effects on the subtidal circulation of Patos Lagoon. Estuaries 24:297-311.

Möller, O.O., Lorenzzetti, J.A., Stech, J.L., Mata, M. M., 1996. The Patos Lagoon summertime circulation and dynamics. Coastal Shelf Research 16:335-351.

Möller, O.O., Piola, A.R., Freitas, A.C., Campos, E.J.D., 2008. The effects of river discharge and seasonal winds on the shelf off southeastern South America. Continental Shelf Research 28, 1607-1624.

Montanher, O.C., Novo, E.M., Filho, E.E., 2018. Temporal trend of the suspended sediment transport of the Amazon River (1984-2016), Hydrological Sciences Journal, DOI: 10.1080/02626667.2018.1546387.

Monteiro, I.O., Marques, W.C., Fernandes, E.H., Gonçalves, R.C., Möller Jr, O.O., 2011. On the effect of earth rotation, river discharge, tidal oscillations, and wind in the dynamics of the patos lagoon coastal plume. Journal of Coastal Research, Editora da Furg, v. 271, p. 120-130.

Moreira, D., Simionato, C.G., 2019. Modeling the suspended sediment transport in a very wide, shallow, and microtidal estuary, the Río de la Plata, Argentina. Journal of Advances in Modeling Earth Systems, 11, 3284-3304.

Moreira, D., Simionato, C.G., Dragani, W., Cayocca, F., Tejedor, M.L.C., 2016. Characterization of Bottom Sediments in the Río de la Plata Estuary. Journal of Coastal Research, 32(6), 1473-1494.

Moreira, D., Simionato, C.G., Gohin, F., Cayocca, F., Tejedor, M.L.C., 2013. Suspended matters mean distribution and seasonal cycle in the Río de la Plata estuary and the adjacent shelf from MODIS and in situ observations. Continental Shelf Research, 68, 51-66.

Oliveira, H., Fernandes, E., Möller, O., García-Rodríguez, F., 2019. Relationships between Wind Effect, Hydrodynamics and Water Level in the World's Largest Coastal Lagoonal System. Water 11 (11), 2209.

Oliveira, H.A., Fernandes, E.H.L., Möller, O.O., Collares, G.L., 2015. Processos Hidrológicos e Hidrodinâmicos da Lagoa Mirim. RBRH vol. 20 no1 Porto Alegre jan./mar. 2015 p. 34-45.

Palma, E. D., Matano, R. P., and Piola, A. R., 2008. A numerical study of the Southwestern Atlantic Shelf circulation: Stratified ocean response to local and offshore forcing, J. Geophys. Res., (C0) 8014.

Partheniades, E., 1965. Erosion and deposition of cohesive soils. Journal of the Hydraulics Division, 91(1), 105-39.

Pasquini, A.I., Depetris, P.J., 2007. ENSO-triggered exceptional flooding in the Paraná River: where is the excess water coming from? J. Hydrol. 383 (2010), 186-193.

Peixoto, D.W.B., Guasselli, L.A., Waterloo, P.F., 2018. Estimativa de Concentração de Sedimentos em Suspensão a Partir de Imagens Landsat 8 em PCHs no Rio Ivaí-RS. São Paulo: Geociências (Online), v. 37, p. 147-154.

Pereira, C.S., 1989. Seasonal variability in the coastal circulation on the Brazilian Continental Shelf (29–351S). Continental Shelf Research 9, 285-289.

Pimenta, F.M., Campos, E.J.D., Miller, J. L., Piola, A. R., 2005. A numerical study of the Plata River plume along the Southeastern South American Continental Shelf. Brazilian Journal of Oceanography, 53(3/4):129-146.

Piola, A.R., Romero, S.I., 2004. Analysis of space-time variability of the Plata River plume. Gayana (Concepción), 68(2, Supl. TIIProc), 482-486.

Piola, A.R., Campos, E.J.D., Möller. O.O., Charo, M., and Martinez, C., 2000. Subtropical Shelf Front off eastern South America. Journal of Geophysical Research. 105(C3), 6565-6578.

Piola, A.R., Matano, R.P., Palma, E.D., Möller, O.O., Campos, E.J.D., 2005. The influence of the Plata River discharge on the western South Atlantic shelf. Geophysical Research Letters. 32.

Rodrigues, A., Oliveira, A., Fonseca, R.; Taborda, R.; Cascalho, J., 2006. Sedimentary dynamics of the southern shelf of Madeira (Portugal). Journal of Coastal Research, SI 39 (Proceeding of the 8th International Coastal Symposium), 454-458. Itajaí, SC, Brazil, ISSN 0749-0208.

Rosa, F., Rufino, M.M., Ferreira, Ó., Matias, A., Brito, A.C., Gaspar, M.B., 2013. The influence of coastal processes on inner shelf sediment distribution: The Eastern Algarve Shelf (Southern Portugal), Geologica Acta, 11, 59-73.

Santoro, P., Fossati, M., Piedra-Cueva, I., 2013. Characterization of circulation patterns in Montevideo Bay (Uruguay). Journal of Coastal Research, 29 (4), 819-835

Santoro, P., Huybrechts, N., Fossati, M., Van Bang, D., Tassi, P., Piedra-Cueva, I., 2016. 2D and 3D numerical study of the Montevideo Bay hydrodynamics and fine sediment dynamics. Proceedings of the XXIIIrd TELEMAC-MASCARET User Conference 2016, 11 to 13 October 2016, Paris, France, 177-188.

Sepúlveda, H.H., Valle-Levinson, A., Framiñan, M., 2004: Observations of subtidal and tidal flows in the Río de la Plata Estuary. Continental Shelf Research, 24, 509-525.

Silva, P., Lisboa, P., Fernandes, E., 2015. Changes on the fine sediment dynamics after the Port of Rio Grande expansion. Adv. Geosci. 39, 123-127.

Simionato, C.G. and Moreira, D., 2018. Modeling the processes that control fine sediments transport in the Río de la Plata Estuary. Journal of Coastal Research, Special Issue No. 85, pp. 31-35.

Simionato, C.G., Meccia, V., Guerrero, R., Dragani, W., Nuñez, M., 2007. The Rio de la Plata estuary response to wind variability in synoptic to intra-seasonal scales: II currents vertical structure and its implications on the salt wedge structure. J. Geophys. Res. C Oceans 112, C07005.

Simionato, C.G., Meccia, V.L., Dragani, W.C., 2009. On the path of plumes of the Río de la Plata estuary main tributaries and their mixing time scales. Geoacta 34, 87-116.

Simionato, C.G., Clara Tejedor, M.L., Campetella, C., Guerrero, R., Moreira, D., 2010. Patterns of sea surface temperature variability on seasonal to sub-annual scales at and offshore the Río de la Plata Estuary. Continental Shelf Research, 30(19), 1983-1997

Simionato, C.G., Nuñez, M.N., Engel, M., 2001. The salinity front of the Río de la Plata - A numerical case study for winter and summer conditions. Geophysical Research Letters, 28(13), 2641-2644.

Simionato, C.G., Vera, C.S., Siegismund, F., 2005. Surface wind variability on seasonal and interannual scales over R´ıo de la Plata area. Journal of Coastal Research, 21(4), 770-783.

Smith, W.H.F., Sandwell, D.T., 1997. Global sea floor topography from satellite altimetry and ship depth soundings. Science 277, 1956-1962.

Soares, I.D., Kourafalou, V., Lee, T.N., 2007a. Circulation on the western South Atlantic continental shelf. Part 1: Numerical process studies on Buoyancy. Journal of Geophysical Research. 112, C04002.

Soares, I.D., Kourafalou, V., Lee, T.N., 2007b. Circulation on the western South Atlantic continental shelf. Part 2: Spring and autumn realistic simulations. Journal of Geophysical Research. 112, C04003.

Souza, R.B., Robinson, I.S., 2004. Lagrangian and satellite observations of the Brazilian Coastal Current. Continental Shelf Research. 24, 241-262.

Sutherland, J., Peet, A.H., Soulsby, R.T., 2004b. Evaluating the performance of morphological models. Coast. Eng. 51, 917-939.

Sutherland, J., Walstra, D.J.R., Chesher, T., Van Rijn, L.C., Southgate, H.N., 2004a. Evaluation of coastal area modelling systems at an estuary mouth. Coast. Eng. 51 (2), 119-142.

Talke, S.A., Stacey, M.T., 2008. Suspended sediment fluxes at an intertidal flat: The shifting influence of wave, wind, tidal, and freshwater forcing. Continental Shelf Research. 28(2008), 710-725.

Távora, J., Fernandes, E.F., Bitencourt L.P., Orozco, P.M.S., 2020. El-Niño Southern Oscillation (ENSO) effects on the variability of Patos Lagoon Suspended Particulate Matter. Regional Studies in Marine Science, 101495.

Toldo Jr., E.E., Corrêa, I.C.S., Almeida, L.E.S.B., Weschenfelder, J., Gruber, N.L.S., 2006. Sedimentação de Longo e curto período na Lagoa dos Patos. Pesquisas em Geociências. 33(2), 79-86.

Toldo Jr., E.E., Ayup Zouain, R.N., Corrêa, I.C.S., Dillenburg, S.R., 1991. Barra Falsa: Hipótese de um paleocanal holocênico de comunicação entre a Laguna dos Patos e o Oceano Atlântico. Pesquisas, 18(2):99-103.

Torrence, C., Compo, G.P., 1997. A practical guide to wavelet analysis. Bull. Am. Meteorol. Soc, 79, 61-78.

Van Leussen, W., 1994. Estuarine macroflocs and their role in fine-grained sediment transport. Utrecht: I. University of Utrecht.

Vaz, A.C., Almeida, T.L., Möller, O., 2006. Sobre a descarga dos rios afluentes da Lagoa dos Patos. Atlântica, v. 28, p. 1-12.

Walstra, L., Van Rijn, L., Blogg, H., Van Ormondt, M., 2001. Evaluation of a Hydrodynamic Area Model Based on the COAST3D Data At Teignmouth 1999. Report TR121-EC MAST Project No. MAS3-CT97-0086, HR Wallinford, UK, pp. D4.1-D4.4.

Warrick, J. A., Simms, A. R., Ritche, A., Steel, E., Dartnell, P., Conrad, J. E., Finlayson, D. P., 2013. Hyperpycnal plume-derived fans in the Santa Barbara Channel, California. Geophysical Research Letters, Vol. 40, 2081-2086.

Winterwerp, J.C., 2002. On the flocculation and settling velocity of estuarine mud. Continental Shelf Research, 22, 1339-1360.

Wright, L.D., Nittrouer, C.A., 1995. Dispersal of river sediments in coastal seas: Six contrasting cases, Estuaries, 18, 494-508.

Wright, L., Friedrichs, C., 2006. Gravity-driven sediment transport on continental shelves: A status report. Continental Shelf Research, 26, 2092-2107.

Ye, S., Ran, Q., Fu, X., Hu, C., Wang, C., Parker, G., Chen, X., Zhang, S., 2019. Emergent stationarity in Yellow River sediment transport and the underlying shift of dominance: from streamflow to vegetation. Hydrology Earth System Sciences, 23, 549-556.

Zavialov, P.O., Ghisolfi, R.D., Garcia, C.A.E.,1998. An inverse model for seasonal circulation over the Southern Brazilian shelf: near-surface velocity from the heat budget, J. Phys. Oceanogr., 28, 545-561.

## Appendix A - Details about the simulation and model set-up

The analysis of the behavior and variability of the dynamics of sediments in suspension for the Southwest Atlantic Inner Continental Shelf was performed with numerical modelling techniques, using the TELEMAC 3D model. Six hydrodynamic simulations were carried out, with a duration of 730 days for the years 2005 to 2006, and 2008 to 2009, with the following configuration:

***Tabela 5 - Table A1 - Artigo 1 - Set-up of the simulations***

| Simulation | Description | La Plata Discharge | Patos Lagoon Discharge | 2005-2006 | 2008-2009 |
|---|---|---|---|---|---|
| SIM 1 | Model forced with all physical forces for the period from 2005 to 2006; | X | X | X | |
| SIM 2 | Forced model with all physical forces for the period from 2008 to 2009; | X | X | | X |

The methodological steps developed in this work are presented in Figure A1, and detailed below.

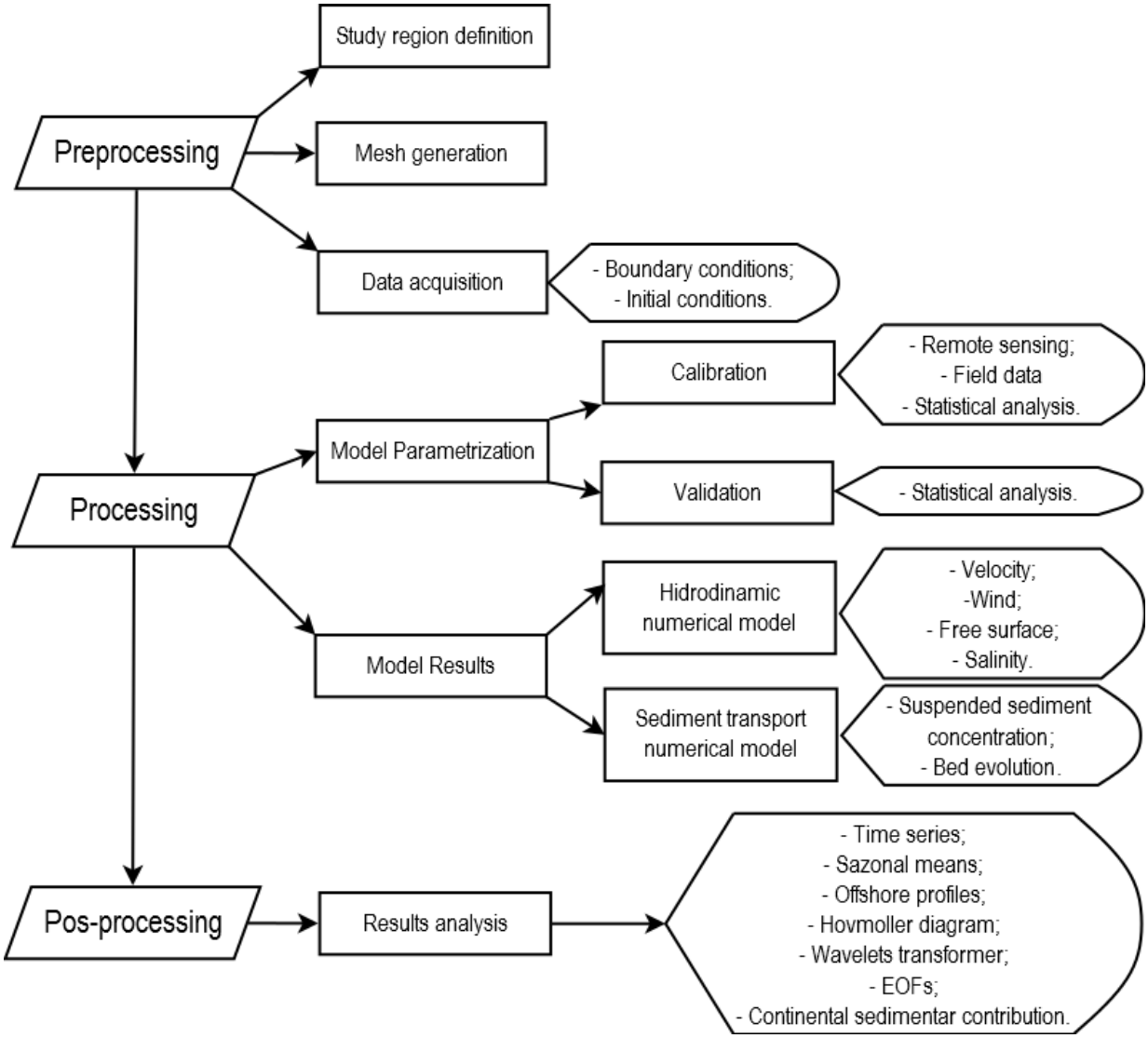


Figura 36 - Figure A1 - Artigo 1 - Summary of the methodological steps used in this work.

## Appendix B - Initial and Boundary Conditions

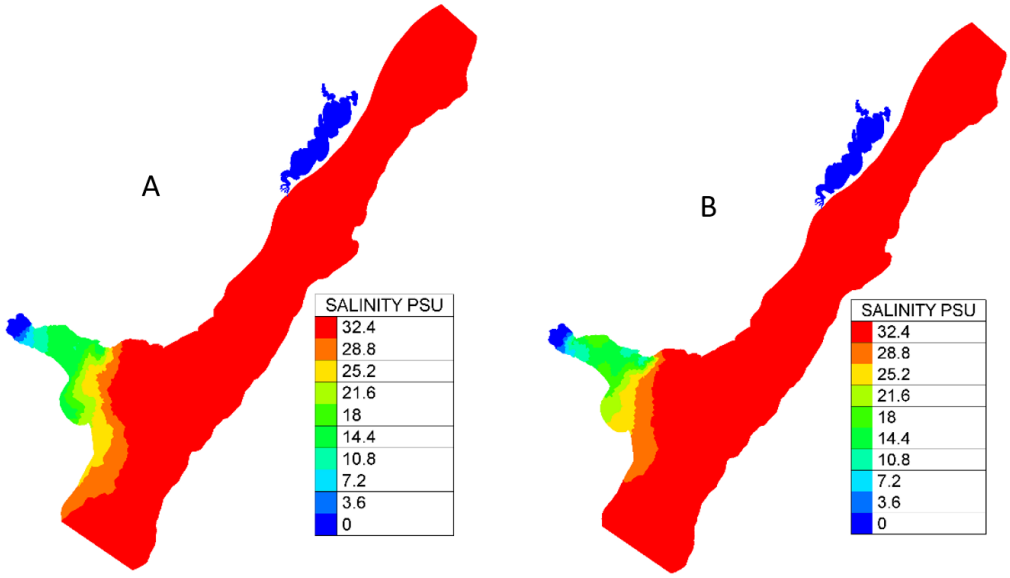


Figura 37 - Figure B1 - Artigo 1 - Salinity fields used as an initial condition in the surface layer of the model in January 2005 (A) and January 2008 (B).

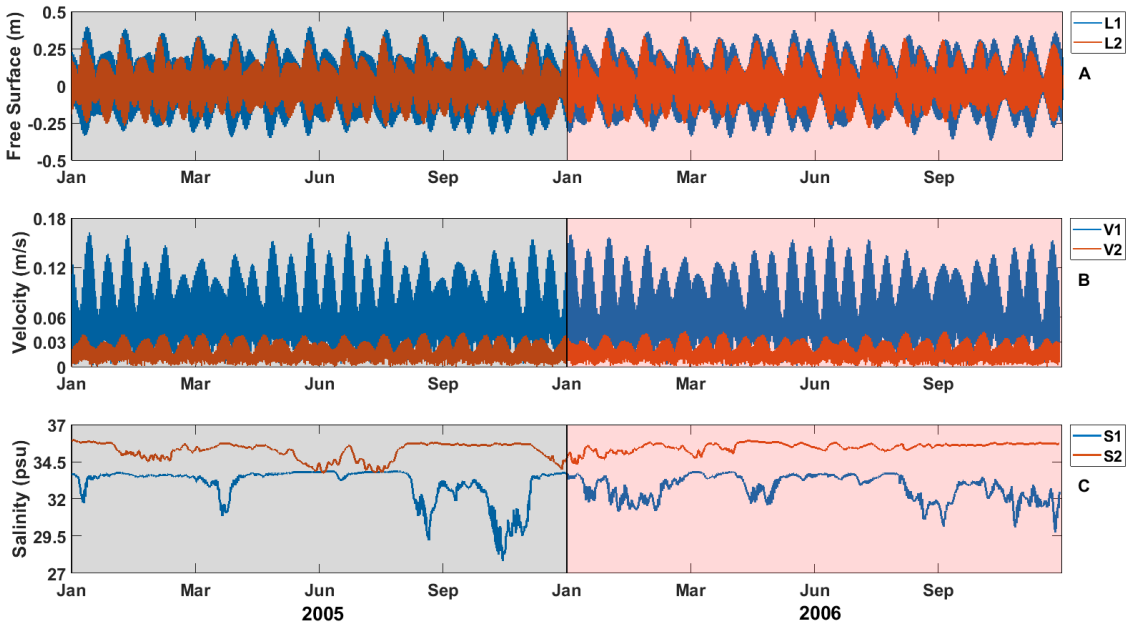


Figura 38 - Figure B2 - Artigo 1 - Data prescribed as the boundary condition at the ocean boundary at points L1 and L2 (sea surface elevation) (A), V1 and V2 (current velocity) (B), and S1 and S2 (salinity) (C) for the period 2005-2006. The boundary conditions for 2008-2009 are not presented.

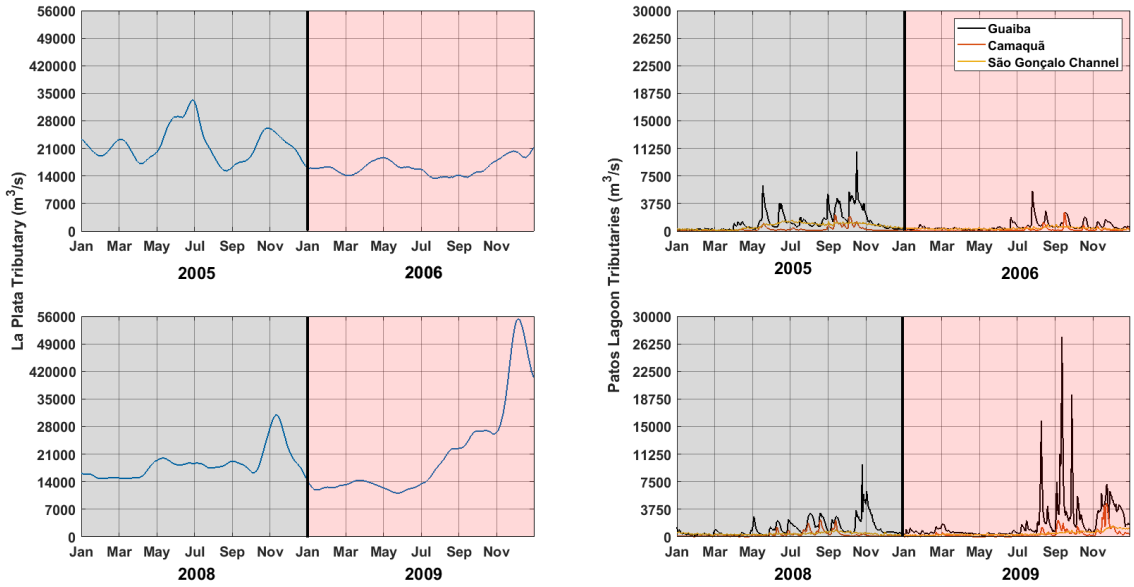


Figura 39 - Figure B3 - Artigo 1 - Time series of the freshwater discharge from the Guaíba River, Camaquã River, São Gonçalo Channel and the La Plata River for both studied periods (2005-2006 and 2008-2009).

Figure B4 shows the frequency distribution of the time series of wind intensity for the simulated periods (2005-2006 and 2008-2009), indicating that the wind velocity varied between 0.19 m/s and 20.3 m/s, with the average around 5.63 m/s for the simulation between the years 2005-2006, and with a predominant northeast direction. The strongest winds, however, are from the southwest. For the simulation between 2008-2009 the wind varied between 0.04 m/s and 7.32 m/s, with a predominant northeast direction and stronger winds in the southeast direction.

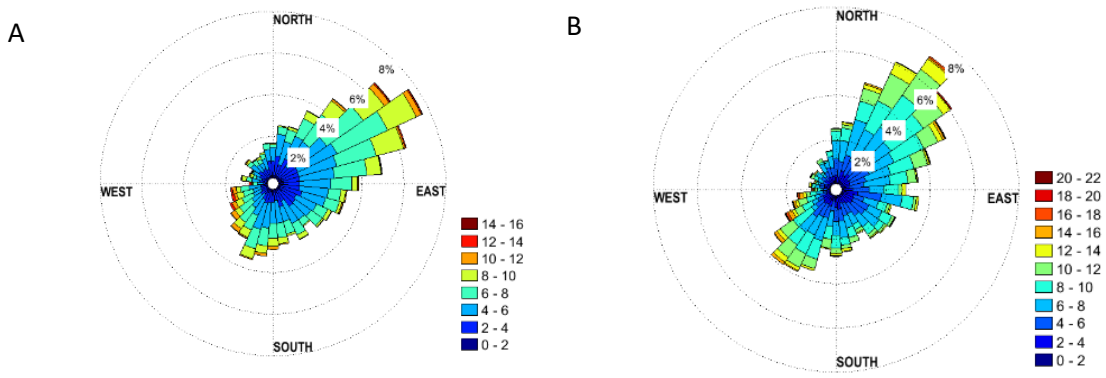


Figura 40 - Figure B4 - Artigo 1 - Wind Rose for the frequency distribution of the time series of wind intensity and direction, for the years 2005-2006 (A) and 2008-2009 (B).

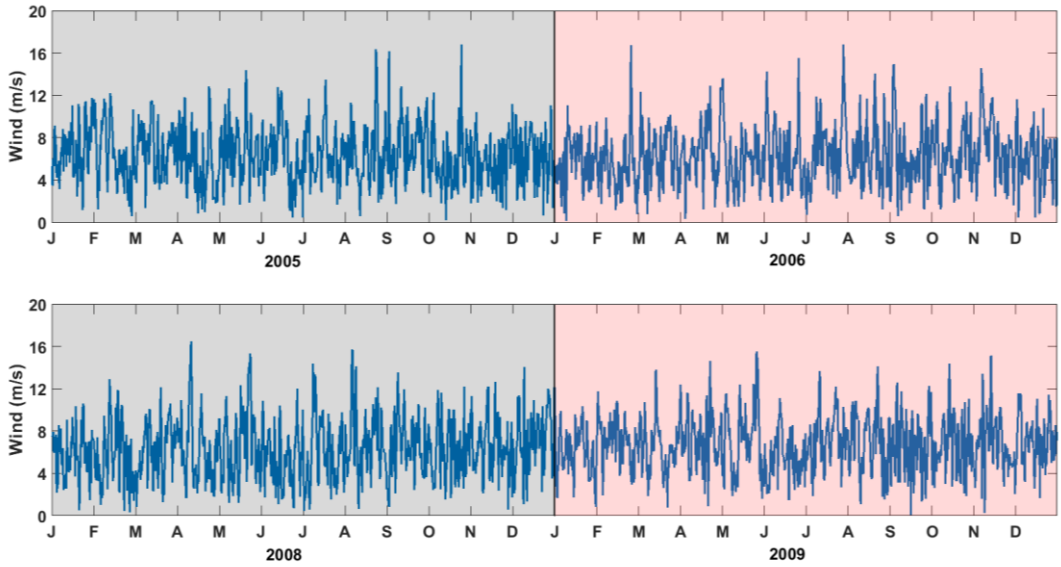


Figura 41 - Figure B5 - Artigo 1 - Time series of intensity used as a superficial forcing in the simulation.

**Tabela 6 - Table B1 - Artigo 1 - Summary of the sources of data prescribed in the initial and boundary conditions.**

| Forcing | Data Source |
|---|---|
| **Continental Discharge** | Guaíba and Camaquã – (National Water Agency);<br>São Gonçalo - Rating Curve Method (Oliveira *et al.,* 2015);<br>La Plata – Naval Hydrography Service of Argentina |
| **Wind** | ECMWF – ERA Interim |
| **Tide** | TPXO |
| **Velocity** | TPXO |
| **Level** | TPXO |
| **Salinity** | HYCOM + NCODA 1/12º |
| **Suspended Sediment** | Fine Silt |
| **Bottom Sediment** | Fine Silt |
| **Suspended Sediment Concentration** | Patos Lagoon - Marques et al., 2010<br>La Plata - Moreira and Simionato, 2019 |

## Appendix C – Statistical parameters for model calibration and validation

The calibration and validation of the model consist of comparisons between model results and in situ data for the same period and location, which are quantified based on statistical analyses such as the root mean square error (RMSE) and the Relative Mean Absolute Error (RMAE) (Janssen et al, 1997; Lalbeharry, 2001; Lalbeharry et al., 2001; Wastra et al., 2001; 2004; Bidlot et al., 2002; Sutherland et al., 2004).

The Root Mean Square Error (RMSE) determines the magnitude of the mean square error module (i.e., without considering if the number is negative or positive) between the observations and the values calculated by the model, according to the following mathematical expression:

$$RMSE = \sqrt{\frac{\sum_{i=1}^{n}(m_i - o_i)^2}{n}} \quad (1)$$

Where, $m$ is a model result, $o$ is measured or observed data point and $n$ is the number of points.

The RMAE indicates the average relative error between the measurements and the results obtained in the model, which was used to quantify the quality of the results found in the best calibration experiment and in the validation tests of the TELEMAC mode (Wastra *et al.,* 2001). The average absolute value of the observed values and the modelled values are given by:

$$\langle |X| \rangle = \frac{1}{n}\sum_{i=1}^{n}|X_n| \quad (2)$$

$$\langle |Y| \rangle = \frac{1}{n}\sum_{i=1}^{n}|Y_n| \quad (3)$$

Where $X$ are observed values, and $Y$ are modelled values, with each of the values being in the same spatial and temporal position. These values can be scalar (wave height or water level) or vectors (currents). The angular parenthesis expresses the mean and, respectively, the $X$ and $Y$ modules. Similarly, the mean absolute error (MAE) is given by:

$$MAE = \langle |Y - X| \rangle \quad (4)$$

The quality of the modelling can be assessed by the RMAE value, as follows:

$$RMAE = \frac{\langle |Y-X| \rangle}{\langle |X| \rangle} = \frac{MAE}{\langle |X| \rangle} \quad (5)$$

**Tabela 7 - Table C1 - Artigo 1 - Rating scale for the relative mean absolute error (RMAE) (Sutherland et al., 2004 and Walstra et al., 2001)**

| Qualification | Excellent | Good | Reasonable | Poor | Bad |
|---|---|---|---|---|---|
| **RMAE** | ≤0.2 | 0.2 – 0.4 | 0.4 – 0.7 | 0.7 – 1.0 | > 1.0 |

**Appendix D – Calibration tests carried out for the hydrodynamic model and respective errors when comparing with data from the Patos Lagoon and the La Plata River.**

**Tabela 8 - Table D1 - Artigoo 1 - Parameters used in the calibration of the model, with the respective RMAE results for each of the tests (Patos Lagoon and La Plata River level). The results of the RMAE for the test with the best approximation in relation to the measured values are marked in bold.**

| Test | Wind Influence Coefficient | Vertical Turbulence | Horizontal Turbulence | Bottom Friction Laws | Friction Coefficient | RMAE Cassino Beach | RMAE La Plata River |
|---|---|---|---|---|---|---|---|
| 01 | $3x10^{-6}$ | K-ε | Smagorinsky | Manning | 0.01 | 0.1452 | 0.2993 |
| 02 | $3x10^{-6}$ | K-ε | Smagorinsky | Manning | 0.02 | 0.3573 | 0.2478 |
| 03 | $3x10^{-6}$ | K-ε | Smagorinsky | Manning | 0.03 | 0.3919 | 0.2612 |
| 04 | $3x10^{-6}$ | K-ε | Smagorinsky | Manning | 0.04 | 0.2547 | 0.3641 |
| 05 | $3x10^{-6}$ | K-ε | K-ε | Manning | 0.01 | 0.1987 | 0.2998 |
| 06 | $3x10^{-6}$ | K-ε | K-ε | Manning | 0.02 | 0.1825 | 0.2664 |
| 07 | $3x10^{-6}$ | K-ε | K-ε | Manning | 0.03 | 0.2564 | 0.2334 |
| 08 | $3x10^{-6}$ | K-ε | K-ε | Manning | 0.04 | 0.2417 | 0.1785 |
| 09 | $3x10^{-6}$ | Prandlt | Smagorinsky | Manning | 0.01 | 0.3214 | 0.4568 |
| **10** | **$3x10^{-6}$** | **Prandlt** | **Smagorinsky** | **Manning** | **0.02** | **0.1521** | **0.1801** |
| 11 | $3x10^{-6}$ | Prandlt | Smagorinsky | Manning | 0.03 | 0.1625 | 0.3698 |
| 12 | $3x10^{-6}$ | Prandlt | Smagorinsky | Manning | 0.04 | 0.1847 | 0.3667 |
| 13 | $3x10^{-6}$ | Prandlt | K-ε | Manning | 0.01 | 0.1965 | 0.3412 |
| 14 | $3x10^{-6}$ | Prandlt | K-ε | Manning | 0.02 | 0.1752 | 0.1987 |
| 15 | $3x10^{-6}$ | Prandlt | K-ε | Manning | 0.03 | 0.3412 | 0.3438 |
| 16 | $3x10^{-6}$ | Prandlt | K-ε | Manning | 0.04 | 0.2987 | 0.3360 |
| 17 | $3x10^{-6}$ | Tsanis | Smagorinsky | Manning | 0.01 | 0.3024 | 0.3978 |
| 18 | $3x10^{-6}$ | Tsanis | Smagorinsky | Manning | 0.02 | 0.4125 | 0.3682 |
| 19 | $3x10^{-6}$ | Tsanis | Smagorinsky | Manning | 0.03 | 0.4187 | 0.3769 |
| 20 | $3x10^{-6}$ | Tsanis | Smagorinsky | Manning | 0.04 | 0.3657 | 0.3572 |
| 21 | $3x10^{-6}$ | Tsanis | K-ε | Nikuradse | $1x10^{-5}$ | 0.4126 | 0.4409 |
| 22 | $3x10^{-6}$ | Tsanis | K-ε | Nikuradse | $2x10^{-5}$ | 0.3952 | 0.4215 |
| 24 | $3x10^{-6}$ | Tsanis | K-ε | Nikuradse | $3x10^{-5}$ | 0.3458 | 0.4712 |
| 25 | $3x10^{-6}$ | Tsanis | K-ε | Nikuradse | $4x10^{-5}$ | 0.2147 | 0.4412 |
| 26 | $3x10^{-6}$ | K-ε | Smagorinsky | Nikuradse | $1x10^{-5}$ | 0.1452 | 0.4181 |
| 27 | $3x10^{-6}$ | K-ε | Smagorinsky | Nikuradse | $2x10^{-5}$ | 0.3878 | 0.4571 |
| 28 | $3x10^{-6}$ | K-ε | Smagorinsky | Nikuradse | $3x10^{-5}$ | 0.2478 | 0.2347 |
| 29 | $3x10^{-6}$ | K-ε | Smagorinsky | Nikuradse | $4x10^{-5}$ | 0.1698 | 0.4516 |
| 30 | $3x10^{-6}$ | K-ε | K-ε | Nikuradse | $1x10^{-5}$ | 0.4215 | 0.3219 |
| 31 | $3x10^{-6}$ | K-ε | K-ε | Nikuradse | $2x10^{-5}$ | 0.4987 | 0.3315 |
| 32 | $3x10^{-6}$ | K-ε | K-ε | Nikuradse | $3x10^{-5}$ | 0.3651 | 0.2669 |
| 33 | $3x10^{-6}$ | K-ε | K-ε | Nikuradse | $4x10^{-5}$ | 0.3412 | 0.2033 |
| 34 | $3x10^{-6}$ | Prandlt | Smagorinsky | Nikuradse | $1x10^{-5}$ | 0.2981 | 0.2155 |
| 35 | $3x10^{-6}$ | Prandlt | Smagorinsky | Nikuradse | $2x10^{-5}$ | 0.2786 | 0.2029 |
| 36 | $3x10^{-6}$ | Prandlt | Smagorinsky | Nikuradse | $3x10^{-5}$ | 0.4127 | 0.9785 |

| | | | | | | | |
|---|---|---|---|---|---|---|---|
| 37 | $3x10^{-6}$ | Prandlt | Smagorinsky | Nikuradse | $4x10^{-5}$ | 0.4579 | 0.2049 |
| 38 | $3x10^{-6}$ | Prandlt | K-ε | Nikuradse | $1x10^{-5}$ | 0.3217 | 0.3284 |
| 39 | $3x10^{-6}$ | Prandlt | K-ε | Nikuradse | $2x10^{-5}$ | 0.3258 | 0.4569 |
| 40 | $3x10^{-6}$ | Prandlt | K-ε | Nikuradse | $3x10^{-5}$ | 0.2569 | 0.5214 |
| 41 | $3x10^{-6}$ | Prandlt | K-ε | Nikuradse | $4x10^{-5}$ | 0.1987 | 0.4396 |
| 42 | $3x10^{-6}$ | Tsanis | Smagorinsky | Nikuradse | $1x10^{-5}$ | 0.2356 | 0.4789 |
| 43 | $3x10^{-6}$ | Tsanis | Smagorinsky | Nikuradse | $2x10^{-5}$ | 0.2147 | 0.2369 |
| 44 | $3x10^{-6}$ | Tsanis | Smagorinsky | Nikuradse | $3x10^{-5}$ | 0.2987 | 0.4213 |
| 45 | $3x10^{-6}$ | Tsanis | Smagorinsky | Nikuradse | $4x10^{-5}$ | 0.4126 | 0.4978 |
| 46 | $3x10^{-6}$ | Tsanis | K-ε | Nikuradse | $1x10^{-5}$ | 0.2713 | 0.2336 |
| 47 | $3x10^{-6}$ | Tsanis | K-ε | Nikuradse | $2x10^{-5}$ | 0.2678 | 0.2245 |
| 48 | $3x10^{-6}$ | Tsanis | K-ε | Nikuradse | $3x10^{-5}$ | 0.2956 | 0.2668 |
| 49 | $3x10^{-6}$ | Tsanis | K-ε | Nikuradse | $4x10^{-5}$ | 0.2456 | 0.2987 |

## Appendix E - Hydrodynamics Analysis

### Analysis of Seasonal Behavior of Estuarine Dynamics and the Inner Shelf

### Sea Level

Figure E1 (A-D) characterizes the seasonal field of sea-level rise for the entire studied domain during the simulated periods 2005-2006 (neutral period) and 2008-2009 (ENSO period), respectively, where the color scale varies from -30 to +30 cm. The results in the summer period (Figures E1-A and E1-B) indicate that the effects of the tide and fluvial discharge promote a pile of water on the Argentine coast of the La Plata River region, while in the northern Patos Lagoon region, the local effect of northeast winds causes a decrease in the water level (Simionato et al., 2001; Castelão and Möller, 2003). This combination of effects will establish a barotropic pressure gradient towards the sea, and favour ebb flows, both for the La Plata River and the Patos Lagoon (Simionato et al., 2001; Castelão and Möller, 2003). The results of the winter period (Figures E1-C and E1-D) show an opposite scenario: the local effect of the south quadrant wind results in the stacking of water on the Uruguayan bank of the La Plata River, while in the Patos Lagoon this stacking occurs in the northern region of the lagoon (Simionato et al., 2001; Castelão and Möller, 2003). In this scenario, the barotropic pressure gradient is weakened, favoring flood flows (Möller et. al.,2001; Fernandes et. al., 2002).

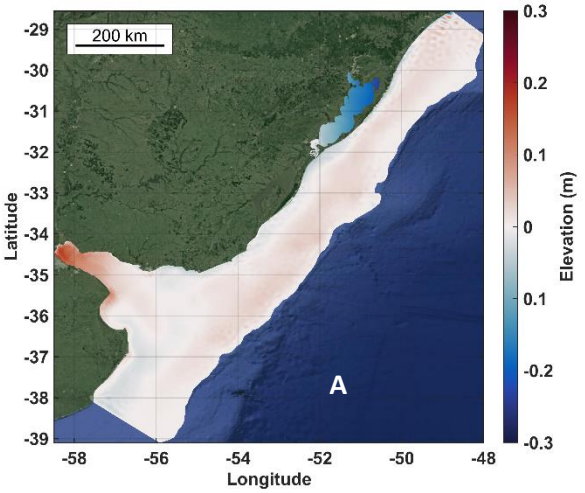


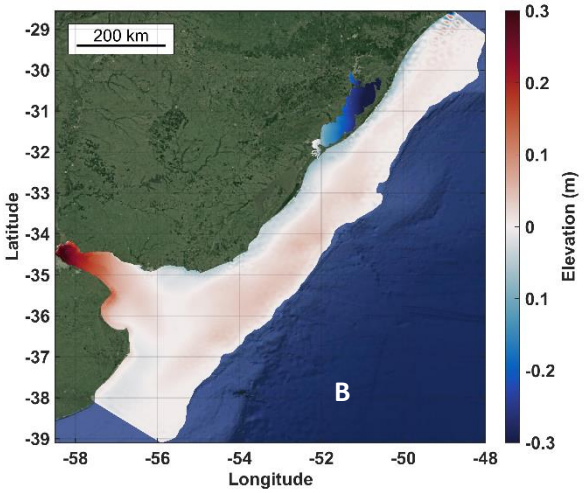

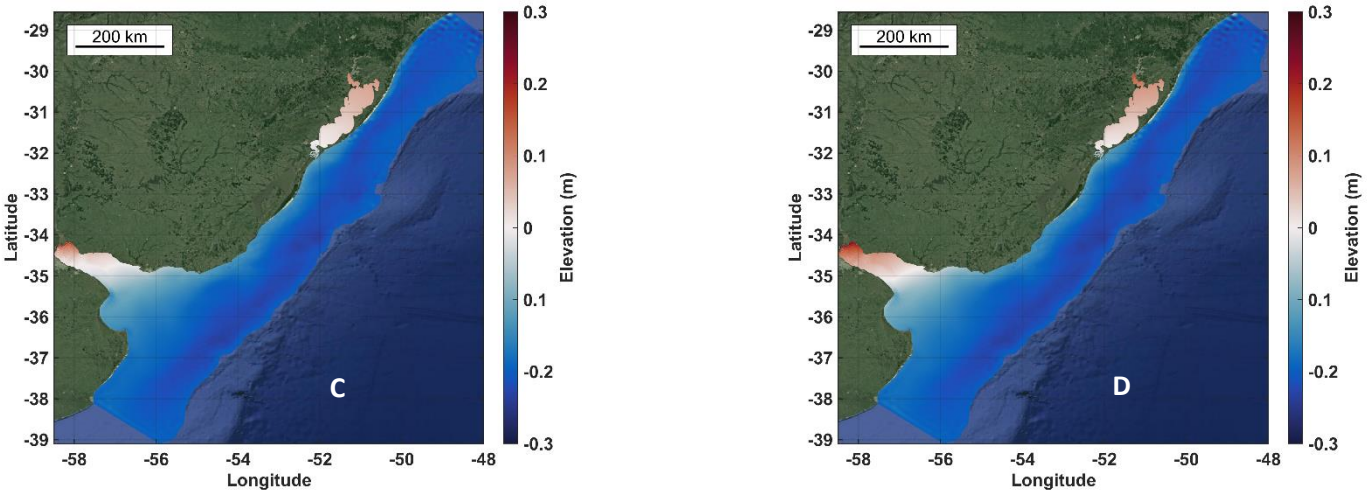


Figura 42 - Figure E1 - Artigo 1 - - Seasonal behavior of sea level for the study region, in the summer 2005-2006 (A), summer 2008-2009 (B), winter 2005-2006 (C) and winter 2008-2009 (D).

In comparing the simulated years, it is clear that there is a decrease in the gradient of elevation of the lagoon level, that is, the difference between the maximum elevation and the minimum elevation. The gradient is smaller in years under the influence of the ENSO phenomenon than in a typical year in the region. As the second modelled period is characteristic of La Niña (January and February, 2008) and El Niño (November and December, 2009), a possible cause for the decrease in the gradient is the high flow of the river that occurs in characteristic El Niño years, and which results in a big difference in the level between the continent and the ocean. For the La Plata River, Guerrero et. al. (2014) explain that despite the change in level between the two periods, the La Plata River discharge is not affected by the ENSO anomaly, as much as by interannual variations caused by local seasonality. Thus, the variation in the La Plata River level gradient is a response to seasonal variability and not to the interference of the El Niño and La Niña events. Matano et. al. (2014) highlight the year of 2009 as an “outbreak” within the pattern presented by the La Plata River discharge.

**Salinity**

Regarding the saline field behavior, it is known from the literature that the Southwest Atlantic Inner Shelf is a region marked by the presence of long strips of low salinity in regions close to the coast (Möller et al., 2008). This is a result of the pattern of freshwater input from the La Plata River and the Patos Lagoon, in addition to the presence of coastal currents from the southern tip of the continent and the local wind regime (Matano et al., 2014). The strong seasonal oscillations

of the southwest wind (i.e., from the southwest) during winter and northeast wind (i.e., from the northeast) during summer, therefore control the saline field in the region.

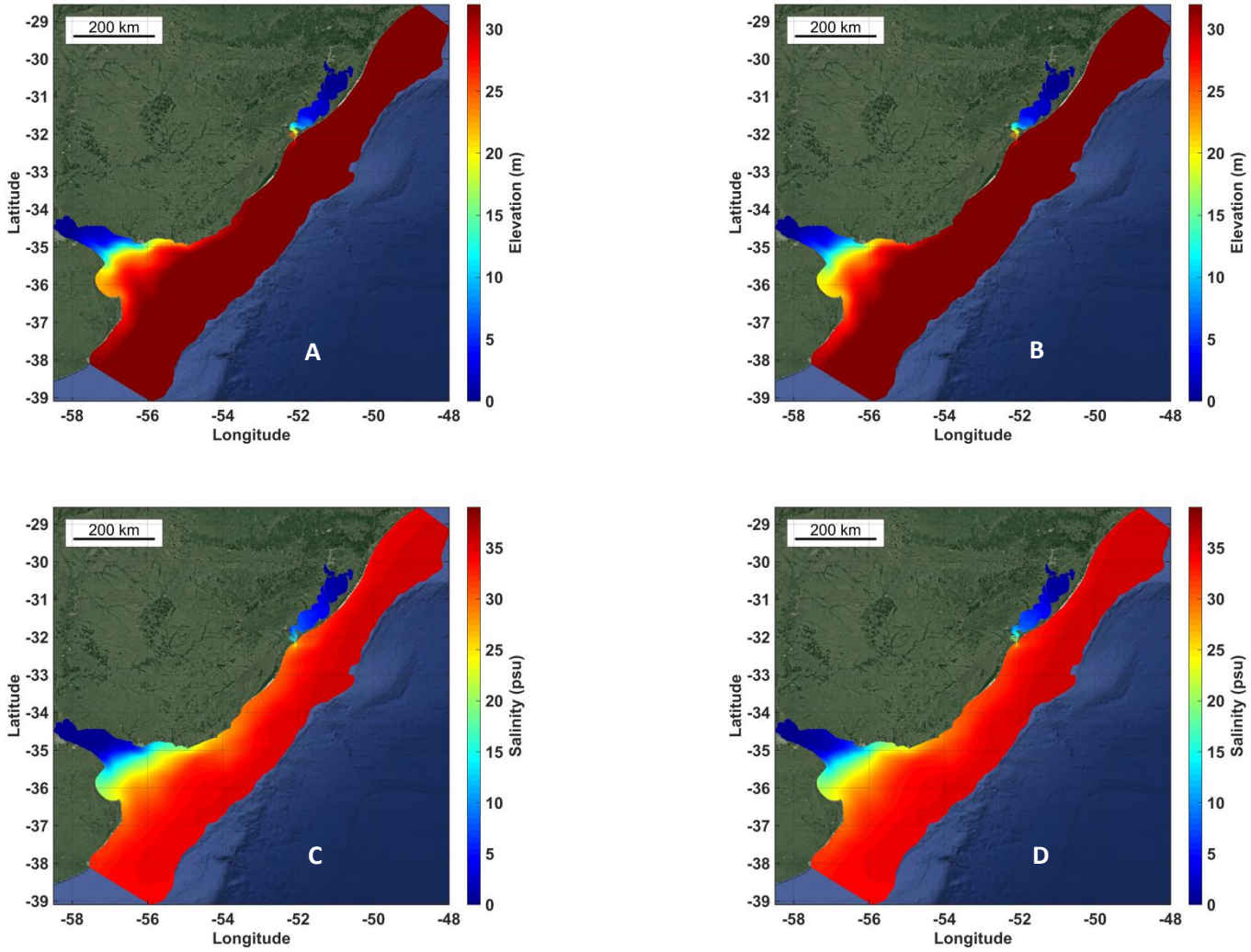


Figura 43 - Figure E2 - Artigo 1 - Seasonal behavior of the salinity field for the study region, in the summer 2005-2006 (A), summer 2008-2009 (B), winter 2005-2006 (C) and winter 2008-2009 (D).

Figure E2 (A-D) characterizes the seasonal salinity field for the entire studied domain during the simulated periods. Analyzing the results of the summer of 2005-2006 (Figure E2A), it appears that the plume retracts and is trapped upstream of the river, as verified by Piola et al. (2000). These upstream extensions are driven by the internal dynamics of the river and the strength of the local wind (Soares et al., 2007b; Palma et al., 2008; Matano and Palma, 2010a; 2010b; 2013) which, in the summer (Figures E2A and E2B), comes predominantly from the northeast and is responsible for trapping the plume in the region near the La Plata River mouth. During the winter (Figures E2C and E2D), the southeast wind predominates in the region and the saline plume

expands further downstream, and with the contribution of the coastal current formed by the southeast wind action, it reaches greater latitudes (28°S) (Piola et al., 2000).

When comparing the simulated years, a significant change in the saline field is not evident in the years 2008-2009 when compared to the period previously simulated. In the summer, a small variation in the saline plume migrating towards northwards can be seen (Figure E2B). The plume is more restricted to the mouth for the years 2008-2009, as it doesn't spread so much along the coast towards the north. In winter, the difference is a little more visible on the platform, where the saline plume expands a lot both to the north and offshore, surpassing the Patos Lagoon mouth and reaching the north of the grid, corroborating the results presented by Piola et al. (2000).

**Current Velocity**

As with the salinity field, the current regimes on the internal platform are strongly modulated by the local action of the wind (Soares et al., 2007a). During the summer, currents therefore migrate towards the south, modulated by the northeast wind characteristic of the region and the season. During the winter, on the other hand, the contribution of the southeast wind in the region intensifies the currents moving in northerly direction along the coast, changing the salinity and level fields as seen previously.

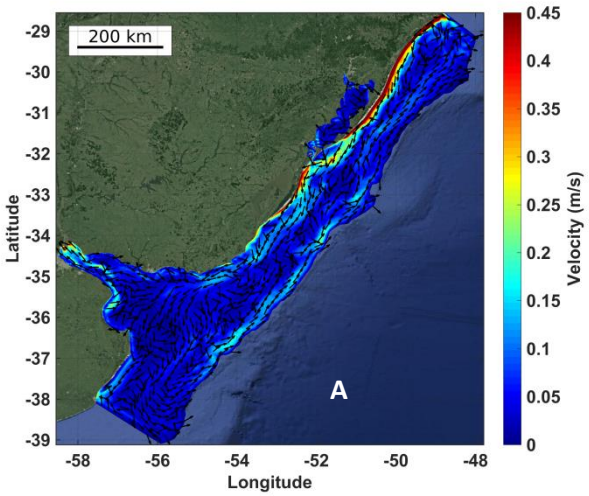


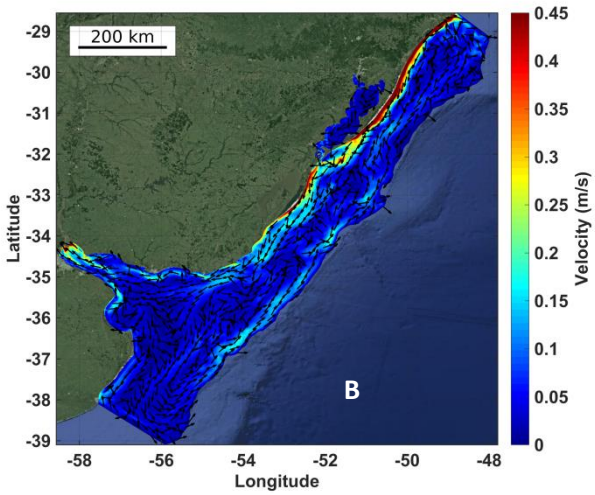

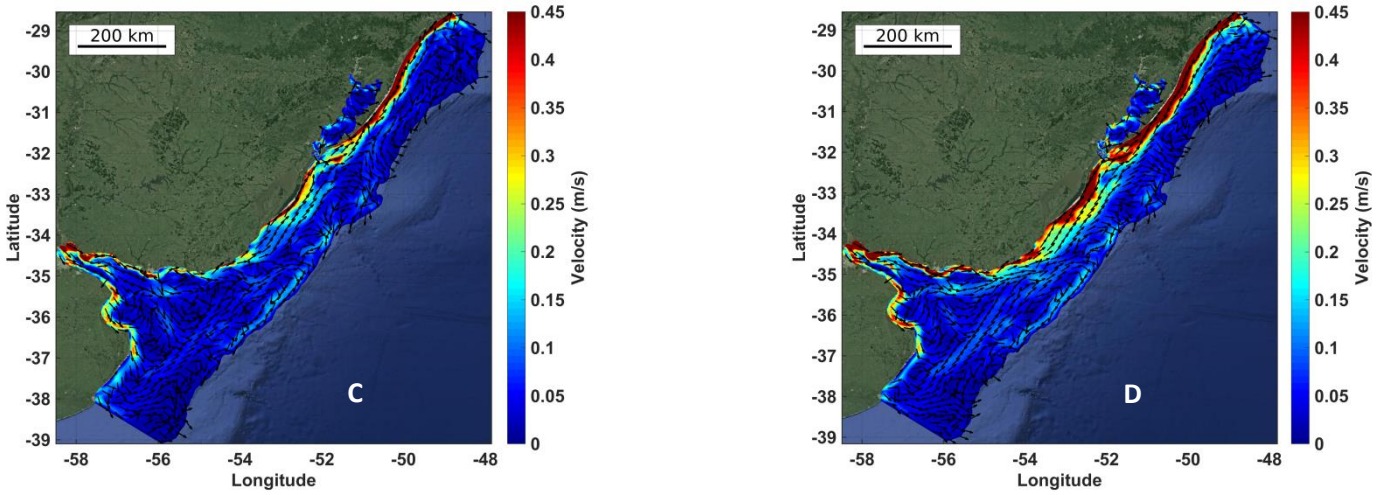


Figura 44 - Figure E3 - Artigo 1 - Seasonal behavior of the speed field for the study region, in the summer 2005-2006 (A), summer 2008-2009 (B), winter 2005-2006 (C) and winter 2008-2009 (D).

Figure 19 shows the results of the current speed field for the summer and winter of the years 2005-2006 (Figures E3A and E3C) and for the summer and winter of 2008-2009 (Figures B3B and B3D). For the first simulated period in the summer, an intensified coastal current towards the south is seen, with speeds ranging from 0.2 to 0.4 m/s, which corroborates the results of Ghisolfi et al. (2003) and Soares et al. (2007a). In winter, the results show that the current is more intensified than in the summer, but in the opposite direction – i.e. northwards through the action of a southeasterly wind - as proposed by Ghisolfi et al. (2003). The currents in the results vary in magnitude from 0.35 to 0.40 m/s.

When comparing the first simulation with the second, an intensification in the currents in both summer and winter is evident. This intensification is more evident in the north of the studied region, where the average velocity surpasses 0.45 m/s, possibly due to the effects of El Niño (Pimenta et al., 2005).

## 6.2. Article 2

# Bottom Evolution Patterns in the Southwest Atlantic Inner Continental Shelf

Paulo Victor Lisboa [a,b,*], Elisa H. Fernandes [a], Aldo Sottolichio [b], Nicolas Huybrecht [c], Raylton Bendô [d].

[a]*Laboratótio de Oceanografia Costeira e Estuarina - LOCOSTE, Instituto de Oceanografia - PPGO, Universidade Federal do Rio Grande, Rio Grande, RS, 96203-900, Brazil*

[b]*Environnements et Paléo-Environnements Océaniques et Continentaux – EPOC Laboratory, University of Bordeaux, 33615 Pessac, France.*

[c] *Cerema, Direction Technique Eau, Mer et Fleuves, 134 rue de Beauvais – CS 60039-60280 Margny-lès-Compiègne – France.*

[d]*Escola de Engenharia – PPGE, Universidade Federal do Rio Grande, Rio Grande, RS, 96203-900, Brazil.*

* Corresponding author

E-mail address: paulovictor_fjv@hotmail.com

### Introdução

The morphology of inner shelves and the distribution of sediments are influenced by complex sedimentary processes acting on different temporal and spatial scales (Sternberg and Nowell, 1999). The transport of bottom sediments in continental shelves is the main one and has been receiving attention from the scientific community in the last decade (Marques et al., 2010; Simionato et al., 2011; Santoro et al., 2017, Simionato and Moreira, 2018; Moreira et al., 2019). These studies are important for the quantification of transport and destination of continental sediments reaching the coastal region as the continent-ocean interactions result in major implications for ecological studies. Sielski et. al. (2017) examined the morphological characteristics of Paraná's inner continental shelf. Their results show that sediments with a mean diameter of silt to very fine sands prevail at all depths and that these sediments have their origin related to large estuarine systems present in the area. Guillén et. al. (2005) analyzed the variability of the bottom

sediment on the inner shelf of the Delta Ebro. As a result, the authors stated that the variability of the sediment is directly related to local seasonality, that is, during the winter the bottom layer is predominantly muddy, while in the summer there is a thickening of the sediment from the inner continental shelf.

Considering that the suspended sediment transport process on the inner shelf is controlled by the balance between oceanographic conditions and the local sedimentary supply, friction becomes an important factor, with currents, wind, and waves being the main responsible for the transport of sediments near the bottom as these forcing induce shear stress and consequently sediment drag at the bottom (Wright et. Al., 1991; Nittrouer and Wright, 1994).

In most inner shelves, however, long time series of simultaneously measured bottom sediment concentration, current, and water level data are relatively rare. Previous studies have shown, that numerical models are powerful and cost-effective tools capable of satisfactorily reproducing the suspended and bottom sediment concentration in coastal regions (Marques et al, 2010; Villaret et al, 2013; Santoro et al., 2019). The hydro-morphodynamic model equations normally reproduce the sedimentary dynamics according to three main processes: erosion, deposition, and bottom transport (Lepesqueur et. al., 2019) and admit that sediment transport occurs when the bottom shear stress exceeds a threshold value, which depends mainly on the grain size and the density of non-cohesive sediments (Villaret et al., 2013; Lepesqueur et. al., 2019). Furthermore, this density has a strong influence on the speed and advection of the sediment that controls the sedimentary balance through the processes of erosion and deposition (Hostache et al., 2014). Therefore, these two parameters are responsible for determining the deposition regions for each type of simulated grain.

La Plata River and Patos Lagoon are examples of important fluvial systems located on the South Atlantic Continental Shelf that contribute to the sedimentary deposits present on the inner shelf. Their continental contribution was discussed by several authors in terms of suspended sediment concentrations and coastal plume behavior. Möller et. al. (2008), analyzed the effect of fluvial discharge and wind on a seasonal scale on the distribution of coastal waters of the Continental Shelf of the Southwest Atlantic. The authors observed that SW winds are predominant in winter and force the plume of the River Plate to propagate to the north, even during the low flow period. While the NE winds move the plume to the south, concentrating the plume near the mouth of the river. Corroborating with Möller et. al. (2008), Soares et. al. (2007b) analyzed the importance of the turbulent mixing process in the evolution of the La Plata plume and its spread on the Continental Shelf of the Southwest Atlantic using numerical modeling results. The authors demonstrated that the plume of La Plata tends to expand along the north bank in the presence of

local winds during fall/winter and is more restricted to the river mouth during spring/summer when winds are weaker and the tidal regime prevails. in the region.

Still on the River Plate, Moreira et. al. (2016) provided a comprehensive and objective characterization of the distribution of bottom sediments. For this, the authors used data from sediment collections from the upper, medium, and lower estuaries. The results show a gradual distribution, starting from more sandy sediment in the region of the upper estuary, passing through siltier sediment in the middle region, until sediments more predominantly clayey in the lower estuary. Simionato and Moreira (2018) using numerical modeling, analyzed the role of different forcing and environmental conditions in determining the distribution of fine sediments in suspension in the La Plata River estuary. The authors concluded that the higher estuary is characterized by having a large amount of suspended sediment, however as the sediment approaches the lower estuary, the area of the estuary widens, producing a large sediment deposition, decreasing the sediment concentration in suspension significantly. Santoro et. al. (2016) in order to explore the effect of the consolidation process on the bed evolution and on the dynamics of fine sediments in the La Plata estuary, used the 2D sediment transport model. The authors used the sedimentation column experiment to calibrate the consolidation model and stated that in general terms, there is not much significant change in the deposition and erosion patterns if we compare the scenarios with and without the consolidation model.

About the influence of the Patos Lagoon on the Continental Shelf of the Southwest Atlantic, Marques et. al. (2009) analyzed the physical forces that are responsible for controlling the dynamics of the Patos Lagoon plume and its expansion on the adjacent shelf. With this, the authors verified that a coastal plume has the characteristic behavior of a small spatial scale plume, and its mode of dominant temporal variability is associated with transport towards the south, being controlled by the combination of dominant winds in the north quadrant and seasonal variability of river discharge in the region. More recently, Lisboa et al. (submitted) analyzing the sedimentary contribution of La Plata River and Patos Lagoon to the Southwest Atlantic Inner Shelf and, their spatial and temporal variability, identified different characteristics of the coastal plumes of the two estuaries. While the La Plata River plume has homopycnal characteristics, the plume of Patos Lagoon behaves in a hipopicnal way. In addition, the authors carried out a qualitative and quantitative analysis of the contribution of both rivers to the adjacent platform, highlighting the effect of the ENOS phenomenon on the region's sedimentary load. The results show that river flows interact with sediments on a seasonal to interannual scale, while the local wind contributes to the concentration of sediments on synoptic scales. As for the exported sedimentary load, the authors stated that the contribution can reach values close to $10^8$ ton / year, this load being strongly influenced by the ENOS effect.

Despite the recognition of the La Plata River and Patos Lagoon influence on the transport of suspended sediment and the sedimentation process of the adjacent inner shelf, little is known about the behavior of the erosion and deposition processes and the resultant bottom sediment evolution on the Southwest Atlantic Inner Shelf. Therefore, these are the goals of this study.

## Data and methods

### Study Area

The studied area is located between latitudes 28ºS and 38ºS (Figure 1), which corresponds to the central region of the Southwestern Atlantic Shelf, which according to Acha et al. (2004) is considered the largest continental platform in the Southern Hemisphere. For Bisbal et al (1995), the study area is known to be one of the most biologically productive areas in the global ocean due to the high level of phytoplantonic biomass from La Plata River and Patos Lagoon, and one of the most economically important areas due to the high fishing activity performed in the region (Haimovic et al, 1989; Castello et al, 1990). The inner shelf has its limit close to the 30 m isoline, resulting in an average width of 100 km on the northern border and 198 km on the southern border (Soares and Möller, 2001), with a slope of 0.6 m / km (Laprida et al, 2007; Violante et al, 2004).

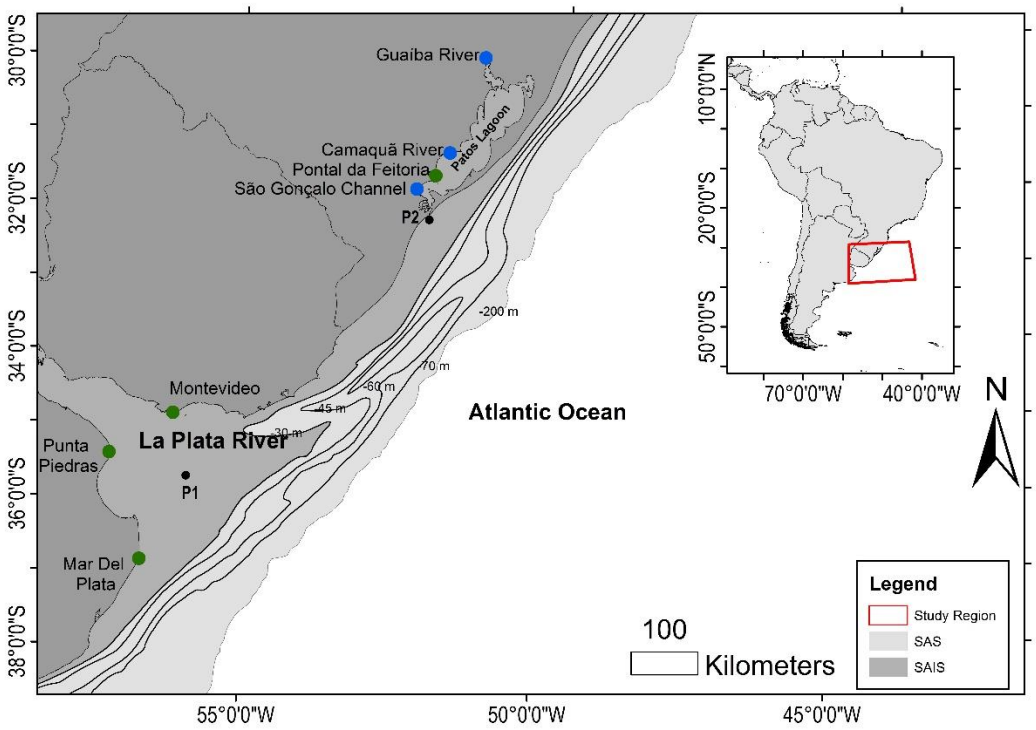


Figura 45 - Figure 1 - Artigo 2 - The study region defined between the latitudes of 28°S (Santa Marta Cape) and 38°S (Mar Del Plata). Blue dots represent the main effluents from Patos

Lagoon (Guaíba River, Camaquã River, and São Gonçalo Channel), green dots are important geomorphological regions in the study area and black dots represent points from where model results where extracted for the Wavelet analysis, the deposition flux and the bed evolution (P1 and P2).

The region is strongly influenced by the continental contribution of the La Plata River and Patos Lagoon. The first is the result of the confluence of two major rivers in South America, Paraná River and Uruguay (Dinápoli et. al., 2020), being responsible for transporting between 80 and 160 million tons of suspended sediment per year to the estuary, in addition to a large amount of nutrients (Sarubbi, 2007; Re et. al., 2010; Menéndez et. al., 2011). The Paraná and Uruguay rivers account for most of the continental discharge to the Rio da Prata (Framinan et. al., 1999), with an average flow of 22,000 $m^3/s$, with peak flow reaching 90,000 $m^3/s$ (Berbery and Barros, 2002; Jaime and Menéndez, 2002).

The Patos Lagoon has an average flow of 2400 $m^3/s$ (Vaz et. al., 2006), with the Guaíba, Camaquã, and São Gonçalo Channel as its main tributaries. The tributaries present standard characteristics for the mid-latitude region, that is, high discharge during the end of winter and spreading towards the beginning of spring, and moderate discharges during the summer and part of fall (Möller et al. 2001). In addition, the location is widely known for being strongly affected by the ENSO cycles, in which the region is assessed as having higher (El Niño) or lower (La Niña) freshwater discharge values. Therefore, when the river discharge is high (reaching 3000 $m^3/s$), there is a control over the dynamics of the lagoon, drastically reducing the entry of seawater. Otherwise, the flow rate is low (300 $m^3/s$), the dynamics control is the responsibility of the action of the local wind, thus allowing saltwater to enter the estuary.

As for the astronomical tidal regime of La Plata River, the region is dominated by micro tide, the main component being M2, followed by O1 (Möller et al, 2001; Fossati et al, 2014). The tidal amplitude is about 0.4 m along the southern coast of Brazil and on the Uruguayan coast, while on the Argentine coast the amplitude can be observed in the order of 1m. An important feature of the River Plate is that the astronomical tide is of the same order of magnitude as the meteorological tide. Meteorological tides in the region are generated mainly on the Argentine continental shelf and spread to the north like waves trapped in the coast until reaching the estuary (Santoro et. Al., 2013).

Meanwhile, in Patos Lagoon, the system is microtidal, mixed with diurne predominance, its effects being restricted to the coastal zone and the region of the lower estuary, with an average amplitude of 0.23 m (Möller et. Ao., 2001; Fernandes et al., 2004). The effect of the astronomical tide is practically null in the Patos Lagoon because in addition to being filtered in the entrance

channel of the estuary (Kjerfve and Knoppers, 1991; Moller et. al., 1996; Fernandes et. al., 2004; Castelão and Moller, 2006), the tides they are also attenuated by long-term oscillations generated offshore (Fernandes et. al., 2004).

The atmospheric circulation in the region is controlled by the influence of the quasi-permanent high-pressure systems in the South Pacific and the South Atlantic. Simionato et. al. (2004b) analyzed the wind variability in the La Plata River region and found that there is a seasonal variability marked by the winds. The direction and intensity of the wind vary throughout the year (Santoro et. Al., 2017). During winter, southeast winds generally predominate, but the strongest average winds blow from the south and southeast. During summer and spring, however, the winds blow from the east and, to a lesser extent, from the northeast. The strongest average winds blowing from the southeast reach values close to 9 m/s during the spring, and the southwest wind in the summer exceeds 9.5 m / s (Simionato et. al. 2004b). Santoro et. al. (2017) stated that the main extreme events in the La Plata region are characterized by strong southwest winds, which can exceed 25 m/s.

In Patos Lagoon the wind regime plays a fundamental role in estuarine dynamics, since, when the flow of the river is below or close to the average, the winds become the main physical force that controls the dynamics over the lagoon. This forcing mechanism is responsible for promoting the transport of saltwater into and out of the estuarine zone (Möller et. al. 2009), conditioned by the wind direction. The northeast wind (NE) is the most frequent during the year (Möller et. al., 2001), but mainly in the spring and southern summer, that is, from October to March. In autumn and southern winter, which extend from April to September, the southwest wind (SW) becomes the strongest and most consistent, as noted by Tomazelli et. al. (1993), and more recently by Tavola et. al. (2020) and Bitencourt et. al. (2020). The flows towards the sea and the land, which generate exchanges between the lagoon and the adjacent region, are the result of the action of NE and SW wind, respectively. The change in wind direction is due to the passage of meteorological fronts on synoptic scales (ranging from 3 to 15 days) (Möller et. al., 2001). These changes in wind direction are important in the generation of saline gradients, which are responsible for the mixing and stratification process typical of estuarine regions. Möller and Castaing (1999) stated that the Patos Lagoon estuary can vary from a salt wedge type estuary, to partially stratified, to a well-mixed one.

**Field data**

For the model calibration and validation exercises, the salinity, sea level, current speed and sediment concentration data sets were used. The velocity current data were collected by an ADP (Acoustic Doppler Profiler) of the Sontek Argonalta 1000 Hz model, moored at the Rio Grande Pilotage station (13 m). For salinity data, the conductivity and temperature probes (CTs) installed at 1 and 10 m depth at the Naval Station. The sea level data were acquired through the tide station at the Rio Grande Pilotage pier. The velocity, salinity and sea level data were collected from October 10 to November 30, 2006, with the same time resolution of 1 h.

For validation, sediment concentration data (SSC) from different parts of the La Plata River, collected during 2010 at different periods of the year, were used. The first data set was collected in the lower estuary region, the second obtained in the middle estuary and the third in the upper estuary (FREPLATA-IFREMER Project). Details on data acquisition procedures have been described by Fossati et. al. (2014).

**The Numerical model**

The proposed numerical modeling study is based on the TELEMAC-MASCARET system (Hervouet, 2007). The local hydrodynamics is simulated by the TELEMAC-3D model (VERSION), which solves the Reynolds averaged equations in hydrostatic mode, considering the Boussinesq approximations for the solution of the Momentum Equation. The morphodynamic and sediment transport modeling is performed using the SISYPHE model (Villaret et al, 2010; Villaret et al, 2013).

The choice of this modeling structure is based on two main aspects: 1) The model is based on a mesh of unstructured finite elements, being suitable for the complex geometries present in the coastal and estuarine regions of the study area; 2) The model allows the internal and dynamic coupling of two different models (TELEMAC 3D and SISYPHE). This coupling is an important and relevant part for the simulation of morphodynamics and sediment transport since it allows that at each step of the simulation, changes in hydrodynamics are reproduced in the morphodynamics, and vice-versa.

SISYPHE divides processes related to sediment dynamics in sediment transport, which is divided into suspended sediment and bottom sediment, and in erosion and deposition fluxes, allowing the calculation of the bottom evolution in the studied area. Tassi & Villaret ( 2014) describe the model in detail. SISYPHE works with both non-cohesive and cohesive sediments. The focus of this study will be on the modeling fine cohesive sediments.

The bottom shear stress ($\tau$) controls sediment transport through variables such as erosion and deposition (Villaret et al, 2013). In TELEMAC 3D, friction dissipates energy from the bottom using a roughness coefficient, which is responsible for the bottom shear stress, which in turn controls bed deposition and erosion. For the present study, friction will be calculated using Nikuradse (Nikuradse, 1923) as the law of bottom friction, and the hydrodynamic and morphodynamic models were internally coupled.

$$\tau_0 = \rho u_*^2 = \rho \left( \frac{k}{log \frac{30 z_1}{k_s}} \right)^2 u_{z_1}^2$$

being $\rho$ the water density, $u_*$ the friction speed, $z_1$ the altitude of the sigma layer close to the bottom, $u_{z_1}$ the bottom speed, $k$ = 0.4 the von Karmán coefficient, $k_s \approx 2.5 d_{50}$ the bottom roughness of Nikuradse and $d_{50}$ the average particle size of the bottom.

The erosion flux in SISYPHE is related to the critical shear stress at the bottom in relation to the bottom shear force in the same place. This flow is calculated from the Partheniades formula:

$$E = \begin{cases} M \left( \frac{\tau_b}{\tau_{ce}} - 1 \right) & if\ \tau_b > \tau_{ce} \\ 0 & otherwise \end{cases}$$

where $M$ is the constant of the Krone-Partheniades erosion law (Kg m$^{-2}$.s$^{-1}$), $\tau_b$ bottom shear and $\tau_{ce}$ critical erosion shear stress, which was considered 1.5 Pa in this study.

The deposition flow is calculated according to the concentration near the bottom. In the case of fine sediment, the bottom concentration is approximately equal to the concentration at the mean depth:

$$D = \begin{cases} w_s C \left( 1 - \frac{\tau_b}{\tau_{cd}} \right) & if\ \tau_b > \tau_{cd} \\ 0 & otherwise \end{cases}$$

where, $\tau_{cd}$ is the critical shear stress for mud deposition, considered as 0.01 Pa in this study, $w_s$ is the sediment setting velocity (m.s$^{-1}$), and $C$ is the suspended sediment concentration (g.L$^{-1}$). If the shear stress is less than the bottom shear, the sediment will be deposited.

The sediment transport is calculated according to the advection-diffusion equation:

$$\frac{\partial C}{\partial t} + U\frac{\partial C}{\partial x} + V\frac{\partial C}{\partial y} = \left[\frac{\partial}{\partial x}\left(\epsilon_s \frac{\partial C}{\partial x}\right) + \frac{\partial}{\partial y}\left(\epsilon_s \frac{\partial C}{\partial y}\right)\right] + \frac{(E-D)_{z=a}}{h}$$

where $C$ is the averaged depth suspended sediment concentration, $\epsilon_s$ is the sediment turbulent diffusive coefficient, $U$ and $V$ are the average depth velocity components in the $x$ and $y$ directions, respectively, and $h$ is the depth.

For the calculation of the bed evolution, SISYPHE uses the Exner equation (Exner, 1920 and Exner, 1925) in all steps of the simulation. The calculation of the bed evolution takes into account the flow of sediment in the bottom and the balance between deposition and erosion.

$$(1-n)\frac{\partial Z_f}{\partial t} + \nabla . Q_b + (E-D)_{z=a} = 0$$

where $n$ is the bottom sediment porosity value, $Z_f$ is the bottom evolution, $Q_b$ is the bottom sediment flow, $E$ and $D$ are the erosion and deposition rates at elevation $z = a$, corresponding to the depth between the water-sediment interface.

**Numerical Mesh**

The numerical domain was defined between the latitudes of 28°S (Santa Marta Cape) and 38°S (Mar Del Plata) and discretized by an unstructured finite element mesh (Figure 2) based on nautical charts from the Brazilian and Argentine Navy, allowing the satisfactory representation of the observed complex geometries and steep depth variations (from 0,40 to 320 m). The unstructured mesh was generated using the Bluekenue software (http://www.nrc-cnrc.gc.ca/eng/solutions/advisory/blue_kenue_index.html), and consisted of 18,275 nodes and 33,296 triangular elements, discretized in the vertical by 11 equally spaced sigma levels.

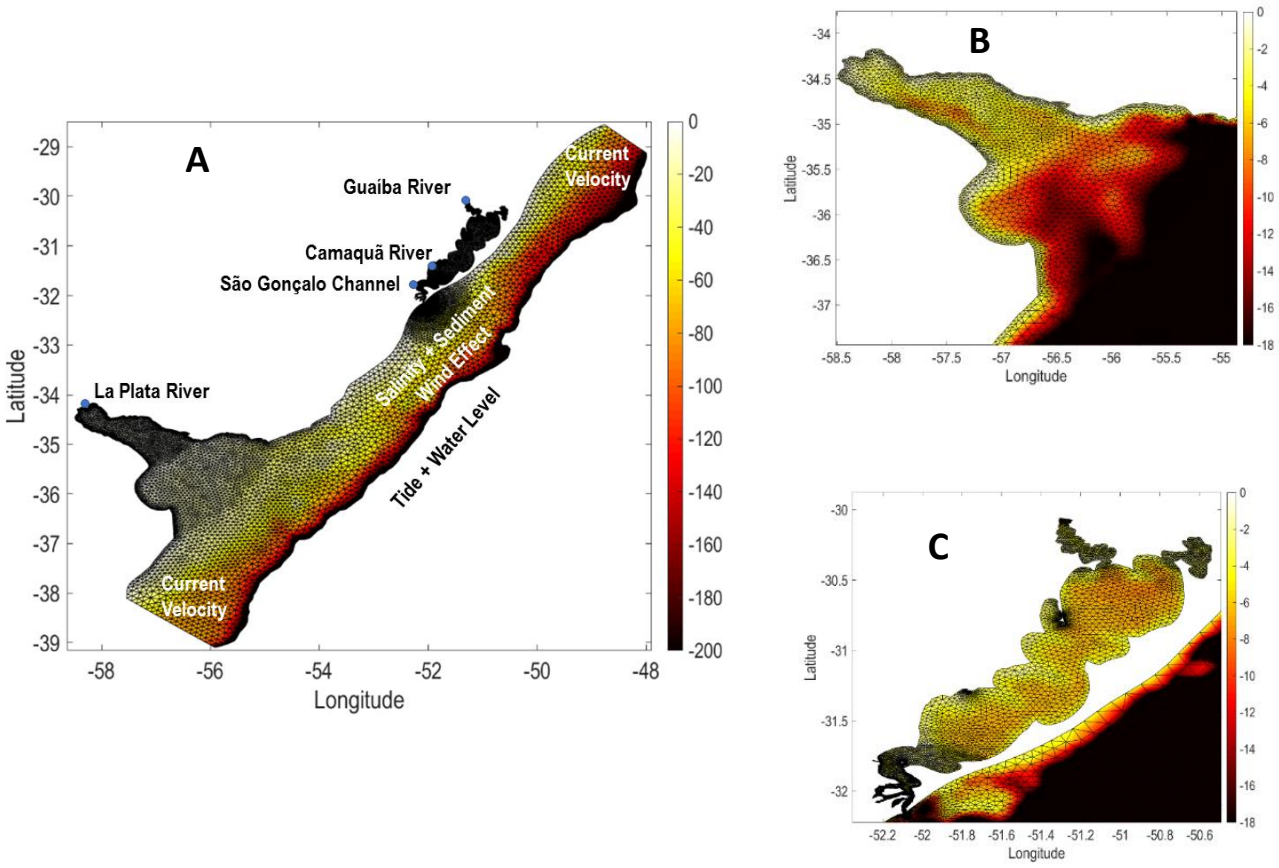


Figure 46 - Figure 2 - Artigo 2 - Computational domain and numerical mesh used for the simulations. (A) Initial and boundary conditions prescribed in the model. (B), detail of La Plata River mouth (C), and Patos Lagoon (C).

**Initial and Boundary Conditions**

Based on the model set-up applied by Lisboa et al. (submitted), Figure 2 also presents the data prescribed as initial and boundary conditions for 8 years (January 1st, 2005 to December 31st, 2012) long simulation. The simulation period was chosen based on the occurrence of ENSO cycles. For that, in all contours (continental or oceanic) time series of data were used in order to better represent the local dynamics. In the ocean, frontiers were used: (I) Elevation and current speed. For the elevation an average value of the sea level (0.4 m) was used, in addition to the estimate of the local tide regime. The tide was calculated by the inverse solution of Laplace's equations (Edgbert et. al., 1994), using 33 harmonic components of the tide to generate a reliable estimate of sea-level behavior (figure 3E). The current speed was calculated based on the regional tidal speed fields obtained by the OSU Tidal Inversion System (OTIS - Egbert and Erofeeva, 2002), internally coupled to TELEMAC (TPXO). (II) The salinity field of the HYCOM + NCODA Global Project (HYbrid Coordinate Ocean Model, https://hycom.org/), was interpolated in time and in all numerical domains (figure 3D), with temporal and spatial resolutions of 3 h and 0.08°, respectively.

In the continental boundary corresponding to the main tributaries of Patos Lagoon, daily flow data (Guaíba River, Camaquã) provided by the National Water Agency (ANA, www.hidroweb.ana.gov.br) were used (figure 3A). As for the main tributary of the Patos Lagoon Estuary (São Gonçalo Channel), there is no time series of systematic fluvial discharge. For this reason, level data obtained from the Mirim Lagoon Agency (ALM, https://wp.ufpel.edu.br/alm/) were converted into daily river discharge data based on the Rating Curve Method, proposed by Oliveira et. al. (2015). For the La Plata River, the daily flow data for the river was obtained through the Argentine Naval Hydrography Service (https://argentina.gob.ar/armada). As there are no systematic measurements of SSC data available to construct a realistic series, values of 200 $mg.l^{-1}$, 100 $mg.l^{-1}$, 150 $mg.l^{-1}$ have been assigned to the Guaíba River, Camaquã River, and Canal de São Gonçalo, respectively (Marques et. Al., 2010), and 230 $mg.l^{-1}$ for the La Plata river (Moreira and Simionato, 2019). The class of suspended sediments used in this study was fine silt (Marques et. al., 2010b; Fossati et. al., 2013).

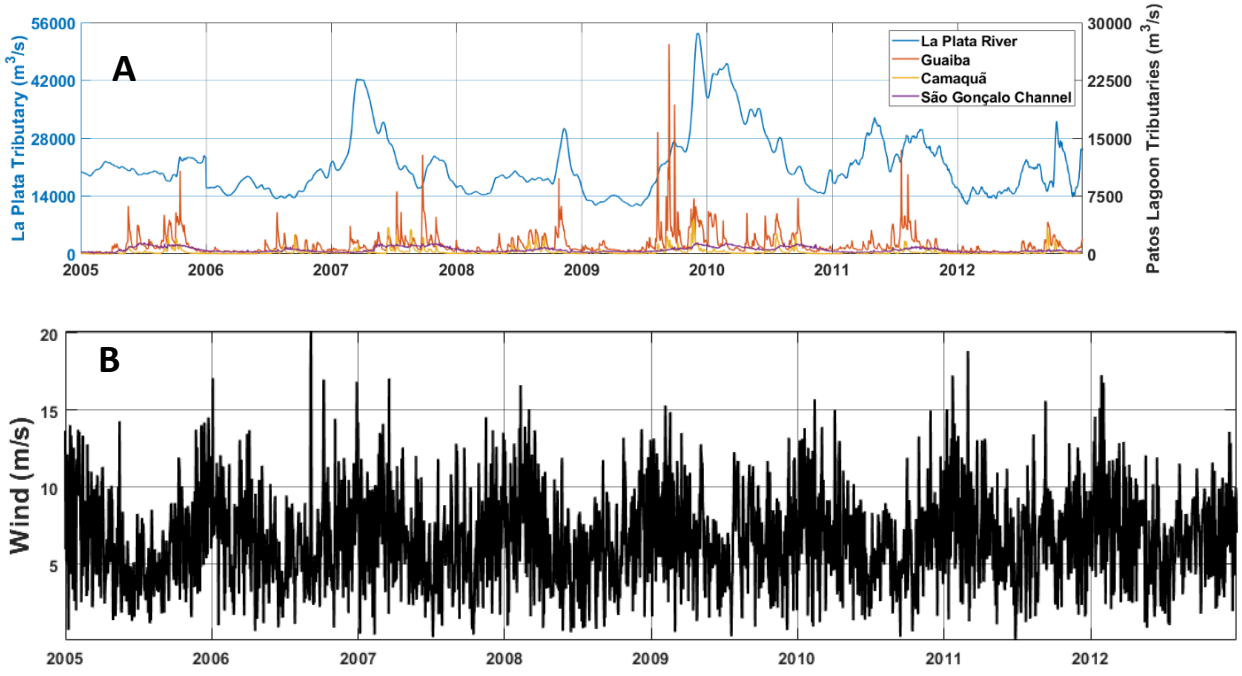

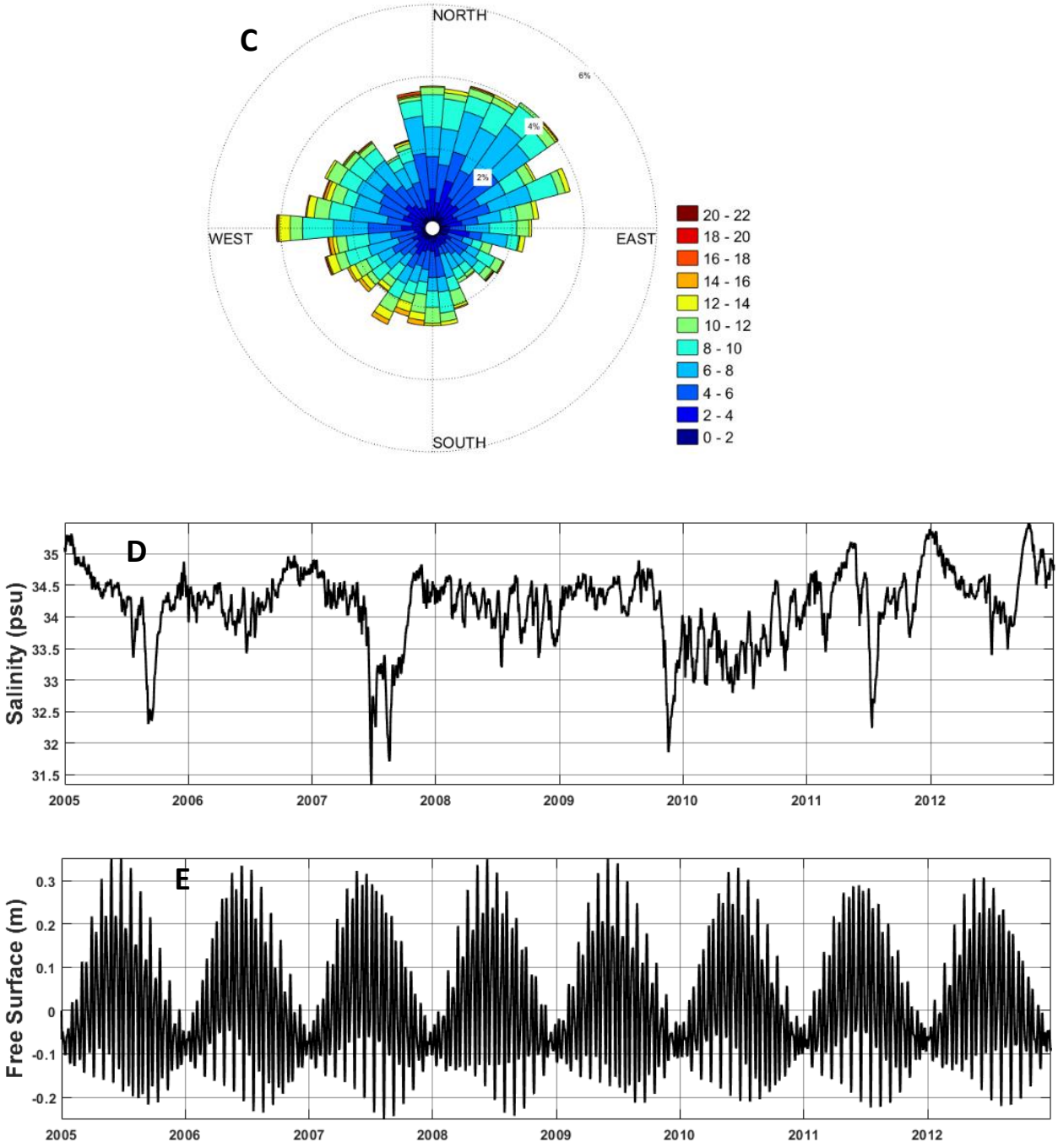


Figura 47 - Figure 3 - Artigo 2 - Time series of fluvial discharge from the Guaíba River, Camaquã River, São Gonçalo Channel and La Plata River for the period studied (2005-2012) (A) Time series of intensity used as surface forcing in the simulation. (B) The wind rose for the frequency distribution of the time series of wind intensity and direction, for the years 2005 to 2012 (C) Times series of salinity from the ocean boundary (D). Times series of tidal from the ocean boundary.

At the surface boundary, wind data from the global ECMWF model (http://www.ecmwf.in) was used, with a 6-hour temporal resolution and 0.75º spatial resolution, being interpolated for the entire mesh, and for all time steps. Figure 3B indicates that the wind intensity varied from 0.2 to 20

$m.s^{-1}$, with the average intensity around 5.5 $m.s^{-1}$. The predominant wind direction during this period was from the northeast followed by the southwest.

**Calibration and Validation**

A model's calibration and validation exercises consist of comparing the model's results with data collected in the field (in situ) for the same period and in the same location. The model's ability to reproduce the measured data is evaluated based on analysis of statistical parameters (Relative Mean Absolute Error (RMAE) and Root Mean Square Error (RMSE)) as presented by Walstra et al., 2001, Fernandes et. al. (2001), Fernandes et. al. (2002), Sutherland et al., 2004, Marques et. al. (2009), Lisboa & Fernandes (2015).

**Tabela 9 - Table 1 - Artigo 2 - Rating scale for the relative mean absolute error (RMAE) (Sutherland et al., 2004 and Walstra et al., 2001)**

| Qualification | Excellent | Good | Reasonable | Poor | Bad |
|---|---|---|---|---|---|
| **RMAE** | ≤0.2 | 0.2 – 0.4 | 0.4 – 0.7 | 0.7 – 1.0 | >1.0 |

The TELEMAC model has been extensively calibrated and validated for the Patos Lagoon (Marques et al., 2009; 2010a; 2010b; 2011; António et al., 2020) and Mirim Lagoon (Oliveira et al., 2019). Lisboa et. al. (submitted) expanded the domain and successfully calibrated and validated the model to the South Atlantic Inner Shelf. For this, forty-nine tests of model calibration exercises were carried out, which consisted of experimenting with different values for the main physical parameters of the model (wind influence coefficient; the horizontal turbulence model and its coefficients for horizontal diffusion of tracers and speed), in addition to comparing them to the time series of model results, with time series of data collected in situ for specific variables (current speed, salinity, sea level, and sediment concentration), in order to define the set of physical parameters that best reproduce environmental behavior of region.

**Tabela 10 - Table 2 - Artigo 2 - Better parameterization of the model found by the calibration exercises.**

| *Parameters* | |
|---|---|
| **Time Step** | 60s |
| **Coriolis Coefficient** | -7.70735 x $10^{-5}$ $N.m^{-1}.s^{-1}$ |
| **Horizontal Turbulence Model** | Smagorinsky |
| **Vertical Turbulence Model** | Mixing Length (Prandlt) |
| **Law of Bottom Friction** | Manning |
| **Bottom Friction Coefficient** | 0.02 $s/m^{1/3}$ |
| **Wind Influence Coefficient** | $3x10^{-6}$ $N.m^{-1}.s^{-1}$ |
| **Suspend Sediment Class** | Fine Silt |
| **Sediment Setting Velocity** | 0.00001 $m.s^{-1}$ |
| **Critical Erosion Shear Stress** | 1.5 $Nm^{-2}$ |
| **Critical Shear Stress for Deposition** | 0.01 $Nm^{-2}$ |

Based on the statistical analyzes presented in table 1, the best results in the calibration exercises are present in figures 4 and 5, where the black lines represent the modeled data, while the red lines the data in situ. In addition, Table 2 shows the best parameterization of the model after the calibration tests. In the model reproduction, the RMAE values found were considered good (0.24 and 0.40) when comparing the measured and calculated salinity on the surface (Figure 4A) and at the bottom (Figure 4B) at Naval Station. In the comparison of the simulated and measured data of the surface (Figure 4C) and bottom velocity current (Figure 4D), at the Pilotage station, the RMAE values (0.16 and 0.18, respectively) found were considered excellent. In the comparison of the free sea surface data (Figure E), the RMAE was 0.37, considered good by Walstra et. al., 2001.

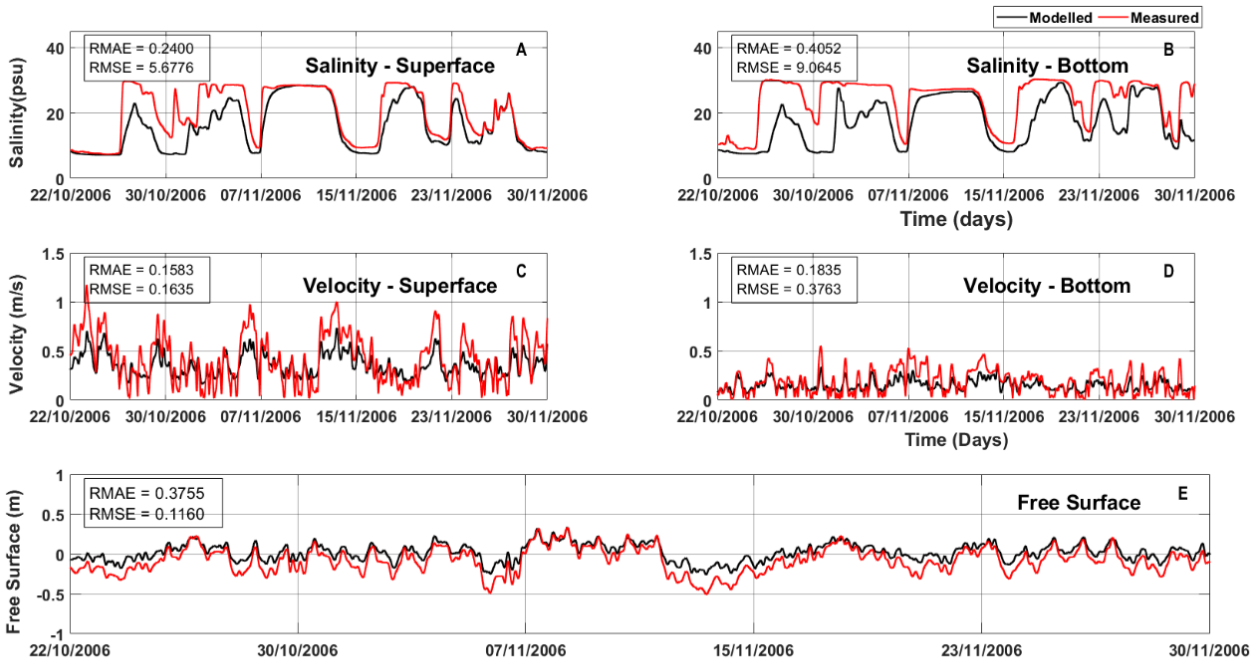


Figura 48 - Figure 4 - Artigo 2 - Comparison between the measured (red line) and calculated (black line) salinity time series at (A) the surface and (B) the bottom, current velocity time series at (C) the surface and (D) the bottom, and free surface time series (E).

Using the best parameterization of the model that the calibration exercises were able to reproduce (Table 2), a validation exercise was carried out with the SSC data for Rio da Prata (Figure 5). The results of the model (black line) were classified as excellent (Table 1) for the three regions, in the three periods analyzed. With RMAE = 0.182, the lower estuary (Figure 5A) obtained the best statistical results, followed by the upper estuary (Figure 5C) with RMAE = 0.1882 and finally the middle estuary (Figure 5B) with RMAE = 0.2073.

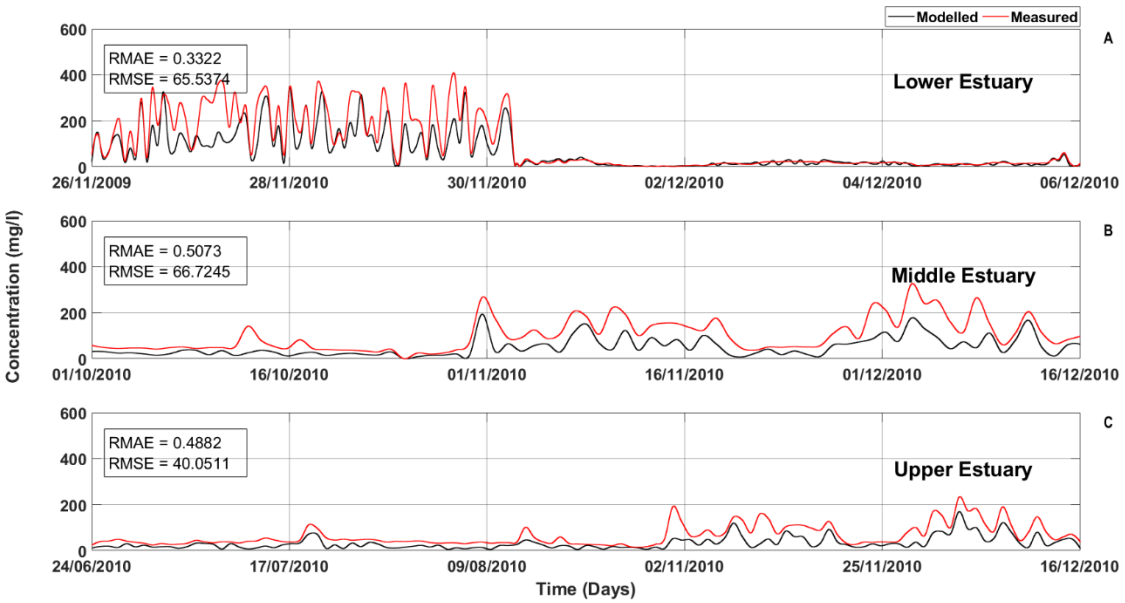


Figura 49 - Figure 5 - Artigo 2 - Comparison between the calculated suspended sediment concentration (black line) and the measured data (red line) in (A) the lower, (B) middle and (C) upper estuary in Rio de La Plata River, between the 24th of June to the 16th of December, 2010.

With the validation exercise, it was evident that the model overestimates the sediment by approximately 15 concentration units (mg / l). This overestimation can be answered by the fact that the continental border is prescribed with constant sediment values. Because of this, it is expected that with the use of a long and systematic time series, the quality of the results will improve.

## Results

### Spatial variability in the Southwest Atlantic Inner Continental Shelf

Figure 6A shows the mean concentration of sediment in the bottom layer, for the 8 simulated years. The result shows a pattern regarding the interference of the plume at the bottom of the seabed. That is, for the La Plata River, where the plume reaches the entire water column (Lisboa et al, 2020), a great concentration can be noticed in the region of the north and south coast of the La Plata estuary, with values above 340 mg/L. In the region of the inner shelf the values of the bottom concentration can reach 200 mg/L in the northern portion of the mouth of Patos Lagoon, and 120 mg/L in the southern region of Patos Lagoon (central portion of the study region).

As for the region close to the mouth of Patos Lagoon, the behavior of the bottom concentration indicates that the regional plume has a superficial profile, presenting low concentration close to the bottom, reaching values close to 10 mg/L. This profile had already been confirmed by Marques et al 2010 and Lisboa et al., 2020. The results confirm that both the La Plata

plume and the Patos Lagoon plume propagate predominantly through the coastal region, indicating a strong contribution to the mean scenario of the bottom sediment concentration on the internal platform (depths less than 30 meters).

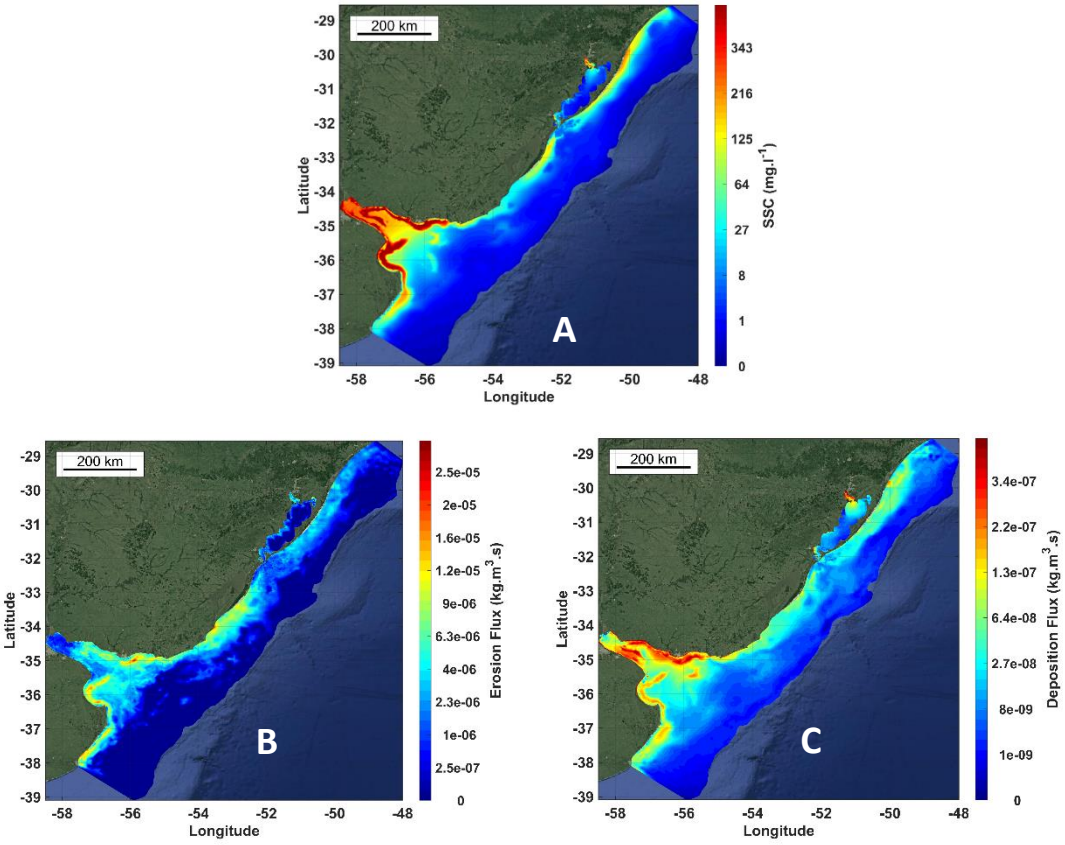


Figura 50 - Figure 6 - Artigo 2 - Mean-field of concentration of bottom sediment (A), Mean-field of erosion flow (B) and deposition flow (C) for the study region, during the period from 2005 to 2012.

The results of the mean erosion flow (figure 6B) over the study region show that erosion occurs more severely in the La Plata River and in the central portion of the coastal region, with wind intensity and fluvial discharge being the main ones responsible for controlling the erosion process (Marques et al 2010). The local dynamics generate erosion rates of approximately $10^5$ kg/m$^2$.s, with the highest rates in areas close to Punta Piedras and Montevideo. Meanwhile, the deposition flow (figure 6C) showed patterns similar to erosion in the coastal region, being more intense in the coastal regions of the La Plata estuary (Uruguayan and Argentine coast), in the northern portion of Patos Lagoon (region of Guaíba River) and in the shallow areas of the inner shelf (up to 10 m deep), with values close to $10^7$ kg/m$^2$.s.

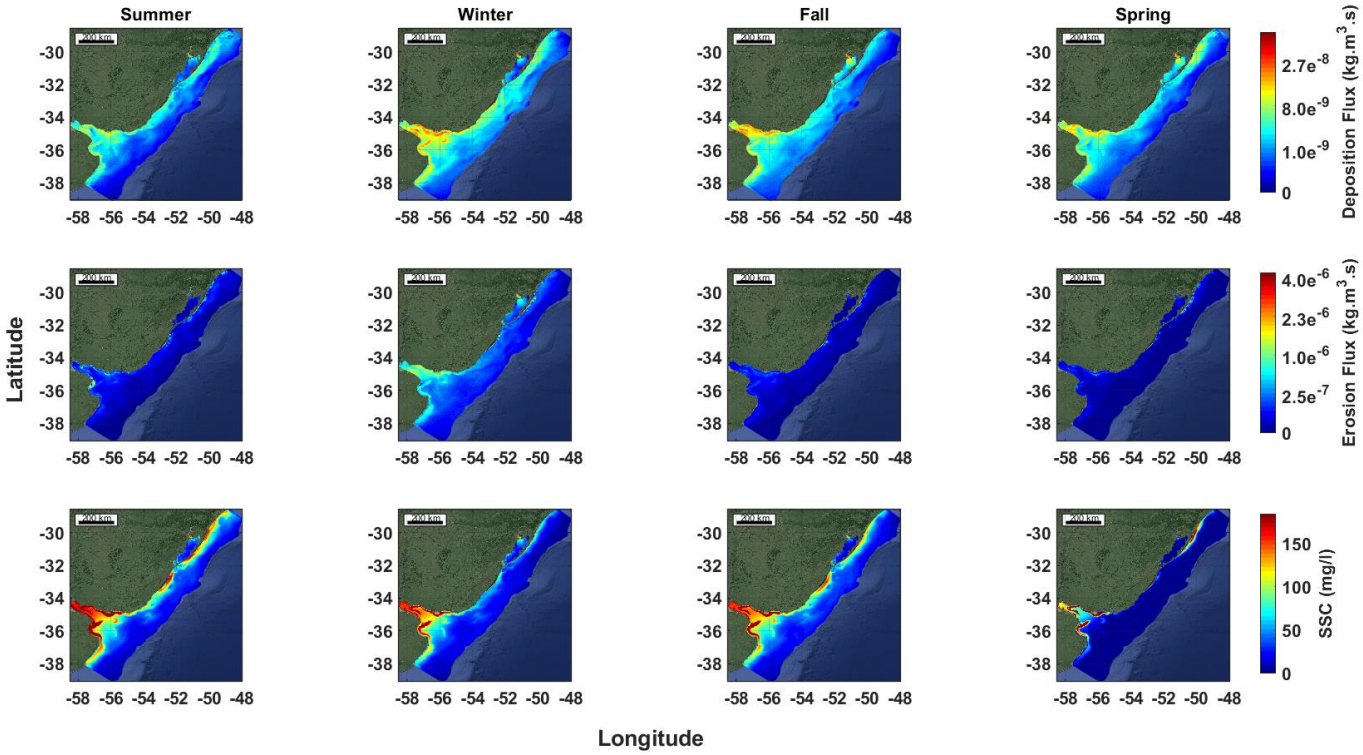


Figura 51 - Figure 7 - Artigo 2 - Seven years (2005–2012) calculated Deposition Flux, Erosion Flux, and SSC means for the austral seasons: a) Summer (Dec – Jan – Feb), b) Winter (Mar – Apr – May), c) Fall (Jun – Jul – Aug), and d) Spring (Sep – Out – Nov).

Figure 7 represents the different seasonal patterns in the deposition and erosion flux, and in the distribution of the bottom sediment concentration (BSC) for the study region. It is noticed that during the summer, high BSC was found in the La Plata River and throughout the inner shelf. This behavior covered the entire coastline, reaching the region of the study area. The same pattern was observed during fall, in which BSC is intensified and distributed throughout the coastal region. The deposition and erosion flux, on the other hand, had opposite behaviors, while the deposition flux reached median to high values, the high erosion flux was restricted only to the region near Punta Piedra, Argentine coast of the La Plata River. During the winter, the BSC in the La Plata region behaves similarly to the summer. What differentiates the seasons is the BSC in the region of the internal platform, which during winter presents a slight decrease. As for erosion and deposition flows, there was an increase in both fluxes during the winter, mainly on the Uruguayan coast of the La Plata.

**Spatial Variability of Bottom Sediment**

In order to analyze and identify the spatial variability of the bottom sediment in the study area, the EOF analysis was performed. Images were generated (Figure 8A, 8B, and 8C) representative of the distribution of spatial variability comprised by the first three modes of EOF for the study period (2005 - 2012). The analysis was implemented on the horizontal representation of the deep layer of the study area.

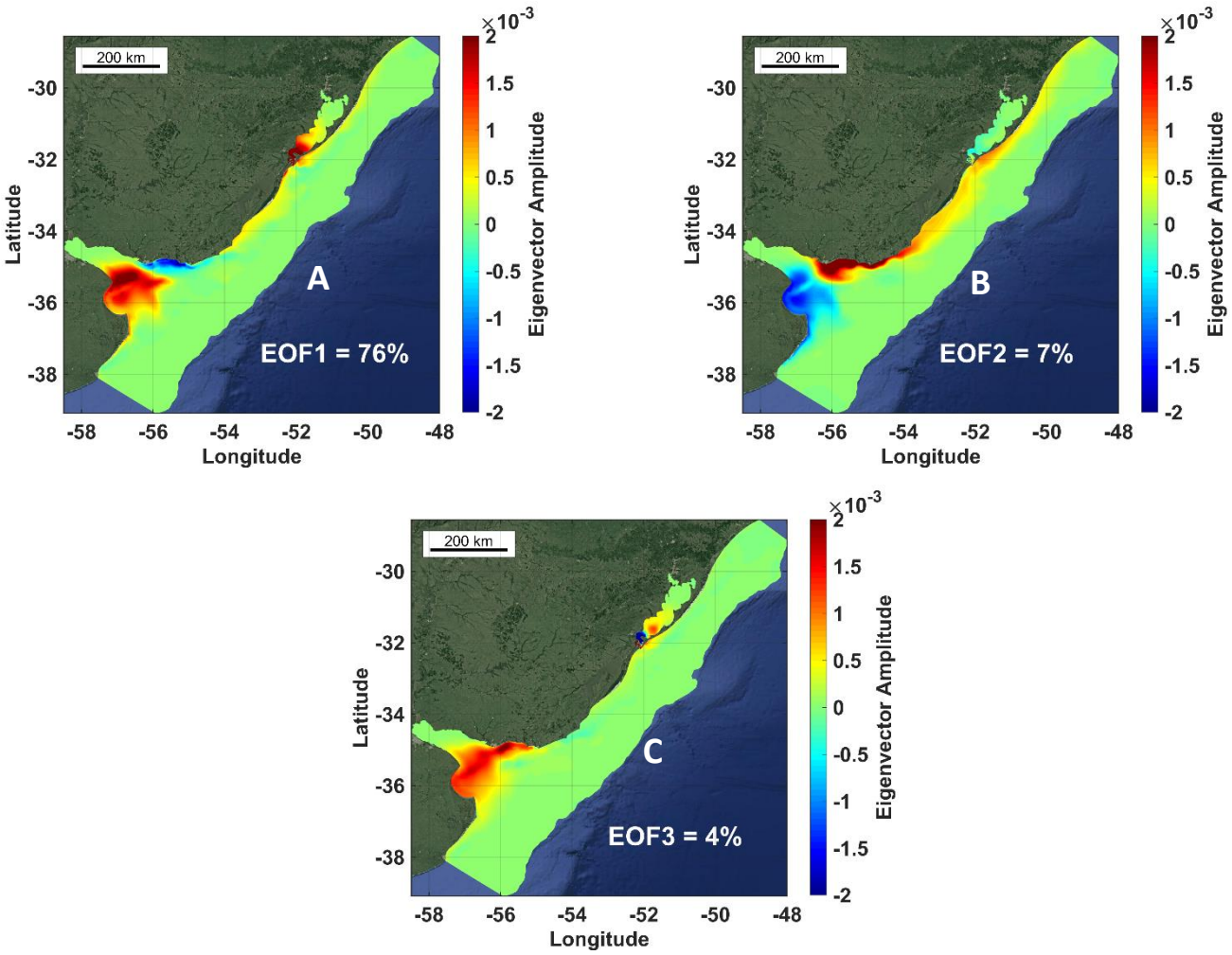


Figure 52 - Figure 8 - Artigo 2 - The first three EOF modes of the bottom sediment concentration for the entire domain in the simulated years (2005 - 2012).

Observing the results of the EOFs, the first mode obtained representativeness of 76% of the variance (Figure 8A), showing a well-defined pattern (area in red) for the presence of the bottom sediment in the regions close to Punta Piedras, in a thin strip in the coastal region, and in the Patos Lagoon Estuary, this means that in 76% of the simulated period the bottom sediment is preferentially concentrated in the regions of the estuary, in the inner shelf, and in the southern region of the mouth of the La Plata River. On the other hand, in the region near Montevideo (blue

area), the sediment concentration has a very high variability during the analyzed period, resulting in a low local pattern for the bottom sediment.

The second and third EOF modes represent 7% and 4%, respectively, of the variance of the bottom sediment for the simulating period. For the second mode of variability, the scenario behaves opposite to the first mode. Thus, in this second mode of EOF, the northern region of the mouth of La Plata presents a low variability (high pattern) in the concentration of the bottom sediment, while on the south coast and a large part of the inner shelf, it became evident a strong pattern defined for the concentration of the bottom sediment. Finally, in the third mode, the region of the high estuary presents a large area where the bottom sediment is largely concentrated, showing a high pattern of bottom sediment for the region.

**Temporal variability of sediment deposition in the Southwest Atlantic Inner Continental Shelf**

Previous studies in the region show that the action of the local wind is one of the main physical forces that control the distribution of suspended sediment in the inner shelf (Marques et al. 2009; 2010a; Monteiro et al., 2011; Lisboa et al., submitted), however, some peculiar patterns may become responsible for the deposition processes on the region. Since the La Plata and Patos Lagoon plumes are different hydrological systems, both are controlled by different time scales. Because of this, wind and fluvial discharge were analyzed in isolation representing the two main mechanisms that provide sediment for the inner shelf. For this, the analysis of cross wavelets of the deposition flow extracted from the mouths of the La Plata River and Patos Lagoon was used.

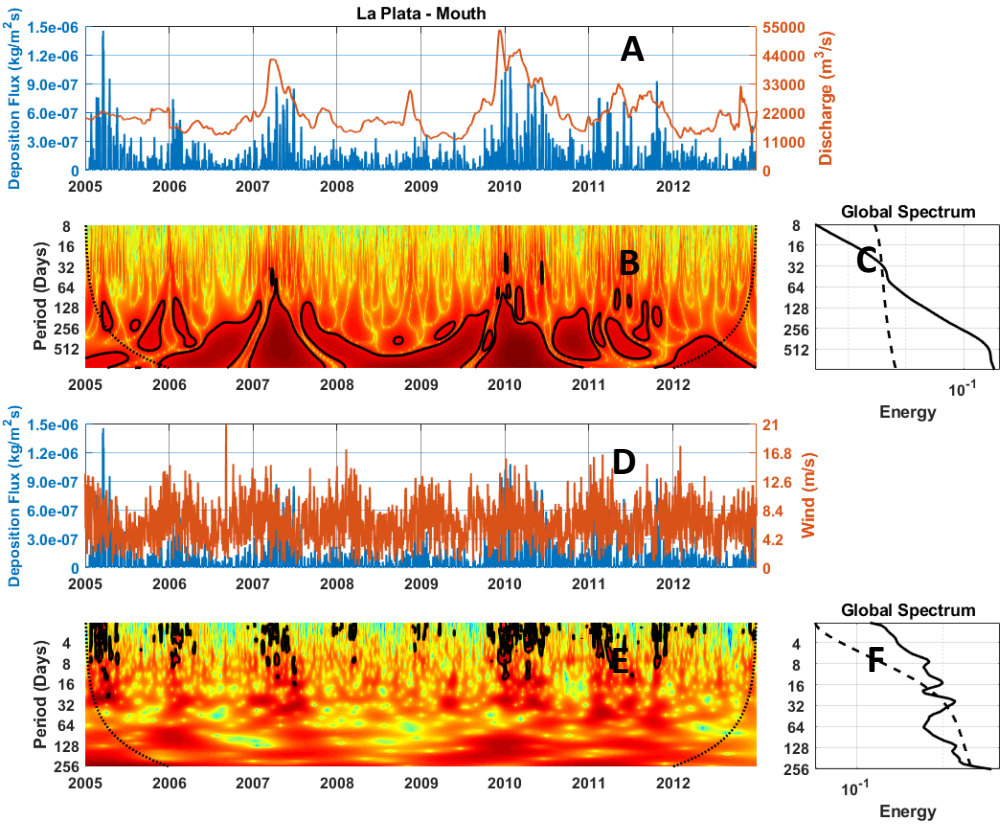


Figura 53 - Figure 9 - Artigo 2 - (A) Time series of deposition flow at the La Plata mouth (blue) and fluvial discharge for the cross-analysis (orange) (black dot - P1, Figure 1). (B) Cross spectra of local energy between the series using Mexican Hat wavelets. The level curves involve regions with a 95% confidence interval. The dashed line indicates the region of influence where the effects of borders become important. (C) Mean global power spectrum. The dashed line represents the 95% confidence level. (D) Time series of deposition flow at the La Plata mouth (blue) and the intensity of the wind for the cross-analysis (orange). (E) Cross spectra of local energy between the series using Morlet wavelets. The level curves involve regions with a 95% confidence interval. The dashed line indicates the region of influence where the effects of borders become important. (F) Mean global power spectrum. The dashed line represents the 95% confidence level.

The cross-wavelet analysis between the continental discharge and the deposition flux for La Plata River is shown in Figure 9A. The wavelets are capable of showing the correlated energy changes throughout the time series in the local spectra (Figure 9B) and their global spectra (Figure 9C), and results indicate that the discharge contributes to the deposition flux on temporal scales bigger than 30 days (Figure 9C) with regions of correlation indicating seasonal variability (Figure 9B). When analyzing the correlation between the deposition flux and the wind velocity, it is evident that these parameters are correlated on time scales smaller than 16 days (Figures 9E and 9F), indicating the contribution wind acting in synoptic scales in the sediment deposition. When looking

at the continental discharge (Figure 10A) and the wind (Figure 10D) with the deposition flux (Figures 10B, 10C, 10D and 10E), respectively, a similar behavior is observed.

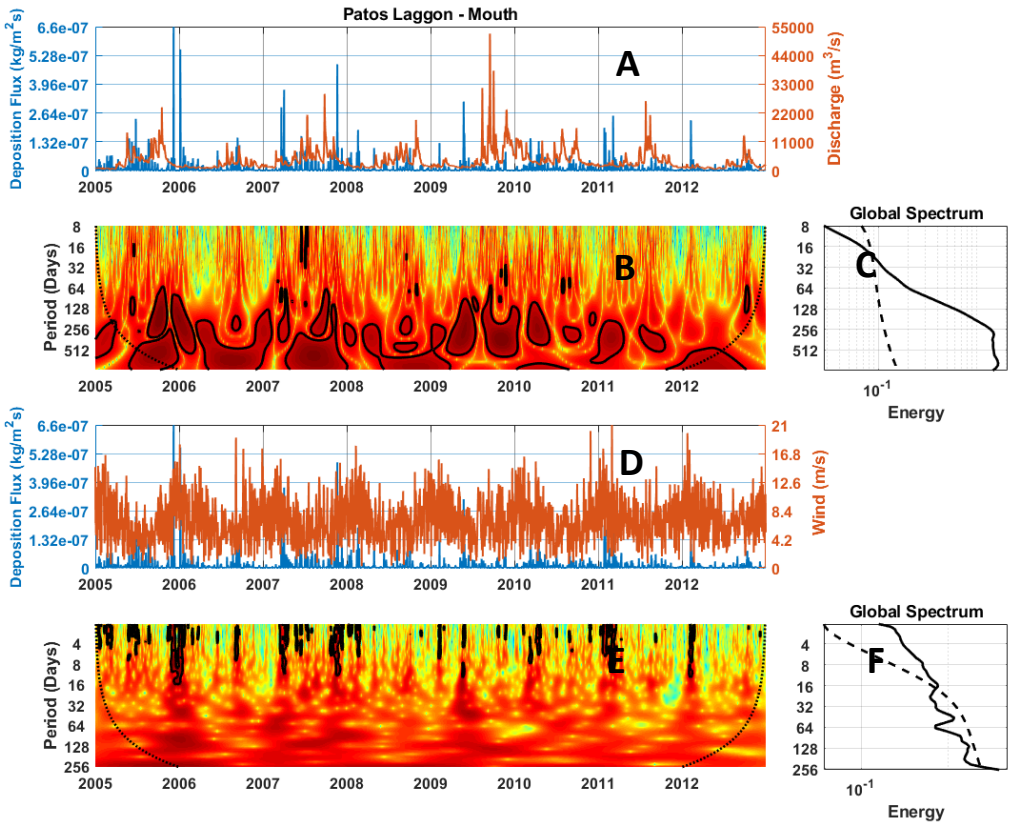


Figura 54 - Figure 10 - Artigo 2 - (A) Time series of deposition flow at the Patos Lagoon mouth (blue) and fluvial discharge for cross-analysis (orange) (black dot - P1, Figure 1). (B) Cross spectra of local energy between the series using Mexican Hat wavelets. The level curves involve regions with a 95% confidence interval. The dashed line indicates the region of influence where the effects of borders become important. (C) Mean global power spectrum. The dashed line represents the 95% confidence level. (D) Time series of deposition flow at the Patos Lagoon mouth (blue) and wind intensity for the cross-analysis (orange). (E) Cross spectra of local energy between the series using Morlet wavelets. The level curves involve regions with a 95% confidence interval. The dashed line indicates the region of influence where the effects of borders become important. (F) Mean global power spectrum. The dashed line represents the 95% confidence level.

Thus, the deposition process in the analyzed period is directly related to the discharge and wind and, consequently, to the availability of sediment and the greater the availability of sediment, the greater the deposition patterns.

**Sedimentation Rate and Bed Evolution of the Inner Shelf**

The balance between the deposition and erosion flow, plus the continental contribution of La Plata River and Patos Lagoon to the coastal region and the continental shelf suggests a positive evolution (areas in red) in most of the study region, with the exception of some area where the erosion process (blue areas) prevails (figure 11A). In the regions close to the coast, the values of the bed evolution rate vary from -1.0 m to 1.0 m during the simulated period, with a large part of the inner shelf being influenced by the deposition process. Coastal erosion was restricted to some regions near the mouth of the La Plata River and much of the northern coast of Patos Lagoon. Considering the 8 years of simulation (2005 - 2012), these values of evolution of the bottom result in an annual sedimentation rate with values close to 125 mm per year.

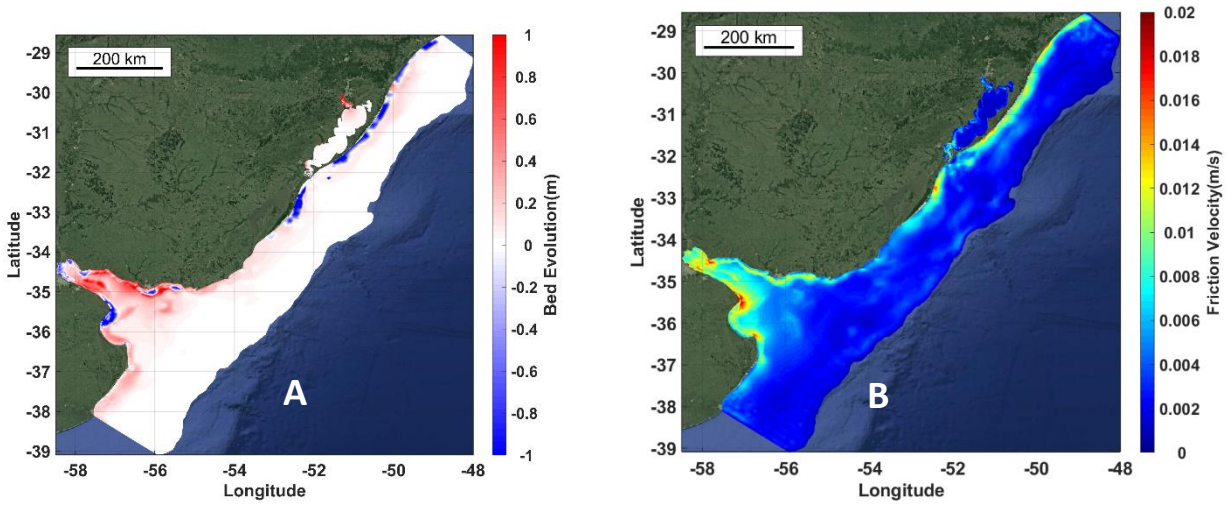


Figure 55 - Figure 10 - Artigo 2 - (A) Bed Evolution rate for the entire domain after 2920 simulated days, (B) Mean friction velocity field.

The result of the bed evolution in the coastal region is an important indication that coastal plumes are important in the dynamics of sediments and play an important role in contributing to the conditioning of the deposition flow in its area of influence. However, the frictional velocity significantly controls the erosion processes, as can be seen in figure 11B. In the regions where the erosive flow has the highest values, it coincides with the highest values of the friction velocity, which reach maximum values close to 0.02 m/s. Thus, the importance of this physical forcing in the erosion process of the inner shelf is evident.

**Influence of ENSO on Bed Evolution**

The results show that during the analyzed period, at least one strong El Niño event (2009/2010) and one strong La Niña event (2007/2008) occurred (figure 12A). For the mouth of La Plata River region (figure 12B) the deposition flux reached values close to 20 mg/m²s, resulting in a 15 cm bed evolution at the end of the analyzed period. At the mouth of Patos Lagoon (figure 12C), the bed evolution was increased by 4.8 cm, as a result of a depositional flux of 1.8 mg/m²s.

When analyzing figure 12, we notice that the deposition flux shows an increase in the years known to be affected by the ENSO event. In the rigorous El Niño of 2009/2010, there is clearly a significant increase in the sediment deposition rate, especially in the region of the mouth of the La Plata River. On the other hand, during the strong La Niña of 2007/2008 the ENSO effect influences the deposition process in order to drastically reduce the deposition flow. This influence can be seen both at the mouth of Patos Lagoon and at the mouth of the La Plata River.

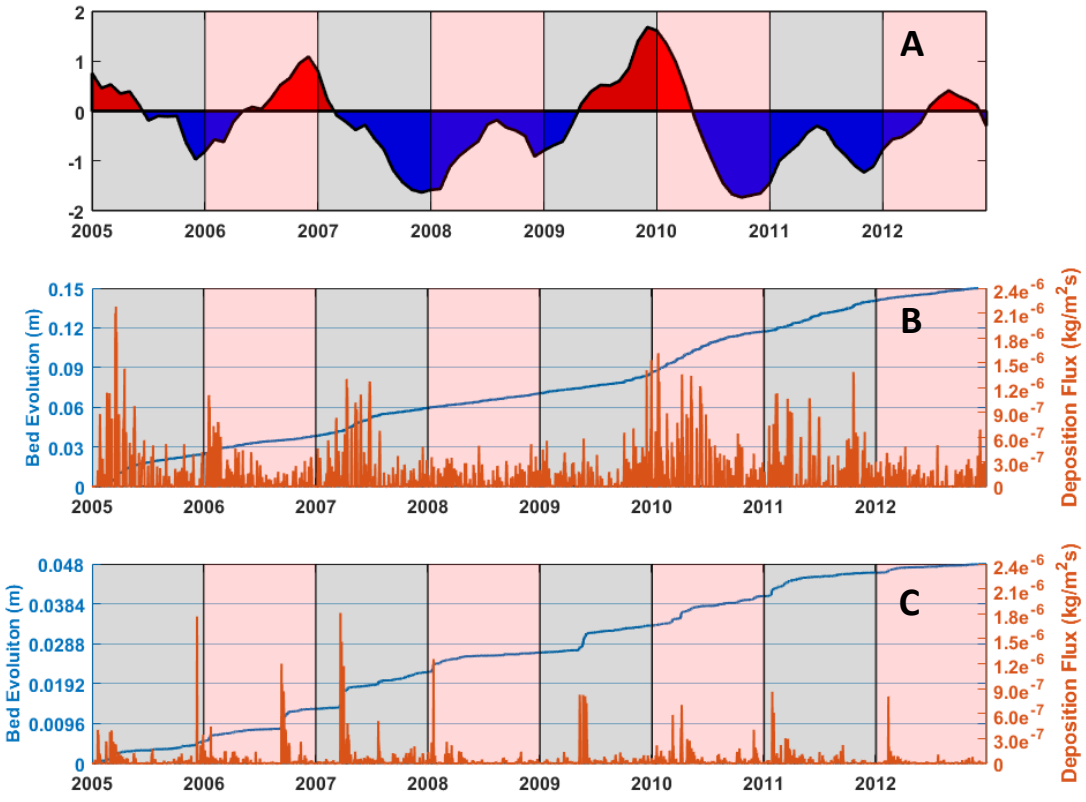


*Figura 56 - Figure 12 - Artigo 2 - (A) The South Oscillation Index (SOI) for the analysis period (2005 - 2012), (B) deposition flux and bed evolution for the mouth of the La Plata River (P1), (C) and deposition flux and bed evolution for the mouth of the Patos Lagoon (P2).*

The bed evolution process is directly related to the local deposition rate. Thus, the ENSO phenomenon interferes with the behavior of this variable. The results show an increase in the thickness of the bottom layer with each increase in the deposition flow.

**Discussion**

Despite the intrinsic limitations in the model, the results of the long-term simulation of sediment transport to the Southwest Atlantic Inner Shelf reproduced the local dynamics satisfactorily. The present study did not take into account some processes that may play an important role in the sediment dynamics for the region, they are waves, sediment consolidation, and biological activity. However, ignoring these processes did not appear to be something that significantly affected the dynamics of the bottom sediment, however, there is an interest in including some of these processes in future work.

**Mean Scenario**

The mean concentration of the bottom sediment in the study region showed the presence of two distinct plumes: one homopycnal, that is, that occupies the entire water column, and another hypopycnal, which occurs only in the upper part of the water column. This differentiation directly reflects the bed evolution in the shallow areas on the internal platform. Thus, the La Plata plume, being a homopycnal plume, significantly influences the concentration of bottom sediment in the region of the mouth of the river as shown in figure 6. Lisboa et al, 2020 show that the influence of the La Plata plume is not restricted only to the mouth of the mouth, which depending on the local dynamics, the plume expands through the adjacent coastal region, intensifying the deposition process throughout the inner shelf.

In the Patos Lagoon plume case, since it is a hypopycnal plume, it has little influence on the mouth of the estuary, as shown by Marques et al. 2010. However, Calliari et al. 2007 already showed that the regions to the north and south of the mouth would be more sensitive to the deposition process stimulated by the Patos Lagoon plume. Marques et al. 2010, further states that these patterns of the bottom evolution caused by the inference of the Patos Lagoon plume are associated with the local circulation pattern, which in turn is predominantly controlled by wind and fluvial discharge. This sensitivity to the deposition process in the coastal region adjacent to Patos Lagoon was also evidenced by other authors such as Holland et al. 2009, Vinzon et al. 2009, and more recently by Lisboa et al. 2020.

The results of this study are compatible with the results presented by Calliari et al. 2009 for the region adjacent to the Patos Lagoon mouth, and with Moreira et al. 2016 for the region of

the La Plata mouth, in which the authors present geomorphological features similar to those presented in this work. According to the authors, these depositional features are preferably between 6 and 2690 meters deep, with layers that vary from a few millimeters to just over 1 meter.

Long-term numerical modeling is an excellent indicator for determining the preferred regions for deposition to occur. However, due to the limitations of the model, the consolidation process was not considered, which is an important process in the formation of muddy banks. Consolidation is a process associated with variations in the density of the sediment and, consequently, in the viscosity of the muddy bench. The muddy benches are hardly remobilized, thus contributing to the deposition process in the region of the inner shelf.

**Spatial Variability**

The analysis of the EOFs indicated the dominance of the first mode for the spatial variability of the bottom sediment in the study region, with a percentage close to 76%. This mode reflects the influence of bathymetry on the concentration of the bottom sediment since a spatial pattern was detected in shallow areas both in the Patos Lagoon estuary and in the La Plata estuary. Simionato and Moreira, 2018 found that fine sediment is mostly concentrated in the southern region of the La Plata mouth, as shown in the first mode of the EOF analyzed. The authors justify this spatial distribution of the bottom sediment concentration because the region presents an abrupt increase in-depth, an abrupt variation in the width of the estuary, in addition to the region being characterized as the front of the saline wedge of the estuary, which favors the accumulation of the sediment in the region.

In the Patos Lagoon estuary, Marques et al, 2010 state that the predominant action of the north quadrant wind helps in stacking water in the Patos Lagoon estuarine region, and consequently, an increase in the bottom sediment concentration in the shallow regions of the estuary. In the inner shelf region, the variability of the bottom sediment is greater when compared to the estuarine regions, that is, a well-defined pattern of the concentration of the bottom sediment on the inner shelf is not shown, indicating that it is a highly variable area due to the coastal dynamics.

**Deposition Pattern**

The analysis of the energetic potential by wavelets has been widely used to determine the temporal variability of two correlated parameters. In the case of the present study, this correlation was made to determine the temporal variability of the deposition flow when correlated with the river

discharge and to determine the time variability of the deposition flow when correlated with the wind, that is, the two main forces that affect the sediment distribution on the inner shelf.

The analysis considered 2920 simulation days and determined that the deposition process is controlled by the wind in synoptic scales (cycles of 16 days), while the fluvial discharge controls the deposition flow in seasonal scales (cycles from 30 to 180 days), both for the La Plata region and for the Patos Lagoon mouth. These values coincide with those found by Marques et al, 2010b for the region of the Patos Lagoon mouth for the period from 1998 to 1999.

The availability of sediment has a positive influence on the deposition process. Therefore, in the study area, this availability is associated with favorable environmental conditions. Moreira et al, 2019 lists that the southeast wind, fluvial discharge, and estuary morphology, associated with coastal dynamics, are among the main conditions that favor the distribution of sediment on the internal platform and generate a pattern of deposition on the site. As for Patos Lagoon, Marques et al 2010a mention that the northeast winds are associated with fluvial discharge, which associated with the local circulation pattern promotes deposition on the inner shelf.

Another factor that interferes with sediment deposition in the coastal region is related to the deceleration of plumes and the velocity of the coastal current (Wright and Nittouer, 1995). This is because in some cases when the fluvial discharge exceeds the amount of sediment supplied to the coastal region, this sediment can reach long distances before being deposited (Wright and Nittouer, 1995). For the region of studies, both the plume of La Plata and the Patos Lagoon plume tends to decelerate abruptly when interacting with the dynamics of the inner shelf. Thus, the fine sediments from the plumes can influence the bottom morphology of regions more distant from the source.

**Bed Evolution**

The Southwest Atlantic Inner Shelf is recognized for being a highly depositional platform, mainly due to the presence of large effluents that contribute to the suspended sediment (Calliari et. Al., 2009). In the present work, the results presented show that most of the inner shelf is dominated by a positive bed evolution, however, it is possible to observe areas in which the bed evolution had a negative behavior. This represents that in these areas in the balance between erosion and deposition, erosion flow predominated over deposition. The highly energetic coastal dynamics, mainly due to the action of the northeast wind, generate bottom friction velocities large enough to exceed the erosion coefficient threshold, resulting in a high erosive flow. In the case of the other depositional areas, the dynamics are not energetic enough to mobilize the sediment at greater distances, thus resulting in an ideal scenario for deposition (Marques et al, 2010).

Santoro et al, 2017 and Fossati et al, 2013 analyzed the bed evolution in the La Plata estuary region and showed similar and distinct features to those found in the present study. The similarities are due to the erosive areas present on the Argentine coast of the estuary. According to the authors, the high local dynamics, associated with the high bathymetric gradient, resulted in a highly erosive character for the region. In contrast, in the present study the areas of the high estuary are predominantly erosive, while Santoro et al., 2017 showed depositional areas. This difference can be explained because the authors used the consolidation model, or even because of the instability present in the model's contours.

For the region near the Patos Lagoon mouth, we can see that there is a positive trend in the bed evolution, both near the east and the west. This is due to the presence of a muddy bench, present in the region, as detailed by Calliari et al, 2009. The presence of a smooth area (bed evolution close to zero) in front of the jetties is also evidenced by Fachin, 1998, who claims to be a predominantly muddy area, which may have traces of mixed sand. Calliari and Fachin, 1993 already stated that this muddy deposit represented by the model, has its origin related to the Patos Lagoon plume, since it can influence the areas close to the 20-meter isoline.

Regarding the influence of the ENSO effect on the bed evolution process, the periods in which deposition rates increased were directly correlated to climatic anomalies due to the strong influence of El Nino / La Nina in the study region. ENSO events are weather patterns that occur at intervals of 3 to 7 years. These episodes cause above-average rainfall in southern Brazil, Uruguay, and northeastern Argentina (Grimm et al. 1998; Philander 1990; Ropelewski and Halpert 1987, 1989; Bitencourt et al, 2020). This cyclical oscillation contributes to the entry of sedimentary cargo on the inner shelf, originating from rivers (Ivanoff et al., 2020). Due to the increase in the sedimentary load that arrives in the coastal region, the deposition flux of this sediment increases, directly affecting the behavior of the bed evolution.

**Conclusion**

The bed evolution of the Southwest Atlantic Inner Shelf and the collaboration of the erosion and deposition processes were investigated for the period from January 1, 2005, to December 31, 2012. The inner shelf has two large effluents that have a fundamental role as source sediment. The La Plata and Patos Lagoon plumes behave differently, while the first has a homopycnal profile, covering the entire water column, the second behaves like a hypopycnal plume, covering only the first meters.

The mean depositional pattern on the adjacent coastal region is the result of a balance between the processes of erosion and deposition, thereby realizing that deposition prevails in much

of the study area, thus characterizing the highly depositional Southwest Atlantic Inner Shelf. The cause of this is in several parameters present in the study area, from the coastal dynamics favorable to deposition, due to the deceleration of the plume, passing through the bathymetric and geomorphological features, to the action of the wind.

The action of wind and fluvial discharge in the main physical mechanisms in the control and distribution of fine sediment across the shelf. These mechanisms have different operating time scales, while the wind acts in the region in a synoptic way, that is, on the 16-day scale, the fluvial discharge is presented on a monthly to the seasonal basis, thus, from 30 to 180 days.

The plume of sediment from La Plata and Patos Lagoon significantly influences the availability of suspended sediment, which over time may become bottom sediment. In addition, the action of the south quadrant wind induces the formation of currents to the north, responsible for transporting the sediment from the La Plata River to the northern region of the inner shelf, as well as the northeast wind in Patos Lagoon is responsible for the local sedimentation that moves to the in the coastal region.

The EOF modes showed that there is a well-defined pattern in the spatial variability of the bottom sediment. This sediment accumulates preferentially close to the central region of the La Plata estuary and dominates the entire Patos Lagoon estuary. In addition, it is possible to notice a small pattern formed in the central region of the inner shelf.

Regarding the bed evolution, the work showed that the Southwest Atlantic Inner Shelf is essentially depositional, despite presenting some erosive areas along the coastal region and on the Argentine coast of the La Plata River. Being highly influenced by the ENSO effect in the region, which increases the deposition flow, reflecting this in the bottom evolution process. The sedimentation rate was around 50 mm/year, with regions with rates that reached values close to 120 mm/year being observed.

**Reference**

Berbery E. H. & Barros V. 2002: The hydrological cycle of the La Plata Basin in South America. J Hydromet 3: 630-645.

Bisbal, G.A., 1995. The Southeast South American shelf large marine ecosystem: Evolution and components. Mar. Policy,19(1),21–38, doi:10.1016/0308-597X(95)92570-W.

Calliari, L. J., J. C. Winterwerp, E. H. Fernandes, D. C. Cuchiara, S. B. Vinzon, M. Sperle, and K. T. Holland (2009), Fine grain sediment transport and deposition in the Patos Lagoon-Cassino beach sedimentary system, Cont. Shelf Res., 29(03), 515–529.

Castello, J., Duarte, A., Möller, O. O., Niencheski, F., Odebredcht, C., Weiss, G., Habiaga, R., Bellotto, V., Kitzmann, D., Souto, C., Souza, R., Ciotti, A., Fillmann, G., Schwingell, P., Bersano, J., Cirano, M., Freire, K., Lima, I., Mello, R., Monteiro, A., Resgalla, C., Soares, I., Suzuki, M. 1990. On the importance of coastal and subantartic waters for the shelf ecosystem off Rio Grande do Sul. Anais do II Simpósio de Estrutura, Função e Manejo de Ecossistemas da Costa Sul e Sudeste, São Paulo – Brazil, I: 112-129.

Egbert, G.D., & S.Y. Erofeeva, 2002. Efficient inverse modeling of barotropic ocean tides. J. Atmos. Oceanic Technol., 19(2), 183-204.

Egbert, G.D., Bennett, A.F., Foreman, M.G.G., 1994. Topex/Poseidon tides estimated using global inverse model. J. Geophys. Res., 99(C12), 24821–24852, doi: 10.1029/ 94JC01894.

Exner, F. M.: Über die Wechselwirkung zwischen Wasser und Geschiebe in Flüssen, Akad. Wiss. Wien Math. Naturwiss. Klasse, 134, 165–204, 1925.

Exner, F. M.: Zur Physik der Dünen, Akad. Wiss. Wien Math. Naturwiss. Klasse, 129, 929–952, 1920.

Fossati, M., Cayocca, F., & Piedra-Cueva, J.C.I. (2014). Fine sediment dynamics in the Río de la Plata. Advances in Geosciences, 39, 75-80.

Haimovici, M.; Pereira, S.; Vieira, P.C.V. 1989. La pesca demersal en el sur de Brasil en el período 1975-l985. Frente Marítimo, 5: 151-163.

Hervouet, J.M. (2007). Hydrodynamics of Free Surface Flows. John Wiley & Sons, Ltd, Chichester, UK. 31, 45, 111, 116, 119, 247, 249, 254.

Holland, K. T., S. B. Vinzon, and L. J. Calliari (2009), A field study of coastal dynamics on a muddy coast offshore of Cassino beach, Brazil, 29(3), 501–502.

Hostache, R., Hissler, C., Matgen, P., Guignard, C., and Bates, P.: Modelling suspended-sediment propagation and related heavy metal contamination in floodplains: a parameter sensitivity analysis, Hydrol. Earth Syst. Sci., 18, 3539 3551, https://doi.org/10.5194/hess-18-3539-2014, 2014.

Jaime, P. R., & Menéndez, A. N. (2002). Análisis del régimen hidrológico de los ríos Paraná y Uruguay. Informe LHA-01-216-02, INA, Ezeiza.

Laprida, C., Chapori, N. G., Violante, R. A., Compagnucci, R. H., 2007. Mid-Holocene evolution and paleoenvironments of the shoreface–offshore transition, north-eastern Argentina: New evidence based on benthic microfauna. Marine Geology, 240(43-56).

Lepesqueur, J., Hostache, R., Martínez-Carreras, N., Montargès-Pelletier, E., Hissler, C. Sediment transport modelling in riverine environments: on the importance of grain-size distribution,

sediment density, and suspended sediment concentrations at the upstream boundary. Hydrol. Earth Syst. Sci., 23, 3901–3915.

Marques, W. C. et al.,2010b. Dynamics of the Patos Lagoon coastal plume and its contribution to the deposition pattern of the Southern Brazilian inner Shelf. Journal of Geophysical Research, v. 115.

Marques, W.C., Fernandes, E.H., Monteiro, I.O., Möller Jr., O.O., 2009. Numerical modeling of the Patos Lagoon coastal plume, Brazil. Continental Shelf Res. 29, 556-571.

Möller Jr OO, Piola AR, Freitas AC, Campos EJD. 2008. The effects of river discharge and seasonal winds on the shelf off southeastern South America. Continental Shelf Research 28(13):1607–24. doi:10.1016/j.csr.2008.03.012

Möller, O. O., J. A. Lorenzzetti, J. L. Stech, and M. M. Mata (1996), The Patos Lagoon summertime circulation and dynamics, Cont. Shelf Res., 16, 335‐351, doi:10.1016/0278-4343(95)00014-R.

Möller, O. O., P. Castaing, J. C. Salomon, and P. Lazure (2001), The influence of local and non-local forcing effects on the subtidal circulation of Patos Lagoon, Estuaries Coasts., 24, 297‐311, doi:10.2307/1352953.

Moreira, D., Simionato, C. G., Dragani, W., Cayocca, F., & Luz Clara Tejedor, M. (2016). Characterization of Bottom Sediments in the Río de la Plata Estuary. Journal of Coastal Research, 32(6), 1473‐1494.

Nikuradse, J.: Gesetzmässigkeiten der Turbulente Strömung in Glatten Rohren, Ver. Deut. Ing. Forschungsheft, 356, Ver. Deut. Ing. Forschungsheft, Düsseldorf, 1932.

Nittrouer, C.A., Wright, L.D., 1994. Transport of particles across continental shelves. Reviews of Geophysics 32 (1), 85‐113.

Santoro, P., Fossati, M., Tassi, P., Huybrechts, N., Pham Van Bang, D., and Piedra-Cueva, J.C.I. (2017). A coupled wave-current-sediment transport model for an estuarine system: Application to the Río de la Plata and Montevideo Bay. Applied Mathematical Modelling, 52, 107-130.

Simionato, C. G., Moreira, D., Re, M., & Fossati, M. (2011). Estudio de la dinámica hidro-sedimentológica del Río de la Plata: observación y modelación numérica de los sedimentos finos. Published by Proyecto FREPLATA, CTMFM-CARP, 109p.

Siminato, C. G., Moreira, D., (2018). Modeling the Processes that Control Fine Sediments Transport in the Río de la Plata Estuary. Journal of Coastal Research, 85(sp1):31-35.

Soares, I.D., & Möller, O.O., 2001. Low-frequency currents and water mass spatial distribution on the southern Brazilian shelf. Continental Shelf Research, 21(16-17):1785-1814. DOI:10.1016/S0278-4343(01)00024-3.

Soares, I.D., Kourafalou, V., Lee T.N., 2007a. Circulation on the western South Atlantic continental shelf: 1. Numerical process studies on buoyancy. J. Geophys. Res., 112, D04002, doi:10.1029/2006JC003618.

Soares, I.D., Kourafalou, V., Lee T.N., 2007b. Circulation on the western South Atlantic continental shelf: 2. Spring and autumn realistic simulations. J. Geophys. Res., Res. 112, C04003, doi:10.1029/2006JC003620.

Sternberg, R.W., Nowell, A.R.M., 1999. Continental shelf sedimentology: scales of investigation define future research opportunities. Journal of Sea Research 41, 55–71.

Tassi, P., Villaret, C., 2014. Sisyphe v6.3 User's Manual - User manual, EDFLNHE report H-P73-2010-01219.

Villaret, C., 2010. Sisyphe user manual, Tech. Rep., EDF R&D, Chatou.

Villaret, C., Hervouet, J. M., Kopmann, R., Merkel, U., and Davies, A. G., 2013 Morphodynamic modelling using the Telemac finiteelement system, Comput. Geosci., 53, 105–113.

Vinzon, S. B., J. C. Winterwerp, R. Nogueira, and G. J. de Boer (2009), Mud deposit formation on the open coast of the larger Patos Lagoon - Cassino Beach system, Cont. Shelf. Res., 29(03), 572–588.

Violante, R.A. & Cavalloto, J.L. 2004. Evolution of the semienclosed basins and surrounding coastal plains adjacent to the Pampean Region, Argentina. Polish Geological Institute Special Papers, 11:59-70.

Wright, L.D., Boon, J.D., Kim, S.C., List, J.H., 1991. Modes of cross-sore sediment transport on the shoreface of the Middle Atlantic Bight. Marine Geology 96, 19–51.

Marques, W.C., Fernandes, E.H., Möller Jr., O.O., 2010a. Straining and advection contributions to the mixing process of the Patos Lagoon coastal plume, Brazil. Continental Shelf Research, doi:10.1029/2009JC005653.

Moreira D, Simionato CG (2019) Modeling the suspended sediment transport in a very wide, shallow, and microtidal estuary, the Río de la Plata, Argentina. J Adv Model Earth Syst 11(10):3284–3304. https:// doi.org/10.1029/2018MS001605.

Wright, I. D., and C. A. Nittrouer (1995), Dispersal of river sediments in coastal seas: Six contrasting cases, Estuaries, 18, 494–508.

Fossati, M. & Piedra-Cueva, I. (2013). A 3d hydrodynamic numerical model of the Río de la Plata and Montevideo's coastal zone. Applied Mathematical Modelling, 37, 1310_1332. 8, 42

Calliari, L.J., Fachin, S., 1993. Laguna dos patos. Influência nos depósitos lamíticos costeiros. Pesquisas, Porto Alegre 20 (1), 57–69.

Fachin, S., 1998. Caracterização do perfil de equilíbrio da antepraia na costa do Rio Grande do Sul. Msc. Dissertation. Universidade Federal do Rio Grande do Sul, Porto Alegre, Brasil, p. 88, unpublished.

# **Capítulo VII**: Síntese das Discussões e Conclusões

# 7. Síntese das Discussões e Conclusões

Apesar das limitações intrínsecas do modelo, os resultados das simulações de curto prazo (2 anos) e de longo prazo (7 anos) do transporte de sedimentos em suspensão e de fundo, respectivamente, para a Plataforma Interna do Atlântico Sudoeste reproduziram a dinâmica local de forma satisfatória. Por motivos operacionais, o presente estudo não levou em consideração alguns processos que podem desempenhar um papel importante na dinâmica dos sedimentos para a região, são eles: ondas, consolidação de sedimentos e atividade biológica. No entanto, ignorar esses processos numa primeira avaliação não parece ter sido algo que afetasse significativamente a dinâmica do sedimento em suspensão e de fundo, uma vez que os exercícios de calibração e validação resultaram em parâmetros estatísticos considerados adequados, habilitando assim o modelo a reproduzir o comportamento realista da dinâmica sedimentar da região. Porém, existe grande interesse dos autores em incluir esses processos em trabalhos futuros.

## 7.1. Sedimento em Suspensão

### 7.1.1. Distribuição das Plumas da Lagoa dos Patos e do Rio La Plata na Plataforma Interna do Atlântico Sul

Ao analisarmos as simulações de curto prazo, notamos que a distribuição de concentrações de sedimento em suspensão na Plataforma Interna do Atlântico Sudoeste (Figura 8 – Artigo 1), apresenta grande relação sazonal com as plumas do Rio de Prata (Guerrero et. al, 1997) e da Lagoa dos Patos (Marques et. al., 2010a) para os dois períodos analisados (2005 – 2005 e 2008 – 2009). Sendo assim, durante o inverno austral (Figura 8A e 8B – Artigo 1) as concentrações de sedimento em suspensão apresentam seus maiores valores (Campos et. al., 1999; Pimenta et. al., 2005; Soares et. al. 2007a; Simionato and Moreira, 2018), isso por que a pluma do Rio da Prata durante esse período se expande pela faixa costeira em direção ao norte, atingindo latitudes próximas a 26ºS (Moreira et. al., 2013), percorrendo assim distâncias maiores de 1000 km. Já durante o verão austral (Figura 8C e 8D – Artigo 1), a atuação das concentrações de sedimento em suspensão fica mais restrita a uma curta faixa costeira atingindo no máximo a latitude de 30ºS, além de outra porção que fica aprisionada na foz do Rio da Prata (Piola et. al., 2004).

A exemplo do Rio da Prata, a Lagoa dos Patos tem o comportamento das concentrações de sedimento em suspensão condicionado a sazonalidade (Marques et. al.,

2010a), isso por que altos valores de concentração ocorrem com mais frequência durante o inverno austral (Figura 8A e 8B – Artigo 1), enquanto que no durante o verão (Figura 8C e 8D – Artigo 1) é esperado valores próximos ou abaixo da média. Em alguns casos, como visto nos resultados, devido a ampla diferença entre as descargas fluviais, é possível que a pluma do Rio da Prata encontre um cenário ideal para penetrar além da entrada e do estuário da Lagoa dos Patos (Burrage et. al., 2008). Além disso, devido a esse panorama, a pluma do Rio da Prata normalmente se funde ou até mesmo domina a pluma da Lagoa dos Patos (Burrage et. al., 2008), como apresentado nos resultados do presente trabalho.

Como visto nos resultados dos artigos, a região é altamente suscetível a ação do efeito ENSO, sendo assim os anos sob influência do El Niño tendem a serem mais úmidos devido alto índice de precipitação (Bitencourt et. al., 2020). Em contrapartida, nos anos afetados pelo fenômeno La Niña é esperado um cenário de seca (Grimm et. al., 1998). Sendo assim, no período analisado sob a influência do ENSO, predominantemente La Niña (Figura 8B e 8D, Artigo 1), foi visto altos valores de turbidez para o Rio da Prata. Porém nem sempre o ENSO é a única previsão de seca (La Niña) ou enchente (El Niño) na região. Pasquini e Depedris (2007) explicam que o principal contribuinte de sedimentos em suspensão para o Rio da Prata, o Rio Bermejo (70% do sedimento total), não sofre com o efeito ENSO. Por outro lado, os afluentes responsáveis por quase 97% da água doce do La Plata (Rio Paraná e Rio Uruguai) são fortemente afetados pelo ENSO (Dogliotti et. al., 2016), consequentemente, o ENSO afeta essencialmente as concentrações de sedimento em suspensão do Rio da Prata diluindo a concentração do sedimento na região por conta do aumento da descarga fluvial (Berbery e Barros, 2002; García-Rodríguez et. al., 2014).

Para a Lagoa dos Patos, ficou demonstrado que existe uma anomalia da descarga fluvial associada ao ENSO, anomalia essa confirmada por diversos autores (Fernandes et. al., 2002; Vaz et. al., 2006; Távora et. al., 2020; Bitencourt et. al., 2020). Essa anomalia gera valores que variam da média para abaixo da média nos anos de La Niña analisados no trabalho (Figuras 8B e 8D – Artigo 1) e valores acima da média para os anos de El Niño (Távora et. al., 2020; Bitencourt et. al., 2020).

As Figuras 9B e 9F (Artigo 1) são resultados relacionados a hidrodinâmica do estuário do Rio da Prata e mostram que os fluxos de enchente e vazante são altamente afetados pela batimetria local, conforme confirmado por Fossati e Cuevas (2013). Pelos resultados fica evidente que os eventos de vazante no Rio da Prata ocorrem

preferencialmente em áreas rasas do estuário. Em compensação, os fluxos de enchente são mais comumente encontrados em regiões mais profundas, como acontece próximo à costa uruguaia. Na Figura 9F (Artigo 1) fica notório a participação do efeito ENSO ao enfraquecer os fluxos de enchente e vazante, em concordância com Guerrero et. al. (1997). Através das figuras 9D e 9H (Artigo 1) foi possível analisar a seção transversal da Lagoa dos Patos e notar um padrão de circulação vazante na região da desembocadura. Para o período de La Niña analisado, o padrão hidrodinâmico da Lagoa dos Patos se assemelha ao do Rio da Prata, sofrendo uma sutil atenuação na velocidade de corrente (Figura 9H – Artigo 1), consequência do período de seca causado pela La Niña (Grimm et. al., 2000).

Um perfil homopycnal (ocupando toda coluna d'água) na pluma do Rio da Prata ficou evidente nos resultados das figuras 9A e 9E (Artigo 1), com maiores concentrações de sedimento em suspensão na região do alto estuário e ao longo do litoral norte (Uruguai) e litoral sul (Argentina). Os resultados corroboram Moreira et. al. (2013), que afirmaram que as concentrações de sedimento em suspensão são maiores ao longo da costa sul do estuário devido a participação do Rio Paraná com alto fluxo sólido em sua vazão, que tende a ocupar o litoral sul do estuário. O efeito ENSO (Figura 9E – Artigo 1) torna-se visível através do aumento das concentrações de sedimento em suspensão tanto na costa sul quanto na costa norte, como também constatado por Dogliotti et. al. (2016) ao investigar o comportamento da turbidez durante os anos de La Niña. Ao analisarmos a hidrodinâmica da Lagoa dos Patos, fica evidente a formação de uma pluma hipopicnal (flutuabilidade positiva), como mostra a figura 9C (Artigo 1). A pluma apresenta em seu núcleo uma alta concentração de sedimento em suspensão, sendo os máximos relacionados a eventos de vazão, migrando para sul na região costeira na maior parte do tempo (ação do vento nordeste).

### 7.1.2. Variabilidade espacial das plumas costeiras

Analisando o período afetado pelo ENSO (Figura 9G – Artigo1), percebemos uma pluma com concentração mais baixa se comparado a anos normais. O mesmo resultado foi visto por Marques et. al. (2010b), no qual afirmaram que a descarga fluvial da Lagoa dos Patos apresenta alta variabilidade interanual, o que interfere diretamente no processo de exportação do material em suspensão para a região costeira.

Os resultados mostram que ambos dos sistemas exportam água e sedimento em suspensão para a Plataforma Atlântica Interior Sudoeste. Ao analisar o fluxo total de

massa exportada pelo Rio da Prata (Figura 10A e 10B – Artigo 1), foi possível perceber uma similaridade nos padrões de importação e exportação, onde os valores máximos estão relacionados aos máximos da descarga fluvial (Figura B3 - Apêndice B), com um mês de atraso entre a vazão máxima e o pico de sedimento em suspensão. Esse atraso também foi observado por Simionato et. al. (2009), Moreira et. al. (2013) e Dogliotti et. al. (2016), sendo a distância percorrida pelo sedimento da jusante até a foz o grande motivo desse atraso. A mesma análise foi feita para a foz da Lagoa dos Patos onde foi observado uma série temporal com perfil semelhante ao da vazão do rio (Figura B3 - Apêndice B), evidenciando uma correlação entre os picos máximos de sedimento em suspensão com o fluxo máximo de vazão.

Considerando que eventuais condições climáticas podem influenciar no comportamento do sedimento em suspensão (Távora et. al., 2020; Bitencourt et. al., 2020), os anos sob ação do ENSO foram analisados e percebe-se que com os índices ENSO acima de 1 (Figuras 10E e 10F – Artigo 1), existe uma resposta manifesta sobre a vazão do rio, atuando significativamente no fluxo de massa. Pode ser visto que no início de 2008 a região está sob influência de um evento de La Niña moderado, que já é suficiente para alterar os valores do fluxo de massa tanto do Rio da Prata quanto da Lagoa dos Patos. Já no evento forte de El Niño (índice acima de 1.5) ao final do ano de 2009, aumentou significativamente a quantidade de material em suspensão exportados pelo Rio da Prata e da Lagoa dos Patos.

Quanto aos valores acumulativos exportados pelos rios, o presente trabalho estimou uma massa acumulativa do Rio da Prata para os anos neutros (2005 – 2006) que se aproxima de $1.2x10^8$ ton/ano, mesmo ordem de magnitude encontrada por Menéndez e Sarubbi (2007). Já nos anos afetados pelo efeito ENSO, a taxa de exportação ficou em torno de $3.0x10^8$ ton/ano. Para a Lagoa dos Patos, nos anos neutros, essa taxa girou em torno de $1.3x10^7$ ton/ano, muito próximo aos $1.4x10^7$ ton/ano encontrados por Marques et. al. (2010b). Para os anos sob influência do ENSO, esse valor aumentou para $1.35x10^7$ ton/ano.

Para analisar a variabilidade espacial das concentrações de sedimento em suspensão exportadas pelo Rio da Prata e pela Lagoa dos Patos, a análise EOF foi utilizada a fim de compreender como o sedimento em suspensão se distribui na região de estudo. Os resultados apontam que o primeiro modo dominante que controla a variabilidade especial das concentrações de sedimento em suspensão no Rio da Prata e na Lagoa dos Patos (Figura 11A – Artigo 1), que explica 61% do período simulado.

Agregado a isso um forte padrão espacial presente no norte da Lagoa dos Patos e nas costas leste e oeste do Rio da Prata. Já ao estudar o período influenciado pelo ENSO (Figura 11B – Artigo1), o primeiro modo explica 51% da variabilidade espacial do sedimento em suspensão.

O padrão definido pelo primeiro modo EOF (Figuras 11A e 11B – Artigo 1) para a Lagoa dos Patos mostra essa correlação não só para o Rio Guaíba, mas também para os outros dois principais afluentes da lagoa, o Rio Camaquã e o Canal de São Gonçalo, como também foi mencionado por Oliveira et. al. (2015). Para o Rio da Prata, o abastecimento de água do rio Paraná ocorre principalmente ao longo da costa argentina do estuário, mostrando sua importância na dinâmica sedimentar local (em vermelho - Figura 11A – Artigo 1). No litoral uruguaio do estuário, onde o Rio Uruguai é o principal responsável pela contribuição sedimentar, a variabilidade dos sedimentos suspensos tem caráter negativo (azul - Figura 11A – Artigo 1), evidenciando a alta variabilidade desse efluente na dinâmica do estuário.

A fim de analisar o comportamento do sedimento em suspensão na coluna d'água, análises EOF semelhantes foram realizadas para seções longitudinais e transversais na foz de ambos os sistemas (Figuras 12, 13, 14 e 15 – Artigo 1). Para a seção longitudinal na foz do Rio da Prata (Figura 12 – Artigo1), os três primeiros modos da EOF são responsáveis por 81% da variabilidade do SSC durante o período neutro (Figuras 12A, 12C e 12E – Artigo 1), enquanto que durante o período ENSO os três primeiros modos são responsáveis por aproximadamente 93% da variabilidade (Figuras 12B, 12D e 12F – Artigo1). Os resultados dos perfis longitudinais mostram que os sedimentos em suspensão estão presentes em toda a região intermediária (principalmente próximo a Punta Piedras; Figura 1 – Artigo), como afirmado por Moreira et. al. (2013) e Dogliotti et. al. (2016). Em contrapartida, no alto estuário é perceptível uma ampla variabilidade no SSC (região azul), resultado da interferência dos principais afluentes do Rio da Prata (Rio Paraná e Rio Uruguai) (Guerrero et. al., 1997; Moreira et. al., 2103; Dogliotti et. al., 2016).

O perfil transversal na foz do Rio da Prata mostra que o primeiro modo da EOF representa 48% do período neutro analisado, com grande exportação de sedimento pela margem sul do estuário, isto é, a margem influenciada pela descarga fluvial do Rio Paraná, enquanto que o segundo modo representa a participação do Rio Uruguai na exportação do sedimento em 32% do período. Ao analisarmos os anos com efeito ENSO, a importância do Rio Paraná aumenta significativamente, indo para 77% do período

analisado, enquanto que o Rio Uruguai só atua como exportador de sedimento em 12% do período.

Apesar da grande contribuição fluvial dos Rios Paraná e Uruguai, é importante enfatizar que o Rio Bermejo é responsável por 70% do suprimento sedimentar exportados para o Rio da Prata, e como dito anteriormente, o Bermejo não sofre significativamente com o efeito ENSO. Assim sendo, ao considerarmos que a quantidade de sedimento exportada pelo Bermejo não varia tanto, o que torna a disponibilidade de água o principal responsável pela concentração sedimento no Rio da Prata. Resultado disso é que a grande quantidade de sedimento exportado para a região costeira é referente a baixa descarga fluvial durante esse período.

Com a análise dos perfis longitudinais à foz da Lagoa dos Patos, foi possível observar que a Lagoa dos Patos apresenta uma pluma flutuante na desembocadura, que de move preferencialmente para SE ao sair do estuário. Esse padrão dominante (Figura 14A e 14B – Artigo 1) é representado por 93% do período em anos normais e 92% em anos de ENSO, ficando evidente que esse padrão não tem tanta relação a anomalias interanuais, mas sim a ação do vento sinótico, como afirmado por Marques et. al. (2009; 2010b). Já os perfis transversais à foz da Lagoa dos Patos, corroboram quanto a presença de uma pluma hipopicnal. Esse padrão dominante é representado pelo primeiro modo da EOF (Figura 15A e 15B – Artigo 1) com uma porcentagem próximo dos 73% para o período neutro e 70% do período do ENSO.

### 7.1.3. Variabilidade Temporal das Plumas Costeiras

Quanto a variabilidade temporal, a análises das ondaletas mostrou que as plumas costeiras do Rio da Prata e da Lagoa dos Patos apresentam escalas temporais de dias a anos, quando relacionados à ação do vento e a descarga fluvial. A atuação do vento é observada em escalas menores que 15 dias, estando assim relacionado a passagem de frentes meteorológicas na região e está de acordo com as escalas sinóticas observadas por Möller et. al. (2001) e Simionato et. al. (2007). Já a descarga fluvial está relacionada às concentrações de sedimento em suspensão em escalas de tempo mensal e anual, cobrindo os ciclos intra-sazonais, sazonais e interanuais associados ao padrão de precipitação da região.

### 7.1.4. Comportamento do sedimento suspenso na plataforma interna

Ao chegar na plataforma interna, o sedimento em suspensão apresenta um padrão bem definido entre a descarga fluvial e as concentrações de sedimento em suspensão exportadas pela Lagoa dos Patos. Pelo Diagrama de Hovmoller (Figura 20 e 21 – Artigo 1) é possível identificar que as maiores concentrações de sedimento em suspensão ocorrem durante o inverno, coincidente aos picos de descarga fluvial. Enquanto no Rio da Prata, existe uma defasagem de tempo entre a vazão e as concentrações de sedimento em suspensão (Simionato et. al.,2009; Moreira et. al.,2013 e Dogliotti et. al., 2016). Como dito anteriormente, essa defasagem está relacionada à distância entre a jusante e o local escolhido para gerar o diagrama (transecto T6 – Figura 1 – Artigo 1).

Com relação às variações interanuais, existe uma diferença se compararmos o período neutro e o afetado pelo ENSO. Os efeitos da La Niña sobre as concentrações de sedimento em suspensão na plataforma interna durante o ano de 2008 e do El Niño no final de 2009 ficaram evidente nos resultados (Figura 21). Porém, essa alteração não é grande o bastante para diferenciar as concentrações de sedimento em suspensão observadas na plataforma interna durante o período neutro (Figura 20). Esses resultados contradizem os achados de Dogliotti et. al. (2006), no qual os autores afirmaram que durante o ano de La Niña acontece um aumento na concentração de material em suspensão em relação aos anos afetados pelo El Niño. Tal variação pode estar relacionada a posição do perfil T6 (Figure 1 – Artigo 1).

Ao analisarmos a variabilidade espacial associada a SSC na plataforma interna, os dois primeiros modos da EOF representam 76% para o período neutro, e 75% no período do ENSO. Nos primeiros modos da EOF (Figura 22A e 22B), é perceptível a semelhança da distribuição das concentrações de sedimento em suspensão na plataforma interna entre os dois períodos analisados, com um padrão bem definido localizado em uma pequena faixa costeira, respondendo à variação sazonal das concentrações de sedimento em suspensão na região (Figura 8 – Artigo 1). Já no segundo modo da EOF, a variabilidade do sedimento em suspensão indica que o vento de NE influencia na dinâmica da pluma do Rio da Prata e da Lagoa dos Patos, movendo-a para sul. À medida que o sedimento se afasta da influência da vazão continental, o vento passa a ser uma importante forçante na plataforma interna (Soares et. al., 2007b; Simionato et. al., 2005)

## 7.2. Sedimento de Fundo

### 7.2.1. Cenário Médio da Concentração do Sedimento de Fundo

Ao analisarmos as simulações de longo prazo, é possível afirmar que a presença de duas plumas distintas na Plataforma Interna do Atlântico Sudoeste (uma homopycnal e a outra hipopicnal), reflete diretamente na diferenciação da evolução do fundo nas áreas rasas da plataforma interna. Sendo assim, a pluma do Rio da Prata, se tratando de uma pluma homopycnal, afeta amplamente a concentração de sedimento de fundo na região da foz do rio, como ilustrado na figura 6 (Artigo 2). Como visto anteriormente, a influência da pluma do Rio da Prata não se restringe apenas à foz do estuário, dependendo da dinâmica local a pluma do Prata pode se expandir para regiões mais distantes, intensificando assim o processo de deposição ao longo de toda a plataforma interna. Já a pluma da Lagoa dos Patos, por ter característica hipopicnal, pouco influencia no processo de deposição na região próxima da foz da lagoa. Calliari et. al. (2007) afirmaram que o sedimento se deposita preferencialmente ao norte ou ao sul da desembocadura, sendo assim regiões mais sensíveis à deposição. Segundo Marques et. al. (2010), o padrão da evolução do fundo causado pela inferência da pluma da Lagoa dos Patos, está associado ao padrão de circulação local, que por sua vez é predominantemente controlado pelo vento e pela descarga fluvial.

### 7.2.2. Variabilidade Espacial do Sedimento de Fundo

Assim como para o sedimento em suspensão, as análises das EOF foram empregadas para determinar a variabilidade espacial da concentração do sedimento de fundo na região de estudo. A análise indicou que o primeiro modo da EOF (Figura 8A – Artigo 2) já foi responsável por 76% da variabilidade especial do sedimento de fundo. Este indica uma certa influência da batimetria na distribuição do sedimento de fundo, uma vez que um padrão espacial foi evidenciado em áreas rasas tanto no estuário da Lagoa dos Patos quanto no Rio da Prata. O resultado da EOF constatou que o sedimento fino se concentra predominantemente na região sul da foz do La Plata, conforme Simmionato e Moreira (2018) constataram. Esse padrão se justifica pelo fato de a região apresentar um aumento abrupto da profundidade, uma variação abrupta na largura do estuário, além da região ser caracterizada como sendo a frente da cunha salina do estuário, o que favorece ao acúmulo de sedimento. Para o estuário da Lagoa dos Patos há participação do vento

no empilhamento da água na região estuarina da Lagoa dos Patos e, consequentemente, no aumento da concentração de sedimento no fundo, mais precisamente, nas regiões rasas do estuário. Na plataforma interna, a variabilidade é maior se comparada as regiões estuarinas, sendo assim, a região da plataforma interna não apresenta um padrão bem definido para a concentração de sedimento de fundo, indicando que é uma região altamente variável devido a dinâmica costeira.

### 7.2.3. Padrão de Deposição do Sedimento

A análise do potencial energético por ondaletas (Figura 9 e 10 – Artigo 2) foi novamente empregada nesse trabalho, mas dessa vez para determinar a variabilidade temporal do sedimento de fundo na região de estudo. Esta análise considerou 7 anos de simulação e determinou que o processo de deposição pode ser controlado pela ação dos ventos em escala sinótica (de 3 a 15 dias), enquanto que a descarga fluvial controla o fluxo de deposição em escalas sazonais (de 30 a 180 dias), tanto para a foz do Rio da Prata quanto para da Lagoa dos Patos.

A disponibilidade de sedimento auxilia no processo de deposição quando associada a condições ambientais favoráveis. Sendo assim, o vento de sudeste, a descarga fluvial e a morfologia do estuário do La Plata, associados à dinâmica costeira, estão entre as principais condições que favorecem a distribuição de sedimentos na plataforma interna e geram assim um padrão deposicional na região (Moreira et. al., 2019). Já para a Lagoa dos Patos, os ventos de NE estão associados à descarga fluvial, que associada ao padrão de circulação local promove o processo de deposição na plataforma interna adjacente.

Outro fator importante que interfere na deposição do sedimento está relacionado à desaceleração das plumas e à velocidade da corrente costeira. Isso porque, em casos que a descarga fluvial ultrapassa a quantidade de sedimento fornecido à região costeira, esse sedimento pode atingir longas distâncias antes de ser depositado. No caso da região de estudo, tanto a pluma do Rio da Prata quanto da Lagoa dos Patos tende a desacelerar abruptamente ao interagir com a dinâmica da plataforma interna. Dessa forma, os sedimentos finos das plumas podem influenciar na morfologia do fundo de regiões mais distantes da fonte.

### 7.2.4. Evolução do Fundo da Plataforma Interna do Atlântico Sudoeste

Pela presença de grandes afluentes que contribuem para o sedimento em suspensão, a Plataforma Interna do Atlântico Sudoeste é amplamente reconhecida por ser uma plataforma altamente deposicional. Os resultados deste trabalho mostram que grande parte da plataforma interna é dominada por uma evolução de fundo positiva, sendo, contudo, possível observar algumas áreas onde a erosão foi predominante. Isso acontece, pois a dinâmica costeira é altamente energética, principalmente devido à ação dos ventos que geram velocidade de fricção de fundo fortes o suficiente para exceder o limiar do coeficiente de erosão, resultando em um alto fluxo erosivo. No caso das demais áreas deposicionais, a dinâmica não é energética o suficiente para remobilizar esse sedimento em distâncias maiores, resultando num cenário ideal para a deposição.

Para a região do La Plata, Santoro et. al. (2017) e Fossati et. al. (2013) analisaram a evolução fundo na região do estuário e apresentaram algumas características semelhantes e outras mais distintas às encontradas no presente estudo. As semelhanças estão relacionadas às áreas erosivas presentes na costa argentina do estuário. A região é altamente dinâmica e associada ao gradiente batimétrico, resulta em um local altamente erosivo. Em contraste, no presente estudo as áreas do alto estuário são predominantemente erosivas, enquanto Santoro et. al. (2017) mostraram um alto estuário deposicional. Essa diferença se explica pela proximidade da área ao contorno continental, o que pode causar instabilidade do modelo.

As regiões norte e sul da desembocadura da Lagoa dos Patos apresentam características deposicionais, sendo assim, uma tendência positiva para a evolução do fundo. Isso se deve à presença de um banco lamítico presente na região, conforme detalhado por Calliari et al. (2009). A presença de uma área lisa (evolução do leito próxima de zero) na frente dos Molhes da Barra também foi evidenciada por Fachin (1998), que afirma ser uma área predominantemente lamítica, que pode apresentar vestígios de areia mista. Calliari e Fachin (1993) já afirmavam que esse depósito lamítico representado pelo modelo, tem sua origem relacionada à pluma da Lagoa dos Patos, pois pode influenciar as áreas próximas à isolinha de 20 metros.

Em relação à influência do efeito ENSO no processo de evolução do fundo, os períodos em que as taxas de deposição aumentaram foram diretamente correlacionados às anomalias climáticas devido à forte influência do El Niño / La Niña na região de estudo. Os eventos ENSO são padrões climáticos que ocorrem em intervalos de 3 a 7 anos. Esses

episódios causam chuvas acima da média no sul do Brasil, Uruguai e nordeste da Argentina (Grimm et al. 1998; Philander 1990; Ropelewski e Halpert 1987, 1989; Bitencourt et al, 2020). Essa oscilação cíclica contribui para a entrada de cargas sedimentares na plataforma interna, oriundas dos rios (Ivanoff et al., 2020). Devido ao aumento da carga sedimentar que chega à região costeira, o fluxo de deposição deste sedimento aumenta, afetando diretamente o comportamento da evolução do fundo.

## 7.3. Conclusão

A Plataforma Interna do Atlântico Sudoeste é uma região influenciada pela descarga continental e vento local. Essa influência é dominante no processo de transporte de sedimentos em suspensão da região, que é afetado significativamente pelas variações sazonais e interanuais promovidas pelos ciclos do ENSO, principalmente em seu regime de descarga fluvial. O Rio da Prata é o maior exportador de sedimentos em suspensão da região, com uma taxa aproximada de $1,2x10^8$ toneladas / ano em um período neutro. Nos anos de influência do ENOS, essa taxa sobe para $3,0x10^8$ toneladas / ano. A Lagoa dos Patos também contribui para o aumento das concentrações de sedimento em suspensão na região costeira ($1,25x10^7$ ton / ano sem efeito ENSO e $1,35 \times 10^7$ ton / ano com ENSO), mas em menor escala em relação ao rio La Plata.

Em relação à variabilidade espacial em anos neutros, há um padrão de concentrações de sedimento em suspensão fortemente definido na região de Punta Piedras, bem como no litoral sul do estuário do Prata, enquanto no litoral norte o comportamento dos sedimentos apresenta maior variabilidade devido à influência da Rio Uruguai na costa uruguaia. Nos períodos afetados pelo ENSO, as concentrações de sedimento em suspensão apresentam baixa variabilidade em praticamente todos os setores do estuário, evidenciando o forte impacto da vazão do rio na distribuição dos sedimentos no estuário. Para a Lagoa dos Patos, não houve grande diferença na variabilidade espacial dos sedimentos em suspensão da região. Um padrão bem definido é observado na região de influência do Rio Guaíba, um dos principais fornecedores de sedimentos em suspensão para a Lagoa dos Patos.

Em relação à variabilidade espacial, os resultados na foz dos rios confirmaram que no Rio da Prata a pluma se comporta com características homopinicais (afetando toda a coluna d'água), e o sedimento se distribui preferencialmente em direção ao litoral sul do estuário, em decorrência da contribuição do Rio Paraná. Na Lagoa dos Patos, a pluma é

classificada como hipopicnal e tende a migrar para o sul principalmente devido à ação do vento predominante do Nordeste.

Quanto à variabilidade temporal, a descarga fluvial interage com as concentrações de sedimento em suspensão em uma escala sazonal até interanual, enquanto o vento contribui para a variabilidade das concentrações de sedimento em suspensão em uma escala de tempo sinótica. Ao chegar à plataforma interna, o sedimento suspenso ocupa preferencialmente uma estreita faixa costeira próxima à costa. O vento, por sua vez, ganha importância na plataforma, à medida que o sedimento se afasta da influência da vazão, tanto do Rio da Prata quanto da Lagoa dos Patos.

O padrão deposicional médio na região costeira adjacente é o resultado de um equilíbrio entre os processos de erosão e deposição, percebendo-se que a deposição prevalece em grande parte da área de estudo, caracterizando a plataforma interna do Atlântico Sudoeste como deposicional. A causa disto está em vários parâmetros presentes na área de estudo, desde a dinâmica costeira favorável à deposição, devido à desaceleração das plumas, passando pelas feições batimétricas e geomorfológicas, até à ação do vento.

A ação do vento e da descarga fluvial nos principais mecanismos físicos de controle e distribuição de sedimentos finos na plataforma. Esses mecanismos possuem diferentes escalas de tempo de operação, enquanto o vento atua na região de forma sinótica, ou seja, na escala de 16 dias, a descarga fluvial é apresentada de forma mensal à sazonal, portanto, de 30 a 180 dias.

A pluma de sedimentos de La Plata e Lagoa dos Patos influencia significativamente a disponibilidade de sedimentos em suspensão, que com o tempo podem se tornar sedimentos de fundo. Além disso, a ação do vento do quadrante sul induz a formação de correntes para o norte, responsáveis pelo transporte do sedimento do Rio da Prata para a região norte da plataforma interna, assim como o vento do nordeste na Lagoa dos Patos é responsável por a sedimentação local que se move para a região costeira.

Em relação à evolução do fundo, o trabalho mostrou que a plataforma interna do Atlântico Sudoeste é essencialmente deposicional, apesar de apresentar algumas áreas erosivas ao longo da região costeira e na costa argentina do rio La Plata. Sendo altamente influenciado pelo efeito ENSO na região, que aumenta o fluxo de deposição, refletindo no processo de evolução do fundo. A taxa de sedimentação ficou em torno de 50 mm/ano, observando-se regiões com taxas que atingiram valores próximos a 120 mm/ano.

Baseado nas conclusões obtidas neste trabalho e nas limitações associadas a modelagem computacional utilizada no estudo, algumas sugestões para a realização de trabalhos futuros podem ser obtidas:

1. É necessária a obtenção de dados da concentração do sedimento em suspensão junto as desembocaduras dos principais afluentes da Lagoa dos Patos e do Rio da Prata, para que se possa ao menos construir uma curva chave que relacione a descarga fluvial e a concentração de sedimento. Além disso, uma medição continua de concentração de sedimento nas desembocaduras da Lagoa dos Patos e do Rio da Prata ajudaria no processo de validação e calibração do TELEMAC acoplado ao SISYPHE.

2. Inserir os dados de maré meteorológica como condição de contorno na fronteira oceânica junto aos dados de nível e maré astronômica. Alguns autores afirmaram a importância da maré na dinâmica de sedimento do Rio da Prata, possivelmente novos resultados quanto as regiões deposicionais e erosivas poderá ser obtido, sendo assim resultados mais realísticos.

3. A implementação e acoplamento do modelo de onda junto com o modelo hidrodinâmica e morfodinâmicos. A onda é um parâmetro vital na dinâmica sedimentar na plataforma interna, visto que, o regime de onda é responsável por remobilização e ressuspensão do sedimento de fundo na coluna d'água, além de transportar o material em suspensão para as regiões mais longínquas da plataforma interna.

4. Desenvolver o módulo de consolidação do fundo de forma a obter uma estimativa mais realística da evolução do fundo em longas escalas de tempos. Além disso, a consolidação do fundo pode alterar parâmetros como fluxo de erosão e fluxo de deposição, o que afetaria de forma significativa os resultados apresentados no presente trabalho.

# **Capítulo VIII**: Referências Bibliográficas

# 8. Referências Bibliográficas


Acha, E.M., Mianzan, H., Guerrero, R., Carreto, J., Giberto, D., Montoya, N., Carignan, M., 2008. An overview of physical and ecological processes in the Rio de la Plata Estuary. Continental Shelf Research, Vol 28 (13),1579-1588.

Acha, E.M., Mianzan, H.W., Guerrero, R., Favero, M., Bava, J., 2004. Marine fronts at the continental shelves of austral South America, Physical and ecological processes, J. Mar. Syst., 44, 83-105.

Bauer, W., Abreu, P.C., Poersch, L.H., 2017. Plankton and water quality variability in an estuary before and after the shrimp farming effluents: possible impacts and regeneration, Brazilian Journal of Oceanography, 65(3):495-508.

Berbery E. H. & Barros V. 2002: The hydrological cycle of the La Plata Basin in South America. J Hydromet 3: 630-645.

Bisbal, G.A., 1995. The Southeast South American shelf large marine ecosystem: Evolution and components. Mar. Policy,19(1),21–38, doi:10.1016/0308-597X(95)92570-W.

Bitencourt, L.P., Fernandes, E.H., Möller, O., Ross, L., 2020.The contribution of ENSO cycles to the salinity spatio-temporal variability in a bar-built microtidal estuary, Regional Studies in Marine Science, Vol 40,101496.

Blanton, J., Oey, L-Y., Amft, J., Lee, T. N., 1989. Advection of momentum and buoyancy in a coastal frontal zone. Journal of Physical Oceanography 19, 98-15.

Brodie, J., Schroeder, T., Rohde, K., Faithful, J., Masters, B., Dekker, A., Brando, V., Maughan, M., 2010. Dispersal of suspended sediments and nutrients in the Great Barrier Reef lagoon during river-discharge event: conclusions from satellite remote sensing and concurrent flood-plume sampling. Marine and Freshwater Research, 61, 651-664.

Burrage, D., Wesson, J., Martinez, C., Pérez, T., Möller Jr, O., Piola, A., 2008. Patos Lagoon outflow within the Río de la Plata plume using an airborne salinity mapper: Observing an embedded plume. Continental Shelf Research. 28, 1625-1638.

Calliari, D., Brugnoli, E., Ferrari, G., Vizziano, D., 2009. Phytoplankton distribution and production along a wide environmental gradient in the South-West Atlantic off Uruguay. Hydrobiology 620, 47-61.

Calliari, L. J., J. C. Winterwerp, E. H. Fernandes, D. C. Cuchiara, S. B. Vinzon, M. Sperle, and K. T. Holland (2009), Fine grain sediment transport and deposition in the Patos Lagoon-Cassino beach sedimentary system, Cont. Shelf Res., 29(03), 515–529.

Calliari, L.J., Fachin, S., 1993. Laguna dos patos. Influência nos depósitos lamíticos costeiros. Pesquisas, Porto Alegre 20 (1), 57–69.

Campos, J.D., Lentini, C.A., Miller, J.L., Piola, R.A., 1999. Inter-annual variability of the sea surface temperature in the South Brazilian Bight. Geophysical Research Letters, 26(14), 2061-2064.

Castelão, R.M., Möller, O.O., 2006. A modeling study of Patos Lagoon (Brazil) flow response to idealized Wind and river discharge: Dynamical analysis. Brazilian Journal of Oceanography. 54(1), 1-17.

Castello, J., Duarte, A., Möller, O. O., Niencheski, F., Odebredcht, C., Weiss, G., Habiaga, R., Bellotto, V., Kitzmann, D., Souto, C., Souza, R., Ciotti, A., Fillmann, G., Schwingell, P., Bersano, J., Cirano, M., Freire, K., Lima, I., Mello, R., Monteiro, A., Resgalla, C., Soares, I., Suzuki, M. 1990. On the importance of coastal and subantartic waters for the shelf ecosystem off Rio Grande do Sul. Anais do II Simpósio de Estrutura, Função e Manejo de Ecossistemas da Costa Sul e Sudeste, São Paulo – Brazil, I: 112-129.

Castello, J.P., Möller Jr., O.O., 1977. Sobre as condições oceanográficas no Rio Grande do Sul, Brasil. Atlântica 2, 25-110.

Chao, S.Y., 1990. Tidal modulation by estuarine plumes. Journal of Phys. Oceanography. 20, 1115-1123.

Ciotti, A.M., Odebrecht, C., Fillmann, G., Möller, O.O., 1995. Freshwater outflow and subtropical convergence influence on phytoplankton biomass on the southern Brazilian continental shelf. Continental Shelf Research. 15(14), 1737-1756.

Costi, J., Marques, W.C., Kirinus, E.P., Duarte, R.F., Arigony-Neto, J., 2018. Water level variability of the Mirim-São Gonçalo System, a large, subtropical, semi-enclosed coastal complex. Adv. Water Resour, 117, 75-86.

Depetris, P.J., Paolini, J.E., 1991. Biogeochemical aspects of South American rivers: the Paraná and the Prinoco. In: Degens, E.T., Demp, S.J.E. Richey (Eds.), En: Biogeochemistry of Major World Rivers, Scope 42. John Wiley & Sons, New York, pp. 165–194.

Depetris, P.J., Pasquini, A.I., 2007b. Discharge trends and flow dynamics of southern southamerican rivers draining the southern Atlantic seabord: an overview. Journal of hydrology 333:385-399.

Diaz, M., Grasso, F., Le Hir, P., Sottolichio, A., Caillaud, M., Thouvenin, B., 2020. Modeling mud and sand transfers between a macrotidal estuary and the continental shelf: Influence of the sediment transport parameterization. Journal of Geophysical Research: Oceans, 125.

Dogliotti, A.I., Ruddick, K., Guerrero, R., 2016. Seasonal and inter-annual turbidity variability in the Río de la Plata from 15 years of MODIS: El Niño dilution effect. Estuar. Coast. Shelf Sci. 182, 27-39.

Edgbert, G.D., Erofeeva, S.Y., 2002. Efficient Inverse Modeling of Barotropic Ocean Tides. Journal of Atmospheric and Oceanic Technology,19:183-204.

Egbert, G.D., Bennett, A.F., Foreman, M.G.G., 1994. Topex/Poseidon tides estimated using global inverse model. J. Geophys. Res., 99(C12), 24821–24852, doi: 10.1029/ 94JC01894.

Emilson, I., 1961. The Shelf and coastal waters off southern Brazil. Boletim do Instituto Oceanográfico da Universidade de São Paulo 11 (2), 101-112.

Exner, F. M.: Über die Wechselwirkung zwischen Wasser und Geschiebe in Flüssen, Akad. Wiss. Wien Math. Naturwiss. Klasse, 134, 165–204, 1925.

Exner, F. M.: Zur Physik der Dünen, Akad. Wiss. Wien Math. Naturwiss. Klasse, 129, 929–952, 1920.

Fachin, S., 1998. Caracterização do perfil de equilíbrio da antepraia na costa do Rio Grande do Sul. Msc. Dissertation. Universidade Federal do Rio Grande do Sul, Porto Alegre, Brasil, p. 88, unpublished.

Farge, M., 1992. Wavelet transforms and their applications to turbulence. Annu. Rev. Fluid Mech. 24, 395-457.

Fernandes, E.H.L., Dyer, K.R., Möller, O.O., 2005. Spatial gradients in the flow of the southern Patos Lagoon. Journal of Coastal Research, v. 21, n. 4, p. 759-769.

Fernandes, E.H.L., Dyer, K.R., Möller, O.O., Niencheski, L.F.H., 2002. The Patos Lagoon Hydrodynamics during an El Nino event (1998). Continental Shelf Research, England, v. 22, n. 11-13, p. 1699-1713.

Fernandes, E.H.L., Dyer, K.R., Niencheski, L.F.H., 2001. Calibration and validation of the TELEMAC-2D model to the Patos Lagoon, Brazil. Journal of Coastal Research, USA, v. 34, p. 470-488.

Fernandes, E.H.L., Mariño-Tapia, I., Dyer, K.R., Möller, O.O., 2004. The attenuation of tidal and subtidal oscillations in the Patos Lagoon estuary. Ocean Dynamics, Alemanha, v. 54, n. 4, p. 348-359.

Fernandes, E.H.L., Monteiro, I., Möller, O.O., 2007. On the dynamics of Mangueira Bay - Patos Lagoon (Brazil). Journal of Coastal Research, v. 47, p. 97-107.

Fossati, M. & Piedra-Cueva, I., 2013. A 3D hydrodynamic numerical model of the Río de la Plata and Montevideo's coastal zone. Applied Mathematical Modelling, 37, 1310_1332. 8, 42

Fossati, M., Cayocca, F., & Piedra-Cueva, J.C.I. (2014). Fine sediment dynamics in the Río de la Plata. Advances in Geosciences, 39, 75-80.

Foster, G., Carter, L., 1997. Mud sedimentation on the continental shelf at an accretionary margin - Poverty Bay, New Zealand, New Zealand Journal of Geology and Geophysics, 40:2, 157-173.

Framiñan, M.B., Brown, O.B., 1996. Study of the Río de la Plata turbidity front: I. Spatial and temporal distribution. Continental Shelf Research, 16, 1259-1282.

Gabioux, M. Vinzon, S.B. and Paiva, A. M., 2005. Tidal propagation over fluid mud layers on the Amazon shelf. Continental Shelf Research 25, 113-125.

García-Rodríguez, F., Brugnoli, E., Muniz, P., Venturini, N., Burone, L., Hutton, M., Rodríguez, Pita, A., Kandratavicius, N., Perez, L., Vercai, J., 2014. Warm-phase ENSO events modulate the continental freshwater input and the trophic state of sediments in a large South American estuary. Marine Freshwater research 65:1-11.

Garvine, R.W., 1999. Penetration of buoyant coastal discharge onto the continental shelf: A numerical model experiment. Journal of Physical Oceanography. 29, 1892-1909.

Geyer, W.R., Hill, P.S., Kineke, G.C., 2004. The transport, transformation and dispersal of sediment by buoyant coastal flows. Continental Shelf Research, v.24, p.927-949.

Grimm, A.M., Barros, V.R., Doyle, M.E., 2000. Climate variability in southern south America associated with El Niño and La Niña events. American Meteorological Society 2000:35-57.

Grimm, A.M., Ferraz, S.E.T., Julio, G., 1998. Precipitation anomalies in southern Brazil associated with El Niño and La Niña events. American Meteorological Society 1998:2863-2879.

Guerrero, R.A., Acha, E.M., Framiñan, M.B., Lasta, C.A., 1997. Physical oceanography of the Río de la Plata estuary Argentina. Continental Shelf Research 17 (7), 727-742.

Guo, X. E. D. & Valle-Levinson, A., 2007. Tidal effects on estuarine circulation and outflow plume in the Chesapeake Bay. Continental Shelf Research. 27(2007), 20-42.

Haimovici, M., Pereira, S.D., Vieira, P.C., 1989. La pesca demersal en el sur de Brasil en el periodo 1975-1985. Frente maritmo, S(A), 151-163.

Haque, A., Rahman, M., 2016. Flow distribution and sediment transport mechanism in the estuary systems of Ganges-Brahmaputra-Meghna Delta. International Journal of Environmental Science and Development, Vol. 7, No. 1.

Hartmann, C. Sano, E.E., Paz, R. S., Möller, O.O., 1986. Avaliação de um período de cheia (junho de 1984) na região sul da Laguna dos Patos, através de dados de sensoriamento remoto, meteorológicos e oceanográficos. 4o Simpósio Brasileiro de Sensoriamento Remoto. Gramado, RS. 685-693.

Hartmann, C., Calliari, L.J., Möller, O.O., 1990. Material Em Suspensão No Estuário da Laguna dos Patos, Rs, Fase I. Obs. Preliminares, Abril 79 A Dez. 80. Sociedade & Natureza.

Hartmann, C., Schettini, C.A.F., 1991. Aspectos hidrológicos na desembocadura da Laguna dos Patos, RS. Revista Brasileira de Geociências, 21(4): 371-377.

He, L., Chen, D., Zhang, S., Liu, M., Duan, G., 2018. Evaluating Regime Change of Sediment Transport in the Jingjiang River Reach, Yangtze River, China. Water, 10, 329.

Helder, W. and Ruardij, P., 1982. A one-dimensional mixing and flushing model of the Ems-Dollard Estuary. Neth. J. Sea Res., 15: 293-312.

Hervouet, J.M. (2007). Hydrodynamics of Free Surface Flows. John Wiley & Sons, Ltd, Chichester, UK. 31, 45, 111, 116, 119, 247, 249, 254.

Hervouet, J-M., 2007. Free surface flows: Modelling with the finite element methods. John Wiley & Sons Ltd, Copyright © 2007, England.

Holland, K. T., S. B. Vinzon, and L. J. Calliari (2009), A field study of coastal dynamics on a muddy coast offshore of Cassino beach, Brazil, 29(3), 501–502.

Hostache, R., Hissler, C., Matgen, P., Guignard, C., and Bates, P.: Modelling suspended-sediment propagation and related heavy metal contamination in floodplains: a parameter sensitivity analysis, Hydrol. Earth Syst. Sci., 18, 3539 3551, https://doi.org/10.5194/hess-18-3539-2014, 2014.

Ivanoff, M.D., Toldo, E.E., Figueira, R.C.L., Ferreira, P.A.L., 2020. Use of 210Pb and 137Cs in the assessment of recent sedimentation in Patos Lagoon, southern Brazil. Geo-Mar Lett.

Jaime, P. R., & Menéndez, A. N. (2002). Análisis del régimen hidrológico de los ríos Paraná y Uruguay. Informe LHA-01-216-02, INA, Ezeiza.

Jalon-Rojas, I., Schmidt, S., Sottolichio, A., 2016. Evaluation of spectral methods for high-frequency multiannual time series in coastal transitional waters: advantages of combined analyses. Limnol. Oceanogr.: Methods 14, 381-396.

Janin, J.M., Marcos, F., 1997. Code TELEMAC-3D – Version 2.2: Note Théorique, Report HE-42/97/049/B, Electricité de France/LNHE, Paris.

Kineke, G.C., Sternberg, R.W., 1995. Distribution of fluids muds on the Amazon continental shelf. Marine Geology, 125, 193-233.

Kjerfve, B., 1986. Comparative oceanography of coastal lagoons, p. 63-81. In D. A. Wolfe (ed.), Estuarine Variability. Academic Press, New York.

Kourafalou, V.H., Oey, L-Y., Wang, J.D., Lee, T.N., 1996a. The fate of river discharge on the continental shelf. 1. Modeling the river plume and the inner shelf coastal current. J. Geophys. Res. 101, 3415-3434.

Laprida, C., Chapori, N. G., Violante, R. A., Compagnucci, R. H., 2007. Mid-Holocene evolution and paleoenvironments of the shoreface–offshore transition, north-eastern Argentina: New evidence based on benthic microfauna. Marine Geology, 240(43-56).

Lee, B.J., Toorman, E., Molz, F.J., Wang, J., 2011. A two-class population balance equation yielding bimodal flocculation of marine or estuarine sediments. Water Research 45(5):2131-2145.

Lepesqueur, J., Hostache, R., Martínez-Carreras, N., Montargès-Pelletier, E., Hissler, C. Sediment transport modelling in riverine environments: on the importance of grain-size distribution, sediment density, and suspended sediment concentrations at the upstream boundary. Hydrol. Earth Syst. Sci., 23, 3901–3915.

Lisboa, P.V., Fernandes, E.H., 2015. Anthropogenic influence on the sedimentary dynamics of a sand spit bar, Patos Lagoon Estuary, RS, Brazil. Journal of Integrated coastal Zone Manegement. 15 (1), 35-46.

Mann, K.H., Lazier, J.R.N., 1991. Dynamics of Marine Ecosystems: Biological–Physical Interactions in the Oceans. Blackwell Scientific Publications, Oxford 466pp.

Marques, W.C., Fernandes, E.H., Möller Jr., O.O., 2010a. Straining and advection contributions to the mixing process of the Patos Lagoon coastal plume, Brazil. Continental Shelf Research, doi:10.1029/2009JC005653.

Marques, W.C., Fernandes, E.H., Monteiro, I.O., Möller Jr., O.O., 2009. Numerical modeling of the Patos Lagoon coastal plume, Brazil. Continental Shelf Res. 29, 556-571.

Marques, W.C., Fernandes, E.H.L., Moraes, B.C., Möller, O.O., Malcherek, A., 2010b. Dynamics of the Patos Lagoon coastal plume and its contribution to the deposition pattern of the Southern Brazilian inner shelf. Journal of Geophysical Research, 115(C10):1-22.

Marques, W.C., Möller, O.O., 2009. Variabilidade temporal em longo período da descarga fluvial e níveis de água da Lagoa dos Patos, Rio Grande do Sul, Brasil. Revista Brasileira de Recursos Hídricos 13, 155-163.

Martins, L.R., Villwock, J.A., 1987. Eastern South America quaternary coastal and marine geology. Reports in Marine Sciences, UNESCO 43, 28-86.

Meade, R.H., 1996. River-sediment inputs to major deltas. In Sea-level Rise and Coastal Subsidence (Milliman, S.D. & Haq, B.U., eds). Kluwer Academic Press, Boston, pp. 63-85.

Meccia, V.L., Simionato, C.G., Fiore, M.M.E., D'Onofrio, E., Dragani, W.C., 2009. Sea surface height variability in the R´ıo de la Plata estuary from

synoptic to inter-annual scales: Results of numerical simulations. Estuarine, Coastal and Shelf Science, 85(2), 327-343

Menandro, P.S., Bastos, A.C., Quaresma, V.S., Vinzón; S.B., 2015. Acoustic response of Amazon Shelf muddy sediments. Revista Brasileira de Geofísica 33(4): 625-636.

Menéndez, A.N., Sarubbi, A., 2007. A Model to Predict the Paraná Delta Front Advancement. Workshop on Morphodynamic Processes in Large Lowland Rivers, (Santa Fe, Argentina), pp. 25.

Milliman, J. D.; Shen, H.; Yang, Z.; Meade, R.H., 1985. Transport and deposition of river sediment in the Changjiang estuary and adjacent continental shelf. Continental Shelf Research, Vol.4, pp. 37-45.

Milliman, J.D., Syvitski, J.P.M., 1992. Geomorphic/tectonic control of sediment discharge to the ocean: the importance of small mountainous rivers. Journal of Geology 100, 525-544.

Möller Jr OO, Piola AR, Freitas AC, Campos EJD. 2008. The effects of river discharge and seasonal winds on the shelf off southeastern South America. Continental Shelf Research 28(13):1607–24. doi:10.1016/j.csr.2008.03.012

Möller, O. O., J. A. Lorenzzetti, J. L. Stech, and M. M. Mata (1996), The Patos Lagoon summertime circulation and dynamics, Cont. Shelf Res., 16, 335–351, doi:10.1016/0278-4343(95)00014-R.

Möller, O. O., P. Castaing, J. C. Salomon, and P. Lazure (2001), The influence of local and non-local forcing effects on the subtidal circulation of Patos Lagoon, Estuaries Coasts., 24, 297–311, doi:10.2307/1352953.

Möller, O.O., Castaing, P., 1999. Hydrographical characteristics of the estuarine area of Patos Lagoon (30° S, Brazil), p. 83-100. In G. M. Perillo, M.C. Piccolo, M. Pino (eds.), Estuaries of South America: Their Geomorphology and Dynamics. Springer Verlag, Berlin.

Möller, O.O., Lorenzzetti, J.A., Stech, J.L., Mata, M. M., 1996. The Patos Lagoon summertime circulation and dynamics. Coastal Shelf Research 16:335-351.

Möller, O.O., Piola, A.R., Freitas, A.C., Campos, E.J.D., 2008. The effects of river discharge and seasonal winds on the shelf off southeastern South America. Continental Shelf Research 28, 1607-1624.

Montanher, O.C., Novo, E.M., Filho, E.E., 2018. Temporal trend of the suspended sediment transport of the Amazon River (1984-2016), Hydrological Sciences Journal, DOI: 10.1080/02626667.2018.1546387.

Monteiro, I.O., Marques, W.C., Fernandes, E.H., Gonçalves, R.C., Möller Jr, O.O., 2011. On the effect of earth rotation, river discharge, tidal oscillations, and wind in the dynamics of the patos lagoon coastal plume. Journal of Coastal Research, Editora da Furg, v. 271, p. 120-130.

Moreira, D., Simionato, C. G., Dragani, W., Cayocca, F., & Luz Clara Tejedor, M. (2016). Characterization of Bottom Sediments in the Río de la Plata Estuary. Journal of Coastal Research, 32(6), 1473–1494.

Moreira, D., Simionato, C.G., 2019. Modeling the suspended sediment transport in a very wide, shallow, and microtidal estuary, the Río de la Plata, Argentina. Journal of Advances in Modeling Earth Systems, 11, 3284-3304.

Moreira, D., Simionato, C.G., Dragani, W., Cayocca, F., Tejedor, M.L.C., 2016. Characterization of Bottom Sediments in the Río de la Plata Estuary. Journal of Coastal Research, 32(6), 1473-1494.

Moreira, D., Simionato, C.G., Gohin, F., Cayocca, F., Tejedor, M.L.C., 2013. Suspended matters mean distribution and seasonal cycle in the Río de la Plata estuary and the adjacent shelf from MODIS and in situ observations. Continental Shelf Research, 68, 51-66.

Nikuradse, J.: Gesetzmässigkeiten der Turbulente Strömung in Glatten Rohren, Ver. Deut. Ing. Forschungsheft, 356, Ver. Deut. Ing. Forschungsheft, Düsseldorf, 1932.

Nittrouer, C.A., Wright, L.D., 1994. Transport of particles across continental shelves. Reviews of Geophysics 32 (1), 85–113.

Oliveira, H., Fernandes, E., Möller, O., García-Rodríguez, F., 2019. Relationships between Wind Effect, Hydrodynamics and Water Level in the World's Largest Coastal Lagoonal System. Water 11 (11), 2209.

Oliveira, H.A., Fernandes, E.H.L., Möller, O.O., Collares, G.L., 2015. Processos Hidrológicos e Hidrodinâmicos da Lagoa Mirim. RBRH vol. 20 no1 Porto Alegre jan./mar. 2015 p. 34-45.

Palma, E. D., Matano, R. P., and Piola, A. R., 2008. A numerical study of the Southwestern Atlantic Shelf circulation: Stratified ocean response to local and offshore forcing, J. Geophys. Res., (C0) 8014.

Partheniades, E., 1965. Erosion and deposition of cohesive soils. Journal of the Hydraulics Division, 91(1), 105-39.

Pasquini, A.I., Depetris, P.J., 2007. ENSO-triggered exceptional flooding in the Paraná River: where is the excess water coming from? J. Hydrol. 383 (2010), 186-193.

Peixoto, D.W.B., Guasselli, L.A., Waterloo, P.F., 2018. Estimativa de Concentração de Sedimentos em Suspensão a Partir de Imagens Landsat 8 em PCHs no Rio Ivaí-RS. São Paulo: Geociências (Online), v. 37, p. 147-154.

Pereira, C.S., 1989. Seasonal variability in the coastal circulation on the Brazilian Continental Shelf (29–351S). Continental Shelf Research 9, 285-289.

Pimenta, F.M., Campos, E.J.D., Miller, J. L., Piola, A. R., 2005. A numerical study of the Plata River plume along the Southeastern South American Continental Shelf. Brazilian Journal of Oceanography, 53(3/4):129-146.

Piola, A.R., Campos, E.J.D., Möller. O.O., Charo, M., and Martinez, C., 2000. Subtropical Shelf Front off eastern South America. Journal of Geophysical Research. 105(C3), 6565-6578.

Piola, A.R., Matano, R.P., Palma, E.D., Möller, O.O., Campos, E.J.D., 2005. The influence of the Plata River discharge on the western South Atlantic shelf. Geophysical Research Letters. 32.

Piola, A.R., Romero, S.I., 2004. Analysis of space-time variability of the Plata River plume. Gayana (Concepción), 68(2, Supl. TIIProc), 482-486.

Rodrigues, A., Oliveira, A., Fonseca, R.; Taborda, R.; Cascalho, J., 2006. Sedimentary dynamics of the southern shelf of Madeira (Portugal). Journal of Coastal Research, SI 39 (Proceeding of the 8th International Coastal Symposium), 454-458. Itajaí, SC, Brazil, ISSN 0749-0208.

Rosa, F., Rufino, M.M., Ferreira, Ó., Matias, A., Brito, A.C., Gaspar, M.B., 2013. The influence of coastal processes on inner shelf sediment distribution: The Eastern Algarve Shelf (Southern Portugal), Geologica Acta, 11, 59-73.

Santoro, P., Fossati, M., Piedra-Cueva, I., 2013. Characterization of circulation patterns in Montevideo Bay (Uruguay). Journal of Coastal Research, 29 (4), 819-835

Santoro, P., Fossati, M., Tassi, P., Huybrechts, N., Pham Van Bang, D., and Piedra-Cueva, J.C.I. (2017). A coupled wave-current-sediment transport

model for an estuarine system: Application to the Río de la Plata and Montevideo Bay. Applied Mathematical Modelling, 52, 107-130.

Santoro, P., Huybrechts, N., Fossati, M., Van Bang, D., Tassi, P., Piedra-Cueva, I., 2016. 2D and 3D numerical study of the Montevideo Bay hydrodynamics and fine sediment dynamics. Proceedings of the XXIIIrd TELEMAC-MASCARET User Conference 2016, 11 to 13 October 2016, Paris, France, 177-188.

Sepúlveda, H.H., Valle-Levinson, A., Framiñan, M., 2004: Observations of subtidal and tidal flows in the Río de la Plata Estuary. Continental Shelf Research, 24, 509-525.

Silva, P., Lisboa, P., Fernandes, E., 2015. Changes on the fine sediment dynamics after the Port of Rio Grande expansion. Adv. Geosci. 39, 123-127.

Siminato, C. G., Moreira, D., (2018). Modeling the Processes that Control Fine Sediments Transport in the Río de la Plata Estuary. Journal of Coastal Research, 85(sp1):31-35.

Simionato, C. G., Moreira, D., Re, M., & Fossati, M. (2011). Estudio de la dinámica hidro-sedimentológica del Río de la Plata: observación y modelación numérica de los sedimentos finos. Published by Proyecto FREPLATA, CTMFM-CARP, 109p.

Simionato, C.G., Clara Tejedor, M.L., Campetella, C., Guerrero, R., Moreira, D., 2010. Patterns of sea surface temperature variability on seasonal to sub-annual scales at and offshore the Río de la Plata Estuary. Continental Shelf Research, 30(19), 1983-1997

Simionato, C.G., Meccia, V., Guerrero, R., Dragani, W., Nuñez, M., 2007. The Rio de la Plata estuary response to wind variability in synoptic to intra-seasonal scales: II currents vertical structure and its implications on the salt wedge structure. J. Geophys. Res. C Oceans 112, C07005.

Simionato, C.G., Meccia, V.L., Dragani, W.C., 2009. On the path of plumes of the Río de la Plata estuary main tributaries and their mixing time scales. Geoacta 34, 87-116.

Simionato, C.G., Nuñez, M.N., Engel, M., 2001. The salinity front of the Río de la Plata - A numerical case study for winter and summer conditions. Geophysical Research Letters, 28(13), 2641-2644.

Simionato, C.G., Vera, C.S., Siegismund, F., 2005. Surface wind variability on seasonal and interannual scales over R´ıo de la Plata area. Journal of Coastal Research, 21(4), 770-783.

Smith, W.H.F., Sandwell, D.T., 1997. Global sea floor topography from satellite altimetry and ship depth soundings. Science 277, 1956-1962.

Soares, I.D., & Möller, O.O., 2001. Low-frequency currents and water mass spatial distribution on the southern Brazilian shelf. Continental Shelf Research, 21(16-17):1785-1814. DOI:10.1016/S0278-4343(01)00024-3.

Soares, I.D., Kourafalou, V., Lee T.N., 2007a. Circulation on the western South Atlantic continental shelf: 1. Numerical process studies on buoyancy. J. Geophys. Res., 112, D04002, doi:10.1029/2006JC003618.

Soares, I.D., Kourafalou, V., Lee T.N., 2007b. Circulation on the western South Atlantic continental shelf: 2. Spring and autumn realistic simulations. J. Geophys. Res., Res. 112, C04003, doi:10.1029/2006JC003620.

Soares, I.D., Kourafalou, V., Lee, T.N., 2007a. Circulation on the western South Atlantic continental shelf. Part 1: Numerical process studies on Buoyancy. Journal of Geophysical Research. 112, C04002.

Soares, I.D., Kourafalou, V., Lee, T.N., 2007b. Circulation on the western South Atlantic continental shelf. Part 2: Spring and autumn realistic simulations. Journal of Geophysical Research. 112, C04003.

Souza, R.B., Robinson, I.S., 2004. Lagrangian and satellite observations of the Brazilian Coastal Current. Continental Shelf Research. 24, 241-262.

Sternberg, R.W., Nowell, A.R.M., 1999. Continental shelf sedimentology: scales of investigation define future research opportunities. Journal of Sea Research 41, 55–71.

Sutherland, J., Peet, A.H., Soulsby, R.T., 2004b. Evaluating the performance of morphological models. Coast. Eng. 51, 917-939.

Sutherland, J., Walstra, D.J.R., Chesher, T., Van Rijn, L.C., Southgate, H.N., 2004a. Evaluation of coastal area modelling systems at an estuary mouth. Coast. Eng. 51 (2), 119-142.

Talke, S.A., Stacey, M.T., 2008. Suspended sediment fluxes at an intertidal flat: The shifting influence of wave, wind, tidal, and freshwater forcing. Continental Shelf Research. 28(2008), 710-725.

Tassi, P., Villaret, C., 2014. Sisyphe v6.3 User's Manual - User manual, EDFLNHE report H-P73-2010-01219.

Távora, J., Fernandes, E.F., Bitencourt L.P., Orozco, P.M.S., 2020. El-Niño Southern Oscillation (ENSO) effects on the variability of Patos Lagoon Suspended Particulate Matter. Regional Studies in Marine Science, 101495.

Toldo Jr., E.E., Ayup Zouain, R.N., Corrêa, I.C.S., Dillenburg, S.R., 1991. Barra Falsa: Hipótese de um paleocanal holocênico de comunicação entre a Laguna dos Patos e o Oceano Atlântico. Pesquisas, 18(2):99-103.

Toldo Jr., E.E., Corrêa, I.C.S., Almeida, L.E.S.B., Weschenfelder, J., Gruber, N.L.S., 2006. Sedimentação de Longo e curto período na Lagoa dos Patos. Pesquisas em Geociências. 33(2), 79-86.

Torrence, C., Compo, G.P., 1997. A practical guide to wavelet analysis. Bull. Am. Meteorol. Soc, 79, 61-78.

Van Leussen, W., 1994. Estuarine macroflocs and their role in fine-grained sediment transport. Utrecht: I. University of Utrecht.

Vaz, A.C., Almeida, T.L., Möller, O., 2006. Sobre a descarga dos rios afluentes da Lagoa dos Patos. Atlântica, v. 28, p. 1-12.

Villaret, C., 2010. Sisyphe user manual, Tech. Rep., EDF R&D, Chatou.

Villaret, C., Hervouet, J. M., Kopmann, R., Merkel, U., and Davies, A. G., 2013 Morphodynamic modelling using the Telemac finiteelement system, Comput. Geosci., 53, 105–113.

Vinzon, S. B., J. C. Winterwerp, R. Nogueira, and G. J. de Boer (2009), Mud deposit formation on the open coast of the larger Patos Lagoon - Cassino Beach system, Cont. Shelf. Res., 29(03), 572–588.

Violante, R.A. & Cavalloto, J.L. 2004. Evolution of the semienclosed basins and surrounding coastal plains adjacent to the Pampean Region, Argentina. Polish Geological Institute Special Papers, 11:59-70.

Walstra, L., Van Rijn, L., Blogg, H., Van Ormondt, M., 2001. Evaluation of a Hydrodynamic Area Model Based on the COAST3D Data At Teignmouth 1999. Report TR121-EC MAST Project No. MAS3-CT97-0086, HR Wallinford, UK, pp. D4.1-D4.4.

Warrick, J. A., Simms, A. R., Ritche, A., Steel, E., Dartnell, P., Conrad, J. E., Finlayson, D. P., 2013. Hyperpycnal plume-derived fans in the Santa Barbara Channel, California. Geophysical Research Letters, Vol. 40, 2081-2086.

Winterwerp, J.C., 2002. On the flocculation and settling velocity of estuarine mud. Continental Shelf Research, 22, 1339-1360.

Wright, I. D., and C. A. Nittrouer (1995), Dispersal of river sediments in coastal seas: Six contrasting cases, Estuaries, 18, 494–508.

Wright, L., Friedrichs, C., 2006. Gravity-driven sediment transport on continental shelves: A status report. Continental Shelf Research, 26, 2092-2107.

Wright, L.D., Boon, J.D., Kim, S.C., List, J.H., 1991. Modes of cross-sore sediment transport on the shoreface of the Middle Atlantic Bight. Marine Geology 96, 19–51.

Wright, L.D., Nittrouer, C.A., 1995. Dispersal of river sediments in coastal seas: Six contrasting cases, Estuaries, 18, 494-508.

Ye, S., Ran, Q., Fu, X., Hu, C., Wang, C., Parker, G., Chen, X., Zhang, S., 2019. Emergent stationarity in Yellow River sediment transport and the underlying shift of dominance: from streamflow to vegetation. Hydrology Earth System Sciences, 23, 549-556.

Zavialov, P.O., Ghisolfi, R.D., Garcia, C.A.E.,1998. An inverse model for seasonal circulation over the Southern Brazilian shelf: near-surface velocity from the heat budget, J. Phys. Oceanogr., 28, 545-561.